

# ANALYTICAL AND NUMERICAL METHODS FOR DIFFERENTIAL EQUATIONS AND APPLICATIONS

EDITED BY: Jesus Martin-Vaquero, Feliz Minhós, Juan L. G. Guirao and  
Bruce Alan Wade

PUBLISHED IN: Frontiers in Applied Mathematics and Statistics and  
Frontiers in Physics



# frontiers

## Frontiers eBook Copyright Statement

The copyright in the text of individual articles in this eBook is the property of their respective authors or their respective institutions or funders. The copyright in graphics and images within each article may be subject to copyright of other parties. In both cases this is subject to a license granted to Frontiers.

The compilation of articles constituting this eBook is the property of Frontiers.

Each article within this eBook, and the eBook itself, are published under the most recent version of the Creative Commons CC-BY licence.

The version current at the date of publication of this eBook is CC-BY 4.0. If the CC-BY licence is updated, the licence granted by Frontiers is automatically updated to the new version.

When exercising any right under the CC-BY licence, Frontiers must be attributed as the original publisher of the article or eBook, as applicable.

Authors have the responsibility of ensuring that any graphics or other materials which are the property of others may be included in the CC-BY licence, but this should be checked before relying on the CC-BY licence to reproduce those materials. Any copyright notices relating to those materials must be complied with.

Copyright and source acknowledgement notices may not be removed and must be displayed in any copy, derivative work or partial copy which includes the elements in question.

All copyright, and all rights therein, are protected by national and international copyright laws. The above represents a summary only. For further information please read Frontiers' Conditions for Website Use and Copyright Statement, and the applicable CC-BY licence.

ISSN 1664-8714

ISBN 978-2-88971-424-7

DOI 10.3389/978-2-88971-424-7

## About Frontiers

Frontiers is more than just an open-access publisher of scholarly articles: it is a pioneering approach to the world of academia, radically improving the way scholarly research is managed. The grand vision of Frontiers is a world where all people have an equal opportunity to seek, share and generate knowledge. Frontiers provides immediate and permanent online open access to all its publications, but this alone is not enough to realize our grand goals.

## Frontiers Journal Series

The Frontiers Journal Series is a multi-tier and interdisciplinary set of open-access, online journals, promising a paradigm shift from the current review, selection and dissemination processes in academic publishing. All Frontiers journals are driven by researchers for researchers; therefore, they constitute a service to the scholarly community. At the same time, the Frontiers Journal Series operates on a revolutionary invention, the tiered publishing system, initially addressing specific communities of scholars, and gradually climbing up to broader public understanding, thus serving the interests of the lay society, too.

## Dedication to Quality

Each Frontiers article is a landmark of the highest quality, thanks to genuinely collaborative interactions between authors and review editors, who include some of the world's best academicians. Research must be certified by peers before entering a stream of knowledge that may eventually reach the public - and shape society; therefore, Frontiers only applies the most rigorous and unbiased reviews. Frontiers revolutionizes research publishing by freely delivering the most outstanding research, evaluated with no bias from both the academic and social point of view. By applying the most advanced information technologies, Frontiers is catapulting scholarly publishing into a new generation.

## What are Frontiers Research Topics?

Frontiers Research Topics are very popular trademarks of the Frontiers Journals Series: they are collections of at least ten articles, all centered on a particular subject. With their unique mix of varied contributions from Original Research to Review Articles, Frontiers Research Topics unify the most influential researchers, the latest key findings and historical advances in a hot research area! Find out more on how to host your own Frontiers Research Topic or contribute to one as an author by contacting the Frontiers Editorial Office: [frontiersin.org/about/contact](http://frontiersin.org/about/contact)

# ANALYTICAL AND NUMERICAL METHODS FOR DIFFERENTIAL EQUATIONS AND APPLICATIONS

Topic Editors:

**Jesus Martin-Vaquero**, University of Salamanca, Spain

**Feliz Minhós**, University of Evora, Portugal

**Juan L. G. Guirao**, Universidad Politécnica de Cartagena, Spain

**Bruce Alan Wade**, University of Louisiana at Lafayette, United States

**Citation:** Martin-Vaquero, J., Minhós, F., Guirao, J. L. G., Wade, B. A., eds. (2021). Analytical and Numerical Methods for Differential Equations and Applications. Lausanne: Frontiers Media SA. doi: 10.3389/978-2-88971-424-7

# Table of Contents

- 04** *Editorial: Analytical and Numerical Methods for Differential Equations and Applications*  
Jesus Martin-Vaquero, Bruce Wade, Juan L. García Guirao and Feliz Minhós
- 06** *Dark-Bright Optical Soliton and Conserved Vectors to the Biswas-Arshed Equation With Third-Order Dispersions in the Absence of Self-Phase Modulation*  
Aliyu Isa Aliyu, Mustafa Inc, Abdullahi Yusuf, Dumitru Baleanu and Mustafa Bayram
- 11** *Fuzzy Type RK4 Solutions to Fuzzy Hybrid Retarded Delay Differential Equations*  
Prasantha Bharathi Dhandapani, Dumitru Baleanu, Jayakumar Thippan and Vinoth Sivakumar
- 17** *Slip and Hall Effects on Peristaltic Rheology of Copper-Water Nanomaterial Through Generalized Complaint Walls With Variable Viscosity*  
Muhammad Awais, Poom Kumam, Nabeela Parveen, Aamir Ali, Zahir Shah and Phatiphat Thounthong
- 28** *The Falling Body Problem in Quantum Calculus*  
Abdulaziz M. Alanazi, Abdelhalim Ebaid, Wadha M. Alhawiti and Ghulam Muhiuddin
- 33** *Application of New Iterative Method to Time Fractional Whitham–Broer–Kaup Equations*  
Rashid Nawaz, Poom Kumam, Samreen Farid, Meshal Shutaywi, Zahir Shah and Wejdan Deebani
- 43** *The Global Attractor of the Allen-Cahn Equation on the Sphere*  
David Medina and Pablo Padilla
- 55** *Invariant Solutions and Conservation Laws of the Variable-Coefficient Heisenberg Ferromagnetic Spin Chain Equation*  
Na Liu
- 65** *ESERK Methods to Numerically Solve Nonlinear Parabolic PDEs in Complex Geometries: Using Right Triangles*  
Jesús Martín-Vaquero
- 73** *Numerical Solutions of Quantum Mechanical Eigenvalue Problems*  
Asif Mushtaq, Amna Noreen and Kåre Olaussen
- 83** *A Vector Series Solution for a Class of Hyperbolic System of Caputo Time-Fractional Partial Differential Equations With Variable Coefficients*  
Ahmad El-Ajou and Zeyad Al-Zhour



# Editorial: Analytical and Numerical Methods for Differential Equations and Applications

Jesus Martin-Vaquero<sup>1\*</sup>, Bruce Wade<sup>2</sup>, Juan L. García Guirao<sup>3</sup> and Feliz Minhós<sup>4</sup>

<sup>1</sup>University of Salamanca, Salamanca, Spain, <sup>2</sup>University of Louisiana at Lafayette, Lafayette, LA, United States, <sup>3</sup>Universidad Politécnica de Cartagena, Cartagena, Spain, <sup>4</sup>University of Evora, Évora, Portugal

**Keywords:** ordinary differential equations, partial differential equations, delay differential equations, fractional PDEs, applied mathematics

## Editorial on the Research Topic

### Analytical and Numerical Methods for Differential Equations and Applications

In the last few decades, new mathematical problems and models, described by differential equations, have brought to light applications in many areas including Physics, Chemistry, Engineering, Biomedicine, and Economics, among others.

This research topic shows the large amount of different types of differential equations, thus it contains a selection of papers with recent advances in subjects as different as delay differential equations, nonlinear partial differential equations (PDEs), studied analytically or numerically, or because of their applications, fractional PDEs, and q-differential equations, etc. We would like to thank all the contributors of this issue, and also the referees. They all worked hard to shed some light on these topics for young researchers who would like to investigate some of these areas. Thus, in this research topic, readers can find papers on varying numerical methods and applications.

Delay differential equations (DDEs): During the last few years, there have been many studies on DDEs. A very special type of retarded delay differential equations called fuzzy hybrid retarded equations are studied in [1]. For these equations, numerical schemes based on Runge-Kutta schemes are a good option to obtain accurate solutions.

Recent advances in stochastic or fractional ODEs and PDEs have been published in the last few years. In this special issue, researchers can find two papers on a fractional PDEs model by [2] and [3], solved numerically with different procedures.

Many scientific papers study PDEs, their applications, and also analytical procedures to study their properties. Thus, an analytical solution of the Biswas-Arshed equation is obtained in [4]. This is a non-linear PDE with important applications in physics. In a similar topic, the variable-coefficient Heisenberg ferromagnetic spin chain (vcHFSC) equation is considered in [5]. This equation is also a nonlinear PDEs method, and it can be solved with Lie-algebra groups.

However, many other nonlinear PDEs are transformed into large systems of nonlinear ordinary differential equations (ODEs), where efficient solvers are necessary. In some cases, these PDEs need to be solved in complex geometries, a recent approach is described in [6], where a new procedure to solve nonlinear parabolic PDEs in triangles is explained. But, in other cases, research groups focus their works on the applications of these PDEs such as in [7]. For example, many physical (such as the magneto-hydrodynamics [MHD] problem analyzed in [8]), industrial, or complex economical situations can be modeled by nonlinear PDEs. Chemistry is another very important area; in Awais-Kuman, the authors modeled the peristaltic flow

## OPEN ACCESS

### Edited and reviewed by:

José S. Andrade,  
Federal University of Ceara, Brazil

### \*Correspondence:

Jesus Martin-Vaquero  
jesmarva@usal.es

**Received:** 21 May 2021

**Accepted:** 17 June 2021

**Published:** 09 August 2021

### Citation:

Martin-Vaquero J, Wade B,  
García Guirao JL and Minhós F (2021)  
Editorial: Analytical and Numerical  
Methods for Differential Equations  
and Applications.  
Front. Appl. Math. Stat. 7:712813.  
doi: 10.3389/fams.2021.712813

dynamics of (Cu-H<sub>2</sub>O) nanofluid in a homogeneous porous medium. They solved their model numerically in order to be able to physically interpret how the different parameters that appear in their equation affect the outcome. Another important area of interest is mechanics, thus two papers in this research topic are related with this field: In a study by Alanazi et al. [9], a  $q$ -differential problem is solved with applications in Newtonian mechanics and Mushtaq et al.

[10] describes a *Python* solver to solve some important quantum mechanical eigenvalue PDE problems (such as the Schroedinger) in one or more dimensions.

## AUTHOR CONTRIBUTIONS

All authors listed have made a substantial, direct, and intellectual contribution to the work and approved it for publication.

## REFERENCES

- Dhandapani PB, Baleanu D, Thippan J, and Sivakumar V. Fuzzy Type RK4 Solutions to Fuzzy Hybrid Retarded Delay Differential Equations. *Front Phys* (2019) 7:168. doi:10.3389/fphy.2019.00168
- Nawaz R, Kumam P, Farid S, Shutaywi M, Shah Z, and Deebani W. Application of New Iterative Method to Time Fractional Whitham-Broer-Kaup Equations. *Front Phys* (2020) 8:104. doi:10.3389/fphy.2020.00104
- El-Ajou A, and Al-Zhour Z. A Vector Series Solution for a Class of Hyperbolic System of Caputo Time-Fractional Partial Differential Equations with Variable Coefficients. *Front Phys* (2021) 9:525250. doi:10.3389/fphy.2021.525250
- Aliyu AI, Inc M, Yusuf A, Baleanu D, and Bayram M. Dark-Bright Optical Soliton and Conserved Vectors to the Biswas-Arshed Equation with Third-Order Dispersions in the Absence of Self-phase Modulation. *Front Phys* (2019) 7:28. doi:10.3389/fphy.2019.00028
- Liu N. Invariant Solutions and Conservation Laws of the Variable-Coefficient Heisenberg Ferromagnetic Spin Chain Equation. *Front Phys* (2020) 8:260. doi:10.3389/fphy.2020.00260
- Martin-Vaquero J. ESERK Methods to Numerically Solve Nonlinear Parabolic PDEs in Complex Geometries: Using Right Triangles. *Front Phys* (2020) 8:367. doi:10.3389/fphy.2020.00367
- Medina D, and Padilla P. The Global Attractor of the Allen-Cahn Equation on the Sphere. *Front Appl Math Stat* (2020) 6:20. doi:10.3389/fams.2020.00020
- Awais M, Kumam P, Parveen N, Ali A, Shah Z, and Thounthong P. Slip and Hall Effects on Peristaltic Rheology of Copper-Water Nanomaterial through Generalized Complaint Walls with Variable Viscosity. *Front Phys* (2020) 7:249. doi:10.3389/fphy.2019.00249
- Alanazi AM, Ebaid A, Alhawiti WM, and Muhiuddin G. The Falling Body Problem in Quantum Calculus. *Front Phys* (2020) 8:43. doi:10.3389/fphy.2020.00043
- Mushtaq A, Noreen A, and Olausen K. Numerical Solutions of Quantum Mechanical Eigenvalue Problems. *Front Phys* (2020) 8:390. doi:10.3389/fphy.2020.00390

**Conflict of Interest:** The authors declare that the research was conducted in the absence of any commercial or financial relationships that could be construed as a potential conflict of interest.

**Publisher's Note:** All claims expressed in this article are solely those of the authors and do not necessarily represent those of their affiliated organizations, or those of the publisher, the editors and the reviewers. Any product that may be evaluated in this article, or claim that may be made by its manufacturer, is not guaranteed or endorsed by the publisher.

Copyright © 2021 Martin-Vaquero, Wade, Garcia Guirao and Minhos. This is an open-access article distributed under the terms of the Creative Commons Attribution License (CC BY). The use, distribution or reproduction in other forums is permitted, provided the original author(s) and the copyright owner(s) are credited and that the original publication in this journal is cited, in accordance with accepted academic practice. No use, distribution or reproduction is permitted which does not comply with these terms.



# Dark-Bright Optical Soliton and Conserved Vectors to the Biswas-Arshed Equation With Third-Order Dispersions in the Absence of Self-Phase Modulation

Aliyu Isa Aliyu<sup>1</sup>, Mustafa Inc<sup>2\*</sup>, Abdullahi Yusuf<sup>1,2</sup>, Dumitru Baleanu<sup>3,4</sup> and Mustafa Bayram<sup>5</sup>

<sup>1</sup> Department of Mathematics, Science Faculty, Federal University Dutse, Jigawa, Nigeria, <sup>2</sup> Department of Mathematics, Science Faculty, Firat University, Elazig, Turkey, <sup>3</sup> Department of Mathematics, Cankaya University, Ankara, Turkey, <sup>4</sup> Institute of Space Sciences, Magurele, Romania, <sup>5</sup> Department of Computer Engineering, Istanbul Gelisim University, Istanbul, Turkey

The form-I version of the new celebrated Biswas-Arshed equation is studied in this work with the aid of complex envelope ansatz method. The equation is considered when self-phase is absent and velocity dispersion is negligibly small. New Dark-bright optical soliton solution of the equation emerge from the integration. The acquired solution combines the features of dark and bright solitons in one expression. The solution obtained are not yet reported in the literature. Moreover, we showed that the equation possess conservation laws (CLs).

**Keywords:** complex envelope ansatz, dark-bright optical soliton, Biswas-Arshed equation, conserved vectors, multiplier, numerical simulations

## OPEN ACCESS

### Edited by:

Jesus Martin-Vaquero,  
University of Salamanca, Spain

### Reviewed by:

Emrullah Yasar,  
Uludağ University, Turkey  
Haci Mehmet Baskonus,  
Harran University, Turkey

### \*Correspondence:

Mustafa Inc  
minc@firat.edu.tr

### Specialty section:

This article was submitted to  
Mathematical Physics,  
a section of the journal  
Frontiers in Physics

**Received:** 04 December 2018

**Accepted:** 18 February 2019

**Published:** 14 March 2019

### Citation:

Aliyu AI, Inc M, Yusuf A, Baleanu D and Bayram M (2019) Dark-Bright Optical Soliton and Conserved Vectors to the Biswas-Arshed Equation With Third-Order Dispersions in the Absence of Self-Phase Modulation. *Front. Phys.* 7:28. doi: 10.3389/fphy.2019.00028

## 1. INTRODUCTION

The study of dynamical systems in non-linear physical models plays an important role in optical fibers, electrical transmission lines, plasma physics, mathematical biology, and many more [1]. This is motivated by the capacity to model the behavior of these systems and other under different physical conditions [2]. These systems are represented by non-linear equations. Seeking the exact solutions of non-linear evolution equations has been an interesting topic in mathematical physics, and the solutions of corresponding models are the ways to well describe their dynamics. Several results have been reported in the last few decades [3–24]. The main principle for the existence of solitons in metamaterials, optical fibers, and crystals is the existence of a balance between non-linearity and dispersion. It is obvious that some situations may lead to. Recently, Biswas and Arshed [3] put forward a new model for soliton transmission in optical fibers in the event when self-phase modulation is negligible in the absence of non-linearity.

The third-order model in the absence of self-phase modulation that will be studied in this paper is given by [3, 4]:

$$i\psi_t + \alpha\psi_{xx} + \gamma\psi_{xt} + i[\sigma\psi_{xxx} + \delta\psi_{xxt}] - i[\Omega(|\psi|^2\psi)_x + \mu(|\psi|^2)_x\psi + \theta|\psi|^2\psi_x] = 0. \quad (1)$$

The function  $\psi(x, t)$  representing the dependent involving  $t$  an  $x$  which denotes the temporal and spatial components. The first term represents the temporal evolution of the wave,  $\gamma$  represents the (STD) coefficient,  $\alpha$  is the coefficient of GVD and  $\sigma$  is the coefficient of the third order

dispersion,  $\delta$  is the coefficient of spatio-temporal 3OD (ST-3OD),  $\Omega$  is the effect of self-steepening. Finally,  $\mu$  and  $\theta$  provide the effect of non-linear dispersion. Dark, bright, combo and singular soliton solutions of Equation (1) have been reported in Biswas and Arshed [3] and Ekici and Sonmezoglu [4]. But to the best of our knowledge, the dark-bright optical soliton and Cls of the equation have not been reported. In this work, this special solution combining the features of dark and bright optical soliton in one expression will be recovered by applying a suitable ansatz. The Cls of the equation will be derived using the multiplier method [8, 9].

## 2. DARK-BRIGHT OPTICAL SOLITON

In order derive the dark-bright soliton solution of the equation, we consider the ansatz solution given by Li et al. [5]:

$$\psi(x, t) = A(x, t) \times e^{i\Psi(x,t)}, \tag{2}$$

with

$$\Psi(x, t) = -kx + \omega t + v. \tag{3}$$

In Equation (2),  $\Psi$  denotes the phase shift,  $k$  denotes the wave number,  $\omega$  represents the frequency and  $v$  is the phase constant. We now utilize the ansatz put forward from Li et al. [5]:

$$A(x, t) = i\beta + \lambda \tanh[\eta(x - vt)] + i\rho \operatorname{sech}[\eta(x - vt)], \tag{4}$$

where  $v$  represents the velocity and  $\eta$  is the pulse width. In the even when  $\lambda \rightarrow 0$  or  $\rho \rightarrow 0$ , the Equation (4) transforms to a bright or dark soliton solution. The intensity of  $A(x, t)$  is given by

$$|A(x, t)| = \left\{ \lambda^2 + \beta^2 + 2\beta\rho \operatorname{sech}[\eta(x - vt)] + (\rho^2 - \lambda^2) \operatorname{sech}^2[\eta(x - vt)] \right\}^{\frac{1}{2}}. \tag{5}$$

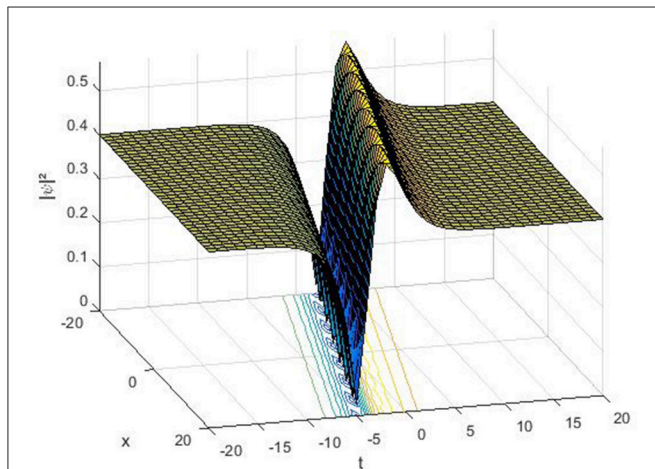


**FIGURE 1** | 3D surface of solution Equation(24) by selecting the parameter values of  $\eta = 0.1, \lambda = 0.1, \theta = 1, \Omega = 0.1$ .

The non-linear phase shift  $\psi_{NL}$  is represented by

$$\psi_{NL} = \arctan \left[ \frac{\beta + \rho \operatorname{sech}[\eta(x - vt)]}{\lambda \tanh[\eta(x - vt)]} \right]. \tag{6}$$

Putting Equation (2) into Equation (1) leads to

$$\begin{aligned} & -A(\omega + k(k(\alpha + k\sigma) - (\gamma + k\delta)\omega) + k(\theta + \mu + \Omega)|A|^2 + 2i\Omega AA_x) - \\ & i((-1 + k(\gamma + k\delta))A_t + (k(2\alpha + 3k\sigma) - (\gamma + 2k\delta)\omega + (\theta + \mu + \Omega)|A|^2)A_x + \\ & i((\gamma + 2k\delta)A_{xt} + (\alpha + 3k\sigma - \delta\omega)A_{xx} + i(\delta A_{xxt} + \sigma A_{xxx}))) = 0. \end{aligned} \tag{7}$$

Now, putting Equation(4) into Equation(7), expanding the result and equating the combination of coefficients of  $\operatorname{sech}(\tau)$  and  $\tanh(\tau)$ , we acquire the independent parametric equations represented by:

**Constants:**

$$-i\beta(\omega + k(-\gamma\omega + k(\alpha + k\sigma - \delta\omega) + (\beta^2 + \lambda^2)(\theta + \mu + \Omega))) = 0, \tag{8}$$

**sech( $\tau$ ):**

$$-i\rho(\omega + k(-\gamma\omega + k(\alpha + k\sigma - \delta\omega) + (3\beta^2 + \lambda^2)(\theta + \mu + \Omega))) = 0, \tag{9}$$

**sech<sup>2</sup>( $\tau$ ):**

$$\begin{aligned} & i(v(-1 + k(\gamma + k\delta))\eta\lambda - 3k^2\eta\lambda\sigma - \eta\lambda \\ & (-\gamma\omega + (\beta^2 + \lambda^2)(\theta + \mu + \Omega)) + \\ & k(-2\alpha\eta\lambda + 2\delta\eta\lambda\omega + \beta(\lambda^2 - 3\rho^2)(\theta + \mu + \Omega))) = 0, \end{aligned} \tag{10}$$

**sech<sup>3</sup>( $\tau$ ):**

$$\begin{aligned} & i\rho(-\alpha\eta^2 + v(\gamma + 2k\delta)\eta^2 - 2\beta\eta\theta\lambda + k\theta\lambda^2 - 2\beta\eta\lambda\mu \\ & + k\lambda^2\mu - k\theta\rho^2 - k\mu\rho^2 - 3k\eta^2\sigma + \\ & \delta\eta^2\omega - 2\beta\eta\lambda\Omega + k\lambda^2\Omega - k\rho^2\Omega) = 0, \end{aligned} \tag{11}$$

**sech<sup>4</sup>( $\tau$ ):**

$$i\eta\lambda(2\eta^2(v\delta - \sigma) + (\lambda - \rho)(\lambda + \rho)(\theta + \mu + \Omega)) = 0, \tag{12}$$

**tanh( $\tau$ ):**

$$-\lambda(\omega + k(-\gamma\omega + k(\alpha + k\sigma - \delta\omega) + (\beta^2 + \lambda^2)(\theta + \mu + \Omega))) = 0, \tag{13}$$

**tanh( $\tau$ )sech( $\tau$ ):**

$$\begin{aligned} & \rho(v(-1 + k(\gamma + k\delta))\eta - 3k^2\eta\sigma - 2k(\alpha\eta - \delta\eta\omega \\ & + \beta\lambda(\theta + \mu + \Omega)) - \eta(-\gamma\omega + \\ & \lambda^2(\theta + \mu + \Omega) + \beta^2(\theta + \mu + 3\Omega))) = 0, \end{aligned} \tag{14}$$

$\tanh(\tau)\text{sech}^2(\tau)$  :

$$(-2\alpha\eta^2\lambda + 2\nu(\gamma + 2k\delta)\eta^2\lambda + k\theta\lambda^3 + k\lambda^3\mu - 2\beta\eta\theta\rho^2 - k\theta\lambda\rho^2 - 2\beta\eta\mu\rho^2 - k\lambda\mu\rho^2 - 6k\eta^2\lambda\sigma + 2\delta\eta^2\lambda\omega + (\lambda^2(2\beta\eta + k\lambda) - (6\beta\eta + k\lambda)\rho^2)\Omega) = 0, \tag{15}$$

$\tanh(\tau)\text{sech}^3(\tau)$  :

$$\eta\rho(5\eta^2\nu\delta - \sigma) + (\lambda - \rho)(\lambda + \rho)(\theta + \mu + 3\Omega) = 0, \tag{16}$$

$\tanh^2(\tau)\text{sech}(\tau)$  :

$$-i\eta\rho(\eta(-\alpha + \nu(\gamma + 2k\delta) - 3k\sigma + \delta\omega) - 2\beta\lambda\Omega) = 0, \tag{17}$$

$\tanh^2(\tau)\text{sech}^2(\tau)$  :

$$-2i\eta\lambda(2\eta^2(\nu\delta - \sigma) + (\lambda - \rho)(\lambda + \rho)\Omega) = 0, \tag{18}$$

$\tanh^3(\tau)\text{sech}(\tau)$  :

$$\eta^3\rho(-\nu\delta + \sigma) = 0, \tag{19}$$

where  $\tau = \eta(x - \nu t)$ . From the solution of Equations(8)–(19), we observed that  $\beta = 0$ . but, for a dark-bright optical soliton to exist, we require both  $\rho \neq 0$  and  $\lambda \neq 0$ . For the sake of compatibility, we considered the case when  $\rho = \lambda$  from the solutions of Equations(8)–(19). We acquire the velocity as

$$\nu = -\rho^2(\theta + \mu + \Omega), \tag{20}$$

the wave number is represented by

$$k = -\frac{\omega}{\rho^2(\theta + \mu + \Omega)}. \tag{21}$$

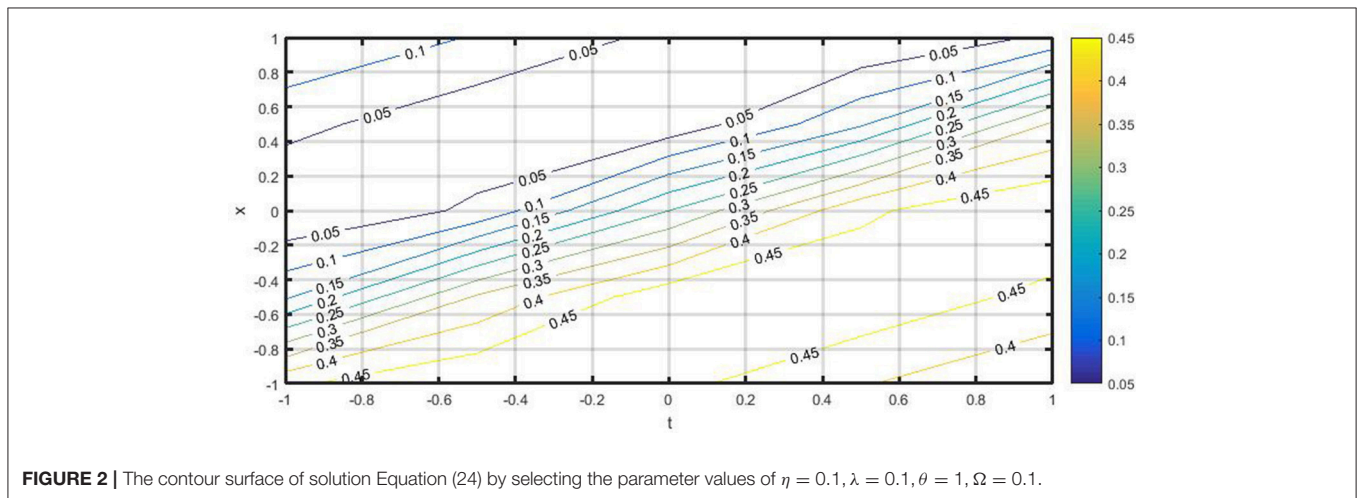
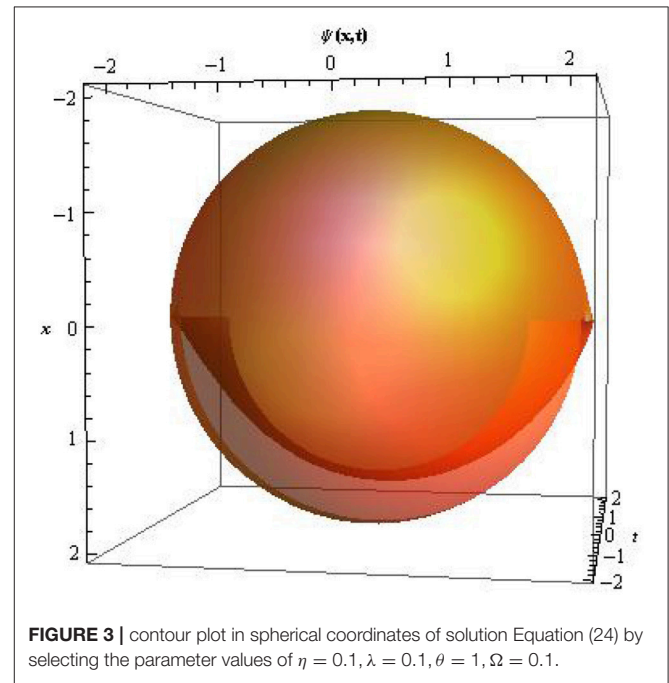
We also acquire the value of  $\delta$  and  $\alpha$  as

$$\delta = -\frac{\sigma}{\rho^2(\theta + \mu + \Omega)}, \tag{22}$$

$$\alpha = -\gamma\rho^2(\theta + \mu + \Omega). \tag{23}$$

The dark-bright optical soliton to the model reads:

$$\psi(x, t) = \left\{ i\lambda\text{sech}[\eta(x + t\lambda^2(\theta + \mu + \Omega))] + \lambda\tanh[\eta(x + t\lambda^2(\theta + \mu + \Omega))] \right\} \times e^{i(\theta + t\omega + \frac{x\omega}{\lambda^2(\theta + \mu + \Omega)})}. \tag{24}$$



and the intensity gives

$$|\psi(x, t)|^2 = \lambda^2. \tag{25}$$

The phase shift is represented by

$$\psi_{NL} = \arctan \left[ \frac{\operatorname{sech}[\eta(x + t\lambda^2(\theta + \mu + \Omega))]}{\tanh[\eta(x + t\lambda^2(\theta + \mu + \Omega))]} \right]. \tag{26}$$

The dark-bright soliton Equation (24) represents a soliton combining the features of dark and bright solitons in one expression. The constant  $\beta = 0$  implies a pronounced “platform” underneath the soliton under non-zero boundary conditions and its asymptotic value approaches  $\lambda$  as  $|t| \rightarrow \infty$ . To analyze the dynamics behavior of the soliton solution Equation (24), we have made numerical evolutions for some perturbations to show the evolution of the dark-bright optical soliton solution. **Figures 1-3** shows the profiles surfaces of the dark-bright soliton Equation (24). The obtained soliton Equation (24) possesses the structure of the physical properties of dark and bright optical solitons in the same expression. These solitons appear temporal solitons observed in optical fibers.

### 3. CONSERVATION LAWS

In this part, we will utilize the multiplier to derive the Cls [8, 9]. To achieve this aim, we apply

$$\psi(x, t) = u(x, t) + iv(x, t), \tag{27}$$

to transform Equation (1) to a system of PDEs. Putting Equation (27) into Equation (1), we acquire:

$$\begin{cases} -v_t + 2(\mu + \Omega)uvu_x + (\theta + \Omega)u^2v_x + (\theta + 2\mu + 3\Omega)v^2v_x \\ + \gamma u_{xt} + \alpha u_{xx} - \delta v_{xxt} - \sigma v_{xxx} = 0. \\ u_t + (-\theta - 2\mu - 3\Omega)u^2u_x + (-\theta - \Omega)v^2u_x - 2(\mu + \Omega)uvv_x \\ + \gamma v_{xt} + \alpha v_{xx} + \delta u_{xxt} + \sigma u_{xxx} = 0. \end{cases} \tag{28}$$

### REFERENCES

1. Whitham GB. *Linear and Nonlinear Waves*. New York, NY: John Wiley (1974).
2. Agrawal GP. *Nonlinear Fiber Optics*. New York, NY: Academic Press (1995).
3. Biswas A, Arshed S. Optical solitons in presence of higher order dispersions and absence of self-phase modulation. *Optik*. (2018) **174**:452–9. doi: 10.1016/j.ijleo.2018.08.037
4. Ekici M, Sonmezoglu A. Optical solitons with Biswas-Arshed equation by extended trial function method. *Optik*. (2018) **177**:13–20. doi: 10.1016/j.ijleo.2018.09.134
5. Li Z, Li L, Tian H. New types of solitary wave solutions for the higher order nonlinear Schrödinger equation, *Phys Rev Lett*. (2000) **84**:4096–9. doi: 10.1103/PhysRevLett.84.4096

Applying the formula for determining equations in [9], we acquires the multipliers of zeroth-order  $\Lambda_1(x, t, u, v)$ ,  $\Lambda_2(x, t, u, v)$  for Equation (1)

$$\begin{aligned} \Lambda_1 &= c_1 u, \\ \Lambda_2 &= c_1 v, \end{aligned} \tag{29}$$

where  $c_1$  is a constant.

1. If  $c_1 = 1$  in Equation(29), then we have the following multipliers:

$$\Lambda^1 = u, \Lambda^2 = v. \tag{30}$$

Subsequently, we acquire the fluxes given by:

$$\begin{aligned} \mathbf{T}^x &= \frac{-\delta(uu_{xx} - vv_{xx})}{\sigma}, \\ \mathbf{T}^t &= \frac{u^3tu_t(3\Omega+2\mu+\theta)+\sigma(uu_{xx}+vv_{xx})}{\sigma}. \end{aligned} \tag{31}$$

### 4. CONCLUDING REMARKS

In this article, we have explored a suitable ansatz solution to derive a dark-bright soliton solution of the new celebrated Biswas-Arshed equation. observing the solutions derived in Biswas and Arshed [3] and Ekici and Sonmezoglu [4], we observed that the solution of the equation acquired in this manuscript is new. The method used here has been proved to be efficient in investigating the combined soliton solution of non-linear models. We finally showed that the equation has conservation laws and we reported the conserved vectors. We hope to apply other techniques to extract additional new forms of solutions of the new model in the future.

### AUTHOR CONTRIBUTIONS

All authors listed have made a substantial, direct and intellectual contribution to the work, and approved it for publication.

### FUNDING

This study was Funded by Cankaya University.

6. Zhou Q, Zhu Q. Combined optical solitons with parabolic law nonlinearity and spatio-temporal dispersion. *J Mod Opt*. (2015) **62**:483–6. doi: 10.1080/09500340.2014.986549
7. Choudhuri A, Porsezian K. Dark-in-the-Bright solitary wave solution of higher-order nonlinear Schrödinger equation with non-Kerr terms. *Opt Commun*. (2012) **285**:364–7. doi: 10.1016/j.optcom.2011.09.043
8. Anco SC, Bluman G. Direct construction method for conservation laws of partial differential equations Part II: general treatment. *Eur J Appl Math*. (2002) **13**:567–85. doi: 10.1017/S0956792501004661
9. Buhe E, Bluman GW. Symmetry reductions, exact solutions, and conservation laws of the generalized Zakharov equations. *J Math Phys*. (2015) **56**:101501. doi: 10.1063/1.4931962
10. Jawad MA, Petkovic MD, Biswas A. Modified simple equation method for nonlinear evolution equations. *Appl Math Comput*. (2010) **217**:869–77. doi: 10.1016/j.amc.2010.06.030

11. Mirzazadeh M, Eslami M, Biswas A. Soliton solutions to KdV6 equation. *Nonlinear Dyn.* (2015) **80**:387–96. doi: 10.1007/s11071-014-1876-1
12. Mirzazadeh M, Mahmood MF, Majid FB, Biswas A, Belic M. Optical solitons in birefringent fibers with riccati equation method. *Optoelectron Adv Mat Rapid Commun.* (2015) **9**:1032–6.
13. Inc M, Aliyu AI, Yusuf A. optical solitons to the nonlinear Schrödinger's equation with Spatio-temporal dispersion using complex amplitude ansatz. *J Mod Opt.* (2017) **64**:2273–80. doi: 10.1080/09500340.2017.1352047
14. Baleanu D, Inc M, Aliyu AI, Yusuf A. Dark optical solitons and conservation laws to the resonance nonlinear Schrödinger equation with Kerr law nonlinearity. *Optik.* (2017) **147**:248–55. doi: 10.1016/j.ijleo.2017.08.080
15. Inc M, Aliyu AI, Yusuf A. Solitons and conservation laws to the resonance nonlinear Schrödinger equation with both spatio-temporal and inter-modal dispersions. *Optik.* (2017) **142**:509–22. doi: 10.1016/j.ijleo.2017.06.010
16. Inc M, Hashemi MS, Aliyu AI. Exact solutions and conservation laws of the Bogoyavlenskii equation, *Acta Phys Polon A.* (2018) **133**:1133–7. doi: 10.12693/APhysPolA.133.1133
17. Aliyu AI, Inc M, Yusuf A, Baleanu D. Symmetry analysis, explicit solutions, and conservation laws of a sixth-order nonlinear ramani equation. *Symmetry.* (2018) **10**:341. doi: 10.3390/sym10080341
18. Inc M, Aliyu AI, Yusuf A, Baleanu D. Novel optical solitary waves and modulation instability analysis for the coupled nonlinear Schrödinger equation in monomode step-index optical fibers. *Superlattices Microstruct.* (2018) **113**:745–53. doi: 10.1016/j.spmi.2017.12.010
19. Inc M, Aliyu AI, Yusuf A, Baleanu D. Optical solitons, conservation laws and modulation instability analysis for the modified nonlinear Schrödinger's equation for Davydov solitons. *J Electromagn Waves Appl.* (2018) **32**:858–73. doi: 10.1080/09205071.2017.1408499
20. Inc M, Aliyu AI, Yusuf A, Baleanu D. Optical solitary waves, conservation laws and modulation instability analysis to the nonlinear Schrödinger's equation in compressional dispersive Alven waves. *Optik.* (2017) **153**:257–66. doi: 10.1016/j.ijleo.2017.10.109
21. Zhou Q, Mirzazadeh M, Ekici M, Sonmezoglu A. Analytical study of solitons in non-Kerr nonlinear negative-index materials. *Nonlinear Dyn.* (2016) **86**:623–38. doi: 10.1007/s11071-016-2911-1
22. Zhou Q. Analytical solutions and modulation instability analysis to the perturbed nonlinear Schrödinger equation. *J Mod Opt.* (2014) **61**:500–3. doi: 10.1080/09500340.2014.897391
23. Taghizadeh N, Mirzazadeh M, Farahrooz F. Exact solutions of the nonlinear Schrodinger equation by the first integral method. *J Math Anal Appl.* (2011) **374**:549–53. doi: 10.1016/j.jmaa.2010.08.050
24. Inc M, Aliyu AI, Yusuf A, Baleanu D. Combined optical solitary waves and conservation laws for nonlinear Chen-Lee-Liu equation in optical fibers. *Optik.* (2018) **158**:297–304. doi: 10.1016/j.ijleo.2017.12.075

**Conflict of Interest Statement:** The authors declare that the research was conducted in the absence of any commercial or financial relationships that could be construed as a potential conflict of interest.

Copyright © 2019 Aliyu, Inc, Yusuf, Baleanu and Bayram. This is an open-access article distributed under the terms of the Creative Commons Attribution License (CC BY). The use, distribution or reproduction in other forums is permitted, provided the original author(s) and the copyright owner(s) are credited and that the original publication in this journal is cited, in accordance with accepted academic practice. No use, distribution or reproduction is permitted which does not comply with these terms.



# Fuzzy Type RK4 Solutions to Fuzzy Hybrid Retarded Delay Differential Equations

Prasanth Bharathi Dhandapani<sup>1\*</sup>, Dumitru Baleanu<sup>2,3</sup>, Jayakumar Thippan<sup>1</sup> and Vinoth Sivakumar<sup>1</sup>

<sup>1</sup> Department of Mathematics, Sri Ramakrishna Mission Vidyalyaya College of Arts and Science, Coimbatore, India,

<sup>2</sup> Department of Mathematics, Cankaya University, Ankara, Turkey, <sup>3</sup> Institute of Space Sciences, Măgurele, Romania

This paper constructs the numerical solution of particular type of differential equations called fuzzy hybrid retarded delay-differential equations using the method of Runge-Kutta for fourth order. The concept of fuzzy number, hybrid-differential equations, and delay-differential equations binds together to form our equations. An example following the algorithm is presented to understand the Concept of fuzzy hybrid retarded delay-differential equations and its accuracy is discussed in terms of decimal places for easy understanding of laymen.

## OPEN ACCESS

### Edited by:

Jesus Martin-Vaquero,  
University of Salamanca, Spain

### Reviewed by:

Haci Mehmet Baskonus,  
Harran University, Turkey  
Andreas Gustavsson,  
University of Seoul, South Korea

### \*Correspondence:

Prasanth Bharathi Dhandapani  
d.prasanthbharathi@gmail.com

### Specialty section:

This article was submitted to  
Mathematical Physics,  
a section of the journal  
Frontiers in Physics

**Received:** 24 September 2019

**Accepted:** 11 October 2019

**Published:** 25 October 2019

### Citation:

Dhandapani PB, Baleanu D, Thippan J  
and Sivakumar V (2019) Fuzzy Type  
RK4 Solutions to Fuzzy Hybrid  
Retarded Delay Differential Equations.  
Front. Phys. 7:168.  
doi: 10.3389/fphy.2019.00168

**Keywords:** hybrid, fuzzy, retarded delay, differential equations, numerical solutions, fourth order, Runge-Kutta Method

## 1. INTRODUCTION

In this manuscript a system is modeled with the concept of retarded delay differential equation and we study it using fuzzy numbers. Nowadays hybrid systems play a vital role in communication systems and retard delay differential equation was considered to be unavoidable in modeling any biological models. In this paper these two separate mathematical concepts were combined under one roof called fuzzy. We call these system of differential equation as fuzzy hybrid retarded delay differential equations (FHRDDE).

The basic properties of fuzzy sets, fuzzy differential equations, fuzzy mappings were studied by various authors [1–7]. We recall that Pederson and Sambandham [8], Abbasbandy and Allahviranloo [9], Al Rawi et al. [10], Bellan and Zennaro [11], and Jayakumar et al. [12] have treated the hybrid, fuzzy, delay, fuzzy delay differential equation numerically, respectively. Prasanth Bharathi et al., studied various types of fuzzy delay differential equations in Prasanth Bharathi et al. [13, 14]. Different methods were used by some authors for solving Hybrid fuzzy differential equations without delay like [15] and [16]. Besides, L.C. Barros regularly studied fuzzy differential equations [15, 17–19]. In Pederson and Sambandham [8], the authors defined and solved the problem of hybrid fuzzy IVP. We extended this hybrid fuzzy IVP to fuzzy hybrid retarded delay IVP. In addition to that of hybrid term  $\Lambda(z_H(t))$ , the retarded delay term  $z_H(t-\delta)$  is also used. So, there occurs some changes in the Runge-Kutta method which can be seen by comparing section 3 with Pederson and Sambandham [8].

The organization of the manuscript is given below. The section 2 treats the fuzzy hybrid retarded delay-differential systems. The section 3 shows the method of Runge-Kutta for fourth order (R-K-4) for dealing a FHRDDE and the section 4 holds algorithm and numerical example to prove the theory.

## 2. FUZZY HYBRID RETARDED DELAY-DIFFERENTIAL SYSTEMS

According to Al Rawi et al. [10] the retarded delay differential equations are defined in the form of  $a_0 Dz_H(t) + b_0 z_H(t) + b_1 z_H(t - \delta) = f(t)$ . When  $f(t) = 0$ , it becomes homogeneous for every first order delay differential equation. Here we take  $f(t)$  as hybrid term and it was termed as hybrid retarded delay differential equations where the constants are given by  $a_0 = 1, b_0 = -1, b_1 = -1, f(t) = \Lambda(z_H(t))$ . Throughout the paper any function of the form  $f_H(t)$  represents the hybrid function satisfying the properties of fuzzy set proposed by Zadeh as followed by Pederson and Sambandham [8] defined over the hybrid term  $\Lambda(z_H(t))$  and delay term  $z_H(t - \delta)$ .

Let us consider the following FHRDDE for  $\alpha \in [0, 1]$

$$\begin{cases} Dz_H(t) = [f(t, z_H(t), \Lambda(z_H(t)), z_H(t - \delta))]^\alpha, & t \geq t_0, \\ z_H(t) = \phi(t), & -\delta \leq t \leq t_0, \\ z_H(t_0) = z_0 = \phi(t_0), \end{cases} \quad (1)$$

where  $\Lambda(z_H(t))$  is the hybrid function and  $z_H(t - \delta)$  is the delay function involving the delay term  $\delta$ . More over the Hybrid function is the function involving two or more sub functions acting differently in specific interval defined over the main functions interval. i.e., The sub functions of main function acts differently in the different sub intervals of main function's domain. In the numerical example below, we have taken the hybrid function  $\Lambda(z_H(t)) = m(t) \cdot \Lambda(z(t))$  where  $m(t)$  and  $\Lambda(z(t))$  will vary for different values defined over the interval  $t \in [t_0, t_n]$ . The delay term  $\delta$  varies in the interval  $(t_0, t_n]$ .  $z_H(t) = \phi(t)$  is the initial function and  $z_H(t_0) = z_0 = \phi(t_0)$  is the initial value defined at  $t_0$ . It is obvious that

$$\begin{aligned} Dz_H(t) &= [f(t, \phi(t), \Lambda(z_H(t)), z_H(t - \delta))]^\alpha, \\ &-\delta \leq t \leq t_0, 0 \leq \alpha \leq 1. \end{aligned}$$

It follows that for  $[f(t, z_H(t), \Lambda(z_H(t)), z(t - \delta))]^\alpha$ . Now we can define the above fuzzy valued function  $Dz_H(t)$  i.e.,  $[f(t, z_H(t), \Lambda(z_H(t)), z_H(t - \delta))]^\alpha$  as follows

$$= \begin{cases} [f(t, z_H(t), \Lambda(z_H(t)), z_H(t - \delta))]^\alpha \\ \left\{ \begin{aligned} \min & f(t, v_H(t), \Lambda(v_H(t)), v_H(t - \delta)) : \\ & v_H(t) \in (z_H(t)^\alpha, \bar{z}_H(t)^\alpha), \\ & \Lambda(v_H(t)) \in (\Lambda(z_H(t)^\alpha), \Lambda(\bar{z}_H(t)^\alpha)), \\ & v_H(t - \delta) \in (z_H(t - \delta)^\alpha, \bar{z}_H(t - \delta)^\alpha), \end{aligned} \right. \\ \left\{ \begin{aligned} \max & f(t, v_H(t), \Lambda(v_H(t)), v_H(t - \delta)) : \\ & v_H(t) \in (z_H(t)^\alpha, \bar{z}_H(t)^\alpha), \\ & \Lambda(v_H(t)) \in (\Lambda(z_H(t)^\alpha), \Lambda(\bar{z}_H(t)^\alpha)), \\ & v_H(t - \delta) \in (z_H(t - \delta)^\alpha, \bar{z}_H(t - \delta)^\alpha), \end{aligned} \right. \end{cases} \quad (2)$$

for  $z_H \in E$  with  $\alpha$ - level sets  $[z_H]^\alpha = [z_H^\alpha, \bar{z}_H^\alpha], 0 \leq \alpha \leq 1$

$$\begin{cases} D(z_H^\alpha)(t) = \min(f(t, v_H(t), \Lambda(v_H(t)), v(t - \delta)) : \\ \quad v_H(t) \in (z_H(t)^\alpha, \bar{z}_H(t)^\alpha), \Lambda(v_H(t)) \\ \quad \in (\Lambda(z_H(t)^\alpha), \Lambda(\bar{z}_H(t)^\alpha)) \\ \quad v_H(t - \delta) \in (z_H(t - \delta)^\alpha, \bar{z}_H(t - \delta)^\alpha)), \\ D(\bar{z}_H^\alpha)(t) = \max(f(t, v_H(t), \Lambda(v_H(t)), v_H(t - \delta)) : \\ \quad v_H(t) \in (z_H(t)^\alpha, \bar{z}_H(t)^\alpha), \Lambda(v_H(t)) \\ \quad \in (\Lambda(z_H(t)^\alpha), \Lambda(\bar{z}_H(t)^\alpha)), \\ \quad v_H(t - \delta) \in (z_H(t - \delta)^\alpha, \bar{z}_H(t - \delta)^\alpha)). \end{cases} \quad (3)$$

for  $t \in I$  and  $0 \leq \alpha \leq 1$ .

## 3. FOURTH-ORDER FUZZY TYPE RUNGE-KUTTA METHOD (R-K-4)

We recall that the R-K-4 plays a vital role in solving differential equations. Also, it holds good for any dynamical system involving delay differential equations. We use the R-K-4 for a FHRDDE (1). Here we use a new simplified form of R-K-4. We define

$$\begin{aligned} z_{t_{n+1};\alpha} - z_{t_n;\alpha} &= \sum_{j=1}^4 w_j K_j(t_n; z_H(t_n; \alpha)), \\ \bar{z}_{t_{n+1};\alpha} - \bar{z}_{t_n;\alpha} &= \sum_{j=1}^4 w_j \bar{K}_j(t_n; z_H(t_n; \alpha)), \end{aligned}$$

where  $w_1, w_2, w_3,$  and  $w_4$  are simple constants and

$$\begin{aligned} K_j &= (\min R_j, \max R_j), j = 1, 2, 3, 4. \\ R_j &= hf \left( t, v_H(t), \Lambda(v_H(t)), v_H(t - \delta), \right), j = 1. \\ R_j &= hf \left( t + \frac{h}{2}, v_H(t), \Lambda(v_H(t)), v_H(t - \delta), \right), j = 2, 3. \\ R_j &= hf \left( t + h, v_H(t), \Lambda(v_H(t)), v_H(t - \delta), \right), j = 4. \end{aligned}$$

Such that,

$$\begin{aligned} v_H(t) &\in [z_H(t_{k,n}; \alpha), \bar{z}_H(t_{k,n}; \alpha)], j = 1. \\ v_H(t) &\in [N_{j-1}, \bar{N}_{j-1}], j = 2, 3, 4. \\ v_H(t - \delta) &\in [z_H(t_{k,n} - \delta; \alpha), \bar{z}_H(t_{k,n} - \delta; \alpha)], j = 1. \\ v_H(t - \delta) &\in [N_{j-1}, \bar{N}_{j-1}], j = 2, 3, 4. \\ v_H(t_l) &\in [z_H(t_{k,0}; \alpha), \bar{z}_H(t_{k,0}; \alpha)], j = 1, 2, 3, 4. \end{aligned}$$

where,

$$\begin{aligned} N_j &= z + \frac{K_j}{2}, j = 1, 2. \\ N_j &= z + K_j, j = 3. \\ N_j &\in \left( N_j(t_{k,n}, z_H(t_{k,n}; \alpha)), \bar{N}_j(t_{k,n}, z(t_{k,n}; \alpha)) \right), \\ K_j &\in \left( K_j(t_{k,n}, z_H(t_{k,n}; \alpha)), \bar{K}_j(t_{k,n}, z(t_{k,n}; \alpha)) \right), \end{aligned}$$

$$Z \in \left( z_H(t_{k,n}; \alpha), \bar{z}(t_{k,n}; \alpha) \right).$$

Next we define the followings

$$P = \underline{K}_1(t, z_H(t; \alpha)) + 2\underline{K}_2(t, z_H(t; \alpha)) + 2\underline{K}_3(t, z_H(t; \alpha)) + \underline{K}_4(t, z_H(t; \alpha)),$$

$$Q = \bar{K}_1(t, z_H(t; \alpha)) + 2\bar{K}_2(t, z_H(t; \alpha)) + 2\bar{K}_3(t, z_H(t; \alpha)) + \bar{K}_4(t, z_H(t; \alpha)).$$

The exact solution at  $t_{n+1}$  is given by

$$\begin{cases} \underline{Z}_H(t_{n+1}; \alpha) = \underline{Z}_H(t_n; \alpha) + \frac{P}{6}, \\ \bar{Z}_H(t_{n+1}; \alpha) = \bar{Z}_H(t_n; \alpha) + \frac{Q}{6}. \end{cases} \tag{4}$$

The approximate solution has the following form

$$\begin{cases} \underline{z}_H(t_{n+1}; \alpha) \approx \underline{z}_H(t_n; \alpha) + \frac{P}{6}, \\ \bar{z}_H(t_{n+1}; \alpha) \approx \bar{z}_H(t_n; \alpha) + \frac{Q}{6}. \end{cases} \tag{5}$$

where P and Q are given by

$$P = P[(t_n, \underline{Z}_H(t_n; \alpha), \bar{Z}_{H_n}(t; \alpha))]$$

and

$$Q = Q[(t_n, \underline{Z}_H(t_n; \alpha), \bar{Z}_{H_n}(t; \alpha))],$$

respectively.

### 4. ALGORITHM AND THE NUMERICAL EXAMPLE

This section consists of an algorithm followed by an example to understand the proposed theory.

**Algorithm (R-K-4):**

**Step:1** Fix  $N=10$ ,

**Step:2** Calculate  $h$  by  $h = \frac{(t_n - t_0)}{t_n * N}$

**Step:3** Set  $t_i = i * h$  for  $i = 0, 1, \dots, n$  and compute  $z(t_i)$ .

**Step:4** Take  $t_0$  as initial point and  $z_0$  as the initial value.

**Step:5** Compute  $K_1, K_2, K_3, K_4, z(t_i)$  using Runge-Kutta method, explained in previous section.

**Step:6** Calculate the upcoming iterations using  $z(t_{i+1}) = z(t_i)$  as described in previous section.

**Step:7** Repeat the steps, Step:2, Step:4 and Step:5 for  $t_i \leq t_n$ .

**Step:8** Quit the process at  $t_i > t_n$ .

**The Numerical Example**

Consider the FHRDDE, extended from Pederson and Sambandham [8], namely

$$\begin{cases} Dz_H(t) = [z_H(t) + \Lambda(z_H(t)) + z(t-1)]^\alpha, & 0 \leq t \leq 3, 0 \leq \alpha \leq 1, \\ z_H(t) = [(\frac{6}{8} + \frac{4\alpha}{8})e^t, (\frac{9}{8} - \frac{\alpha}{8})e^t], & -1 \leq t \leq 0. \end{cases} \tag{6}$$

The hybrid function is defined as  $\Lambda(z_H(t)) = m(t) \cdot \Lambda(z(t))$  as mentioned in section 2 where,

$$m(t) = |\sin(\pi \cdot t)|, \quad \text{fort } t \in [0, 3].$$

$$\Lambda(v(t)) = \begin{cases} 0, & \text{for } t = 0, \\ v, & \text{for } t \in (0, 3]. \end{cases}$$

(4) Then the above Equation (6)

$$\begin{cases} Dz_H(t) = [z_H(t) + m(t)\Lambda(z(t)) + z(t-1)]^\alpha, & 0 \leq t \leq 3, 0 \leq \alpha \leq 1, \\ z_H(t) = [(\frac{6}{8} + \frac{4\alpha}{8})e^t, (\frac{9}{8} - \frac{\alpha}{8})e^t], & -1 \leq t \leq 0. \end{cases} \tag{7}$$

The exact solution of (7) is given by

$$\begin{aligned} Z_H(t; \alpha) = & \begin{cases} [(\frac{6}{8} + \frac{4\alpha}{8})e^t, (\frac{9}{8} + \frac{\alpha}{8})e^t], & t \in [-1, 0], \\ [(\frac{6}{8} + \frac{4\alpha}{8})e^{t-1} - \frac{e \cos(\pi t)}{\pi} - \frac{1}{e} + \frac{e}{\pi} + 1, & t \in [0, 1], \\ [(\frac{6}{8} + \frac{4\alpha}{8})(-\frac{t}{e} + \frac{et}{\pi} + t + e^{t-2} + \frac{e \sin(\pi t)}{\pi} - \frac{e \cos(\pi t)}{\pi} - \frac{1}{e} + 1), & t \in [1, 2], \\ [(\frac{6}{8} + \frac{4\alpha}{8}) & t \in [2, 3], \end{cases} \tag{8} \\ & \begin{cases} (\frac{1}{2}(-\frac{t^2}{e} + \frac{et^2}{\pi} + t^2 - \frac{2et}{\pi} + 2e^{t-3} + \frac{2e \sin(\pi t)}{\pi^2} - \frac{2e(\pi^2-1) \cos(\pi t)}{\pi^3} - \frac{4}{e} + \frac{4e}{\pi} - \frac{2e}{\pi^3} + 4)), \\ (\frac{9}{8} + \frac{\alpha}{8}) & \\ (\frac{1}{2}(-\frac{t^2}{e} + \frac{et^2}{\pi} + t^2 - \frac{2et}{\pi} + 2e^{t-3} + \frac{2e \sin(\pi t)}{\pi^2} - \frac{2e(\pi^2-1) \cos(\pi t)}{\pi^3} - \frac{4}{e} + \frac{4e}{\pi} - \frac{2e}{\pi^3} + 4)), & t \in [2, 3], \end{cases} \end{aligned}$$

where  $Z_H(t; \alpha) = [\underline{Z}_H(t; \alpha), \bar{Z}_H(t; \alpha)]$ .

Let  $z_H(n; \alpha) = [\underline{z}_H(n; \alpha), \bar{z}_H(n; \alpha)]$  and,

$$\begin{aligned} A_1 &= c_0 \sum_{s=0}^{2n} (e^{(-1+\frac{sh}{2})}), A_2 = c_0 \sum_{s=0}^{2n} (H\text{Sin}(\frac{sh\pi}{2})), B_1 = c_1 \sum_{s=1}^{20} (e^{(-1+\frac{sh}{2})}), \\ B_2 &= c_2 \sum_{s=20}^{2n} e^{(-2+\frac{sh}{2})}, B_3 = (\frac{(n-10)H}{\pi}), B_4 = c_2 \sum_{s=20}^{2n} (\frac{H\text{Cos}(\frac{sh\pi}{2})}{\pi}), \\ B_5 &= c_3 \sum_{s=1}^{2n} (H\text{Sin}(\frac{sh\pi}{2})), D_1 = c_1 \sum_{s=1}^{20} (e^{(-1+\frac{sh}{2})}), D_2 = c_4 \sum_{s=20}^{40} (e^{(-2+\frac{sh}{2})}), \\ D_3 &= c_5 \sum_{s=40}^{2n} (e^{(-3+\frac{sh}{2})}), D_4 = (\frac{(30-n)H}{\pi}), D_5 = c_2 \sum_{s=20}^{2n} (\frac{H\text{Cos}(\frac{sh\pi}{2})}{\pi}), \end{aligned}$$

**TABLE 1** | Comparing the exact and the approximate solution.

$\alpha$ 's	Approximate		Exact	
	$z_H(n; \alpha)$	$\bar{z}_H(n; \alpha)$	$z_H(t; \alpha)$	$\bar{z}_H(t; \alpha)$
0	6.62032538253014	9.93048807379521	6.62032351488858	9.93048527233288
0.1	6.84100289528115	9.82014931741971	6.84100096538487	9.82014654708473
0.2	7.06168040803215	9.70981056104421	7.06167841588116	9.70980782183659
0.3	7.28235792078316	9.59947180466870	7.28235586637744	9.59946909658845
0.4	7.50303543353416	9.48913304829320	7.50303331687373	9.48913037134030
0.5	7.72371294628516	9.37879429191770	7.72371076737002	9.37879164609216
0.6	7.94439045903617	9.26845553554220	7.94438821786630	9.26845292084402
0.7	8.16506797178717	9.15811677916670	8.16506566836259	9.15811419559588
0.8	8.38574548453818	9.04777802279119	8.38574311885887	9.04777547034773
0.9	8.60642299728918	8.93743926641569	8.60642056935516	8.93743674509959
1	8.82710051004019	8.82710051004019	8.82709801985145	8.82709801985145

$$D_6 = c_3 \sum_{s=1}^{2n} (H \text{Sin}(\frac{sh\pi}{2})), D_7 = c_6 \sum_{s=40}^{2n} (\frac{H \text{Sin}(\frac{sh\pi}{2})}{\pi^2}),$$

The approximate solution is given by

$$z_H(n; \alpha) = \begin{cases} [(\frac{6}{8} + \frac{4\alpha}{8}), (\frac{9}{8} + \frac{\alpha}{8})], & (-10 \leq n \leq 0), \\ [(\frac{6}{8} + \frac{4\alpha}{8})(z_0 + h(A_1 + A_2)), (\frac{9}{8} + \frac{\alpha}{8})(z_0 + h(A_1 + A_2))], & (1 \leq n \leq 10), \\ [(\frac{6}{8} + \frac{4\alpha}{8})(z_0 + h(n-10) - \frac{h}{6e}(6n-1) + h(\sum_{i=1}^5 B_i)), (\frac{9}{8} + \frac{\alpha}{8})(z_0 + h(n-10) - \frac{h}{6e}(6n-1) + h(\sum_{i=1}^5 B_i))], & (11 \leq n \leq 20), (9) \\ [(\frac{6}{8} + \frac{4\alpha}{8})(z_0 + ((h^2(\frac{n^2-(400)}{2}))) (1 - \frac{1}{e} + \frac{H}{\pi})) + h(10 - \frac{59}{6e}) + h \sum_{i=1}^7 (D_i)), (\frac{9}{8} + \frac{\alpha}{8})(z_0 + ((h^2(\frac{n^2-(400)}{2}))) (1 - \frac{1}{e} + \frac{H}{\pi})) + h(10 - \frac{59}{6e}) + h \sum_{i=1}^7 (D_i)), & (21 \leq n \leq 30), \end{cases}$$

where the coefficients are written as

$$c_0 = \begin{cases} 1/6, s = 0, 2n. \\ 2/3, s = 1, 3, \dots, 2n - 1. \\ 1/3, s = 2, 4, \dots, 2n - 2. \end{cases} \quad c_1 = \begin{cases} 1/6, s = 20. \\ 2/3, s = 1, 3, \dots, 19. \\ 1/3, s = 2, 4, \dots, 18. \end{cases}$$

$$c_2 = \begin{cases} 1/6, s = 20, 2n. \\ 2/3, s = 21, 23, \dots, 2n - 1. \\ 1/3, s = 22, 24, \dots, 2n - 2. \end{cases} \quad c_3 = \begin{cases} 1/6, s = 2n \\ 2/3, s = 1, 3, \dots, 2n - 1. \\ 1/3, s = 2, 4, \dots, 2n - 2. \end{cases}$$

$$c_4 = \begin{cases} 1/6, s = 20, 40. \\ 2/3, s = 21, 23, \dots, 39. \\ 1/3, s = 22, 24, \dots, 38. \end{cases} \quad c_5 = \begin{cases} 1/6, s = 40, 2n \\ 2/3, s = 41, 43, \dots, 2n - 1. \\ 1/3, s = 42, 44, \dots, 2n - 2. \end{cases}$$

$$c_6 = \begin{cases} -1/6, s = 40, 2n. \\ -2/3, s = 41, 43, \dots, 2n - 1. \\ -1/3, s = 42, 44, \dots, 2n - 2. \end{cases}$$

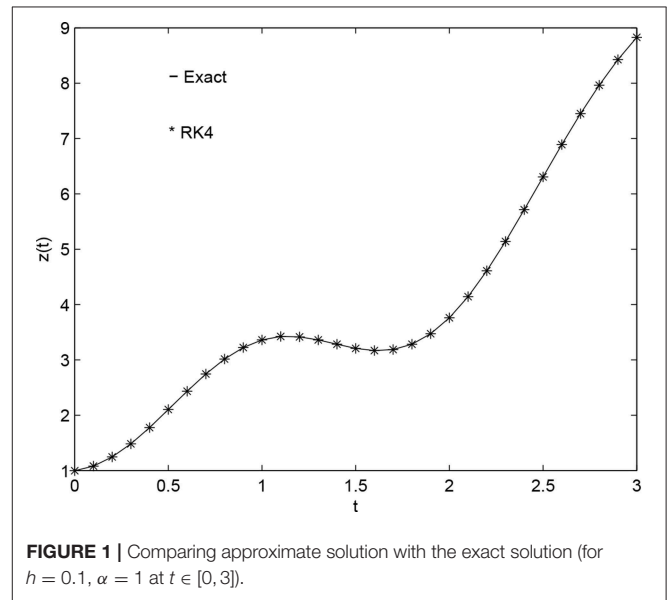
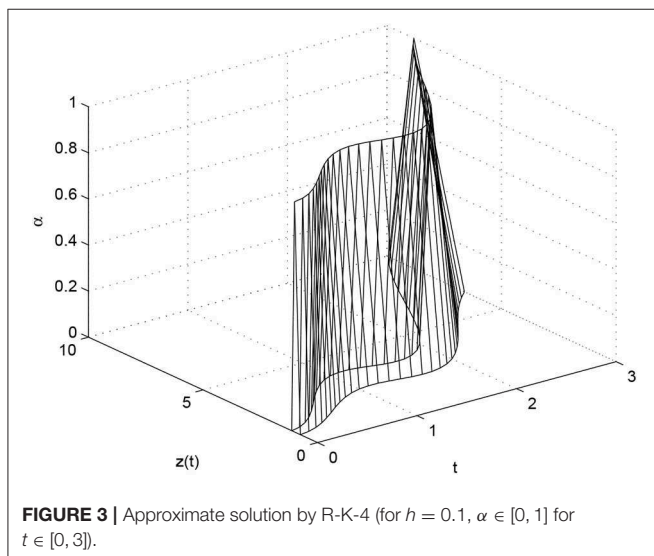
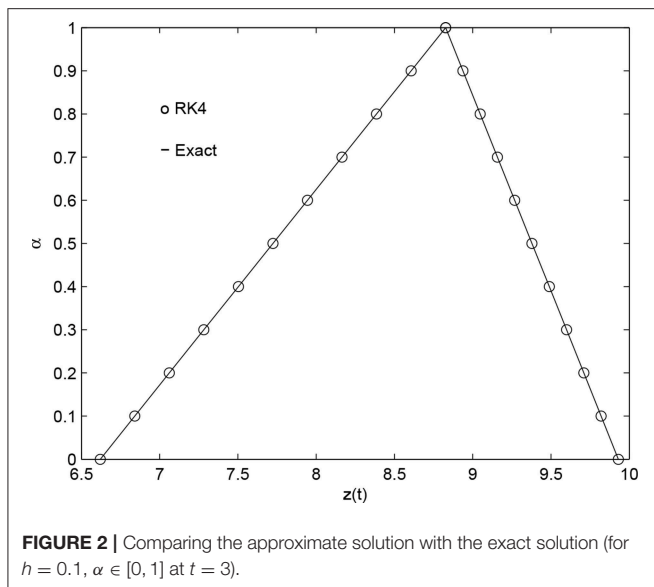


**FIGURE 1** | Comparing approximate solution with the exact solution (for  $h = 0.1, \alpha = 1$  at  $t \in [0, 3]$ ).

Consider another  $H = (1 + h + \frac{h^2}{2} + \frac{h^3}{6} + \frac{h^4}{24})^{10}, t \in [t_0, t_n]$ , i.e.,  $t \in [0, 3], h = 0.1$  Set  $n = 10t$  and  $z_H(10t) = z_H(n)$ .

### 5. CONCLUSION

We have used the R-K-4 method to find the numerical solution of FHRDDE. We presented the **Table 1** only for  $t = 3, h = 0.1$  for  $\alpha \in [0, 1]$ . The values of  $z_H$  for  $t \in [0, 3]$  are plotted in **Figure 1** for  $\alpha = 1$  and in **Figure 3** for  $\alpha \in [0, 3]$ . The comparison of the solutions represented in **Figure 1** for non-fuzzy IVP and the **Figure 2** for fuzzy IVP prove the accuracy of R-K-4 with that of the exact solution. From the **Table 1** we can conclude that the accuracy of the method proposed is about four decimal places. Also if we increase the order of the Runge-Kutta method the accuracy of our numerical solutions will increase. The analytical and numerical results obtained by this paper ensures



the hybrid system with time lag (delay) can be solved. Thus, we can solve properly any FHRDDE using the R-K-4 method. We followed [10] to write the retarded delay differential equation in regular homogeneous form and we added a hybrid term to make it as non-homogenous equation which in turn makes

our governing Equation 1 as the hybrid fuzzy retarded delay differential equation. Thus, our results differ from results on the delay papers like [11, 12] or as in hybrid papers like [8, 20]. There are differences between the traditional Runge-Kutta methods presented in Pederson and Sambandham [8] and the reported method because in our case the Runge-Kutta method involves both hybrid and retarded delay term. The previously published papers varies only the hybrid term in regular intervals. However, we constructed a system in which both hybrid term  $\Lambda(z_H(t))$  and delay term  $z_H(t - \delta)$  are subject to vary in some regular intervals. We also generalized the numerical solution which will provide very closer solution for any values in the given intervals. In the above example, we have taken  $(\frac{6}{8} + \frac{4\alpha}{8})$  and  $(\frac{9}{8} - \frac{\alpha}{8})$  as our fuzzy numbers. But one can choose different fuzzy numbers with in the interval  $\alpha \in [0, 1]$ . In all the cases the non-member, partial member and the full member of both approximate and analytical solution will coincide as they are defined in  $[0 \leq \alpha \leq 1]$ . According to our knowledge the researchers working with the numerical solutions of hybrid systems like [8, 20] did not considered the system with time lag. In this paper we solved the hybrid system with time lag and we open a gate for the related future research in areas like communication systems and signal processing.

## DATA AVAILABILITY STATEMENT

All datasets generated for this study are included in the article/supplementary material.

## AUTHOR CONTRIBUTIONS

PD formulated the problem, converted it into fuzzy functions, and solved the problem analytically. DB solved the problem numerically and carefully proof-read the whole paper. JT generalized both numerical and exact solutions. VS plotted all the three graphs for various values. All the authors equally typeset their parts in the journal template and checked the final version of the manuscript.

## ACKNOWLEDGMENTS

The authors would like to thank the reviewers for their kind suggestions toward the improvement of the paper.

## REFERENCES

- Goetschel R, Voxman W. Elementary fuzzy calculus. *Fuzzy Sets Syst.* (1986) **18**:31–43. doi: 10.1016/0165-0114(86)90026-6
- Kaleva O. Fuzzy differential equations. *Fuzzy Sets Syst.* (1987) **24**:301–17. doi: 10.1016/0165-0114(87)90029-7
- Bukley JJ, Feuring T. Fuzzy differential equations. *Fuzzy Sets Syst.* (2000) **110**:43–54.
- Seikkala S. On the fuzzy initial value problem. *Fuzzy Sets Syst.* (1987) **24**:319–30. doi: 10.1016/0165-0114(87)90030-3
- Lupulescu V. On a class of fuzzy functional differential equations. *Fuzzy Sets Syst.* (2009) **160**:1547–62. doi: 10.1016/j.fss.2008.07.005
- Dubois D, Prade H. Towards fuzzy differential calculus, Part 3. Differentiation. *Fuzzy Sets Syst.* (1982) **8**:225–33. doi: 10.1016/S0165-0114(82)80001-8
- Chang SL, Zadeh LA. On fuzzy mapping and control. *IEEE Trans Syst Man Cybern.* (1972) **2**:30–4. doi: 10.1109/TSMC.1972.5408553

8. Pederson S, Sambandham M. The Runge-Kutta method for hybrid fuzzy differential equations. *Nonlinear Anal Hybrid Syst.* (2008) **2**:626–34. doi: 10.1016/j.nahs.2006.10.013
9. Abbasbandy S, Allahviranloo T. Numerical solution of fuzzy differential equation by Runge-Kutta Method. *Nonlinear Stud.* (2004) **11**:117–29.
10. AL Rawi SN, Salih RS, Mohammed AA. Numerical Solution of  $N^{\text{th}}$  order linear delay differential equation using Runge-Kutta method. *Um Salama Sci J.* (2006) **3**:140–6.
11. Bellen A, Zennaro M. Numerical methods for delay differential equations. In: Golub GH, Schwab CH, Light WA, Suli E, editors. *Numerical Mathematics and Scientific Computation*. Oxford: Oxford Science Publications; Clarendon Press (2003). p. 1–10; 63–70.
12. Jayakumar T, Parivallal A, Prasantha Bharathi D. Numerical solutions of Fuzzy delay differential equations by fourth order Runge Kutta Method. *Adv Fuzzy Sets Syst.* (2016) **21**:135–61. doi: 10.17654/FS021020135
13. Prasantha Bharathi D, Jayakumar T, Vinoth S. Numerical solution of fuzzy pure multiple retarded delay differential equations. *Int J Res Advent Technol.* (2018) **6**:3693–8.
14. Prasantha Bharathi D, Jayakumar T, Vinoth S. Numerical solution of fuzzy pure multiple neutral delay differential equations. *Int J Adv Sci Res Manage.* (2019) **4**:172–8.
15. Paripour M, Hajilou E, Hajilou A, Heidari H. Application of Adomian decomposition method to solve hybrid fuzzy differential equations. *J Taibah Univ Sci.* (2015) **9**:95–103. doi: 10.1016/j.jtusci.2014.06.002
16. Sepahvandzadeh A, Ghazanfari B. Variational Iteration Method for solving Hybrid Fuzzy differential equation. *J Math Extens.* (2016) **10**:76–85.
17. de Barros LC, Pedro FS. Fuzzy differential equations with interactive derivative. *Fuzzy Sets Syst.* (2017) **309**:64–80. doi: 10.1016/j.fss.2016.04.002
18. Barros LC, Gomes LT, Tonelli PA. Fuzzy differential equations: an approach via fuzzification of the derivative operator. *Fuzzy Sets Syst.* (2013) **230**:39–52. doi: 10.1016/j.fss.2013.03.004
19. Mizukoshi MT, Barros LC, Chalco-Cano Y, Roman-Flores H, Bassanezi RC. Fuzzy differential equations and the extension principle. *Inform Sci.* (2007) **177**:3627–35. doi: 10.1016/j.ins.2007.02.039
20. Sambandham M. Perturbed Lyapunov-like functions and hybrid fuzzy differential equations. *Int J. Hybrid Syst.* (2002) **2**:23–34.

**Conflict of Interest:** The authors declare that the research was conducted in the absence of any commercial or financial relationships that could be construed as a potential conflict of interest.

Copyright © 2019 Dhandapani, Baleanu, Thippan and Sivakumar. This is an open-access article distributed under the terms of the Creative Commons Attribution License (CC BY). The use, distribution or reproduction in other forums is permitted, provided the original author(s) and the copyright owner(s) are credited and that the original publication in this journal is cited, in accordance with accepted academic practice. No use, distribution or reproduction is permitted which does not comply with these terms.



# Slip and Hall Effects on Peristaltic Rheology of Copper-Water Nanomaterial Through Generalized Complaint Walls With Variable Viscosity

Muhammad Awais<sup>1</sup>, Poom Kumam<sup>2,3,4\*</sup>, Nabeela Parveen<sup>1</sup>, Aamir Ali<sup>1</sup>, Zahir Shah<sup>5\*</sup> and Phatiphat Thounthong<sup>6</sup>

<sup>1</sup> Department of Mathematics, COMSATS University Islamabad, Attock Campus, Attock, Pakistan, <sup>2</sup> KMUTT-Fixed Point Research Laboratory, Department of Mathematics, Faculty of Science, King Mongkut's University of Technology Thonburi, Bangkok, Thailand, <sup>3</sup> KMUTT-Fixed Point Theory and Applications Research Group, Faculty of Science, Theoretical and Computational Science Center, King Mongkut's University of Technology Thonburi, Bangkok, Thailand, <sup>4</sup> Department of Medical Research, China Medical University Hospital, China Medical University, Taichung, Taiwan, <sup>5</sup> Center of Excellence in Theoretical and Computational Science, King Mongkut's University of Technology Thonburi, Bangkok, Thailand, <sup>6</sup> Department of Teacher Training in Electrical Engineering, Faculty of Technical Education, Renewable Energy Research Centre, King Mongkut's University of Technology North Bangkok, Bangkok, Thailand

## OPEN ACCESS

### Edited by:

Bruce Alan Wade,  
University of Louisiana at Lafayette,  
United States

### Reviewed by:

Andreas Gustavsson,  
University of Seoul, South Korea  
Ebenezer Bonyah,  
University of Education,  
Winneba, Ghana

### \*Correspondence:

Poom Kumam  
poom.kum@kmutt.ac.th  
Zahir Shah  
zahir.sha@kmutt.ac.th

### Specialty section:

This article was submitted to  
Mathematical Physics,  
a section of the journal  
Frontiers in Physics

Received: 04 October 2019

Accepted: 23 December 2019

Published: 31 January 2020

### Citation:

Awais M, Kumam P, Parveen N, Ali A, Shah Z and Thounthong P (2020) Slip and Hall Effects on Peristaltic Rheology of Copper-Water Nanomaterial Through Generalized Complaint Walls With Variable Viscosity. *Front. Phys.* 7:249. doi: 10.3389/fphy.2019.00249

Current research is intended to examine the hydro-magnetic peristaltic flow of copper-water nanofluid configured in a symmetric three-dimensional rotating channel having generalized complaint boundaries incorporating second-order velocity slip conditions and temperature-dependent viscosity effects. Strong magnetic field with Hall properties, viscous dissipation, thermal radiations, and heat source/sink phenomenon have been studied. Constitutive partial differential equations are modeled and then simplified into a coupled system of ordinary differential equations by employing lubrication approximation. Consequential governing model is tackled numerically, and the results for flow quantities and Nusselt number are physically interpreted via graphs and bar charts toward the assorted parameters. Interpreted numerical results indicate that velocity components are accelerated with augmentation in first- and second-order velocity slip parameters and variable viscosity parameter, while it is reduced with a rise in Grashof number possessing dominant effects in the central region. Also, the temperature of the fluid increases with an increase in temperature-dependent viscosity effect.

**Keywords:** nanofluid, peristalsis, rotation, slip conditions, hall effects, variable viscosity

## INTRODUCTION

Peristalsis is a transport process of a decisive kind for moving fluids inside a conduit that occurs due to its surface deformation. Analysis of peristalsis has gained plausible importance in the last few years due to its wide applications in medical and chemical fields. Peristalsis comes from the Greek word "Peristalsiskos," which means spontaneous squeezing and grasping along the flexible walls of tubular structures. It is a self-regulating and necessary procedure that is precisely useful to move food in the digestive system, with commercial peristaltic pumping and blood pumping

in the heart–lung machine, where it is essential to split the fluid from the walls of the pumping device and move forward without being infected due to the collision with the machinery. The idea of peristalsis has been pioneered by Shapiro et al. [1] and Latham [2], primarily. From then on, several researchers and scientists have studied the peristaltic transport under different aspects and assumptions. Representatively, mixed convection and Joule heating effects on peristaltic transport of water-based nanofluid by assuming convective boundary conditions have been examined by Hayat et al. [3]. Eventually, magneto-hydrodynamics (MHD) peristaltic transport of electrically conducting fluids is paramount in the medical field. Abbas et al. [4] have inspected peristalsis of blood transport carrying nanoparticles with magnetic field effects through a non-uniform channel, which is applicable in drug delivery. Further, magnetic field effects on ciliary-induced peristaltic motion of nanofluid with second law analysis have been investigated by Abrar et al. [5]. For strong magnetic field and rarefied medium, electric conductivity of the magnetic fluids becomes anisotropic due to which Hall current appears prominently and this has been initially presented by Hall [6]. Recently, Hall effects on peristaltic transport of Carreau fluid through a channel were examined by Hayat et al. [7]. The incompressible Eyring–Powell fluid is used to fill the channel. A distinctive description in this regard is given in Hayat et al., Rashidi et al., Hasona and Qureshi et al. [8–12].

Fluids have a major role in augmentation of heat transfer rate in several physiological applications involving heat transfer in connection with peristalsis such as oxygenation, hemodialysis, photodynamic therapy, etc. In this regard, suspension of nanoparticles including metal oxides, metals, and carbide/nitride etc. are of the essence to boost up the thermal properties of ordinary fluids like water, engine oil, ethylene glycol, etc. and friction reduction, which enhances the bioactivity and bioavailability of therapeutics. In biomedical processes, nanotechnology is used as a substitute during envisioning accurate medication of rheumatoid arthritis and it makes selective targeting possible to damaged joints. Awais et al. [13] examined analytically and numerically the boundary layer Maxwell nanofluid transport over stretchable surface presuming the impacts of heat generation/absorption. Awais et al. [14] analyzed slippage phenomenon in the flow of non-Newtonian nanofluid over a stretchable surface. Hayat et al. [15] studied the nanofluid on the stretched surface. They analyzed the flow in the presence of magneto-hydrodynamics and chemical reactions. The generative/absorptive thermal effects have been analyzed. Several attempts in this regime have been made by investigators [16–20]. Recently, Shah et al. [21, 22] studied thermally and electrically conducting nanofluid and heat transfer in different geometries with their applications.

In many physiological and medical procedures, since no-slip boundary conditions do not remain authentic, slip effects are important [23–25]. Moreover, variable viscosity is significant when the physical properties of fluids vary significantly with the distance and temperature and thus studied intensively by researchers [26–29]. None of the above-cited attempts

include combined effects of variable viscosity and second-order velocity slip through a channel with generalized wall properties; therefore, it is the subject of research in this study along with the peristaltic flow of nanofluid within a rotating frame. Modeled system of partial differential equations is a simplified lubrication approach and analyzed numerically by employing NDSolve command in MATHEMATICA based on the standard shooting method with fourth-order Runge-Kutta integration procedure. Several graphical illustrations and tables have been prepared to present the real insight of the current investigation.

## MATHEMATICAL FORMULATION OF PROBLEM

Consider peristaltic flow dynamics of (Cu–H<sub>2</sub>O) nanofluid in a homogeneous porous medium through complaint channel walls sculptured as spring-backed plates having temperature of upper/lower walls as  $T_1/T_0$ . The nanofluid and channel rotate with uniform angular speed  $\Omega$  parallel to the  $z$ -axis (**Figure 1**). Flow occurs by expansion of waves having speed  $c$ , wavelength  $\lambda$ , and amplitude  $a$  parallel to the walls placed at  $z = \pm\eta$  having the form:

$$z = \pm\eta(x, t) = \pm[d + a \sin(\frac{2\pi}{\lambda}(x - ct))], \quad (1)$$

in which  $t$  and  $d$  stand for time and half channel width, respectively. Moreover, magnetic field  $B_0$  is applied along the  $z$ -direction. In view of these facts, conservation laws of mass, momentum, and energy in the presence of generalized Hall properties, rotation, dissipative, radiative, internal heat generation/absorption, and buoyancy effects are of the form [30–33]:

$$\frac{\partial u}{\partial x} + \frac{\partial w}{\partial z} = 0 \quad (2)$$

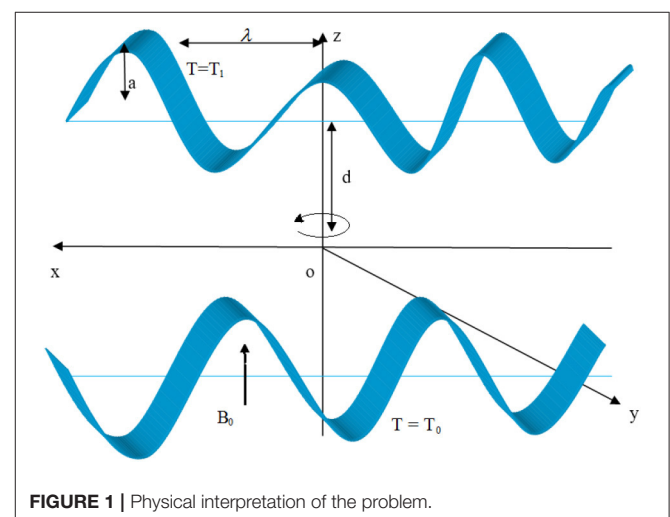


FIGURE 1 | Physical interpretation of the problem.

$$\rho_{eff} \left[ \frac{du}{dt} - 2\Omega v \right] = -\frac{\partial \hat{P}}{\partial x} + \mu_{eff} \left[ \frac{\partial^2 u}{\partial x^2} + \frac{\partial^2 u}{\partial z^2} \right] + \frac{A_1 \sigma_f B_0^2}{1 + (A_1 m)^2} (-u + A_1 m v) - \frac{\mu_{eff} u}{k_1} + g(\rho\beta)_{eff}(T - T_0), \tag{3}$$

$$\rho_{eff} \left[ \frac{dv}{dt} + 2\Omega u \right] = -\frac{\partial \hat{P}}{\partial y} + \mu_{eff} \left[ \frac{\partial^2 v}{\partial x^2} + \frac{\partial^2 v}{\partial z^2} \right] - \frac{A_1 \sigma_f B_0^2}{1 + (A_1 m)^2} (v + A_1 m u) - \frac{\mu_{eff} v}{k_1}, \tag{4}$$

$$\rho_{eff} \left[ \frac{dw}{dt} \right] = -\frac{\partial \hat{P}}{\partial z} + \mu_{eff} \left[ \frac{\partial^2 w}{\partial x^2} + \frac{\partial^2 w}{\partial z^2} \right], \tag{5}$$

$$(\rho C_p)_{eff} \frac{dT}{dt} = K_{eff} \left[ \frac{\partial^2 T}{\partial x^2} + \frac{\partial^2 T}{\partial z^2} \right] + \mu_{eff} \left[ 2 \left\{ \left( \frac{\partial u}{\partial x} \right)^2 + \left( \frac{\partial w}{\partial z} \right)^2 \right\} + \left\{ \frac{\partial u}{\partial z} + \frac{\partial w}{\partial x} \right\}^2 \right] + \frac{16\sigma^* T_m^3}{3k^*} \left[ \frac{\partial^2 T}{\partial x^2} + \frac{\partial^2 T}{\partial z^2} \right] + \frac{\mu_{eff} u^2}{k_1} + \Phi, \tag{6}$$

Moreover  $u, v,$  and  $w$  symbolize the velocities in the respective directions, while  $\sigma_f, k_1, g, A_1, m, \sigma^*, k^*, T, T_m,$  and  $\Phi,$  respectively, represent the electrical conductivity, permeability of porous medium, gravitational force, effective thermal conductivity, Hall effect, Stefan-Boltzmann constant, mean absorption coefficient, fluid temperature, mean temperature of nanofluid, and internal heat generation/absorption effects. The relations for effective density  $\rho_{eff},$  specific heat  $C_{p,eff},$  thermal conductivity  $K_{eff},$  effective viscosity  $\mu_{eff}$  with  $\alpha$  as variable viscosity parameter and thermal expansion coefficient  $\beta_{eff}$  for the dual phase flow model of the nanofluid are [29]:

$$\begin{aligned} \rho_{eff} &= (1 - \phi)\rho_f + \phi\rho_p, & (\rho C_p)_{eff} &= (1 - \phi)(\rho C_p)_f + \phi(\rho C_p)_p, \\ \frac{K_{eff}}{K_f} &= \frac{K_p + 2k_f - 2\phi(K_f - K_p)}{K_p + 2k_f + \phi(K_f - K_p)}, & \mu_{eff} &= \frac{\mu_f \exp[-\alpha(T - T_m)]}{(1 - \phi)^{2.5}}, \\ (\rho\beta)_{eff} &= (1 - \phi)(\rho\beta)_f + \phi(\rho\beta)_p. \end{aligned} \tag{8}$$

As the wall properties decompose the pressure as rigidity, stiffness, and damping, thus expression for motion of generalized compliant boundaries is [29, 30]:

where modified pressure  $\hat{P}$  involving centrifugal effect is given by

$$\hat{P} = P - \frac{1}{2} \rho \Omega^2 (x^2 + y^2). \tag{7}$$

$$L(\eta) = p - p_0 = \left[ -\tau \frac{\partial^2}{\partial x^2} + m' \frac{\partial^2}{\partial t^2} + d' \frac{\partial}{\partial t} + \beta' \frac{\partial^4}{\partial x^4} + k \right] \eta. \tag{9}$$

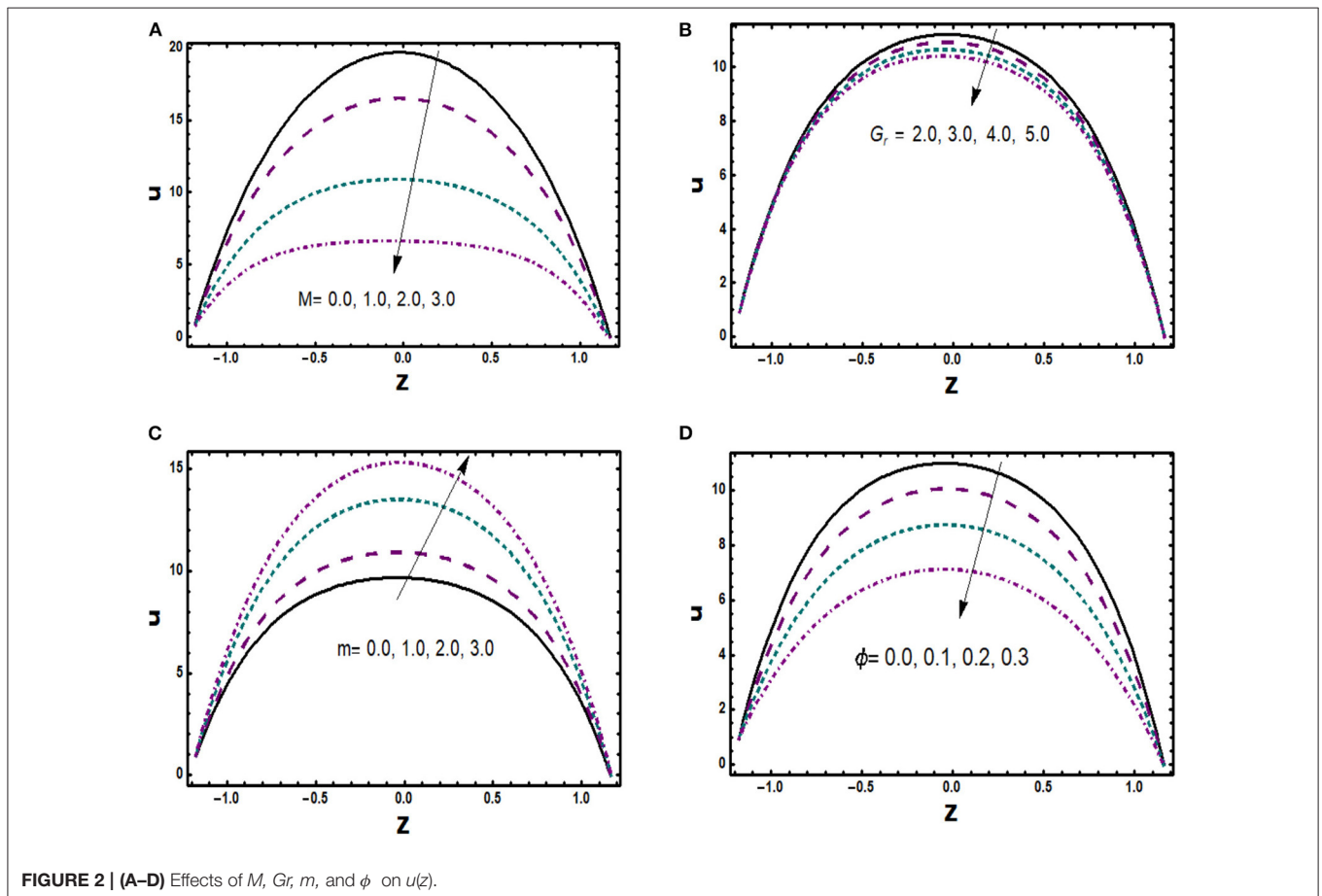


FIGURE 2 | (A–D) Effects of  $M, Gr, m,$  and  $\phi$  on  $u(z).$

In the above relation,  $L$  is the operator that symbolizes the movement of elastic walls possessing viscous damping force,  $P_0$  represents the pressure outside the elastic walls due to muscular tension,  $\tau$  expresses the longitudinal tension per unit area,  $m'$  is mass of the plate,  $d'$  is the wall damping coefficient,  $\beta'$  is the flexural rigidity, and  $k$  is the stiffness effect. Utilizing the generalized complaint wall-pressure relation in Equation (3) with the assumption that  $P_0 = 0$ , we get

$$\begin{aligned} \frac{\partial L}{\partial x} &= \frac{\partial p}{\partial x} \tag{10} \\ &= \frac{\mu_f \exp[-\alpha(T - T_m)]}{(1 - \phi)^{2.5}} \left[ \frac{\partial^2 u}{\partial x^2} + \frac{\partial^2 u}{\partial z^2} \right] \\ &+ \frac{A_1 \sigma_f B_0^2}{1 + (A_1 m)^2} (-u + A_1 m v) - \frac{\mu_f \exp[-\alpha(T - T_m)] u}{(1 - \phi)^{2.5} k_1} \\ &+ g(\rho\beta)_{\text{eff}}(T - T_m) - [(1 - \phi)\rho_f + \phi\rho_p] \left[ \frac{du}{dt} - 2\Omega v \right]. \end{aligned}$$

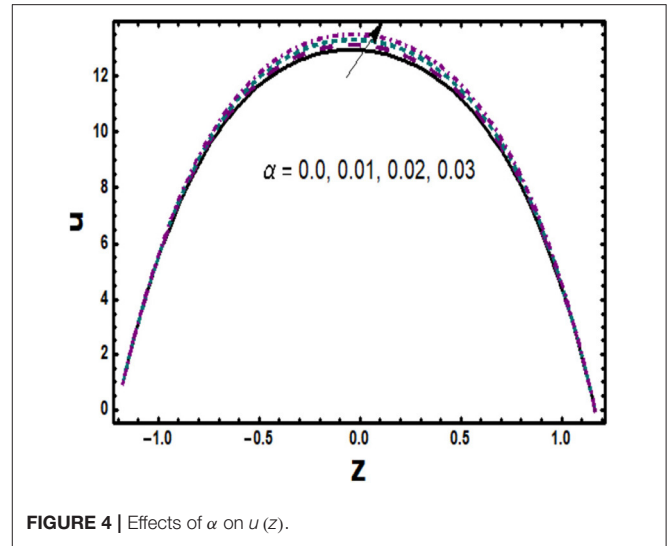


FIGURE 4 | Effects of  $\alpha$  on  $u(z)$ .

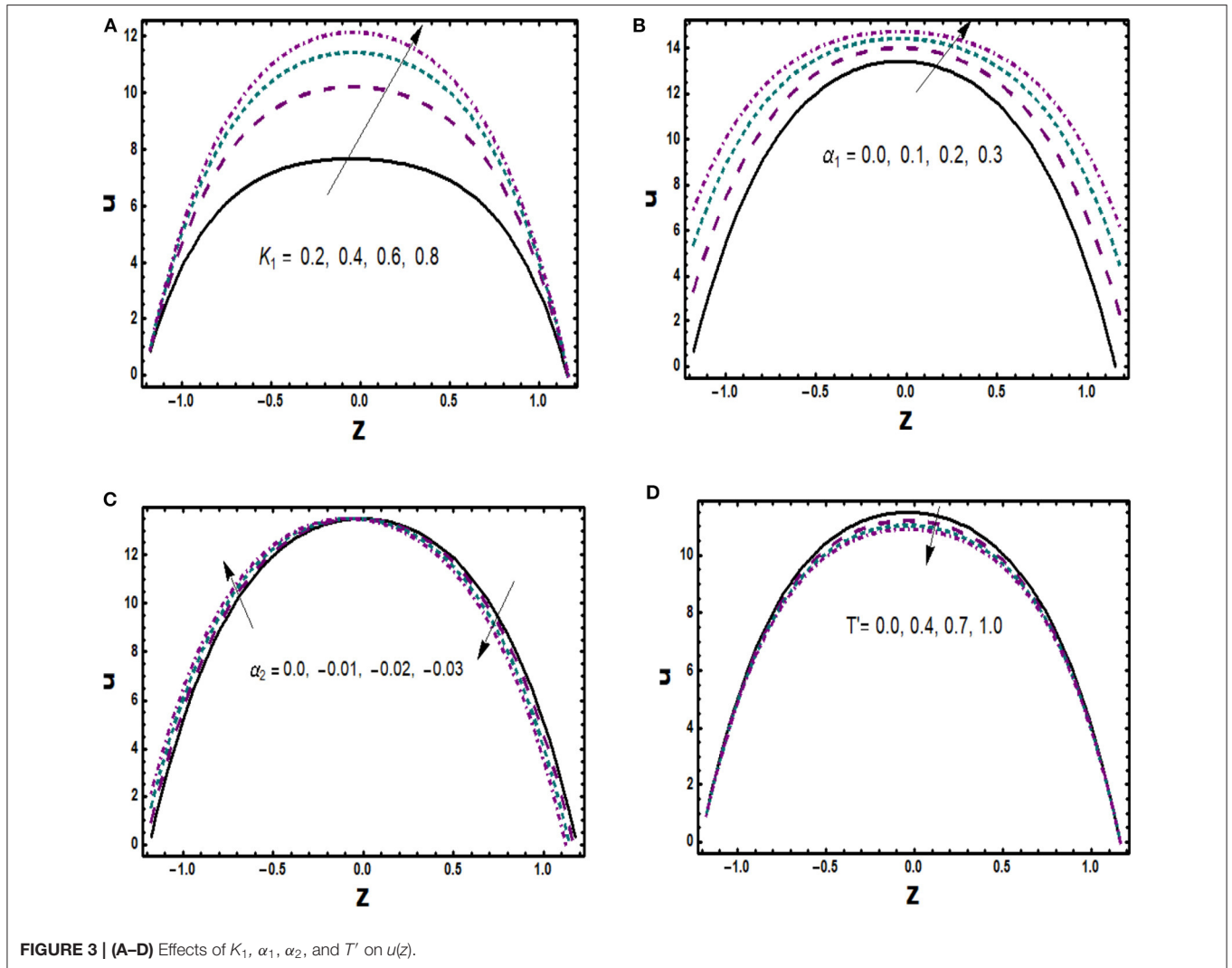


FIGURE 3 | (A–D) Effects of  $K_1$ ,  $\alpha_1$ ,  $\alpha_2$ , and  $T'$  on  $u(z)$ .

Scaling transformations utilized in the above equations are

$$\begin{aligned}
 x^* &= \frac{x}{\lambda}, \quad y^* = \frac{y}{\lambda}, \quad z^* = \frac{z}{d}, \quad \delta = \frac{d}{\lambda}, \quad p = \frac{d^2 \widehat{P}}{c\mu_f \lambda}, \quad t^* = \frac{ct}{\lambda}, \\
 u^* &= \frac{u}{c}, \quad v^* = \frac{v}{c}, \quad w^* = \frac{w}{c}, \quad \eta^* = \frac{\eta}{d}, \\
 \theta &= \frac{T - T_m}{T_1 - T_0}, \quad T_m = \frac{T_1 + T_0}{2}, \quad \alpha_1^* = \frac{\alpha_1}{d}, \quad \alpha_2^* = \frac{\alpha_2}{d}, \\
 \beta_1^* &= \frac{\beta_1}{d}, \quad \beta_2^* = \frac{\beta_2}{d}.
 \end{aligned}
 \tag{11}$$

Here,  $\alpha_1, \alpha_2, \beta_1,$  and  $\beta_2,$  respectively, express first-order velocity slip, second-order velocity slip, secondary velocity slip, and thermal slip parameters ( $T_1, T_0$ ) are upper and lower wall temperatures while  $\delta$  is wave number. Further, introducing stream function  $\psi$  such that  $u = \frac{\partial \psi}{\partial z}$  and  $w = -\delta \frac{\partial \psi}{\partial x}$  and suppressing bar notations for ease, conservation laws with the assumption of long wavelength and small inertial forces, we reach:

$$\begin{aligned}
 -2T' \left[ (1 - \phi) + \phi \frac{\rho_p}{\rho_f} \right] v &= -\frac{\partial p}{\partial x} + \frac{\exp(-\alpha(T - T_0))}{(1 - \phi)^{2.5}} \left( \frac{\partial^2 u}{\partial z^2} \right) \\
 &- \frac{A_1 M^2}{1 + (A_1 m)^2} \left( \frac{\partial \psi}{\partial z} - A_1 m v \right) - \frac{\exp(-\alpha(T - T_0))}{(1 - \phi)^{2.5} K_1} \frac{\partial \psi}{\partial z} \\
 &+ Gr(T - T_m),
 \end{aligned}
 \tag{12}$$

$$\begin{aligned}
 2T' \left[ (1 - \phi) + \phi \frac{\rho_p}{\rho_f} \right] u &= -\frac{\partial p}{\partial y} + \frac{\exp(-\alpha(T - T_0))}{(1 - \phi)^{2.5}} \frac{\partial^2 v}{\partial z^2} \\
 &- \frac{A_1 M^2}{1 + (A_1 m)^2} \left( v + A_1 m \frac{\partial \psi}{\partial z} \right) - \frac{\exp(-\alpha(T - T_0)) v}{(1 - \phi)^{2.5} K_1},
 \end{aligned}
 \tag{13}$$

$$\begin{aligned}
 \left( A_2 + \frac{4}{3} R \right) \left( \frac{\partial^2 \theta}{\partial z^2} \right) &+ \frac{Br \exp(-\alpha(T - T_0))}{(1 - \phi)^{2.5} K_1} \left( \frac{\partial \psi}{\partial z} \right)^2 + \varepsilon_1 \\
 &+ \frac{Br \exp(-\alpha(T - T_0))}{(1 - \phi)^{2.5}} \left( \frac{\partial^2 \psi}{\partial z^2} \right)^2 = 0.
 \end{aligned}
 \tag{14}$$

In the above equations,  $Re = \frac{\rho_f c d}{\mu_f}$  denotes the Reynolds number,  $\delta = \frac{d}{\lambda}$  represents wave number,  $T' = \frac{Re \Omega d}{c}$  is the Taylor number,

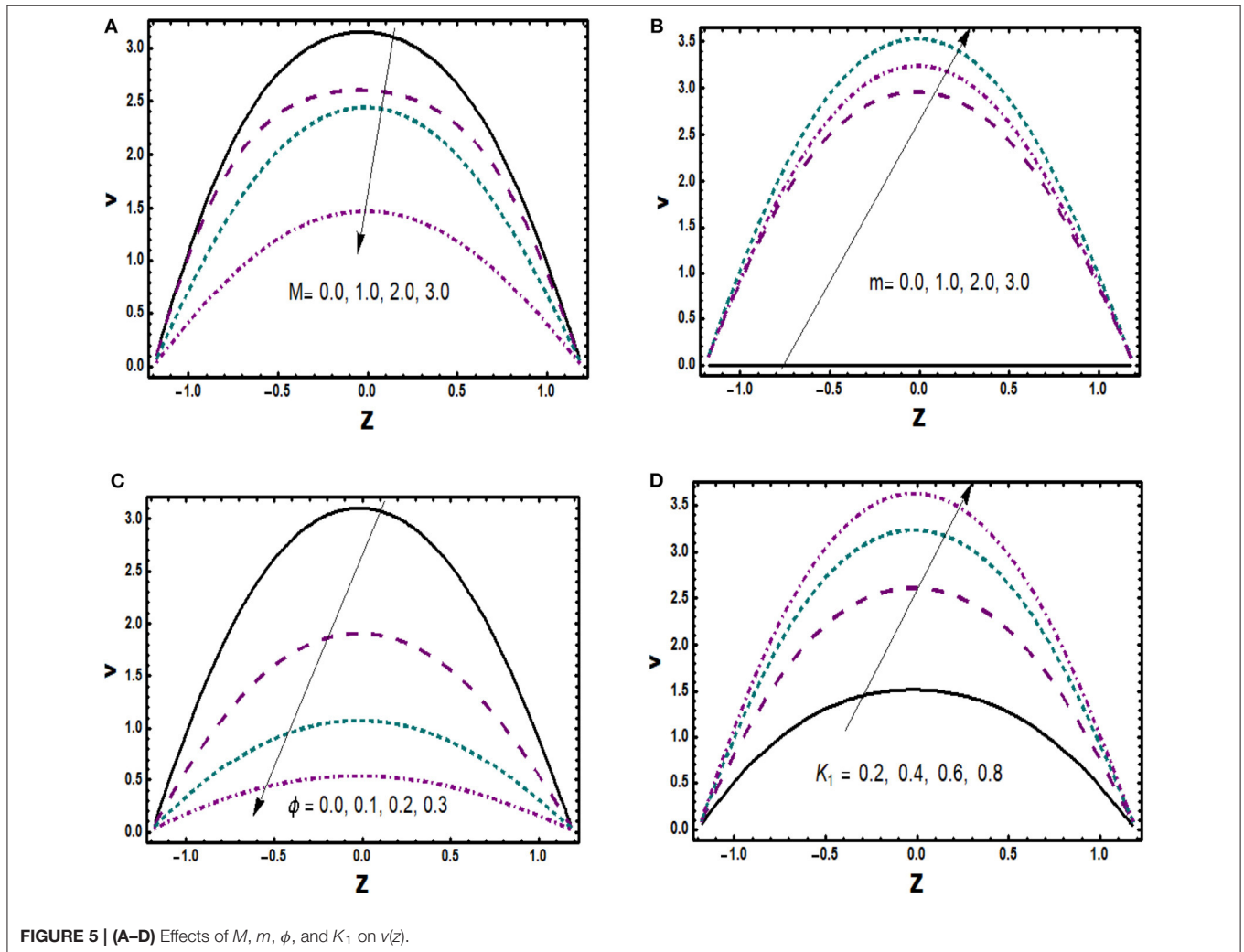


FIGURE 5 | (A–D) Effects of  $M, m, \phi,$  and  $K_1$  on  $v(z).$

$M = B_0 d \sqrt{\frac{\sigma_f}{\mu_f \exp[-\alpha(T-T_0)]}}$  is the Hartman number,  $R = \frac{4\sigma^* T_m^3}{k^* \kappa_f}$  is radiation parameter,  $K_1 = \frac{k_1}{d^2}$  is the permeability parameter,  $Pr = \mu_f \exp[-\alpha(T-T_0)] \frac{C_f}{k_f}$  is the Prandtl number,  $Br = Ec Pr$  expresses the Brinkman number,  $Ec = \frac{c^2}{C_f(T_1-T_0)}$  stands for the Eckert number,  $\varepsilon_1 = \frac{d^2 \Phi}{k_f(T_1-T_0)}$  shows heat generation/absorption parameter,  $m = \frac{\sigma_f B_0}{en_e}$  is the Hall parameter, and  $Gr = \frac{d^2}{c \mu_f} g(\rho\beta)_{eff}$  is the Grashof number. Moreover, the nanofluidics parameters  $A_1$  and  $A_2$  are expressed as

$$A_1 = 1 + \frac{3(\frac{\sigma_p}{\sigma_f} - 1)\phi}{(\frac{\sigma_p}{\sigma_f} + 2) - (\frac{\sigma_p}{\sigma_f} - 1)\phi}, A_2 = \frac{K_p + 2k_f - 2\phi(K_f - K_p)}{K_p + 2K_f + \phi(K_f - K_p)} \tag{15}$$

The wall properties for  $\eta = 1 + \varepsilon \sin(2\pi(x-t))$  with  $\varepsilon$  representing amplitude ratio parameter becomes:

$$\frac{\partial \psi}{\partial z} \pm \frac{\alpha_1}{(1-\phi)^{2.5}} \frac{\partial^2 \psi}{\partial z^2} \pm \frac{\alpha_2}{(1-\phi)^{2.5}} \frac{\partial^3 \psi}{\partial z^3} = 0, \quad z = \pm \eta, \tag{16}$$

$$\begin{aligned} & \left[ E_1 \frac{\partial^3}{\partial x^3} + E_2 \frac{\partial^3}{\partial x \partial t^2} + E_3 \frac{\partial^2}{\partial x \partial t} + E_4 \frac{\partial^5}{\partial x^5} + E_5 \frac{\partial}{\partial x} \right] \eta \\ & = \frac{\exp(-\alpha(T-T_0))}{(1-\phi)^{2.5}} \frac{\partial^3 \psi}{\partial z^3} + \frac{d^2}{c \mu_f} g(\rho\beta)_{nf}(T-T_0) \\ & - \frac{A_1 M^2}{1 + (A_1 m)^2} \left( \frac{\partial \psi}{\partial z} - A_1 m v \right) - \frac{\exp(-\alpha(T-T_0))}{(1-\phi)^{2.5} K_1} \frac{\partial \psi}{\partial z} \\ & + 2T' \left[ (1-\phi) + \phi \frac{\rho_p}{\rho_f} \right] v, \quad \text{at } z = \pm \eta, \end{aligned} \tag{17}$$

$$v \pm \frac{\beta_1}{(1-\phi)^{2.5}} \frac{\partial v}{\partial z} = 0, \quad \theta \pm \beta_2 \frac{\partial \theta}{\partial z} = \pm \frac{1}{2} \quad \text{at } z = \pm \eta. \tag{18}$$

where  $(E_1, E_2, E_3, E_4, E_5)$  exposed the dimensionless wall parameters.

$$\begin{aligned} E_1 &= -\frac{\tau d^3}{\lambda^3 \mu_f \exp[-\alpha(T-T_0)]c}, \quad E_2 = \frac{m_1 c d^3}{\lambda^3 \mu_f \exp[-\alpha(T-T_0)]c}, \\ E_3 &= \frac{d' d^3}{\lambda^2 \mu_f \exp[-\alpha(T-T_0)]c}, \quad E_4 = \frac{\beta' d^3}{\lambda^5 \mu_f c}, \quad E_5 = \frac{k d^3}{\lambda \mu_f c}. \end{aligned} \tag{19}$$

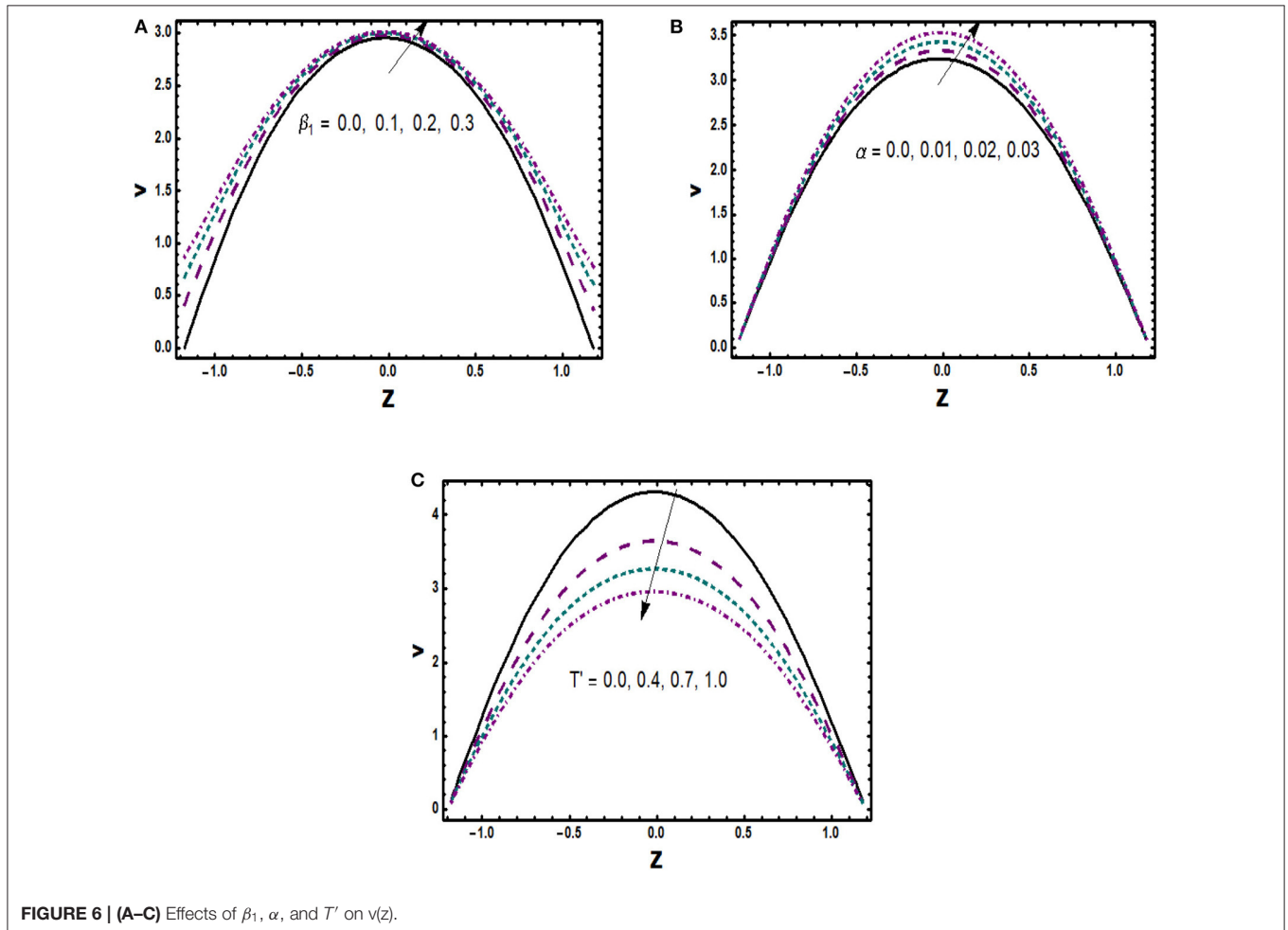


FIGURE 6 | (A–C) Effects of  $\beta_1$ ,  $\alpha$ , and  $T'$  on  $v(z)$ .

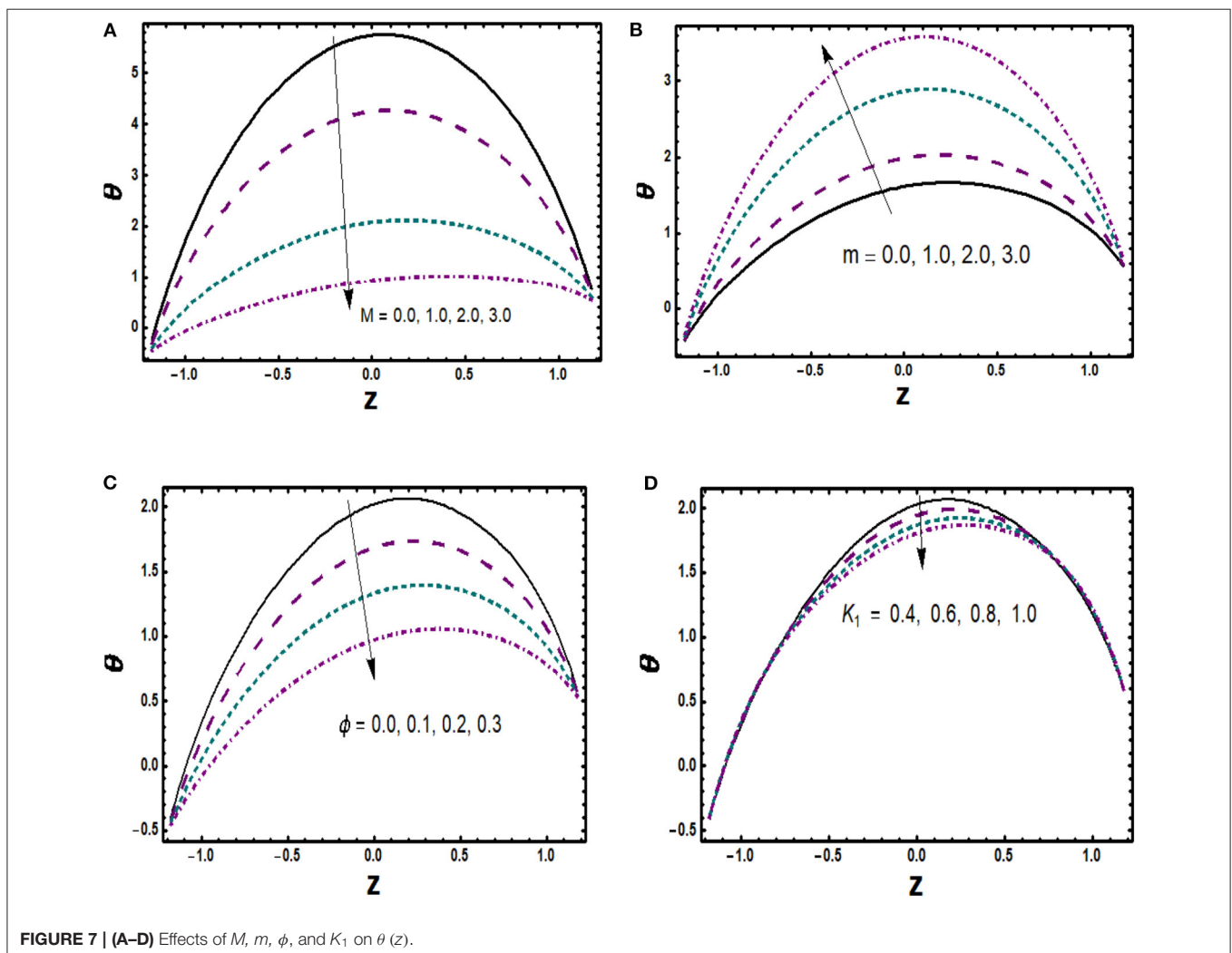
## NUMERICAL RESULTS AND DISCUSSION

A series of analysis is physically interpreted in this section in order to understand behaviors of primary and secondary velocities, temperature, and heat exchange rate against involving parameters for  $x = 0.2$ ,  $t = 0.1$ ,  $\varepsilon = 0.3$ ,  $\phi = 0.01$ ,  $E_1 = 0.03$ ,  $E_2 = 0.02$ ,  $E_3 = 0.01$ ,  $E_4 = 0.03$ ,  $E_5 = 0.02$ .

### Analysis of Axial Velocity

The physical behavior of the axial velocity component is exploited in **Figures 2–4** for various substantial parameters with the numerical values  $\alpha = 0.03$ ,  $\alpha_1 = 0.01$ ,  $\alpha_2 = -0.01$ ,  $\beta_1 = \beta_2 = 0.02$ ,  $m = 1.0$ ,  $M = 2.0$ ,  $Gr = 3.0$ ,  $Br = 0.01$ ,  $T' = 1.0$ ,  $R = 0.1$ ,  $\varepsilon_1 = 0.3$ ,  $K_1 = 0.5$ . **Figure 2A** depicts the consequence of applied magnetic field on velocity associated with Hartmann number  $M$ . Enhancement in values of  $M$  makes the impact of Lorentz force strong, which opposes the body forces with dominant retarding effects, and therefore, axial velocity is observed as a decreasing function of  $M$ . It is described in **Figure 2B** that velocity at the boundaries of

channel shows almost a negligible variation against  $Gr$ , whereas it is trimmed down in the center of the channel, which clearly shows that thermal convection opposes the flow in an important manner. Variational trend of velocity toward Hall parameter  $m$  is noticed in **Figure 2C**. Effective viscosity of copper nanoparticles abbreviates with rise in values of  $m$ , which consequently reduces magnetic damping force, and thus, velocity seems to be accelerating. Furthermore, an augmentation in nanoparticle volume fraction ( $\phi$ ) offers more resistance to the fluid transport, which drops the flow velocity. This trend is represented in **Figure 2D**. Behavior of  $u(z)$  for non-identical values of permeability parameter  $K_1$  is illustrated in **Figure 3A**. Large values of porosity parameter lessen frictional effects as well as lead to high permeability, which causes flow rate to accelerate. The effect of hydrodynamic slip parameter  $\alpha_1$  on velocity is depicted physically in **Figure 3B**. One can notice that as the values of slip parameter enlarge, fluid flows smoothly since it indicates that fluid velocity is unaffected by surface motion and that slippage reduces the resistive forces. A relevant behavior of second slip parameter  $\alpha_2$  is exposed in **Figure 3C** as well.



An increase in  $\alpha_2$  accelerates flow in the vicinity of the lower half of the channel while a completely conflicting trend is seen in the region of the upper half. It is depicted in **Figure 3D** that velocity in axial direction is reduced for rising values of rotation parameter  $T'$ . It validates physically that a flow in the perpendicular direction is generated due to angular velocity with consequences in axial flow abbreviation. Moreover, it can be seen interestingly that velocity has its maximum values in absence of rotation. The effect of variable viscosity parameter is shown in **Figure 4** in which velocity  $u(z)$  rises due to reducing frictional forces with increment in  $\alpha$ .

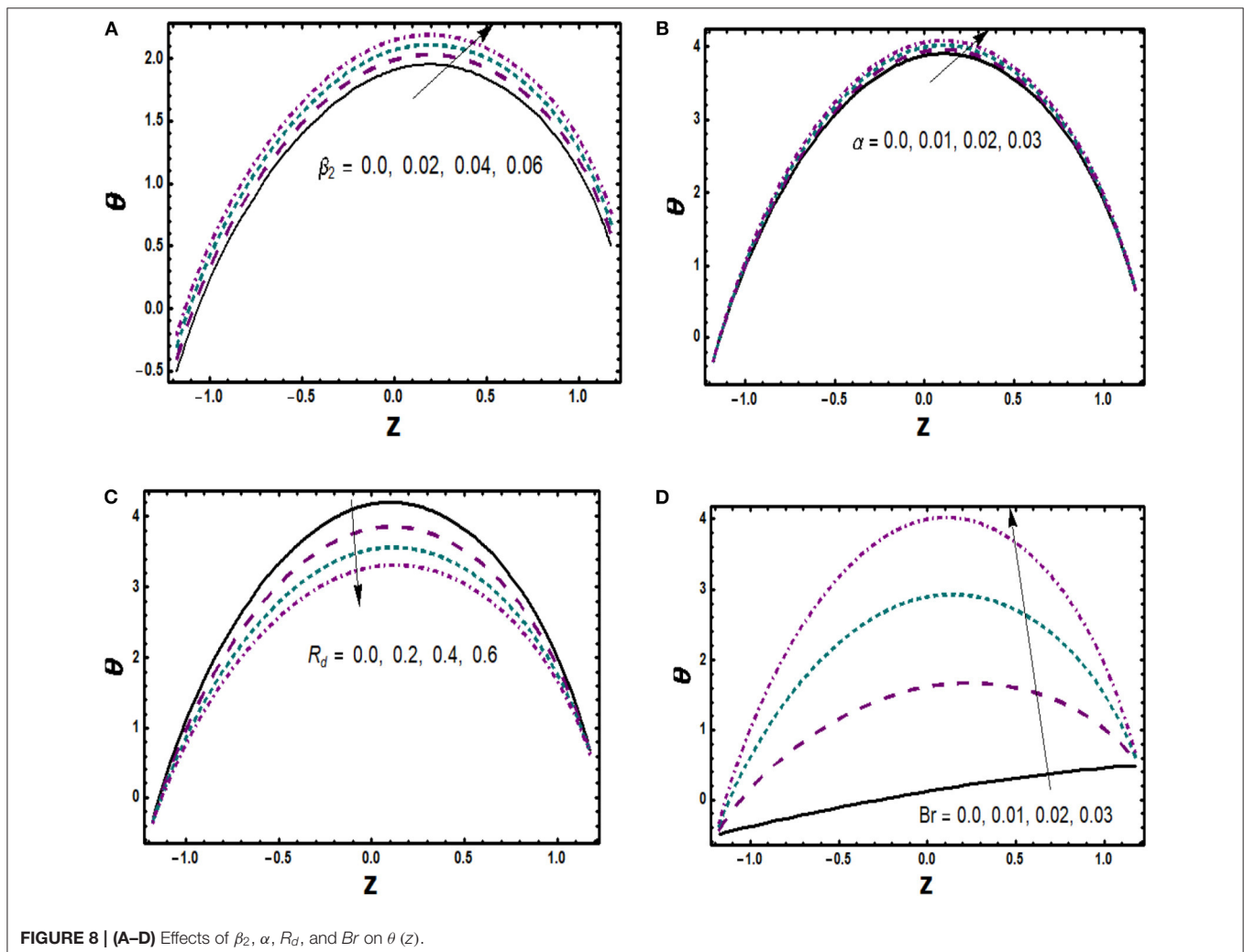
## Secondary Velocity

Effect of rotating motion induces a velocity component perpendicular to axial direction, which is known as secondary velocity  $v(z)$ . In order to understand physical insight of secondary velocity against pertinent parameters for numerical values  $\alpha = 0.03$ ,  $\alpha_1 = 0.1$ ,  $\alpha_2 = 0.1$ ,  $\beta_1 = \beta_2 = 0.02$ ,  $m = 1.0$ ,  $M = 2.0$ ,  $Br = 0.1$ ,  $Gr = 3.0$ ,  $T' = 1.0$ ,  $R = 0.1$ ,  $\varepsilon_1 = 0.3$ ,  $K_1 = 0.5$ , **Figures 5, 6** are prepared. **Figure 5A** presents secondary velocity  $v(z)$  as a decreasing function of  $M$  whereas Hall effects enhance

the secondary velocity as noticed in **Figure 5B**. Moreover, inspection of other plots in **Figures 5, 6** signifies that physical behaviors of velocity  $v(z)$  for escalating values of  $\phi$ ,  $K_1$ ,  $\beta_1$ ,  $\alpha$ , and  $T'$  as well as motivation behind such behaviors are similar to those for axial velocity. Also, graphical estimation reveals that maximum velocity occurs in the middle region of the channel.

## Temperature Distribution

Variational trends of dimensionless temperature distribution toward the influence of substantial parameters in case of  $\alpha = 0.02$ ,  $\alpha_1 = 0.01$ ,  $\alpha_2 = -0.01$ ,  $\beta_1 = \beta_2 = 0.5$ ,  $m = 2.0$ ,  $M = 2.0$ ,  $Gr = 3.0$ ,  $Br = 0.01$ ,  $T' = 1.0$ ,  $R = 0.2$ ,  $\varepsilon_1 = 0.3$ , and  $K_1 = 0.5$  is plotted and presented in **Figures 7–9**. As demonstrated in **Figure 7A**, the temperature of the fluid decreases owing to the enhancing values of Hartmann number. This happens because magnetic field clustered the nanoparticles, thereby increasing viscous effects that reduce average kinetic energy leading to temperature rise. An increment in  $\theta(z)$  corresponding to enlargement in Hall parameter is seen in **Figure 7B**. It is of factual significance that augmentation in  $m$  enhances electrical conductivity, i.e.,



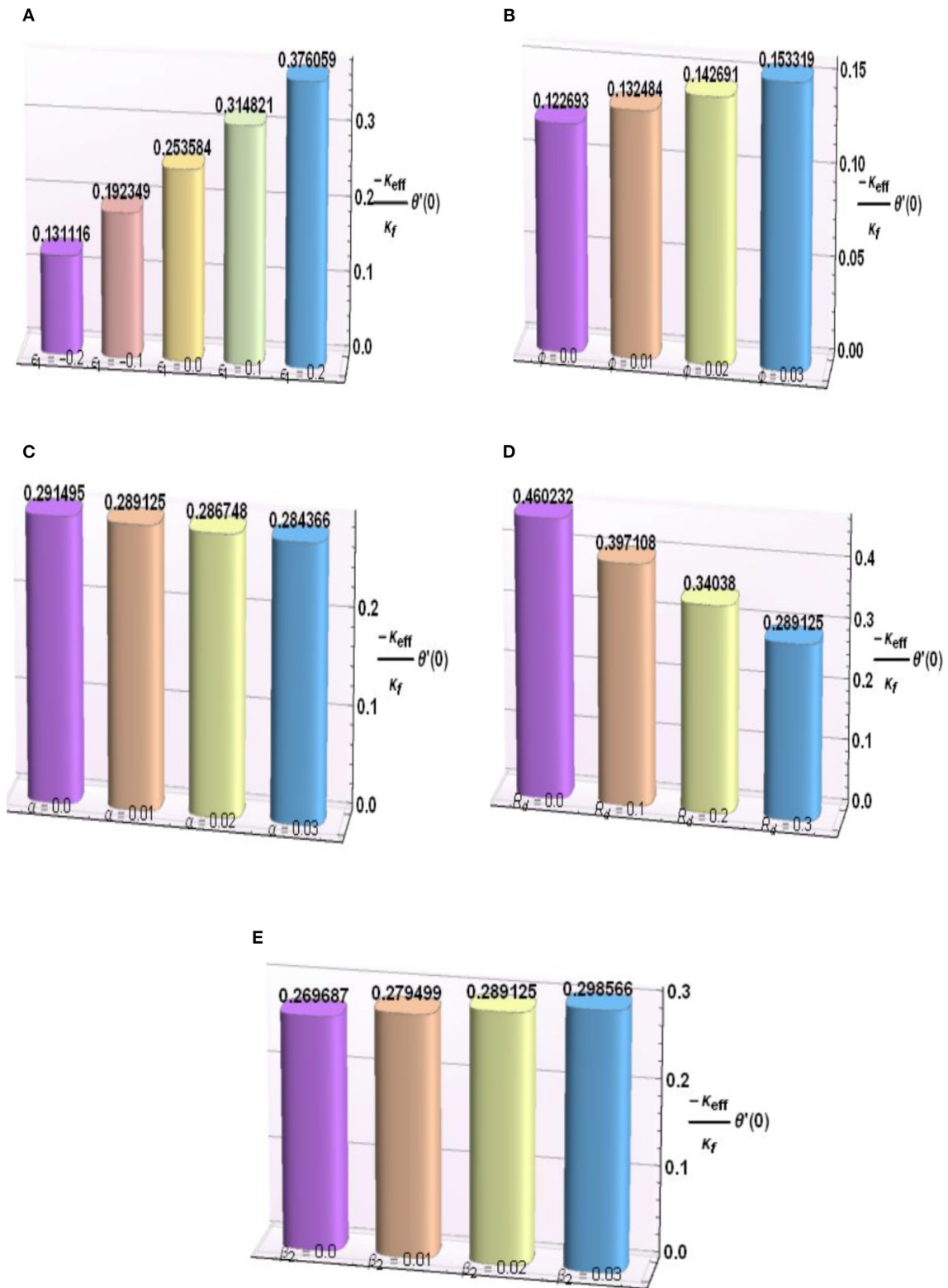


**FIGURE 9 | (A–E)** Variation in  $-\frac{K_{eff}}{K_f} \theta'(0)$  against  $\epsilon_1$ ,  $\phi$ ,  $\alpha$ ,  $R_d$ , and  $\beta_2$ .

**TABLE 1** | Numerical values of thermal properties of copper and water.

Phase	$\rho(\text{kg m}^{-3})$	$C(\text{J kg}^{-1} \text{K}^{-1})$	$K(\text{Wm}^{-1}\text{K}^{-1})$	$\beta(\text{K}^{-1}) \times 10^{-6}$	$\sigma(\Omega\text{m})^{-1}$
Water	997.1	4,179	0.613	210	0.05
Copper	8,933	385	401	16.65	$5.96 \times 10^7$

**TABLE 2** | Comparison of results for  $-\kappa_{\text{eff}}/\kappa_f\theta'(0)$  with Tanveer et al. [27] when  $\alpha = \alpha_2 = E_4 = E_5 = \varepsilon_1 = Gr = R = 0$ .

$\phi$	<b>M</b>	<b>m</b>	<b><math>K_1</math></b>	<b>Present results</b>	<b>Tanveer et al. [27]</b>
0.0	1.0	1.0	0.8	0.352189	0.352191
0.02				0.381989	0.381991
0.04				0.413208	0.413211
0.1	0.0			0.516370	0.516373
	0.5			0.516282	0.516284
	1.0			0.516065	0.516068
	1.0	0.0		0.515520	0.515523
		0.2		0.515060	0.515063
		0.4		0.514906	0.514908
		1.0	1.0	0.516113	0.516115
			2.0	0.516979	0.516981
			3.0	0.517233	0.517235

number of free electrons to conduct electric current increases and correspondingly rising conduction rate leads to temperature increase. **Figure 7C** exposed a reduction in temperature for rise in  $\phi$  due to increasing thermal exchange rate. More to the point, an increase in porosity parameter increases the permeability of channel walls and corresponds to larger time relaxation, which enhances resistive effects and, hence, temperature dropoff. This fact can be observed in **Figure 7D**. A corresponding enhancement in temperature profile vs. gradually mounting values of thermal slip parameter is observed in **Figure 8A**. This behavior is consistent with the physics of the problem that a rise in  $\beta_2$  leads to a reduction in retarding effects and dominates the temperature difference between fluid and boundaries of the channel due to which temperature rises accordingly. The purpose of **Figure 8B** is to explore the impact of the non-uniform viscosity parameter on  $\theta(z)$ , which serves to boost the temperature markedly due to the fact that  $\alpha$  is inversely related to viscous forces and its growing values reduce such forces. Obstinate, **Figure 8C** signifies a contour of the variation in  $\theta(z)$  for increasing values of  $R_d$  evolving. It is known that an increase in  $R_d$  values corresponds to a drop in mean absorption parameter prominently and in so doing refers to less energy absorption and temperature decreases accordingly. Further, **Figure 8D** portrays the variation in  $\theta(z)$  toward  $Br$ . It is seen that temperature absolutely grows for the increase in  $Br$  due to increasing thermal energy generated by internal friction of fluid.

Deviation in a few of the emerging parameters for heat transfer rate is probed as well. For this purpose, bar charts are structured and exhibited in **Figures 9A–E**. An increment in rate of heat exchange for increasing values of  $\varepsilon_1$  and  $\phi$  is

expressed in **Figures 9A,B** due to internal heat production and ever-increasing thermal conduction, accordingly. **Figures 9C,D**, respectively, depict a decreasing trend in heat transfer rate as the values of  $\alpha$  and  $R_d$  become larger while an acceleration is reported for  $\beta_2$  as demonstrated in **Figure 9E**. Additionally, experimental numerical values of thermal properties are articulated in **Table 1**. A comparative analysis has been carried out and results are displayed in **Table 2**. A very good agreement is observed between existing results and those of Hayat et al. [27].

## CONCLUDING REMARKS

Peristaltic flow dynamics of Cu-H<sub>2</sub>O nanofluid through channel with complaint walls having porous medium in a rotating frame is investigated in the presence of Hall current along with some physical factors. Major outcomes are recapped as:

- Enhancement in slip parameters  $\alpha_1$ ,  $\alpha_2$ , and  $\beta_1$  has consequences in axial and secondary velocity acceleration while the impact of  $Gr$  shows a decrease in axial velocity.
- Variation in  $M$  and  $T'$  corresponds to a decrease in velocities as well as temperature but the profiles show a conflicting trend toward  $m$ .
- Increase in values of  $K_1$  enhances velocities and drops fluid temperature, whereas consequences of  $\phi$  depict a dropoff in velocities as well as temperature.
- Comparatively, both the axial and secondary velocities correspond to a similar variational trend.
- Dimensionless temperature distribution increases toward a rise in  $\beta_2$ ,  $Br$ ,  $\alpha$ , and  $\varepsilon_1$ , whereas a conflicting variation is noticed for  $R_d$ .
- Heat transfer rate is maximum in the vicinity of the surface of the channel for boosting values of  $\varepsilon_1$ ,  $\phi$ , and  $\alpha$ , but it decreases for radiation and thermal slip parameters.
- Both velocity and temperature fields exhibit their maximum values in the central region of complaint walled channel.

## DATA AVAILABILITY STATEMENT

The datasets generated for this study are available on request to the corresponding author.

## AUTHOR CONTRIBUTIONS

All authors listed have made a substantial, direct and intellectual contribution to the work, and approved it for publication.

## FUNDING

This project was supported by the Theoretical and Computational Science (TaCS) Center under the Computational and Applied Science for Smart Innovation Research Cluster (CLASSIC), Faculty of Science, KMUTT.

## REFERENCES

- Shapiro AH, Jafferin MY, Weinberg SL. Peristaltic pumping with long wavelengths at low Reynolds number. *J Fluid Mech.* (1969) **37**:799–825. doi: 10.1017/S0022112069000899
- Latham TW. *Fluid motions in a peristaltic pump* (Doctoral dissertation). Massachusetts Ins Tech. (1966). Available online at: <http://dspace.mit.edu/handle/1721.1/7582>.
- Hayat T, Nawaz S, Alsaedi A, Rafiq M. Mixed convective peristaltic flow of water based nanofluids with joule heating and convective boundary conditions. *PLoS ONE.* (2016) **11**:e0153537. doi: 10.1371/journal.pone.0153537
- Abbas MA, Bai Y, Rashidi MM, Bhatti MM. Application of drug delivery in magnetohydrodynamics peristaltic blood flow of nano fluid in a non-uniform channel. *J Mech Med Biol.* (2016) **16**:1650052. doi: 10.1142/S0219519416500524
- Abrar MN, Haq RU, Awais M, Rashid I. Entropy analysis in a cilia transport of nanofluid under the influence of magnetic field. *Nucl Eng Tech.* (2017) **49**:1680–8. doi: 10.1016/j.net.2017.09.007
- Hall E. On a new action of the magnet on electric current. *Amer J Math.* (1879) **2**:287–92. doi: 10.2307/2369245
- Hayat T, Iqbal M, Yasmin H, Alsaadi F, Alotaibi N. Nonlinear flow of a Carreau fluid in the presence of Hall current and convective effect. *Eur Phys J Plus.* (2014) **129**:107. doi: 10.1140/epjp/i2014-14107-2
- Hayat T, Bibi A, Yasmin H, Ahmad B. Simultaneous effects of Hall current and homogeneous/heterogeneous reactions on peristalsis. *J Taiwan Inst Chem Eng.* (2016) **58**:28–38. doi: 10.1016/j.jtice.2015.05.037
- Hayat T, Iqbal M, Yasmin H, Alsaadi FE. Hall effects on peristaltic flow of couple stress fluid in an inclined asymmetric channel. *J Biomath.* (2014) **7**:1450057. doi: 10.1142/S1793524514500570
- Rashidi MM, Yang Z, Awais M, Nawaz M, Hayat T. Generalized magnetic field effects in Burgers nano-fluid model. *PLoS ONE.* (2017) **12**:e0168923. doi: 10.1371/journal.pone.0168923
- Hasona WM. Hall current effect on the peristaltic motion of synovial nanofluid with magnetohydrodynamic. *Heat Trans Asian Res.* (2019) **48**:1–18. doi: 10.1002/hjt.21469
- Qureshi IH, Nawaz M, Shehzad A. Numerical study of dispersion of nanoparticles in magnetohydrodynamic liquid with Hall and ion slip currents. *AIP Adv.* (2019) **9**:025219. doi: 10.1063/1.5084311
- Awais M, Hayat T, Irum S, Alsaedi A. Heat generation/absorption effects in a boundary layer stretched flow of Maxwell nanofluid: analytical and Numerical solutions. *PLoS ONE.* (2015) **10**:e0129814. doi: 10.1371/journal.pone.0129814
- Awais M, Hayat T, Ali A, Irum S. Velocity, thermal and concentration slip effects on a magneto-hydrodynamic nano-fluid flow. *Alex Eng J.* (2016) **55**:2107–14. doi: 10.1016/j.aej.2016.06.027
- Hayat T, Rashid M, Imtiaz M, Alsaedi A. Magneto-hydrodynamic (MHD) stretched flow of nano-fluid with power-law velocity and chemical reaction. *AIP Adv.* (2015) **5**:2158–3226. doi: 10.1063/1.4935649
- Abbasi FM, Hayat T, Ahmad B, Chen GQ. Slip effect on mixed convective peristaltic transport of copper-water nano-fluid in an inclined channel. *PLoS ONE.* (2014) **9**:e105440. doi: 10.1371/journal.pone.0105440
- Awais M, Farooq S, Hayat T, Ahmad B. Comparative study of silver and copper water magneto nanoparticles with homogeneous-heterogeneous reactions in a tapered channel. *Int J Heat Mass Trans.* (2017) **115**:108–14. doi: 10.1016/j.ijheatmasstransfer.2017.07.129
- Awan SE, Khan ZA, Awais M, Rehman SU, Raja MAZ. Numerical treatment for hydro-magnetic unsteady channel flow of nanofluid with heat transfer. *Results Phys.* (2018) **9**:1543–54. doi: 10.1016/j.rinp.2018.04.068
- Awais M, Hayat T, Muqaddass N, Ali A, Aqsa, Awan SE. Nanoparticles and nonlinear thermal radiation properties in the rheology of polymeric material. *Results Phys.* (2018) **8**:1038–45. doi: 10.1016/j.rinp.2018.01.041
- Khan WA, Ali M, Irfan M, Khan M, Shahzad M, Sultan F. A rheological analysis of nanofluid subjected to melting heat transport characteristics. *Appl Nanosci.* (2019) **1**–10. doi: 10.1007/s13204-019-01067-5
- Shah Z, Alzahrani EO, Dawar A, Ullah A, Khan I. Influence of Cattaneo-Christov model on Darcy-Forchheimer flow of micropolar ferrofluid over a stretching/shrinking sheet. *Int Commun Heat Mass Transfer.* (2020) **110**:104385. doi: 10.1016/j.icheatmasstransfer.2019.104385
- Shah Z, Khan A, Khan W, Alam MK, Islam S, Kumam P, et al. Micropolar gold blood nanofluid flow and radiative heat transfer between permeable channels. *Comput Methods Programs Biomed.* (2020) **186**:105197. doi: 10.1016/j.cmpb.2019.105197
- Hayat T, Awais M, Imtiaz A. Heat source/sink in a magneto-hydrodynamic non-Newtonian fluid flow in a porous medium: Dual solution. *PLoS ONE.* (2016) **11**:e0162205. doi: 10.1371/journal.pone.0162205
- Salahuddin T, Hussain A, Malik MY, Awais M, Khan M. Carreau nano-fluid impinging over a stretching cylinder with generalized slip effects: using finite difference scheme. *Results Phys.* (2017) **7**:3090–9. doi: 10.1016/j.rinp.2017.07.036
- Aly EH, Ebad A. Effect of the velocity second slip boundary condition on the peristaltic flow of nanofluids in an asymmetric channel: exact solution. *Abst Appl Anal.* (2014) **2014**:11. doi: 10.1155/2014/191876
- Awais M, Bukhari U, Ali A, Yasmin H. Convective and peristaltic viscous fluid flow with variable viscosity. *J Eng Thermophys.* (2017) **26**:69–78. doi: 10.1134/S1810232817010088
- Tanveer A, Hayat T, Alsaedi A. Variable viscosity in peristalsis of Sisko fluid. *Appl Math Mech Ed.* (2018) **39**:501–12. doi: 10.1007/s10483-018-2313-8
- Shah Z, Kumam P, Dawar A, Alzahrani EO, Thounthong P. Study of the couple stress convective micropolar fluid flow in a Hall MHD generator system. *Front Phys.* (2019) **7**:171. doi: 10.3389/fphy.2019.00171
- Shah Z, Babazadeh H, Kumam P, Shafee A, Thounthong P. Numerical simulation of magnetohydrodynamic nanofluids under the influence of shape factor and thermal transport in a porous media using CVFEM. *Front Phys.* (2019) **7**:164. doi: 10.3389/fphy.2019.00164
- Hayat T, Ayub S, Alsaedi A, Ahmad B. Numerical simulation of buoyancy peristaltic flow of Johnson-Segalman nanofluid in an inclined channel. *Results Phys.* (2018) **9**:906–15. doi: 10.1016/j.rinp.2018.03.037
- Hayat T, Rafique M, Alsaedi A. Investigation of Hall and slip conditions on peristaltic transport of Cu-water nanofluid in a rotating medium. *Int J Heat Mass Trans.* (2017) **112**:129–41. doi: 10.1016/j.ijthermalsci.2016.10.004
- Sharma RP, Raju MC, Makinde OD, Reddy PRK, Reddy PC. Buoyancy effects on unsteady MHD chemically reacting and rotating fluid flows past a plate in porous medium. *Def Diff Forum.* (2019) **392**:1–9. doi: 10.4028/www.scientific.net/DDF.392.1
- Ali N, Hayat T, Asghar S. Peristaltic flow of Maxwell fluid in a channel with compliant walls. *Chaos Sol Fract.* (2009) **39**:407–16. doi: 10.1016/j.chaos.2007.04.010

**Conflict of Interest:** The authors declare that the research was conducted in the absence of any commercial or financial relationships that could be construed as a potential conflict of interest.

Copyright © 2020 Awais, Kumam, Parveen, Ali, Shah and Thounthong. This is an open-access article distributed under the terms of the Creative Commons Attribution License (CC BY). The use, distribution or reproduction in other forums is permitted, provided the original author(s) and the copyright owner(s) are credited and that the original publication in this journal is cited, in accordance with accepted academic practice. No use, distribution or reproduction is permitted which does not comply with these terms.



# The Falling Body Problem in Quantum Calculus

Abdulaziz M. Alanazi, Abdelhalim Ebaid\*, Wadha M. Alhawiti and Ghulam Muhiuddin

Department of Mathematics, Faculty of Sciences, University of Tabuk, Tabuk, Saudi Arabia

The quantum calculus,  $q$ -calculus, is a relatively new branch in which the derivative of a real function can be calculated without limits. In this paper, the falling body problem in a resisting medium is revisited in view of the  $q$ -calculus to the first time. The  $q$ -differential equations describing the vertical velocity and distance of the body are obtained. Accordingly, exact expressions for the vertical velocity and the vertical distance are provided. The solutions are expressed in terms of the small  $q$ -exponential function which is an elementary function in the  $q$ -calculus. The dimensionality of the obtained formulae of the velocity and the distance are also analyzed. In addition, the present exact solutions reduce to the corresponding solutions in classical Newtonian mechanics when the quantum parameter  $q$  tends to one.

## OPEN ACCESS

### Edited by:

Jesus Martin-Vaquero,  
University of Salamanca, Spain

### Reviewed by:

Praveen Agarwal,  
Anand International College of  
Engineering, India  
Ding-fang Zeng,  
Beijing University of Technology, China

### \*Correspondence:

Abdelhalim Ebaid  
aebaid@ut.edu.sa

### Specialty section:

This article was submitted to  
Mathematical Physics,  
a section of the journal  
Frontiers in Physics

**Received:** 02 November 2019

**Accepted:** 13 February 2020

**Published:** 06 March 2020

### Citation:

Alanazi AM, Ebaid A, Alhawiti WM and  
Muhiuddin G (2020) The Falling Body  
Problem in Quantum Calculus.  
Front. Phys. 8:43.  
doi: 10.3389/fphy.2020.00043

**Keywords:**  $q$ -calculus,  $q$ -series, exact solution, falling body problem,  $q$ -differential equation

**2010 Mathematics Subject Classification:** 35A24, 49K15

## 1. INTRODUCTION

Basically, the regular calculus uses limits in calculating the derivatives of real functions. However, the calculus without limits is nowadays known as quantum calculus or  $q$ -calculus. Historically, in the eighteenth century, Euler obtained the basic formulae in  $q$ -calculus. However, Jackson [1] may have been the first to introduce the notion of the definite  $q$ -derivative and  $q$ -integral. Currently, there is a significant interest in implementing the  $q$ -calculus due to its applications in several areas, such as mathematics, number theory, and combinatorics [2]. Ernst [3, 4] pointed out that the majority of scientists who use  $q$ -calculus are physicists. Baxter [5] introduced the exact solutions of several models in Statistical Mechanics. Bettaibi and Mezlini [6] solved some  $q$ -heat and  $q$ -wave equations. Many interesting results in such area of research were also introduced by several authors in the literature [7–12].

In this paper, we aim to extend the applications of the  $q$ -calculus to study the falling body problem in a resisting medium. This problem and also the full projectile motion have been investigated by several authors [13–17] using various definitions in fractional calculus. However, the present paper may be the first to analyze the falling body problem in view of the  $q$ -calculus.

The basic formulae in  $q$ -calculus will be used to analyze the motion of a falling body in a resisting medium. Moreover, it will be shown that the exact solutions for the vertical velocity and distance reduce to the classical ones as  $q \rightarrow 1$ . The paper is organized as follows. Section 2 presents the main aspects of the  $q$ -calculus. Section 3 discusses the application of the  $q$ -calculus on the falling body problem. Section 4 includes an additional analysis. Finally, section 5 outlines the conclusions.

## 2. THE MAIN ASPECTS OF THE $q$ -CALCULUS

Let  $q \in \mathbb{R}$  and  $n \in \mathbb{N}$ , then  $[n]_q$  is defined as (first chapter in [18])

$$[n]_q = \frac{1 - q^n}{1 - q}, \tag{1}$$

and as  $q \rightarrow 1$ , we have

$$\lim_{q \rightarrow 1} [n]_q = n. \tag{2}$$

The  $q$ -factorial  $[n]_q!$  of a positive integer  $n$  is given by

$$[n]_q! = [1]_q \times [2]_q \times [3]_q \times \dots \times [n]_q. \tag{3}$$

The definition of  $q$ -differential is  $d_q f(t) = f(t) - f(qt)$  and the  $q$ -derivative of a function  $f(t)$  is defined by [18]

$$D_q f(t) := \frac{d_q f(t)}{d_q t} = \frac{f(t) - f(qt)}{(1 - q)t}, \quad t \neq 0, \tag{4}$$

such that

$$\lim_{q \rightarrow 1} D_q f(t) = f'(t), \tag{5}$$

if  $f$  is differentiable at  $t$ , and we have at  $t = 0$  that

$$D_q f(0) = \lim_{t \rightarrow 0} D_q f(t). \tag{6}$$

According to (4) we have

$$D_q t^n = [n]_q t^{n-1}. \tag{7}$$

The small  $q$ -analog of the exponential function  $e^t$  denoted by  $e_q(t)$  (also called the small  $q$ -exponential function) is given as

$$e_q(t) = \sum_{j=0}^{\infty} \frac{t^j}{[j]_q!}. \tag{8}$$

The definite Jackson  $q$ -integral is defined by

$$\int_0^x f(t) d_q t = (1 - q)x \sum_{j=0}^{\infty} q^j f(q^j x), \tag{9}$$

and according to (4) and (9), we have

$$\int_0^x D_q f(t) d_q t = f(x) - f(0). \tag{10}$$

The indefinite Jackson  $q$ -integral of the small  $q$ -exponential function  $e_q(\alpha t)$  is given as [18]

$$\int e_q(\alpha t) d_q t = \frac{1}{\alpha} e_q(\alpha t) + c, \tag{11}$$

where  $c$  is a real constant. The correctness of dimensionality of the physical quantities is actually guaranteed by the definition (4).

## 3. THE FALLING BODY PROBLEM

Consider the falling of an object of mass  $m$  in the Earth gravitational field through the air from a height  $h$  with initial velocity  $v_0$ . The classical equation of motion for the particle is given by [15, 16]

$$m \frac{dv}{dt} = -mg - mkv, \tag{12}$$

where  $k$  is a positive constant and its dimensionality is the inverse of seconds, i.e.,  $[k] = s^{-1}$ . The initial conditions are given as

$$v(0) = v_0, \quad z(0) = h, \tag{13}$$

where  $z(t)$  is the vertical distance of the particle at arbitrary time  $t$  and  $\frac{dz(t)}{dt} = v(t)$ . The equation of motion (12) in view of the quantum calculus becomes

$$\frac{d_q v}{d_q t} := -g - kv, \quad q \in (0, 1]. \tag{14}$$

In order to solve Equation (14), we assume the solution in the series form:

$$v(t) = \sum_{n=0}^{\infty} a_n t^n, \tag{15}$$

and therefore

$$\begin{aligned} \frac{d_q v}{d_q t} &= \sum_{n=0}^{\infty} [n]_q a_n t^{n-1}, \\ &= \sum_{n=1}^{\infty} [n]_q a_n t^{n-1}, \quad \text{where } [0]_q = 0, \\ &= \sum_{n=0}^{\infty} [n+1]_q a_{n+1} t^n. \end{aligned} \tag{16}$$

Substituting (15) and (16) into (14), yields

$$\sum_{n=0}^{\infty} [n+1]_q a_{n+1} t^n = -g - k \sum_{n=0}^{\infty} a_n t^n, \tag{17}$$

or

$$[1]_q a_1 + \sum_{n=1}^{\infty} [n+1]_q a_{n+1} t^n = -g - ka_0 - k \sum_{n=1}^{\infty} a_n t^n, \tag{18}$$

which gives

$$\begin{aligned} a_1 &= \frac{-g - ka_0}{[1]_q}, \\ a_{n+1} &= \frac{-ka_n}{[n+1]_q}, \quad n \geq 1, \end{aligned} \tag{19}$$

From (19), we have

$$\begin{aligned}
 a_2 &= \frac{-ka_1}{[2]_q} = \frac{(-1)^2kg + (-k)^2a_0}{[1]_q[2]_q}, \\
 a_3 &= \frac{-ka_2}{[3]_q} = \frac{(-1)^3k^2g + (-k)^3a_0}{[1]_q[2]_q[3]_q}, \\
 a_4 &= \frac{-ka_3}{[4]_q} = \frac{(-1)^4k^3g + (-k)^4a_0}{[1]_q[2]_q[3]_q[4]_q}, \\
 &\vdots \\
 a_n &= \frac{(-1)^nk^{n-1}g + (-k)^na_0}{[1]_q[2]_q[3]_q \dots [n]_q}, \quad n \geq 1. \tag{20}
 \end{aligned}$$

This  $n$ -term coefficient can be expressed in terms of the  $q$ -factorial  $[n]_q!$  as

$$a_n = \frac{(-1)^nk^{n-1}g + (-k)^na_0}{[n]_q!}, \quad n \geq 1. \tag{21}$$

The instantaneous velocity is obtained as

$$\begin{aligned}
 v(t) &= a_0 + \sum_{n=1}^{\infty} a_n t^n, \\
 &= a_0 + \sum_{n=1}^{\infty} \left[ \frac{(-1)^nk^{n-1}g + (-k)^na_0}{[n]_q!} \right] t^n. \\
 &= a_0 + \sum_{n=1}^{\infty} \left[ \frac{(g/k)(-kt)^n + (-kt)^na_0}{[n]_q!} \right], \tag{22}
 \end{aligned}$$

which can be written as

$$v(t) = a_0 + \left( \frac{g}{k} + a_0 \right) \sum_{n=1}^{\infty} \frac{(-kt)^n}{[n]_q!}. \tag{23}$$

In terms of the small exponential function  $e_q(-kt)$ , we have

$$v(t) = a_0 + \left( \frac{g}{k} + a_0 \right) [e_q(-kt) - 1]. \tag{24}$$

Applying the first initial condition in (13) on (24), we obtain  $a_0 = v_0$  and therefore  $v(t)$  becomes

$$v(t) = v_0 + \left( \frac{g}{k} + v_0 \right) [e_q(-kt) - 1], \tag{25}$$

which can be simplified as

$$v(t) = -\frac{g}{k} + \left( \frac{g}{k} + v_0 \right) e_q(-kt). \tag{26}$$

The vertical distance  $z(t)$  in quantum calculus is governed by,

$$D_q z(t) = -\frac{g}{k} + \left( \frac{g}{k} + v_0 \right) e_q(-kt), \tag{27}$$

where  $v(t) = D_q z(t)$ . Integrating (27), it then follows;

$$\int_0^t D_q z(\tau) d_q \tau = \int_0^t \left( -\frac{g}{k} \right) d_q \tau + \left( \frac{g}{k} + v_0 \right) \int_0^t e_q(-k\tau) d_q \tau, \tag{28}$$

and hence,

$$z(t) - z(0) = -\frac{g}{k} \left[ \frac{\tau}{[1]_q} \right]_0^t + \left( \frac{g}{k} + v_0 \right) \left[ -\frac{e_q(-k\tau)}{k} \right]_0^t, \tag{29}$$

or

$$z(t) = h - \frac{g}{k} \left( \frac{t}{[1]_q} \right) + \left( \frac{g}{k} + v_0 \right) \left( -\frac{e_q(-kt)}{k} + \frac{1}{k} \right), \tag{30}$$

i.e.,

$$z(t) = h - \frac{gt}{k} + \frac{1}{k} \left( \frac{g}{k} + v_0 \right) (1 - e_q(-kt)), \tag{31}$$

where  $[1]_q = 1$ . The exact solutions (26) and (31) should be reduced to the corresponding solutions in classical Newtonian mechanics when  $q \rightarrow 1$ . In addition, if the acceleration due to gravity is measured in  $ms^{-2}$ , then the vertical velocity in (26) must have dimension  $ms^{-1}$  and the vertical distance in (31) must have dimension  $m$ . These issues are addressed in the following section.

### 4. ANALYSIS AND APPLICATIONS

First of all, we investigate the solutions (26) and (31) when  $q \rightarrow 1$ . In this case, the small exponential function  $e_q(-kt)$  reduces to the standard exponential function  $e^{-kt}$  in classical calculus. Hence, (26) becomes

$$v(t) = -\frac{g}{k} + \left( v_0 + \frac{g}{k} \right) e^{-kt}, \tag{32}$$

which is the analytic expression for velocity in the case of the classical Newtonian mechanics (see Equation 16 in reference [15]). Besides, the vertical distance in (31) reduces to

$$z(t) = h - \frac{gt}{k} + \frac{1}{k} \left( \frac{g}{k} + v_0 \right) (1 - e^{-kt}), \tag{33}$$

which is also the analytic expression for the vertical distance in the classical Newtonian mechanics (see Equation 17 in reference [15]).

In addition, in the case of no air resistance, i.e., the parameter  $k$  vanishes, we obtain from (32) that

$$\begin{aligned}
 v(t)|_{k \rightarrow 0} &= \lim_{k \rightarrow 0} \left[ v_0 e^{-kt} + g \left( \frac{e^{-kt} - 1}{k} \right) \right], \\
 &= v_0 + g \lim_{k \rightarrow 0} \left( \frac{e^{-kt} - 1}{k} \right), \\
 &= v_0 + g \lim_{k \rightarrow 0} \left( \frac{-te^{-kt}}{1} \right), \\
 &= v_0 - gt. \tag{34}
 \end{aligned}$$

Also, the vertical distance in (33) in the absence of air resistance becomes

$$\begin{aligned}
 z(t)|_{k \rightarrow 0} &= h + \lim_{k \rightarrow 0} \left[ \frac{-gtk + (g + kv_0)(1 - e^{-kt})}{k^2} \right], \\
 &= h + \lim_{k \rightarrow 0} \left[ \frac{v_0 - gt + [(g + kv_0)t - v_0]e^{-kt}}{2k} \right], \\
 &= h + \lim_{k \rightarrow 0} \left[ \frac{-[(g + kv_0)t - v_0]te^{-kt} + v_0te^{-kt}}{2} \right], \\
 &= h + \left( \frac{-(gt - v_0)t + v_0t}{2} \right), \\
 &= h + v_0t - \frac{1}{2}gt^2. \tag{35}
 \end{aligned}$$

Here, it should be noted that L'Hôpital's rule was applied to calculate the above limits. The Equations (34) and (35) are the same of the corresponding equations for the vertical velocity and vertical distance in Newtonian mechanics in the absence of air resistance.

Regarding the dimensions of the  $q$ -forms of  $v(t)$  and  $z(t)$  in (26) and (31), respectively, it should be first to specify the dimensions of the quantities  $e_q(-kt)$  and  $(1 - e_q(-kt))$  as indicated below:

$$\begin{aligned}
 [kt] &= [k] \times [s] = s^{-1} \times s = \text{Scalar}, \\
 [e_q(-kt)] &= \text{Scalar}, \\
 [1 - e_q(-kt)] &= \text{Scalar}. \tag{36}
 \end{aligned}$$

By this,  $e_q(-kt)$  and  $(1 - e_q(-kt))$  are dimensionless quantities, i.e.,  $e_q(-kt)$  and  $(1 - e_q(-kt))$  are scalar quantities. Accordingly,  $v(t)$  in (26) always has dimension  $ms^{-1}$  for all values of the quantum parameter  $q$ . Also  $z(t)$  in (31) always has dimension  $m \forall q \in (0, 1]$ . The correctness of dimensions of the  $q$ -vertical velocity and the  $q$ -height was actually guaranteed by the definition (4) without any need to involve an auxiliary parameter as in the literature [15, 16].

Although the present model of the falling body problem seems simple, the authors believe that the current work is worthy of

exploration. This is because the present solution was provided to the first time for the falling problem in view of  $q$ -calculus. In addition, it was shown in this paper the way of obtaining the solutions in exact forms and also how to check the dimensions of the physical quantities in terms of  $q$ -parameter. Furthermore, the obtained solutions can be verified by direct substitutions into the governing equations. Therefore, the present work is a first step for further studies in future to explore various physical models in applied mathematics implementing the  $q$ -calculus.

## 5. CONCLUSION

In this paper, the quantum calculus was applied to solve the falling body problem. The exact solutions for the  $q$ -vertical velocity and the  $q$ -distance have been obtained. The obtained exact solutions were expressed in terms of the small  $q$ -exponential function. The correctness of dimensionality of the obtained formulae of the velocity and the distance was proved. Moreover, The present exact solutions reduced to the corresponding solutions in classical Newtonian mechanics when the quantum parameter  $q$  tends to one. The present work can be further extended to explore the physical properties of the projectile motion in two and three dimensions in view of the  $q$ -calculus.

## DATA AVAILABILITY STATEMENT

All datasets generated for this study are included in the article/supplementary material.

## AUTHOR CONTRIBUTIONS

All authors listed have made a substantial, direct and intellectual contribution to the work, and approved it for publication.

## FUNDING

The authors extend their appreciation to the Deanship of Scientific Research at University of Tabuk for funding this work through Research Group no. RGP-0207-1440.

## REFERENCES

- Jackson FH. On a  $q$ -definite integrals. *Q J Pure Appl Math.* (1910) **41**:193–203.
- Andrews GE. *q-Series: Their Development and Applications in Analysis, Number Theory, Combinatorics, Physics and Computer Algebra*. CBMS Regional Conference Series in Mathematics, Vol. **66**. Providence, RI: American Mathematical Society (1986).
- Ernst T. *The history of  $q$ -calculus and a new method* (Licentiate thesis), U.U.D.M. Report 2000: 16. Available online at: <https://pdfs.semanticscholar.org/895b/4f8b059dc7ad18807f5aabdf09f2158d0c66.pdf>
- Ernst T. A method for  $q$ -calculus. *J Nonlin Math Phys A Method.* (2003) **10**:487–525. doi: 10.2991/jnmp.2003.10.4.5
- Baxter R. *Exact Solved Models in Statistical Mechanics*. New York, NY: Academic Press (1982).
- Bettaibi N, Mezlini K. On the use Of the  $q$ -Mellin transform to solve some  $q$ -heat and  $q$ -wave equations. *Int J Math Arch.* (2012) **3**:446–55.
- Li YQ, Sheng ZM. A deformation of quantum mechanics. *J Phys A Math Gen.* (1992) **25**:6779–88. doi: 10.1088/0305-4470/25/24/028
- Annaby MH, Mansour ZS. *q-Fractional Calculus and Equations*. Heidelberg: New York, NY: Springer (2012).
- Koca I, Demirci E. On local asymptotic stability of  $q$ -fractional nonlinear dynamical systems. *Appl Appl Math.* (2016) **11**:174–83. Available online at: <http://pvamu.edu/aam>
- Rangaig NA, Pada CT, Convicto VC. On the existence of the solution for  $q$ -Caputo fractional boundary value problem. *Appl Math Phys.* (2017) **5**:99–102. doi: 10.12691/amp-5-3-4
- Tang Y, Zhang T. A remark on the  $q$ -fractional order differential equations. *Appl Math Comput.* (2019) **350**:198–208. doi: 10.1016/j.amc.2019.01.008
- Chanchlani L, Alha S, Gupta J. Generalization of Taylor's formula and differential transform method for composite fractional  $q$ -derivative. *Ramanujan J.* (2019) **48**:21–32. doi: 10.1007/s11139-018-9997-7

13. Kwok SF. A falling body problem through the air in view of the fractional derivative approach. *Phys A*. (2005) **350**:199–206. doi: 10.1016/j.physa.2004.11.041
14. Ebaid A. Analysis of projectile motion in view of the fractional calculus. *Appl Math Model*. (2011) **35**:1231–9. doi: 10.1016/j.apm.2010.08.010
15. Garcia JJR, Calderon MG, Ortiz JM, Baleanu D. Motion of a particle in a resisting medium using fractional calculus approach. *Proc Roman Acad Ser A*. (2013) **14**:42–7.
16. Ebaid A, Masaedeh B, El-Zahar E. A new fractional model for the falling body problem. *Chin Phys Lett*. (2017) **34**:020201. doi: 10.1088/0256-307X/34/2/020201
17. Alharbi FM, Baleanu D, Ebaid A. Physical properties of the projectile motion using the conformable derivative. *Chin J Phys*. (2019) **58**:18–28. doi: 10.1016/j.cjph.2018.12.010
18. Kac VG, Cheung P. *Quantum Calculus*. New York, NY: Springer-Verlag (2002).

**Conflict of Interest:** The authors declare that the research was conducted in the absence of any commercial or financial relationships that could be construed as a potential conflict of interest.

Copyright © 2020 Alanazi, Ebaid, Alhawiti and Muhiuddin. This is an open-access article distributed under the terms of the Creative Commons Attribution License (CC BY). The use, distribution or reproduction in other forums is permitted, provided the original author(s) and the copyright owner(s) are credited and that the original publication in this journal is cited, in accordance with accepted academic practice. No use, distribution or reproduction is permitted which does not comply with these terms.



# Application of New Iterative Method to Time Fractional Whitham–Broer–Kaup Equations

Rashid Nawaz<sup>1†</sup>, Poom Kumam<sup>2,3,4\*\*†</sup>, Samreen Farid<sup>1†</sup>, Meshal Shutaywi<sup>5†</sup>, Zahir Shah<sup>6\*\*†</sup> and Wejdan Deebani<sup>5†</sup>

<sup>1</sup> Department of Mathematics, Abdul Wali Khan University Mardan, Mardan, Pakistan, <sup>2</sup> KMUTT-Fixed Point Theory and Applications Research Group, Faculty of Science, Theoretical and Computational Science Center (TaCS), King Mongkut's University of Technology Thonburi (KMUTT), Bangkok, Thailand, <sup>3</sup> Department of Medical Research, China Medical University Hospital, China Medical University, Taichung, China, <sup>4</sup> Center of Excellence in Theoretical and Computational Science (TaCS-CoE), SCL 802 Fixed Point Laboratory, King Mongkut's University of Technology Thonburi (KMUTT), Bangkok, Thailand, <sup>5</sup> Department of Mathematics, College of Science and Arts, King Abdul-Aziz University, Rabigh, Saudi Arabia, <sup>6</sup> Center of Excellence in Theoretical and Computational Science (TaCS-CoE), SCL 802 Fixed Point Laboratory, King Mongkut's University of Technology Thonburi (KMUTT), Bangkok, Thailand

## OPEN ACCESS

### Edited by:

Jesus Martin-Vaquero,  
University of Salamanca, Spain

### Reviewed by:

Kehui Sun,  
Central South University, China  
Shaobo He,  
Central South University, China

### \*Correspondence:

Poom Kumam  
poom.kum@kmutt.ac.th  
Zahir Shah  
zahir.sha@kmutt.ac.th

<sup>†</sup>These authors have contributed  
equally to this work

### Specialty section:

This article was submitted to  
Mathematical Physics,  
a section of the journal  
Frontiers in Physics

**Received:** 21 December 2019

**Accepted:** 20 March 2020

**Published:** 13 May 2020

### Citation:

Nawaz R, Kumam P, Farid S,  
Shutaywi M, Shah Z and Deebani W  
(2020) Application of New Iterative  
Method to Time Fractional  
Whitham–Broer–Kaup Equations.  
*Front. Phys.* 8:104.  
doi: 10.3389/fphy.2020.00104

This article presents the fractional Laplace transform with the help of new iterative method (NIM) is extended for an estimated solution of coupled system of fractional order PDEs. The time fractional Whitham–Broer–Kaup system is taken as a test example where derivatives are given in the Caputo sense. Numerical results found by the proposed method are compared with that of ADM, VIM, and OHAM. Numerical consequences display that the proposed method is reliable and operative for solution of fractional order coupled system of PDEs. The proposed method shows better accuracy in even two iterations compared to the methods given above.

**Keywords:** fractional Whitham–Broer–Kaup equations, coupled system of time fractional PDEs, new iterative method, fractional calculus (FC), Whitham–Broer–Kaup system, Caputo sense, ADM, VIM and OHAM

## INTRODUCTION

As we know that many technical and engineering issues that arises in day-by-day existence are modeled via mathematical tools form fractional calculus (FC), i.e., fractional calculus can be used to simulate various real phenomena involving long memory, e.g., using fractional derivative, one can model HIV/AIDS model based on the effect of screening of unaware infectives [1]. Maximum problems that arise are non-linear, and it is not usually probable to locate systematic results of such problems since some researchers introduced new approaches for finding the exact solution of FPDEs [2]. However, these methods also have some drawbacks, and we cannot use it for any type of problems. To fulfill these need, researchers introduced many semi analytical techniques such as HPM [3], HPTM [4], HAM [5], FDM [6], RPSM [7], etc.

NIM was introduced by Daftardar-Gejji and Jafari in 2006 and is also known as the DJ method for the solution of non-linear equations. This method is the modification of ADM in which the complex Adomian polynomials are replaced by Jafari polynomials. Therefore, we have no need to compute tedious Adomian's polynomial in each iteration.

In this presentation, we have extended the applications of the DJ method to a solution of coupled WBK equations of fractional order using the fractional Laplace Transform. Using the Laplace

transform for fractional PDEs is effortless compared to the Riemann Liouville integral operator for fractional PDEs as well as a system of fractional PDEs.

The fractional-order WBK equations describe the propagation of shallow water waves [8] with different dispersion relations. The WBK equations are of the form:

$$D_t^\alpha u + uu_x + v_x + bu_{xx} = 0$$

$$D_t^\alpha v + (uv)_x + au_{xxx} - bv_{xx} = 0,$$

where  $u(x, t)$  denotes the horizontal velocity,  $v(x, t)$  is the height that deviates from the equilibrium position,  $a, b$  are real constants that are represented in different diffusion powers, and  $D_t^\alpha 0 < \alpha \leq 1$  is the Caputo derivative operator. For  $\alpha = 1$ , we get the usual WBK equations. It is also essential to show that when  $a = 1$  and  $b = 0$ , we have fractional order modified Boussinesq (MB) equation, and when  $a = 0, b = 1/2$ , we get the fractional order approximate long wave (ALW) equation. These equations took the attention of many researchers in recent decades [9–11].

The present paper is divided into five sections. The Fundamental Theory of Proposed Method section is devoted to the analysis of the DJ method as well as the implementation of the Laplace transform for fractional PDEs are given. In the Application of Laplace Transform with DJ method to Fractional Whitham-Broer-Kaup Equations section, the application of Laplace transform to FPDEs are given. In the Results and Discussion section, the results of the proposed method are compared with VIM, ADM, and OHAM solutions for time-fractional WBK, time fractional MB, and time-fractional ALW equations, while in the Conclusion section, the conclusion of the work is given.

## FUNDAMENTAL THEORY OF PROPOSED METHOD

### New Iterative Method [12–16]

Daftardar-Gejji and Jafari consider the following equation [12]:

Consider the equations of the form:

$$v_i = f_i + \varsigma_i(v_1, v_2) + \xi_i(v_1, v_2), \quad i = 1, 2. \tag{1}$$

where  $f_i$  are known functions,  $\varsigma_i, \xi_i$  are linear and non-linear functions of  $v_i$ . Assuming that equation (1) have a solution of the series form:

$$v_i = \sum_{j=0}^{\infty} v_{i,j}, \quad i = 1, 2. \tag{2}$$

Since  $\varsigma_i$  is linear, so we write it as:

$$\varsigma_i \left( \sum_{j=0}^{\infty} (v_{1,j}, v_{2,j}) \right) = \sum_{j=0}^{\infty} \varsigma_i(v_{1,j}, v_{2,j}), \tag{3}$$

Decomposition of non-linear operators is as follows:

$$\xi_i \left( \sum_{j=0}^{\infty} v_{i,j} \right) = \xi_i(v_{1,0}, v_{2,0})$$

$$+ \sum_{j=1}^{\infty} \left\{ \xi_i \left( \sum_{k=0}^j v_{1,k}, \sum_{k=0}^j v_{2,k} \right) - \xi_i \left( \sum_{k=0}^{j-1} v_{1,k}, \sum_{k=0}^{j-1} v_{2,k} \right) \right\},$$

$$= \sum_{j=0}^{\infty} G_{i,j}. \tag{4}$$

where  $G_{i,0} = \xi_i(v_{1,0}, v_{2,0})$  and  $G_{i,j} = \xi_i \left( \sum_{k=0}^j v_{1,k}, \sum_{k=0}^j v_{2,k} \right) - \xi_i \left( \sum_{k=0}^{j-1} v_{1,k}, \sum_{k=0}^{j-1} v_{2,k} \right), j \geq 1. \quad i = 1, 2.$

Hence, equation (1) is equivalent to:

$$\sum_{j=0}^{\infty} v_{i,j} = f_i + \sum_{j=0}^{\infty} \varsigma_i(v_{1,j}, v_{2,j}) + \sum_{j=0}^{\infty} G_{i,j}. \tag{5}$$

Further, the recurrence relation is defined as follows:

$$v_{i,0} = f_i,$$

$$v_{i,1} = \varsigma_i(v_{1,0}, v_{2,0}) + G_{i,0},$$

$$v_{i,2} = \varsigma_i(v_{1,1}, v_{2,1}) + G_{i,1},$$

$$\dots$$

$$v_{i,m+1} = \varsigma_i(v_{1,m}, v_{2,m}) + G_{i,m}, \quad m = 1, 2, \dots \tag{6}$$

The  $k$ th-order approximation is given by:

$$v_i = \sum_{j=0}^{k-1} v_{i,j}.$$

For convergence analysis, we refer to Daftardar-Gejji and Jafari [13] where explanatory example is solved.

### Laplace Transform and Fractional Partial Differential Equations [4]

Consider the following equations:

$$D_t^\alpha v_i(x, t) + \varsigma v_i(x, t) + \xi v_i(x, t) = 0, \tag{7}$$

$0 < \alpha \leq 1,$   
with ICs.

$$v_i(x, 0) = f_i(x). \tag{8}$$

where  $\varsigma$  is the linear operator,  $\xi$  is the non-linear operator, and  $D_t^\alpha v_i(x, t)$  is the Caputo fractional derivative of a function  $v_i(x, t)$ , which is defined as:

$$D_t^\alpha v_i(x, t) = \frac{1}{\Gamma(n - \alpha)} \int_0^t \left( \frac{v_i^n(x, \gamma)}{(t - \gamma)^{\alpha+1-n}} \right) d\gamma, \quad (9)$$

$$L[D_t^\alpha v_i(x, t)] + L[\zeta v_i(x, t)] + L[\xi v_i(x, t)] = 0. \quad (11)$$

$(n - 1 < \alpha \leq n, n \in \mathbb{N})$ .

Using the property of Laplace transform for Caputo fractional derivatives is:

Using equation (10), we have:

$$L[D_t^\alpha v_i] = s^\alpha L[v_i(x, t)] - \sum_{k=0}^{n-1} v_i^k(x, 0^+) s^{\alpha-1-k}. \quad (10)$$

$$L[v_i(x, t)] = \frac{1}{s} v_i(x, 0) - \frac{1}{s^\alpha} L[\zeta v_i(x, t)] - \frac{1}{s^\alpha} L[\xi v_i(x, t)]. \quad (12)$$

Taking the Laplace transform on both sides of equation (10) we get:

Taking the inverse Laplace transform on both sides of equation (12), we get:

**TABLE 1** | Second-order DJ solution for  $u(x, t)$  in comparison with ADM, VIM, and OHAM solutions at  $\alpha = 1$  for WBK equation.

$(x, t)$	Absolute error of ADM [17]	Absolute error of VIM [18]	Absolute error of OHAM [19]	Absolute error of 2nd-order NIM
(0.1,0.1)	$1.04892 \times 10^{-4}$	$1.23033 \times 10^{-4}$	$1.07078 \times 10^{-4}$	$1.67111 \times 10^{-12}$
(0.1,0.3)	$9.64474 \times 10^{-5}$	$3.69597 \times 10^{-4}$	$3.04565 \times 10^{-4}$	$4.51196 \times 10^{-11}$
(0.1,0.5)	$8.88312 \times 10^{-5}$	$6.16873 \times 10^{-4}$	$4.81303 \times 10^{-4}$	$2.08888 \times 10^{-10}$
(0.2,0.1)	$4.25408 \times 10^{-4}$	$1.19869 \times 10^{-4}$	$1.04388 \times 10^{-4}$	$1.57879 \times 10^{-12}$
(0.2,0.3)	$3.91098 \times 10^{-4}$	$3.60098 \times 10^{-4}$	$2.97260 \times 10^{-4}$	$4.26227 \times 10^{-11}$
(0.2,0.5)	$3.60161 \times 10^{-4}$	$6.01006 \times 10^{-4}$	$4.70138 \times 10^{-4}$	$1.97328 \times 10^{-10}$
(0.3,0.1)	$9.71922 \times 10^{-4}$	$1.16789 \times 10^{-4}$	$1.01776 \times 10^{-4}$	$1.49181 \times 10^{-12}$
(0.3,0.3)	$8.93309 \times 10^{-4}$	$3.50866 \times 10^{-4}$	$2.90150 \times 10^{-4}$	$4.02799 \times 10^{-11}$
(0.3,0.5)	$8.22452 \times 10^{-4}$	$5.85610 \times 10^{-4}$	$4.59590 \times 10^{-4}$	$1.86481 \times 10^{-10}$
(0.4,0.1)	$1.75596 \times 10^{-3}$	$1.13829 \times 10^{-4}$	$9.92418 \times 10^{-5}$	$1.41043 \times 10^{-12}$
(0.4,0.3)	$1.61430 \times 10^{-3}$	$3.41948 \times 10^{-4}$	$2.83229 \times 10^{-4}$	$3.80803 \times 10^{-11}$
(0.4,0.5)	$1.48578 \times 10^{-3}$	$5.70710 \times 10^{-4}$	$4.49118 \times 10^{-4}$	$1.76298 \times 10^{-10}$
(0.5,0.1)	$2.79519 \times 10^{-3}$	$1.10936 \times 10^{-4}$	$9.67808 \times 10^{-4}$	$1.33388 \times 10^{-12}$
(0.5,0.3)	$2.56714 \times 10^{-3}$	$3.33274 \times 10^{-4}$	$2.76492 \times 10^{-4}$	$3.60145 \times 10^{-11}$
(0.5,0.5)	$2.36184 \times 10^{-3}$	$5.56235 \times 10^{-4}$	$4.38895 \times 10^{-4}$	$1.66734 \times 10^{-10}$

**TABLE 2** | Second-order DJ solution for  $u(x, t)$  in comparison with ADM, VIM, and OHAM solutions at  $\alpha = 1$  for MB equation.

$(x, t)$	Absolute error of ADM [17]	Absolute error of VIM [18]	Absolute error of OHAM [19]	Absolute error of 2nd-order NIM
(0.1,0.1)	$8.16297 \times 10^{-7}$	$6.35269 \times 10^{-5}$	$6.35267 \times 10^{-5}$	$4.57301 \times 10^{-13}$
(0.1,0.3)	$7.64245 \times 10^{-7}$	$1.90854 \times 10^{-4}$	$1.90854 \times 10^{-4}$	$1.23478 \times 10^{-11}$
(0.1,0.5)	$7.16083 \times 10^{-7}$	$3.18549 \times 10^{-4}$	$3.18548 \times 10^{-4}$	$5.71662 \times 10^{-11}$
(0.2,0.1)	$3.26243 \times 10^{-6}$	$6.18930 \times 10^{-5}$	$6.18931 \times 10^{-5}$	$4.32265 \times 10^{-13}$
(0.2,0.3)	$3.05458 \times 10^{-6}$	$1.85945 \times 10^{-4}$	$1.85945 \times 10^{-4}$	$1.16698 \times 10^{-11}$
(0.2,0.5)	$2.86226 \times 10^{-6}$	$3.10352 \times 10^{-4}$	$3.10352 \times 10^{-4}$	$5.40272 \times 10^{-11}$
(0.3,0.1)	$7.33445 \times 10^{-6}$	$6.03095 \times 10^{-5}$	$6.03098 \times 10^{-5}$	$4.08618 \times 10^{-13}$
(0.3,0.3)	$6.86758 \times 10^{-6}$	$1.81187 \times 10^{-4}$	$1.81187 \times 10^{-4}$	$1.10335 \times 10^{-11}$
(0.3,0.5)	$6.43557 \times 10^{-6}$	$3.02408 \times 10^{-4}$	$3.02408 \times 10^{-4}$	$5.10809 \times 10^{-11}$
(0.4,0.1)	$1.30286 \times 10^{-5}$	$5.87746 \times 10^{-5}$	$5.87749 \times 10^{-5}$	$3.86524 \times 10^{-13}$
(0.4,0.3)	$1.22000 \times 10^{-5}$	$1.76574 \times 10^{-4}$	$1.76574 \times 10^{-4}$	$1.04358 \times 10^{-11}$
(0.4,0.5)	$1.14333 \times 10^{-5}$	$2.94707 \times 10^{-4}$	$2.94708 \times 10^{-4}$	$4.83143 \times 10^{-11}$
(0.5,0.1)	$2.03415 \times 10^{-5}$	$5.72867 \times 10^{-5}$	$5.72865 \times 10^{-4}$	$3.65707 \times 10^{-13}$
(0.5,0.3)	$1.90489 \times 10^{-5}$	$1.72102 \times 10^{-4}$	$1.72102 \times 10^{-4}$	$9.87438 \times 10^{-12}$
(0.5,0.5)	$1.78528 \times 10^{-5}$	$2.87241 \times 10^{-4}$	$2.87240 \times 10^{-4}$	$4.5715 \times 10^{-11}$

$$v_i(x, t) = v_i(x, 0) - L^{-1}\left[\frac{1}{s^\alpha}L[\zeta v_i(x, t)]\right] - L^{-1}\left[\frac{1}{s^\alpha}L[\xi v_i(x, t)]\right]. \tag{13}$$

$$\begin{aligned} D_t^\alpha u + uu_x + v_x + bu_{xx} &= 0, \\ D_t^\alpha v + (uv)_x + au_{xxx} - bv_{xx} &= 0. \end{aligned} \tag{14}$$

Subject to ICs

Now, we apply a new iterative technique that was derived in the New Iterative Method section.

### APPLICATION OF LAPLACE TRANSFORM WITH DJ METHOD TO FRACTIONAL WHITHAM-BROER-KAUP EQUATIONS

$$\begin{aligned} u(x, 0) &= \lambda - 2Bk \coth(k\xi), \\ v(x, 0) &= -2B(B + b)k^2 \operatorname{csch}^2(k\xi), \end{aligned} \tag{15}$$

where  $\beta = \sqrt{a + b^2}$ ,  $\xi = x + \text{cand } \lambda, c, k$ , are any constants. For  $\alpha = 1$ , the exact solution of the system is as follows:

#### Problem 3.1: Time Fractional WBK Equation

**TABLE 3 |** Second-order DJ solution for  $u(x, t)$  in comparison with ADM, VIM, and OHAM solutions at  $\alpha = 1$  for ALW equation.

$(x, t)$	Absolute error of ADM [17]	Absolute error of VIM [18]	Absolute error of OHAM [19]	Absolute error of 2nd-order NIM
(0.1,0.1)	$8.02989 \times 10^{-6}$	$3.17634 \times 10^{-5}$	$3.17634 \times 10^{-5}$	$1.20348 \times 10^{-13}$
(0.1,0.3)	$7.38281 \times 10^{-6}$	$9.54273 \times 10^{-5}$	$9.54269 \times 10^{-5}$	$3.25026 \times 10^{-12}$
(0.1,0.5)	$6.79923 \times 10^{-6}$	$1.59274 \times 10^{-4}$	$1.59274 \times 10^{-4}$	$1.50478 \times 10^{-11}$
(0.2,0.1)	$3.23228 \times 10^{-5}$	$3.09466 \times 10^{-5}$	$3.09465 \times 10^{-5}$	$1.13895 \times 10^{-13}$
(0.2,0.3)	$2.97172 \times 10^{-5}$	$9.29725 \times 10^{-5}$	$9.29723 \times 10^{-5}$	$3.07447 \times 10^{-12}$
(0.2,0.5)	$2.73673 \times 10^{-5}$	$1.55176 \times 10^{-4}$	$1.55176 \times 10^{-4}$	$1.42339 \times 10^{-11}$
(0.3,0.1)	$7.32051 \times 10^{-5}$	$3.01549 \times 10^{-5}$	$3.01549 \times 10^{-5}$	$1.07747 \times 10^{-13}$
(0.3,0.3)	$6.73006 \times 10^{-5}$	$9.05935 \times 10^{-5}$	$9.05932 \times 10^{-5}$	$2.90939 \times 10^{-12}$
(0.3,0.5)	$6.19760 \times 10^{-5}$	$1.51204 \times 10^{-4}$	$1.51204 \times 10^{-4}$	$1.34695 \times 10^{-11}$
(0.4,0.1)	$1.31032 \times 10^{-4}$	$2.93874 \times 10^{-5}$	$2.93874 \times 10^{-5}$	$1.02029 \times 10^{-13}$
(0.4,0.3)	$1.20455 \times 10^{-4}$	$8.82871 \times 10^{-5}$	$8.82870 \times 10^{-5}$	$2.75424 \times 10^{-12}$
(0.4,0.5)	$1.10919 \times 10^{-4}$	$1.47354 \times 10^{-4}$	$1.47354 \times 10^{-4}$	$1.27514 \times 10^{-11}$
(0.5,0.1)	$2.06186 \times 10^{-4}$	$2.86433 \times 10^{-5}$	$2.86432 \times 10^{-5}$	$9.66033 \times 10^{-14}$
(0.5,0.3)	$1.89528 \times 10^{-4}$	$8.60509 \times 10^{-5}$	$8.60506 \times 10^{-5}$	$2.60846 \times 10^{-12}$
(0.5,0.5)	$1.74510 \times 10^{-4}$	$1.43620 \times 10^{-4}$	$1.43620 \times 10^{-4}$	$1.20763 \times 10^{-11}$

**TABLE 4 |** Second-order DJ solution for  $v(x, t)$  in comparison with ADM, VIM, and OHAM solutions at  $\alpha = 1$  for WBK equation.

$(x, t)$	Absolute error of ADM [17]	Absolute error of VIM [18]	Absolute error of OHAM [19]	Absolute error of 2nd-order NIM
(0.1,0.1)	$6.41419 \times 10^{-3}$	$1.10430 \times 10^{-4}$	$5.86860 \times 10^{-5}$	$3.28081 \times 10^{-12}$
(0.1,0.3)	$5.99783 \times 10^{-3}$	$3.31865 \times 10^{-4}$	$3.04565 \times 10^{-4}$	$8.85812 \times 10^{-11}$
(0.1,0.5)	$5.61507 \times 10^{-3}$	$5.54071 \times 10^{-4}$	$3.08812 \times 10^{-4}$	$4.10099 \times 10^{-10}$
(0.2,0.1)	$1.33181 \times 10^{-2}$	$1.07016 \times 10^{-4}$	$5.56884 \times 10^{-5}$	$3.07768 \times 10^{-12}$
(0.2,0.3)	$1.24441 \times 10^{-2}$	$3.21601 \times 10^{-4}$	$2.97260 \times 10^{-4}$	$8.30963 \times 10^{-11}$
(0.2,0.5)	$1.16416 \times 10^{-2}$	$5.36927 \times 10^{-4}$	$2.92626 \times 10^{-4}$	$3.84706 \times 10^{-10}$
(0.3,0.1)	$2.07641 \times 10^{-2}$	$1.03737 \times 10^{-4}$	$5.28609 \times 10^{-5}$	$2.88849 \times 10^{-12}$
(0.3,0.3)	$1.93852 \times 10^{-2}$	$3.11737 \times 10^{-4}$	$2.90150 \times 10^{-4}$	$7.79908 \times 10^{-11}$
(0.3,0.5)	$1.81209 \times 10^{-2}$	$5.20447 \times 10^{-4}$	$2.77382 \times 10^{-4}$	$3.6107 \times 10^{-10}$
(0.4,0.1)	$2.88100 \times 10^{-2}$	$1.00579 \times 10^{-4}$	$5.01929 \times 10^{-5}$	$2.71246 \times 10^{-12}$
(0.4,0.3)	$2.68724 \times 10^{-2}$	$3.02245 \times 10^{-4}$	$2.83229 \times 10^{-4}$	$7.32356 \times 10^{-11}$
(0.4,0.5)	$2.50985 \times 10^{-2}$	$5.04593 \times 10^{-4}$	$2.63019 \times 10^{-4}$	$3.39055 \times 10^{-10}$
(0.5,0.1)	$3.75193 \times 10^{-2}$	$9.75385 \times 10^{-5}$	$4.76741 \times 10^{-5}$	$2.54828 \times 10^{-12}$
(0.5,0.3)	$3.49617 \times 10^{-2}$	$2.93107 \times 10^{-4}$	$2.76492 \times 10^{-4}$	$6.88039 \times 10^{-11}$
(0.5,0.5)	$3.26239 \times 10^{-2}$	$4.89335 \times 10^{-4}$	$2.49480 \times 10^{-4}$	$3.18537 \times 10^{-10}$

Now, using the basic idea of the DJ method discussed in the Fundamental Theory of Proposed Method section, we have:

$$\begin{aligned}
 u(x, t) &= \lambda - 2Bk \coth(k(\xi - \lambda t)), \\
 v(x, t) &= -2B(B + b)k^2 \operatorname{csch}^2(k(\xi - \lambda t)).
 \end{aligned}
 \tag{16}$$

Applying Laplace transform and inverse Laplace transform to equation (3.1), we have:

$$\begin{aligned}
 u(x, t) &= u(x, 0) \\
 &+ L^{-1} \left[ \frac{1}{s^\alpha} L \left[ - \left( u(x, t) u_x(x, t) + v_x(x, t) + b u_{xx}(x, t) \right) \right] \right], \\
 v(x, t) &= v(x, 0) + L^{-1} \left[ \frac{1}{s^\alpha} L \left[ - \left( (u(x, t) v(x, t))_x \right. \right. \right. \\
 &\left. \left. \left. + a u_{xxx}(x, t) - b v_{xx}(x, t) \right) \right] \right].
 \end{aligned}
 \tag{17}$$

$$\begin{aligned}
 u_0 &= \lambda - 2Bk \coth(k\xi), \\
 v_0 &= -2B(B + b)k^2 \operatorname{csch}^2(k\xi),
 \end{aligned}
 \tag{18}$$

$$u_1 = \frac{-2Bk^2 t^\alpha \lambda \operatorname{csc} h^2(k(x + c))}{\Gamma(1 + \alpha)},
 \tag{19}$$

$$\begin{aligned}
 v_1 &= \frac{1}{\Gamma(1 + \alpha)} 4Bk^3 t^\alpha \operatorname{csc} h^2(k(x + c)) (- (b + B) \lambda \coth(k(x + c)) \\
 &- (a + b^2 - B^2) k (2 + 3 \operatorname{csc} h^2(k(c + x))),
 \end{aligned}
 \tag{20}$$

**TABLE 5** | Second-order DJ solution for  $v(x, t)$  in comparison with ADM, VIM, and OHAM solutions at  $\alpha = 1$  for MB equation.

$(x, t)$	Absolute error of ADM [17]	Absolute error of VIM [18]	Absolute error of OHAM [19]	Absolute error of 2nd-order NIM
(0.1,0.1)	$5.88676 \times 10^{-5}$	$1.65942 \times 10^{-5}$	$1.65942 \times 10^{-5}$	$2.59213 \times 10^{-13}$
(0.1,0.3)	$5.56914 \times 10^{-5}$	$4.98691 \times 10^{-5}$	$4.98691 \times 10^{-5}$	$6.99872 \times 10^{-12}$
(0.1,0.5)	$5.27169 \times 10^{-5}$	$8.32598 \times 10^{-5}$	$8.26491 \times 10^{-4}$	$3.24016 \times 10^{-11}$
(0.2,0.1)	$1.18213 \times 10^{-4}$	$1.60813 \times 10^{-5}$	$1.60812 \times 10^{-5}$	$2.43233 \times 10^{-13}$
(0.2,0.3)	$1.11833 \times 10^{-4}$	$4.83269 \times 10^{-5}$	$4.83269 \times 10^{-5}$	$6.56712 \times 10^{-12}$
(0.2,0.5)	$1.05858 \times 10^{-4}$	$8.06837 \times 10^{-5}$	$7.94290 \times 10^{-4}$	$3.04035 \times 10^{-11}$
(0.3,0.1)	$1.78041 \times 10^{-4}$	$1.55880 \times 10^{-5}$	$1.55880 \times 10^{-5}$	$2.28336 \times 10^{-13}$
(0.3,0.3)	$1.68429 \times 10^{-4}$	$4.68440 \times 10^{-5}$	$4.68439 \times 10^{-5}$	$6.16531 \times 10^{-12}$
(0.3,0.5)	$1.59428 \times 10^{-4}$	$7.82068 \times 10^{-5}$	$7.63646 \times 10^{-4}$	$2.85432 \times 10^{-11}$
(0.4,0.1)	$2.38356 \times 10^{-4}$	$1.51135 \times 10^{-5}$	$1.51135 \times 10^{-5}$	$2.14485 \times 10^{-13}$
(0.4,0.3)	$2.25483 \times 10^{-4}$	$4.54174 \times 10^{-5}$	$4.54174 \times 10^{-5}$	$5.79099 \times 10^{-12}$
(0.4,0.5)	$2.13430 \times 10^{-4}$	$7.58243 \times 10^{-5}$	$7.34471 \times 10^{-4}$	$2.68103 \times 10^{-11}$
(0.5,0.1)	$2.99162 \times 10^{-4}$	$1.46569 \times 10^{-5}$	$1.46569 \times 10^{-5}$	$2.01559 \times 10^{-13}$
(0.5,0.3)	$2.83001 \times 10^{-4}$	$4.40448 \times 10^{-5}$	$4.40448 \times 10^{-5}$	$5.44208 \times 10^{-12}$
(0.5,0.5)	$2.67868 \times 10^{-4}$	$7.35317 \times 10^{-5}$	$7.06678 \times 10^{-4}$	$2.51949 \times 10^{-11}$

**TABLE 6** | Second-order DJ solution for  $v(x, t)$  in comparison with second-order ADM, VIM, and OHAM solutions at  $\alpha = 1$  for ALW equation.

$(x, t)$	Absolute error of ADM [17]	Absolute error of VIM [18]	Absolute error of OHAM [19]	Absolute error of 2nd-order NIM
(0.1,0.1)	$4.81902 \times 10^{-4}$	$8.29712 \times 10^{-6}$	$8.29711 \times 10^{-6}$	$6.71962 \times 10^{-14}$
(0.1,0.3)	$4.50818 \times 10^{-4}$	$2.49346 \times 10^{-5}$	$2.49345 \times 10^{-5}$	$1.81427 \times 10^{-12}$
(0.1,0.5)	$4.22221 \times 10^{-4}$	$4.16299 \times 10^{-5}$	$4.16298 \times 10^{-5}$	$8.39947 \times 10^{-12}$
(0.2,0.1)	$9.76644 \times 10^{-4}$	$8.04063 \times 10^{-6}$	$8.04063 \times 10^{-6}$	$6.30876 \times 10^{-14}$
(0.2,0.3)	$9.13502 \times 10^{-4}$	$2.41634 \times 10^{-5}$	$2.41634 \times 10^{-5}$	$1.70328 \times 10^{-12}$
(0.2,0.5)	$8.55426 \times 10^{-4}$	$4.03419 \times 10^{-5}$	$4.03418 \times 10^{-5}$	$7.88563 \times 10^{-12}$
(0.3,0.1)	$1.48482 \times 10^{-3}$	$7.79401 \times 10^{-6}$	$7.79400 \times 10^{-6}$	$5.92521 \times 10^{-14}$
(0.3,0.3)	$1.38858 \times 10^{-3}$	$2.34220 \times 10^{-5}$	$2.34219 \times 10^{-5}$	$1.59992 \times 10^{-12}$
(0.3,0.5)	$1.30009 \times 10^{-3}$	$3.91034 \times 10^{-5}$	$3.91034 \times 10^{-5}$	$7.40708 \times 10^{-12}$
(0.4,0.1)	$2.00705 \times 10^{-3}$	$7.55675 \times 10^{-6}$	$7.55675 \times 10^{-6}$	$5.56907 \times 10^{-14}$
(0.4,0.3)	$1.87661 \times 10^{-3}$	$2.27087 \times 10^{-5}$	$2.27087 \times 10^{-5}$	$1.50359 \times 10^{-12}$
(0.4,0.5)	$1.75670 \times 10^{-3}$	$3.79121 \times 10^{-5}$	$3.79121 \times 10^{-5}$	$6.96112 \times 10^{-12}$
(0.5,0.1)	$2.54396 \times 10^{-3}$	$7.32847 \times 10^{-6}$	$7.32846 \times 10^{-6}$	$5.23618 \times 10^{-14}$
(0.5,0.3)	$2.37815 \times 10^{-3}$	$2.20224 \times 10^{-5}$	$2.20224 \times 10^{-5}$	$1.41377 \times 10^{-12}$
(0.5,0.5)	$2.22578 \times 10^{-3}$	$3.67658 \times 10^{-5}$	$3.67658 \times 10^{-5}$	$6.54527 \times 10^{-12}$

$$u_2 = \frac{1}{(\Gamma(1 + \alpha))^2 \Gamma(1 + 2\alpha) \Gamma(1 + 3\alpha)} (2Bk^3 t^{2\alpha} \coth(k(x+c)) \csc h^4(k(x+c)) (4Bk^2 t^\alpha \lambda^2 (\Gamma(1 + 2\alpha))^2 + (-20(a + b^2 - B^2)k^2 + \lambda^2 - (4(a + b^2 - B^2)k^2 + \lambda^2) \cos h(2k(x+c))) (\Gamma(1 + \alpha))^2 \Gamma(1 + 3\alpha))), \tag{21}$$

$$v_2 = Bk^4 t^{2\alpha} \csc h^6(k(x+c)) \left[ \frac{1}{\sqrt{\pi} \Gamma(1 + \alpha) \Gamma(1 + 3\alpha)} 2^{3+2\alpha} Bk^2 t^\alpha \lambda \csc h(k(x+c)) \right]$$

$$\begin{aligned} & \Gamma\left(\frac{1}{2} + \alpha\right) (16(a + b^2 - B^2)k \cosh(k(x+c)) \\ & + 2(a + b^2 - B^2)k \cosh(3k(x+c)) \\ & + (b + B)\lambda(2 \sinh(k(c+x)) + \sinh(3k(x+c)))) \\ & - \frac{1}{\Gamma(1 + 2\alpha)} (12(11b - 5B)(a + b^2 - B^2)k^2 \\ & - 3(b + B)\lambda^2 + 2(4(13b - 7B)(a + b^2 - B^2)k^2 \\ & + (b + B)\lambda^2) \cosh(2k(x+c)) + (4(b - B)(a + b^2 - B^2)k^2 \\ & + (b + B)\lambda^2) \cosh(4k(x+c)) \\ & + 4(a + b^2 - B^2)k\lambda(10 \sinh(2k(x+c)) + \sinh(4k(x+c))))]. \end{aligned} \tag{22}$$

Three terms approximate the solution for equation (14):

$$\begin{aligned} u &= u_0 + u_1 + u_2, \\ v &= v_0 + v_1 + v_2. \end{aligned} \tag{23}$$

We take  $k = 0.1, \lambda = 0.005, a = b = 1.5$  and  $c = 10$  in the above problem.

**Problem 3.2:** Time Fractional MB Equation

$$\begin{aligned} D_t^\alpha u + uu_x + v_x &= 0, \\ D_t^\alpha v + (uv)_x + u_{xxx} &= 0, \end{aligned} \tag{24}$$

Subject to ICs

$$\begin{aligned} u(x, 0) &= \lambda - 2k \coth(k\xi), \\ v(x, 0) &= -2k^2 \csc h^2(k\xi). \end{aligned} \tag{25}$$

where  $\xi = x + c$  and  $k, \lambda, c$  are arbitrary constants.

For  $\alpha = 1$ , the exact solution of the system is as follows:

$$\begin{aligned} u(x, t) &= \lambda - 2k \coth(k(\xi - \lambda t)), \\ v(x, t) &= -2k^2 \csc h^2(k(\xi - \lambda t)). \end{aligned} \tag{26}$$

According to the DJ method described in the Fundamental Theory of Proposed Method section, we have:

$$\begin{aligned} u(x, t) &= u(x, 0) + L^{-1} \left[ \frac{1}{S^\alpha} L[-(u(x, t)u_x(x, t) + v_x(x, t))] \right], \\ v(x, t) &= v(x, 0) + L^{-1} \left[ \frac{1}{S^\alpha} L[-((u(x, t)v(x, t))_x + u_{xxx}(x, t))] \right], \end{aligned} \tag{27}$$

so that

$$\begin{aligned} u_0 &= \lambda - 2k \coth(k(x+c)), \\ v_0 &= -2k^2 \csc h^2(k(x+c)), \end{aligned} \tag{28}$$

$$u_1 = -\frac{2k^2 t^\alpha \lambda \csc h^2(k(x+c))}{\Gamma(1 + \alpha)}, \tag{29}$$

$$v_1 = -\frac{4k^3 t^\alpha \lambda \coth(k(x+c)) \csc h^2(k(x+c))}{\Gamma(1 + \alpha)}, \tag{30}$$

$$\begin{aligned} u_2 &= \frac{2k^3 t^{2\alpha} \lambda^2 \csc h^4(k(x+c))}{\Gamma(1 + 2\alpha)} \left\{ \frac{4k^2 t^\alpha \coth(k(x+c)) (\Gamma(1 + 2\alpha))^2}{(\Gamma(1 + \alpha))^2 \Gamma(1 + 3\alpha)} \right. \\ & \left. - \sinh(2k(x+c)) \right\}, \end{aligned} \tag{31}$$

$$\begin{aligned} v_2 &= \frac{4k^4 t^{2\alpha} \lambda^2 \csc h^4(k(x+c))}{\Gamma(1 + 2\alpha)} \{-2 - \cosh(2k(x+c)) + \\ & \frac{2k^2 t^\alpha (3 + 2 \cosh(2k(x+c))) \csc h^2(k(x+c)) (\Gamma(1 + 2\alpha))^2}{(\Gamma(1 + \alpha))^2 \Gamma(1 + 3\alpha)}\}. \end{aligned} \tag{32}$$

Three terms approximate the solution for equation (25):

$$\begin{aligned} u &= u_0 + u_1 + u_2, \\ v &= v_0 + v_1 + v_2. \end{aligned} \tag{33}$$

**Problem 3.3:** Time Fractional ALW Equation

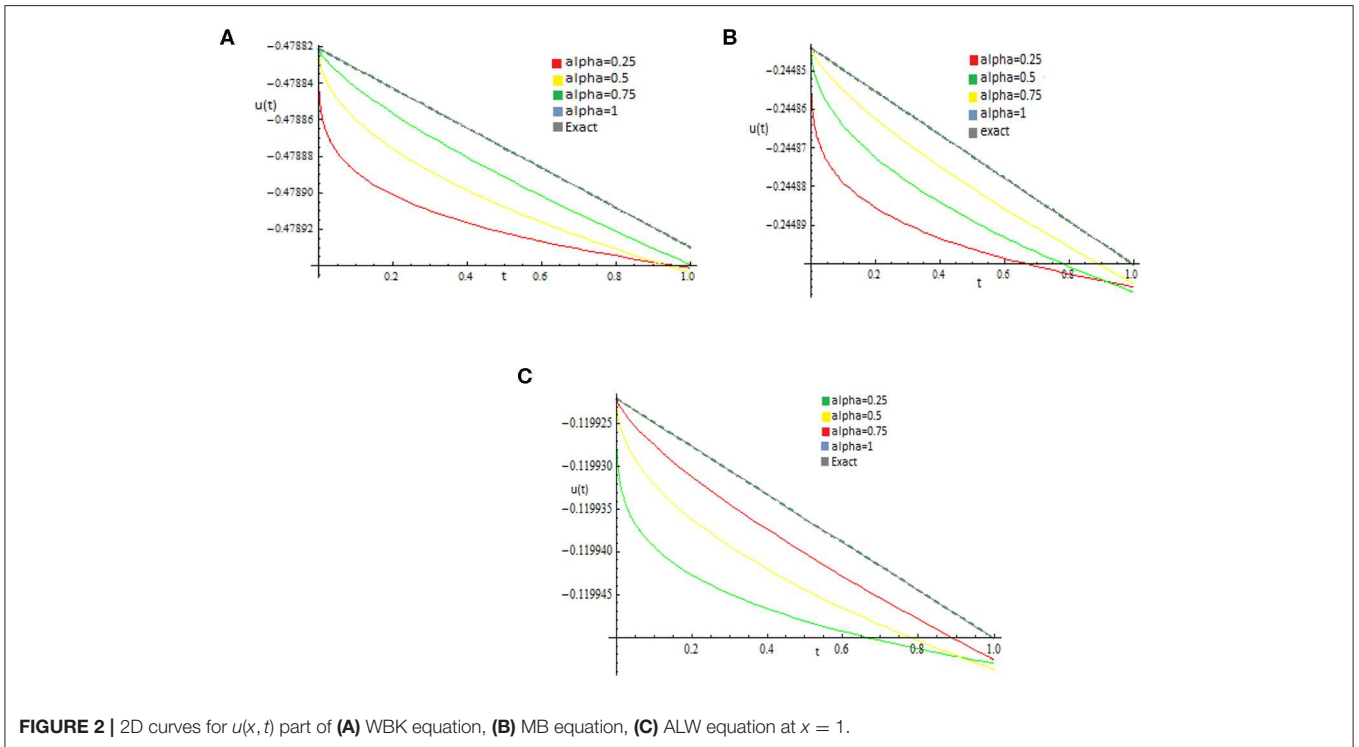
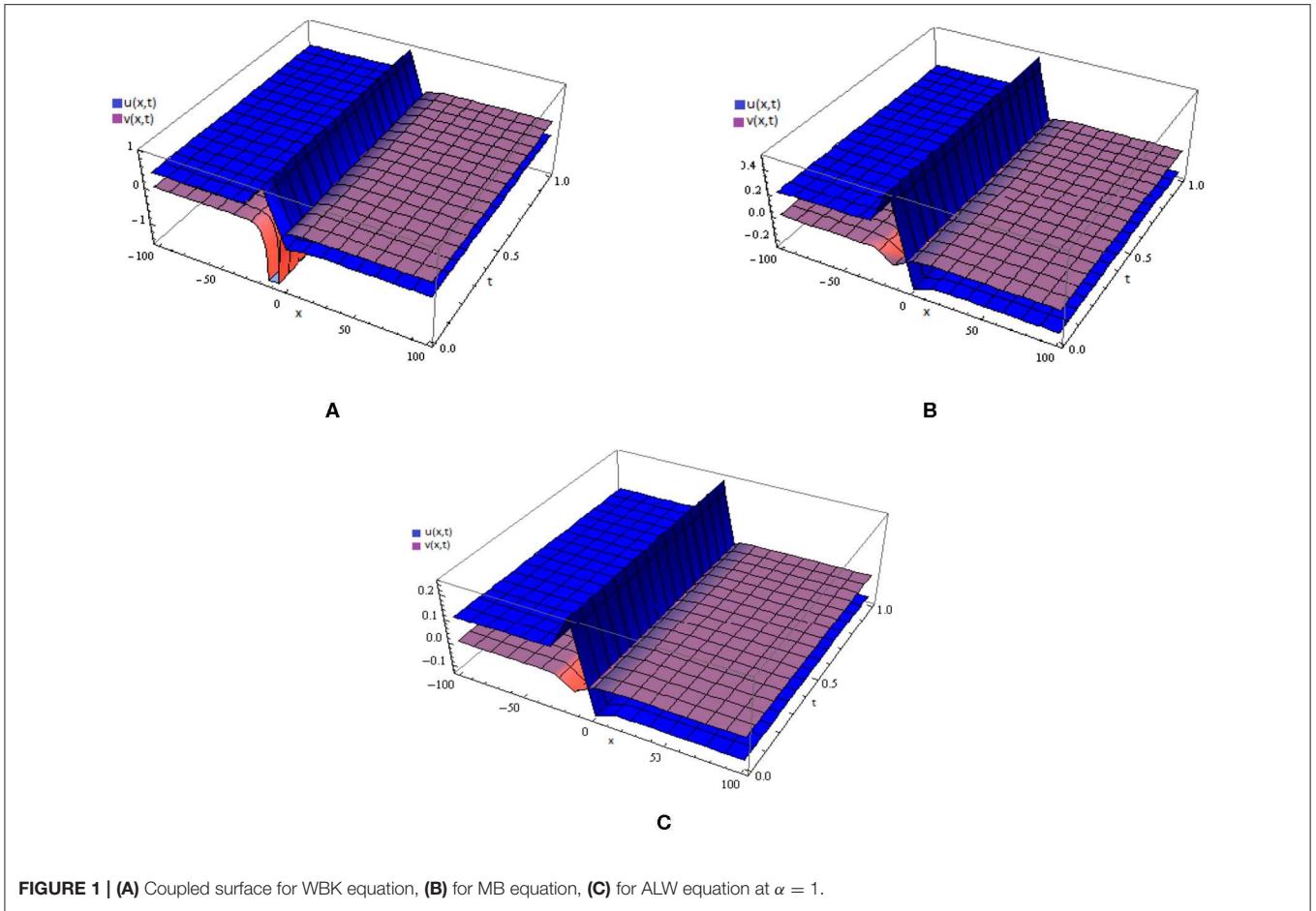
$$\begin{aligned} D_t^\alpha u + uu_x + \frac{1}{2} u_{xx} + v_x &= 0, \\ D_t^\alpha v + (uv)_x - \frac{1}{2} v_{xx} &= 0, \end{aligned} \tag{34}$$

subject to Ics

$$\begin{aligned} u(x, 0) &= \lambda - k \coth(k\xi), \\ v(x, 0) &= -k^2 \csc h^2(k\xi). \end{aligned} \tag{35}$$

where  $\xi = x + c$  and  $\lambda, c, k$  are arbitrary constants.

For  $\alpha = 1$ , the exact solution of the system is as follows:



$$\begin{aligned} u(x, t) &= \lambda - k \coth(k(\xi - \lambda t)), \\ v(x, t) &= -k^2 \csc h^2(k(\xi - \lambda t)). \end{aligned} \tag{36}$$

According to the DJ method described in the Fundamental Theory of Proposed Method section, we have:

$$\begin{aligned} u(x, t) &= u(x, 0) \\ &+ L^{-1} \left[ \frac{1}{S^\alpha} L[-(u(x, t)u_x(x, t) + v_x(x, t) + \frac{1}{2}u_{xx}(x, t))] \right], \\ v(x, t) &= v(x, 0) + L^{-1} \left[ \frac{1}{S^\alpha} L[-((u(x, t)v(x, t))_x - \frac{1}{2}v_{xx}(x, t))] \right]. \end{aligned} \tag{37}$$

So that

$$\begin{aligned} u_0 &= \lambda - k \coth(k(x + c)), \\ v_0 &= -k^2 \csc h^2(k(x + c)), \end{aligned} \tag{38}$$

$$u_1 = -\frac{k^2 t^\alpha \lambda \csc h^2(k(x + c))}{\Gamma(1 + \alpha)}, \tag{39}$$

$$v_1 = -\frac{2k^3 t^\alpha \lambda \coth(k(x + c)) \csc h^2(k(x + c))}{\Gamma(1 + \alpha)}, \tag{40}$$

$$\begin{aligned} u_2 &= \frac{1}{\Gamma(1 + 2\alpha)} k^3 t^{2\alpha} \lambda^2 \csc h^4(k(x + c)) \\ &\left\{ \frac{2k^2 t^\alpha \coth(k(x + c))(\Gamma(1 + 2\alpha))^2}{(\Gamma(1 + \alpha))^2 \Gamma(1 + 3\alpha)} - \sinh(2k(c + x)) \right\}, \end{aligned} \tag{41}$$

$$\begin{aligned} v_2 &= \frac{2k^4 t^{2\alpha} \lambda^2 \csc h^4(k(x + c))}{\Gamma(1 + 2\alpha)} \{-2 - \cosh(2k(x + c))\} \\ &+ \frac{1}{(\Gamma(1 + \alpha))^2 \Gamma(1 + 3\alpha)} (k^2 t^\alpha \\ &(3 + 2 \cosh(2k(x + c))) \csc h^2(k(x + c))(\Gamma(1 + 2\alpha))^2). \end{aligned} \tag{42}$$

Three terms approximate the solution for equation (26):

$$\begin{aligned} u &= u_0 + u_1 + u_2, \\ v &= v_0 + v_1 + v_2. \end{aligned} \tag{43}$$

Values of the parameters are taken to be same as problem 3.1.

## RESULTS AND DISCUSSION

The DJ method is experienced upon the fractional WBK, MB, and ALW equations. Mathematical 7 have been used for most computations.

Tables 1–3 show the estimation of absolute errors of the second-order DJ solution with ADM, VIM, and second-order OHAM solutions for  $u(x, t)$  of fractional WBK, MB, and ALW equations at  $\alpha = 1$ , respectively. Tables 4–6 shows the estimation of absolute errors of second-order DJ solution with ADM, VIM, and second-order OHAM solutions for  $v(x, t)$  of fractional WBK, MB, and ALW equations at  $\alpha = 1$ , respectively. The tabulated results show that the second-order approximate solutions by the DJ method are

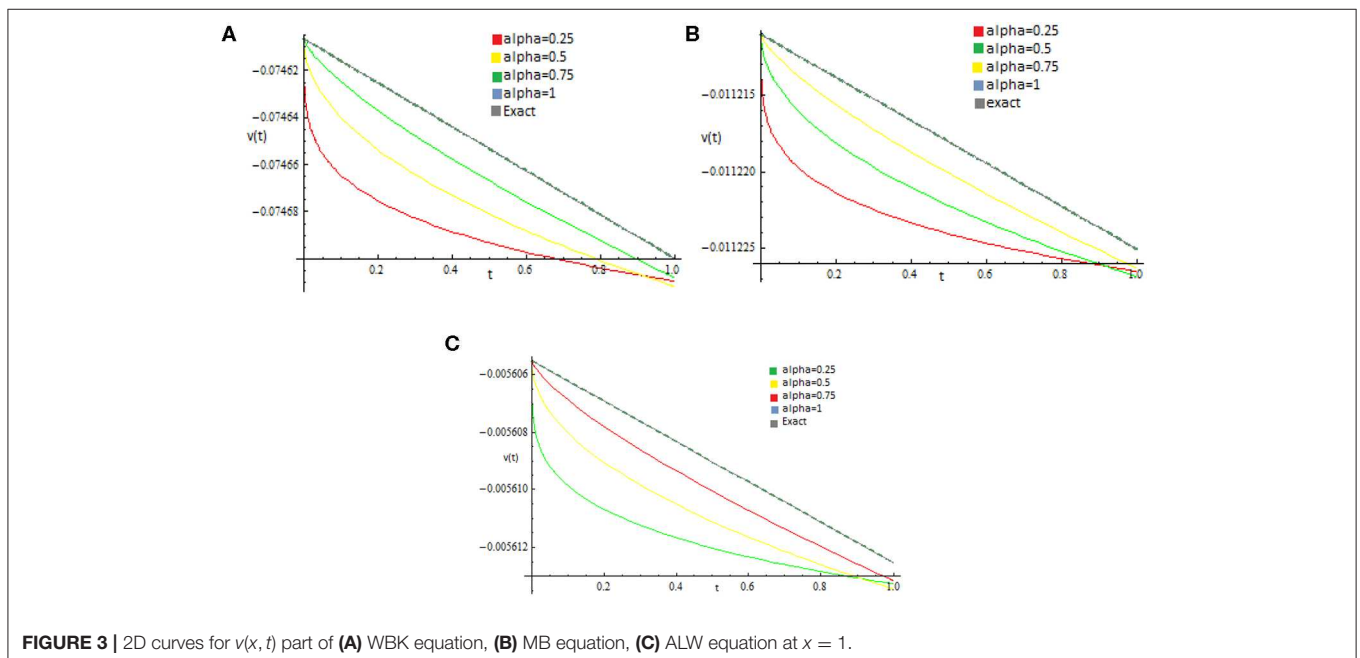
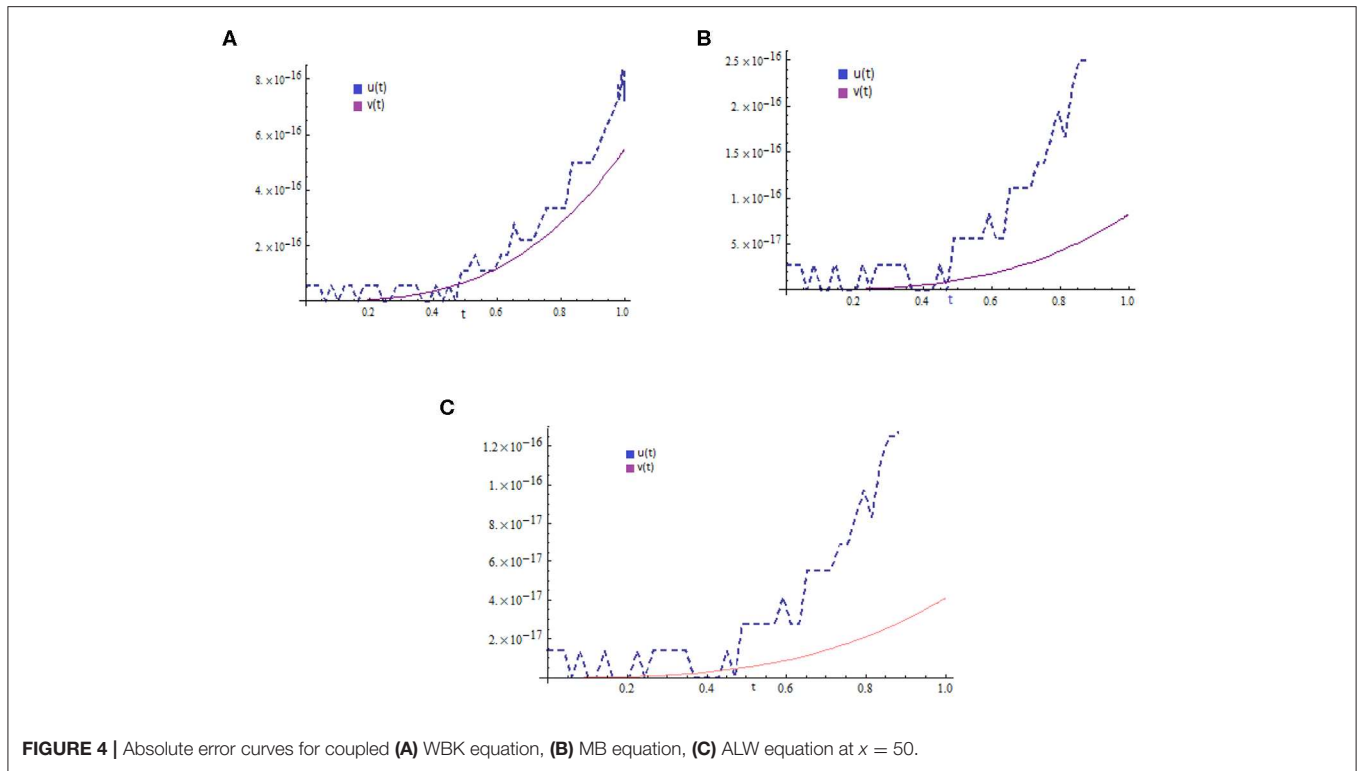


FIGURE 3 | 2D curves for  $v(x, t)$  part of (A) WBK equation, (B) MB equation, (C) ALW equation at  $x = 1$ .



closer to exact solutions than those of ADM, VIM, and OHAM solutions.

**Figures 1A–C** show the coupled surface of the second-order approximate solution by NIM for  $u(x, t)$  and  $v(x, t)$ , part of WBK, MB, and ALW equations at  $\alpha = 1$ , respectively. **Figures 2, 3** show the 2D plots of the second-order approximate solution by NIM for  $u(x, t)$  and  $v(x, t)$  of WBK, MB, and ALW equations at  $x = 1$  and different values of  $\alpha$ , respectively. **Figures 4A–C** show the absolute error graph for the coupled WBK, MB, and ALW equation at  $x = 50$ .

It is clear from 2D figures that as the value of  $\alpha$  increases to 1, the approximate solutions tend closer to the exact solution.

## CONCLUSION

The DJ method converges rapidly to the exact solution at lower order of approximations for the WBK system. The results obtained by the proposed method are very encouraging in assessment with ADM, VIM, and OHAM. As a result, it would be more appealing for researchers to apply this method for solving systems of non-linear PDEs in different fields of science especially in fluid dynamics and physics. The accurateness of the technique can more be improved by taking higher-order estimation of the proposed method.

## DATA AVAILABILITY STATEMENT

All data and related metadata underlying the findings is reported in a submitted article.

## AUTHOR CONTRIBUTIONS

RN and PK developed the numerical method and led the manuscript preparation. ZS and SF contributed to the code development and to the article preparation. MS and WD contributed to the analysis and discussion of the results and help in revision. All authors listed have made a substantial, direct and intellectual contribution to the work, and approved it for publication.

## FUNDING

This research was funded by the Center of Excellence in Theoretical and Computational Science (TaCS-CoE), KMUTT.

## ACKNOWLEDGMENTS

This project was supported by the Theoretical and Computational Science (TaCS) Center under Computational and Applied Science for Smart Innovation Research Cluster (CLASSIC), Faculty of Science, KMUTT.

## REFERENCES

- Babeai A, Jafari H, Ahmadi M. A fractional order HIV/AIDS model based on the effect of screening of unaware infectives. *Meth Appl Sci.* (2019) **42**:2334–43. doi: 10.1002/mm.a.5511
- Kadkhoda N, Jafari H. An analytical approach to obtain exact solutions of some space-time conformable fractional differential equations. *Adv Differ Equ.* (2019) **2019**:428. doi: 10.1186/s13662-019-2349-0
- Javeed S, Baleanu D, Waheed A, Shaukat Khan M, Affan H. Analysis of homotopy perturbation method for solving fractional order differential equations. *Mathematics.* (2019) **7**:40. doi: 10.3390/math7010040
- Singh PK, Vishal K, Som T. Solution of fractional Drinfeld-Sokolov-Wilson equation using homotopy perturbation transform method. *Appl Math.* (2015). **10**:460–472.
- Demir A, Bayrak MA, Ozbilg E. A new approach for the approximate analytical solution of space-time fractional differential equations by the homotopy analysis method. *Adv Math Phys.* (2019) **2019**:12. doi: 10.1155/2019/5602565
- Singh A, Das S, Ong SH, Jafari H. Numerical solution of nonlinear reaction-advection-diffusion equation, *J Comput Nonlinear Dynamics.* (2019) **14**:041003. doi: 10.1115/1.4042687
- Az-Zo'bi, E. A, exact analytic solutions for nonlinear diffusion equations via generalized residual power series method. *Int. J. Math. Comput Sci.* (2019) **4**:69–78.
- Atangana A, D. Baleanu. Nonlinear fractional jaulent-miodek and whitham-broer-kaup equations within sumudu transform. *Abs Appl Anal.* (2013). **2013**:160681. doi: 10.1155/2013/160681
- Ali A, Shah K, Khan RA. Numerical treatment for solving wave solutions of fractionalwhitham-broer-kaupequations. *Alexan Eng J.* (2018) **57**:1991–8. doi: 10.1016/j.aej.2017.04.012
- wang Y, Zhang YF, Jiang Z, Iqbal M. A fractional whitham-Broer-Kaup equation and its possible application to tsunami prevention. *Ther Sci.* (2017) **24**:1847–55. doi: 10.2298/TSCI160510079W
- Guo S, Mei L, Li Y, Sun Y. The improved fractional sub equation method and its applications to the space-time fractional differential equations in fluid mechanics. *Phys Lett A.* (2012) **376**:407–11. doi: 10.1016/j.physleta.2011.10.056
- Bhalekar S, Daftardar-Geji V. Solving a system of nonlinear functional equations using revised new iterative method. *Int. J. Math. Comp Phys Elect Comp Eng.* (2012) **6**:8–21. doi: 10.1155/2012/975829
- Daftardar-Geji V, Jafari H. An iterative method for solving nonlinear functional equations. *J Math Anal Appl.* (2006) **316**:753–63. doi: 10.1016/j.jmaa.2005.05.009
- Khalouta A, Kadem A. Comparison of new iterative method and natural homotopy perturbation method for solving nonlinear time-fractional wave-like equations with variable coefficients. *Nonlinear Dyn Syst Theory.* (2019) **19**:160–9.
- Khan MJ, Nawaz R, Farid S, Iqbal J. New iterative method for the solution of fractional damped burger and fractional Sharma-Tasso-Olver equations. *Complexity.* (2018) **2018**:3249720. doi: 10.1155/2018/3249720
- Jena RM, Chakraverty S. A new iterative method based solution for fractional black-scholes option pricing equations (BSOPE). *Appl Sci.* (2019) **1**:95. doi: 10.1007/s42452-018-0106-8
- El-Sayed SM, Kaya D. Exact and numerical traveling wave solutions of Whitham- Broer- Kaup equations. *Appl Math Comput.* (2005)**167**:1339–49. doi: 10.1016/j.amc.2004.08.012
- Rafei M, Daniali H. Application of the variational iteration method to the Whitham-Broer-Kaup equations. *Comput Math Appl.* (2007) **54**:1079–85. doi: 10.1016/j.camwa.2006.12.054
- Sirajul H, Ishaq M. Solution of coupled Whitham-Broer-Kaup equations using optimal homotopy asymptotic method. *Ocean Eng.* (2014) **84**:81–8. doi: 10.1016/j.oceaneng.2014.03.031

**Conflict of Interest:** The authors declare that the research was conducted in the absence of any commercial or financial relationships that could be construed as a potential conflict of interest.

Copyright © 2020 Nawaz, Kumam, Farid, Shutaywi, Shah and Deebani. This is an open-access article distributed under the terms of the Creative Commons Attribution License (CC BY). The use, distribution or reproduction in other forums is permitted, provided the original author(s) and the copyright owner(s) are credited and that the original publication in this journal is cited, in accordance with accepted academic practice. No use, distribution or reproduction is permitted which does not comply with these terms.



# The Global Attractor of the Allen-Cahn Equation on the Sphere

David Medina<sup>1</sup> and Pablo Padilla<sup>2\*</sup>

<sup>1</sup> Tecnológico Nacional de México/ITS Perote, Perote, Mexico, <sup>2</sup> Departamento de Matemáticas y Mecánica, IIMAS-UNAM, Mexico City, Mexico

In this paper we study the attractor of a parabolic semiflow generated by a singularly perturbed PDE with a non-linear term given by a bistable potential, in an oval surface; the Allen-Cahn equation being a prototypical example. An additional constraint motivated by a variational principle for closed geodesics originally proposed by Poincaré arising from geometric considerations is introduced. The existence of a global attractor is established by modifying standard techniques in order to handle the constraint. Based on previous work on the elliptic case, it is known that when the perturbation parameter tends to zero, minimal energy solutions exhibit a sharp interface concentrated on a closed geodesic. We provide numerical simulations using Galerkin's method. Based on the analytical and numerical results we conjecture that, when the perturbation parameter tends to zero and for large times, the transition layers of the solutions of this PDE consists of closed geodesics or a union of arcs of such geodesics, thus characterizing the structure of the attractor.

**Keywords:** attractors, parabolic semiflow, closed geodesics, Galerkin method, oval surfaces

## OPEN ACCESS

### Edited by:

Jesus Martin-Vaquero,  
University of Salamanca, Spain

### Reviewed by:

Bulent Karasozen,  
Middle East Technical University,  
Turkey

Andreas Gustavsson,  
University of Seoul, South Korea

### \*Correspondence:

Pablo Padilla  
pablo@mym.iimas.unam.mx

### Specialty section:

This article was submitted to  
Mathematical Physics,  
a section of the journal  
Frontiers in Applied Mathematics and  
Statistics

**Received:** 20 February 2020

**Accepted:** 07 May 2020

**Published:** 17 June 2020

### Citation:

Medina D and Padilla P (2020) The  
Global Attractor of the Allen-Cahn  
Equation on the Sphere.  
Front. Appl. Math. Stat. 6:20.  
doi: 10.3389/fams.2020.00020

## 1. INTRODUCTION

The qualitative study of dynamical systems in infinite dimensions has been of fundamental importance. In the case of dynamical systems associated with partial differential equations of evolution having variational structure, many of the ideas and methodologies of gradient-like systems can be extended to infinite dimensions. In particular, the study and characterization of attractors is of special interest.

In this paper, we prove the existence of the global attractor of the parabolic equation associated to:

$$-\epsilon^2 \Delta u + W'(u) = 0, \quad (1)$$

on an oval surface  $M^1$  (see **Figure 1**) where  $u: M \rightarrow \mathbb{R}$ ,  $0 < \epsilon \ll 1$ ,  $\Delta$  represents the Laplace-Beltrami operator on  $M$  and  $W(u)$  is a non-linear term, which in particular includes the Allen-Cahn non-linearity. The flow will be considered in a space of functions satisfying a geometric constraint to be explained later.

Equation (1) arises in many contexts among which we may mention materials science, superconductivity, population dynamics, and pattern formation.

An important case for  $W(u)$  is given by  $W(u) = (1 - u^2)^2$ , which has been widely studied both analytically and numerically for example in Hutchinson and Tonewaga [1] and Padilla and Tonewaga [2] and references therein.

<sup>1</sup>A closed and compact surface enclosing a strictly convex set in  $\mathbb{R}^3$ .

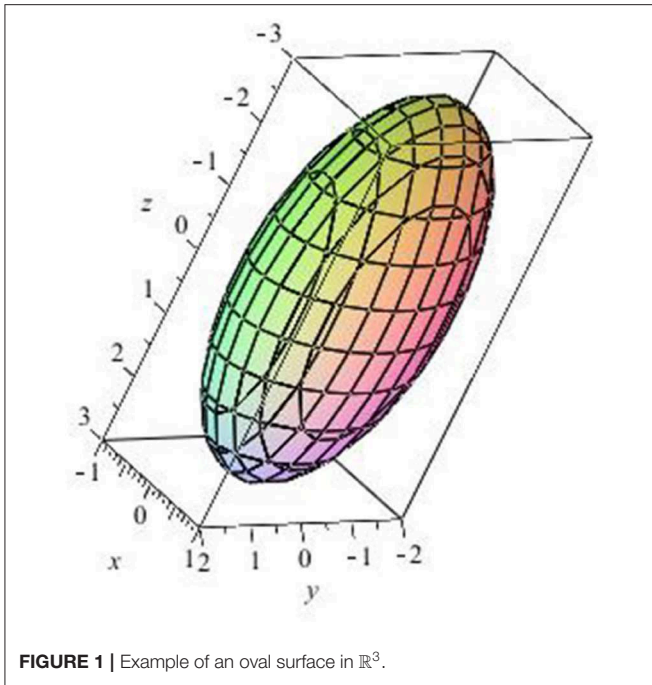


FIGURE 1 | Example of an oval surface in  $\mathbb{R}^3$ .

In a bounded domain  $\Omega \subset \mathbb{R}^n$ ,  $n \geq 2$ , with suitable initial and boundary conditions, in Bronsard and Kohn [3], it is shown that, when  $\epsilon \rightarrow 0$ , the solution  $u$  of (1) separates  $\Omega$  in two regions where  $u \approx 1$  and  $u \approx -1$ , respectively, and the transition layer, moves with normal velocity equal to its principal curvatures. A similar behavior occurs on an oval surface for non-trivial solutions of (1). Using results in Hutchinson and Tonewaga [1] and Padilla and Tonewaga [2], in Garza-Hume and Padilla [4] it is established that, when  $\epsilon \rightarrow 0$ , non-trivial minima of the corresponding energy function (with a suitable restriction) have a transition layer located at the shortest closed geodesic.

This fact is obtained using the variational structure of the problem, because (1) is the Euler Lagrange equation of the functional:

$$E_\epsilon(u) = \int_M \left( \frac{\epsilon}{2} |\nabla u|^2 + \frac{1}{\epsilon} W(u) \right), \tag{2}$$

in a suitable functional space.

For  $\epsilon \rightarrow 0$ , functions  $u$  with uniformly bounded energy  $E_\epsilon(u) < E_0$ , can be proved to be close to  $\pm 1$  in most of the domain, except for a transition curve. The proof follows from a classical result in differential geometry due to Birkhoff that guarantees the existence of a closed geodesic on a surface diffeomorphic to the sphere (see Poincaré [5] where the corresponding variational principle was first conjectured, later demonstrated by Berger and Bombieri [6]):

**Proposition 1.** *Suppose that  $\gamma$  is a closed curve on  $M$  that under the Gauss map,  $g$ , divides the unit sphere in two parts of equal measure. Assume further that among all the curves satisfying the above conditions,  $\gamma$  has minimal length. Then  $\gamma$  is a closed geodesic.*

This fact suggests a natural constraint for the problem under consideration. The function  $u$  belongs to the space of functions that satisfies:

$$\int_{S^2} u(g^{-1}(y)) dy = 0, \tag{3}$$

where  $g$  is the Gauss map.

On the other hand, solutions of (1) correspond to stationary points of the associated gradient flow:

$$u_t = \epsilon \Delta u - \frac{1}{\epsilon} W'(u). \tag{4}$$

The main goal of this paper is show the existence of the attractor of the associated parabolic equation to (1) (i.e., Equation 4), and conjecture its structure in terms of functions that possess transition layers determined by closed geodesics or arcs of geodesics. In other words, given any initial condition, the corresponding parabolic semiflow determined by (4) approaches a function with transitions in geodesics. This will be done by considering the special case in which  $M = S^2$  and  $W(u) = (1 - u^2)^2$ . This will simplify both the analysis and the numerics.

From now on we consider solutions of (4) satisfying the constraint (3). Under the above restrictions, it becomes:

$$\int_{S^2} u = 0, \tag{5}$$

which will be incorporated into the equation later on as a Lagrange multiplier. As a first step, we will proof the existence of an attractor for (4) under the constraint (5). We will recall some standard facts in dynamical systems theory, Sobolev spaces on Riemannian manifolds as well as Gronwall's inequality, which are presented in the following section. This is done for the sake of completeness and to introduce notation and may be skipped by readers familiar with dynamical systems and analysis on manifolds.

Having shown the existence of the attractor, some numerical experiments are performed using the Galerkin method. A few words are in order regarding the limitations of our numerical approach. Even when in principle the method should be applicable for any initial condition, we only considered some that already exhibit a relatively well-defined interface. The aim of the numerical simulations is to make plausible our conjecture on the structure of the global attractor and a more detailed study of the method is not carried out. As for the analytical approach, we remark that the problem of establishing the existence of a global attractor for other surfaces or manifolds in similar situations seems to be a reasonable extension of the methods and ideas here presented. In particular for the case of surfaces with non-zero Euler characteristic as is done in Del Río et al. [14] for the elliptic case.

## 2. GENERAL RESULTS

### 2.1. Semigroups of Operators

The notation and terminology used in this section is adapted or quoted from Temam [7], although arguments and results in

Sell and You [8] and Robinson [9] are also used. Since these are standard results and references, no explicit references are made.

We will consider dynamical systems whose state is described by an element  $u(t)$  of a metric space  $H$ . In most cases, and in particular for dynamical systems associated with partial or ordinary differential equations, the parameter  $t$  (the time or the timelike variable) varies continuously in  $\mathbb{R}$  or in some interval of  $\mathbb{R}$ . Usually the space  $H$  will be a Hilbert or Banach space.

The evolution of the dynamical system is described by a family of operators  $S(t)$ ,  $t \geq 0$ , that map  $H$  into itself and enjoy the usual semigroup properties:

$$\begin{cases} S(t+s) = S(t) \cdot S(s) \quad \forall s, t \geq 0. \\ S(0) = I, \quad \text{Identity in } H. \end{cases} \quad (6)$$

If  $\phi$  is the state of the dynamical system at time  $s$ , then  $S(t)\phi$  is the state of the system at time  $t + s$ , and

$$u(t) = S(t)u(0) \quad (7)$$

$$u(t+s) = S(t)u(s) = S(s)u(t), \quad s, t \geq 0. \quad (8)$$

The semigroup  $S(t)$  will be determined in our case by the solution of a PDE. The basic properties of the operators  $S(t)$  which are needed will be established in the next subsection but, for the time being, we assume that:

$$\begin{aligned} S(t) \quad &\text{is a continuous (non-linear) operator from } H \text{ into itself} \\ &\forall t \geq 0. \end{aligned} \quad (9)$$

These operators may or may not be one-to-one; the injectivity property is equivalent to the *backward uniqueness* property for the dynamical system. When  $S(t)$ ,  $t > 0$ , is one-to-one we denote by  $S(-t)$  its inverse which maps  $S(t)H$  onto  $H$ ; we then obtain a family of operators  $S(t)$ ,  $t \in \mathbb{R}$ , which have the property (6) on their domains of definition,  $\forall s, t \in \mathbb{R}$ . It is clear that for  $t < 0$ , the operators  $S(t)$ , are not usually defined everywhere in  $H$ .

**Definition 1.** For  $u_0 \in H$  the *orbit* or *trajectory* starting in  $u_0$  is the set  $\bigcup_{t \geq 0} S(t)u_0$ .

**Definition 2.** When it exists, an orbit or trajectory ending at  $u_0$  is the set  $\bigcup_{t \geq 0} S(-t)^{-1}u_0$ .

**Definition 3.** For  $u_0 \in H$  or for  $\mathcal{A} \in H$ , the  $\omega$ -limit set of  $u_0$  (or  $\mathcal{A}$ ) is

$$\omega(u_0) = \bigcap_{s \geq 0} \overline{\bigcup_{t \geq s} S(t)u_0},$$

or

$$\omega(\mathcal{A}) = \bigcap_{s \geq 0} \overline{\bigcup_{t \geq s} S(t)\mathcal{A}},$$

where closures are taken in  $H$ .

**Definition 4.** When it exists, the  $\alpha$ -limit set of  $u_0 \in H$  or  $\mathcal{A} \subset H$  is

$$\alpha(u_0) = \bigcap_{s \leq 0} \overline{\bigcup_{t \leq s} S(-t)^{-1}u_0},$$

or

$$\alpha(\mathcal{A}) = \bigcap_{s \leq 0} \overline{\bigcup_{t \leq s} S(-t)^{-1}\mathcal{A}}.$$

**Proposition 2.**  $\phi \in \omega(\mathcal{A})$  if and only if there exists a sequence of elements of  $\phi_n \in \mathcal{A}$  and a sequence  $t_n \rightarrow \infty$  such that

$$S(t_n)\phi_n \rightarrow \phi \text{ as } n \rightarrow \infty. \quad (10)$$

**Remark 1.** Analogously,  $\phi \in \alpha(\mathcal{A})$  if and only if there exists a sequence  $\psi_n$  converging to  $\psi$  in  $H$  and a sequence  $t_n \rightarrow \infty$ , such that  $\phi_n = S(t_n)\psi_n \in \mathcal{A}$ ,  $\forall n$ .

**Definition 5.** A *fixed point*, or an *equilibrium point* is a point  $u_0 \in H$  such that

$$S(t)u_0 = u_0 \quad \forall t \geq 0.$$

## 2.2. Invariant Sets

We say that a set  $X \subset H$  is positively invariant for the semigroup  $\{S(t)\}_{t \geq 0}$  if

$$S(t)X \subset X \quad \forall t \geq 0.$$

It is said to be negatively invariant if  $\{S(t)\}_{t \geq 0}$  if

$$S(t)X \supset X \quad \forall t \geq 0.$$

When the set is both positively and negatively invariant, we call it an invariant set or a functional invariant set.

**Definition 6.** A set  $X \subset H$  is a invariant set for the semigroup  $\{S(t)\}_{t \geq 0}$  if

$$S(t)X = X \quad \forall t \geq 0.$$

The simplest examples of invariant sets are equilibrium points, heteroclinic orbits and limit cycles.

**Lemma 1.** Assume that for some subset  $\mathcal{A} \in H$ ,  $\mathcal{A} \neq \emptyset$ , and for some  $t_0 > 0$ , the set  $\bigcup_{t \geq 0} S(t)\mathcal{A}$  is relatively compact in  $H$ . Then  $\omega(\mathcal{A})$  is non-empty, compact, and invariant.

## 2.3. Absorbing Sets and Attractors

**Definition 7.** An attractor is a set  $\mathcal{A} \in H$  that enjoys the following properties:

1.  $\mathcal{A}$  is an invariant set.
2.  $\mathcal{A}$  possesses an open neighborhood  $\mathcal{U}$  such that, for every  $u_0 \in \mathcal{U}$ ,  $S(t)u_0$  converges to  $\mathcal{A}$  as  $t \rightarrow \infty$ . This means that:

$$\text{dist}(S(t)u_0, \mathcal{A}) \rightarrow 0,$$

as  $t \rightarrow \infty$ .

The distance in (2) is understood to be the distance of a point to a set:

$$\text{dist}(x, \mathcal{A}) = \inf_{y \in \mathcal{A}} d(x, y),$$

$d(x, y)$  denoting the distance of  $x$  to  $y$  in  $H$ .

**Definition 8.** If  $\mathcal{A}$  is an attractor, the largest open set  $\mathcal{U}$  that satisfies (2) is called the *basin of attraction* of  $\mathcal{A}$ . Alternatively, we say that  $\mathcal{A}$  attracts the points of  $\mathcal{U}$ .

**Definition 9.** It is said that  $\mathcal{A}$  uniformly attracts a set  $\mathcal{B} \subset \mathcal{U}$  if

$$d(S(t)\mathcal{B}, \mathcal{A}) \rightarrow 0$$

as  $t \rightarrow \infty$ .

$d(\mathcal{B}_0, \mathcal{B}_1)$  is now the semidistance of two sets:

$$d(\mathcal{B}_0, \mathcal{B}_1) = \sup_{x \in \mathcal{B}_0} \inf_{y \in \mathcal{B}_1} d(x, y).$$

The convergence in the above definition is equivalent to the following: for every  $\epsilon > 0$ , there exists  $t_\epsilon$  such that for  $t \geq t_\epsilon$ ,  $S(t)\mathcal{B}$  is included in  $\mathcal{U}_\epsilon$ , the  $\epsilon$ -neighborhood of  $\mathcal{A}$ . When no confusion can occur we simply say that  $\mathcal{A}$  attracts  $\mathcal{B}$ .

**Definition 10.** We say that  $\mathcal{A} \in H$  is a global (or universal) attractor for the semigroup  $\{S(t)\}_{t \geq 0}$  if  $\mathcal{A}$  is a compact attractor that attracts the bounded sets of  $H$  (and its basin of attraction is then all of  $H$ ).

It is easy to see that such a set is necessarily unique. Also such a set is maximal for the inclusion relation among the bounded attractors and among the bounded functional invariant sets. For this reason it is also called the maximal attractor.

In order to establish the existence of attractors, a useful concept is the related concept of absorbing sets.

**Definition 11.** Let  $\mathcal{B}$  be a subset of  $H$  and  $\mathcal{U}$  an open set containing  $\mathcal{B}$ . We say that  $\mathcal{B}$  is *absorbing* in  $\mathcal{U}$  if the orbit of any bounded set of  $\mathcal{U}$  enters  $\mathcal{B}$  after a certain time (which may depend on the set):

$$\begin{cases} \forall \mathcal{B}_0 \subset \mathcal{U} & \mathcal{B}_0 \text{ bounded} \\ \exists t_1(\mathcal{B}_0) & \text{such that } S(t)\mathcal{B}_0 \subset \mathcal{B}, \forall t \geq t_1(\mathcal{B}_0) \end{cases}$$

We say also that  $\mathcal{B}$  absorbs the bounded sets of  $\mathcal{U}$ .

The existence of global attractor  $\mathcal{A}$  for a semigroup  $\{S(t)\}_{t \geq 0}$  implies that of an absorbing set. Indeed, for  $\epsilon > 0$ , let  $\mathcal{V}_\epsilon$  denote the  $\epsilon$ -neighborhood of  $\mathcal{A}$  (i.e., the union of open balls of radius  $\epsilon$  centered on  $\mathcal{A}$ ). Then, for any bounded set  $\mathcal{B}_0$ ,  $d(S(t)\mathcal{B}_0, \mathcal{A}) \rightarrow 0$  as  $t \rightarrow \infty$ ; hence  $d(S(t)\mathcal{B}_0, \mathcal{A}) \leq \frac{\epsilon}{2}$  for  $t \geq t(\epsilon)$  and  $S(t)\mathcal{B}_0 \subset \mathcal{V}_\epsilon$  for such  $t$ 's. This shows that  $\mathcal{V}_\epsilon$  is an absorbing set.

Conversely, it is a standard result that a semigroup that possesses an absorbing set and enjoys some other properties possesses an attractor.

In order to prove existence of an attractor when the existence of an absorbing set is known, we need further assumptions on the semigroup  $\{S(t)\}_{t \geq 0}$ , and we will make one of the two following:

- The operators  $S(t)$  are *uniformly compact* for  $t$  large. By this we mean that for every bounded set  $\mathcal{B}$  there exists  $t_0$  which may depend on  $\mathcal{B}$  such that

$$\bigcup_{t \geq t_0} S(t)\mathcal{B} \tag{11}$$

is relatively compact in  $H$ .

Alternatively, if  $H$  is a Banach space, we may assume that  $S(t)$  is the perturbation of an operator satisfying (11) by a (non-necessarily linear) operator which converges to 0 as  $t \rightarrow \infty$ . More precisely:

- If  $H$  is a Banach space and for every  $t$ ,  $S(t) = S_1(t) + S_2(t)$  where the operators  $S_1(\cdot)$  are uniformly compact for  $t$  large and  $S_2(t)$  is a continuous mapping from  $H$  into itself such that the following holds:

For every bounded set  $C \subset H$ ,

$$r_c(t) = \sup_{\phi \in C} |S_2(t)\phi|_H \rightarrow 0 \tag{12}$$

as  $t \rightarrow \infty$ .

Of course, if  $H$  is a Banach space, any family of operator satisfying (11) also satisfies (12) with  $S_2 = 0$ .

**Theorem 1.** Assume that  $H$  is a metric space and that the operators  $S(t)$  are given and satisfying (6), (9) and either (11) or (12). We also assume that there exists an open set  $\mathcal{U}$  and a bounded set  $\mathcal{B}$  of  $\mathcal{U}$  such that  $\mathcal{B}$  is absorbing in  $\mathcal{U}$ .

Then the  $\omega$ -limit set of  $\mathcal{B}$ ,  $\mathcal{A} = \omega(\mathcal{B})$ , is a compact attractor which attracts the bounded sets of  $\mathcal{U}$ . It is the maximal bounded attractor in  $\mathcal{U}$  (for the inclusion relation).

Furthermore, if  $H$  is a Banach space, if  $\mathcal{U}$  is convex, and the mapping  $t \mapsto S(t)u_0$  is continuous from  $\mathbb{R}^+$  into  $H$ , for every  $u_0$  in  $H$ ; then  $\mathcal{A}$  is connected too.

The proof of this theorem is carried out through several steps, which can be found in Temam [7].

## 2.4. Sobolev Spaces in Riemannian Manifolds

The notation and terminology used in this section can be found in Hebey [11] and Aubin [12].

Let  $(M, g)$  be a smooth Riemannian manifold. Given  $k$  an integer, and  $p \geq 1$  real, set

$$\mathcal{C}_k^p(M) = \left\{ u \in C^\infty(M) : \forall j = 0, \dots, k, \int_M |\nabla^j u|^p dv(g) < \infty \right\}.$$

When  $M$  is compact, one clearly has that  $\mathcal{C}_k^p(M) = C^\infty(M)$  for any  $k$  and any  $p \geq 1$ . For  $u \in \mathcal{C}_k^p(M)$ , set also

$$\|u\|_{H_k^p} = \left( \sum_{j=0}^k \left( \int_M |\nabla^j u|^p dv(g) \right)^{1/p} \right)^{1/p}.$$

We define the Sobolev space  $H_k^p$  as follows:

**Definition 12.** Given  $(M, g)$  a smooth Riemannian manifold,  $k$  an integer, and  $p \geq 1$  real, the Sobolev space  $H_k^p$  is the completion of  $\mathcal{C}_k^p$  with respect to  $\|\cdot\|_{H_k^p}$ .

Note here that one can look at these spaces as subspaces of  $L^p(M)$ , in which the norm of  $L^p(M)$ ,  $\|\cdot\|_p$  is defined by

$$\|u\|_p = \left( \int_M |u|^p dv(g) \right)^{1/p}.$$

**Definition 13.** Given  $(E, \|\cdot\|_E)$  and  $(F, \|\cdot\|_F)$  two normed vector spaces with the property that  $E$  is a subspace of  $F$ , we say that the embedding of  $E$  in  $F$  is compact if bounded subsets of  $(E, \|\cdot\|_E)$  are relatively compact in  $(F, \|\cdot\|_F)$ . This fact is written as  $E \subset\subset F$ .

This means that bounded sequences in  $(E, \|\cdot\|_E)$  possess convergent subsequences in  $(F, \|\cdot\|_F)$ . Clearly, if the embedding of  $E$  in  $F$  is compact, it is also continuous, i.e., if there exists  $C > 0$  such that for any  $x \in E$ ,  $\|x\|_F \leq C\|x\|_E$ .

The following theorem is needed in order to prove the existence of the attractor of the equation in consideration.

**Theorem 2.** Let  $(M, g)$  be a smooth, compact Riemannian  $n$ -manifold. For any real numbers  $1 \leq q < p$  and any integers  $0 \geq m < k$ , if  $1/p = 1/q - (k - m)/n$ , then  $H_k^q(M) \subset\subset H_m^p(M)$ . In particular, for any  $q \in [1, n)$ ,  $H_1^q(M) \subset\subset L^p(M)$  where  $1/p = 1/q - 1/n$ .

The first part of the above theorem has the following consequence:

**Corollary 1.** For any  $q \in [1, n)$ ,  $H_1^q(M) \subset\subset H_1^q(M)$ , thus  $H_1^q(M) \subset\subset L^p(M)$  for all  $p \geq 1$ .

### 2.5. Differential Inequalities

The following inequality is derived from Gronwall's lemma and will be used later on.

**Lemma 2.** Let  $y$  a positive absolutely continuous function on  $(0, \infty)$  which satisfies:

$$y' + \gamma y^p \leq \delta,$$

with  $p > 1$ ,  $\gamma > 0$ ,  $\delta \geq 0$ . Then, for  $t > 0$ ,

$$y(t) \leq \left(\frac{\delta}{\gamma}\right)^{1/p} + (\gamma(p-1)t)^{-1/(p-1)}.$$

*Proof.* If  $y(0) \leq (\gamma/\delta)^{1/p}$ , then  $y(t) \leq (\gamma/\delta)^{1/p}$ ,  $\forall t \geq 0$ . If  $y(t) > (\gamma/\delta)^{1/p}$ , then there exists  $t_0 \in (0, \infty)$  such that  $y(t) \geq (\gamma/\delta)^{1/p}$  for  $0 \leq t \leq t_0$ , and  $y(t) \leq (\gamma/\delta)^{1/p}$  for  $t \geq t_0$ .

For  $t \in [0, t_0]$  we write  $z(t) = y(t) - (\gamma/\delta)^{1/p} \geq 0$  and since  $(a + b)^p \geq a^p + b^p$  for  $a, b \geq 0$ ,  $p > 1$ , we have

$$y^p = (z + (\gamma/\delta)^{1/p})^p \geq z^p + \gamma/\delta.$$

Hence

$$z' + \gamma z^p \leq y' + \gamma \left(y^p - \frac{\gamma}{\delta}\right) \leq 0,$$

and then by integration

$$z(t)^{p-1} \leq \frac{1}{z_0^{1-p} + \gamma(p-1)t} \leq \frac{1}{\gamma(p-1)t},$$

This implies the desired result for  $t \in [0, t_0]$ , and since, this inequality holds for  $t \geq t_0$ , the lemma is proved.

## 3. EXISTENCE AND STRUCTURE OF ATTRACTOR

The main result is the following in which the existence of a global attractor is shown for equation (4) subject to constraint (5).

**Theorem 3.** The semigroup  $\{S(t)\}_{t \geq 0}$  associated with (4) - (5) possesses a maximal attractor which is bounded in  $H_1^2(S^2)$ , compact and connected in  $L^2(S^2)$ . Its basin of attraction is the whole space  $L^2(S^2)$ , and attracts bounded sets of  $L^2(S^2)$ .

*Proof.* The existence of a solution proposed equation is equivalent to finding the minimum of:

$$\inf E_\epsilon(u) = \inf \int_M \left( \frac{\epsilon}{2} |\nabla u|^2 + \frac{1}{\epsilon} W(u) \right)$$

for all  $u \in H_1^2(M)$ , subject to the constraint:

$$G(u) = \int_M u(y)f(y) = 0,$$

where  $f(y)$  is the Jacobian determinant of the transformation of  $S^2$  into  $M$ . This determinant can be considered to be positive, and this factor is the Gaussian curvature in  $y$ .

For fixed  $\epsilon > 0$ , the existence of this minimum is a consequence of this functional satisfies the Palais–Smale condition (see Struwe [13]), is bounded below and the constraint defines a closed lineal subspace.

On other hand it should be noted that:

$$\frac{d}{dt} E_\epsilon(u) = -\epsilon \int_{S^2} u_t^2 \leq 0. \tag{13}$$

This last statement ensures the existence of a global solution for  $t > 0$ . This is sufficient to define the associated semiflow to given equation.

Another way to verify the above statement, is to first prove the existence and uniqueness of a solution of (4)–(5) subject to a suitable initial condition; then the backward uniqueness in order to show existence for all  $t \in \mathbb{R}$ . Finally apply the theorem 4 for the characterization of global attractor.

In the usual way, we shall see the existence of an absorbent set in  $L^2(S^2)$  and subsequently, the compactness of the mentioned semigroup, according to theorem 1.

The Euler–Lagrange equation associated to (2) with the constraint (3) (for each  $\epsilon_i$ ), contain a Lagrange multiplier  $\lambda_i$  as follows:

$$u_t - \epsilon_i \Delta u + \frac{4}{\epsilon_i} (u^3 - u) + \lambda_i f = 0. \tag{14}$$

In Del Río et al. [14], it is shown that these multipliers are bounded. This fact will be used later.

In order to prove the existence of an absorbing set in  $L^2(S^2)$ , we multiply (2) by  $u$  and integrate over  $S^2$ . Using Green's formula we obtain:

$$\frac{1}{2} \frac{d}{dt} \|u\|_{L^2}^2 + \epsilon_i \int_{S^2} |\nabla u|^2 + \int_{S^2} \left( \frac{4}{\epsilon_i} (u^4 - u^2) + \lambda_i f u \right) = 0, \tag{15}$$

where  $\|\cdot\|_{L^2}$  denotes the norm  $L^2(S^2)$ .

By a standard corollary (see for instance 1)  $H_1^2(S^2) \subset\subset L^2(S^2)$ , therefore there exists a constant  $c_0$  such that  $\|u\|_{L^2} \leq c_0 \|u\|_{H_1^2}$ , and there exists a  $c_1$  such that:

$$\int_{S^2} |u|^2 \leq c_1 \int_{S^2} |\nabla u|^2. \tag{16}$$

An estimate of the third integral in (15) is required, for which the following inequality is used:

$$-\lambda_i f u \leq \frac{1}{2} \lambda_i^2 f^2 + \frac{1}{2} u^2,$$

and by Hölder's inequality, for a  $C > 0$ :

$$\begin{aligned} \int_{S^2} \left( \frac{4}{\epsilon_i} - \lambda_i f u \right) &\leq \left( \frac{4}{\epsilon_i} + \frac{1}{2} \right) \int_{S^2} u^2 + \frac{1}{2} \lambda_i^2 \int_{S^2} f^2 \\ &\leq C \sqrt{\int_{S^2} u^4} + C, \end{aligned}$$

and for certain  $A, B > 0$ :

$$\begin{aligned} \int_{S^2} \left( \frac{4}{\epsilon_i} (u^4 - u^2) + \lambda_i f u \right) &\geq \frac{4}{\epsilon_i} \int_{S^2} u^4 - C \sqrt{\int_{S^2} u^4} + C = \\ &\frac{4}{\epsilon_i} \left( \sqrt{\int_{S^2} u^4} - A \right)^2 - B. \end{aligned}$$

Thanks to (15) and the previous relationship, we conclude that there exists a  $c'_1 > 0$  such that:

$$\begin{aligned} \frac{1}{2} \frac{d}{dt} \|u\|_{L^2}^2 + \epsilon_i \int_{S^2} |\nabla u|^2 + \int_{S^2} \left( \frac{4}{\epsilon_i} u^4 - c'_1 \right) &\leq \\ \frac{1}{2} \frac{d}{dt} \|u\|_{L^2}^2 + \epsilon_i \int_{S^2} |\nabla u|^2 + \int_{S^2} \left( \frac{4}{\epsilon_i} (u^4 - u^2) + \lambda_i f u \right) &= 0. \end{aligned}$$

Thus:

$$\frac{1}{2} \frac{d}{dt} \|u\|_{L^2}^2 + \epsilon_i \int_{S^2} |\nabla u|^2 + \int_{S^2} \left( \frac{4}{\epsilon_i} u^4 - c'_1 \right) \leq 0,$$

this meaning that:

$$\frac{1}{2} \frac{d}{dt} \|u\|_{L^2}^2 + \epsilon_i \int_{S^2} |\nabla u|^2 + \int_{S^2} \left( \frac{4}{\epsilon_i} u^4 \right) \leq 4\pi c'_1. \tag{17}$$

According to (16) concluded from (17), there exists a  $c'_2 = 2(4\pi c'_1)$  such that:

$$\frac{d}{dt} \|u\|_{L^2}^2 + \frac{2\epsilon_i}{c_1^2} \|u\|_{L^2}^2 \leq c'_2.$$

By using the classical Gronwall lemma, we obtain that:

$$\|u(t)\|_{L^2}^2 \leq \|u_0\|_{L^2}^2 \exp\left(-\frac{2\epsilon_i}{c_1^2} t\right) + \frac{c'_2 c_1^2}{2\epsilon_i} \left(1 - \exp\left(-\frac{2\epsilon_i}{c_1^2} t\right)\right).$$

Therefore:

$$\limsup_{t \rightarrow \infty} \|u(t)\|_{L^2} \leq \rho_0, \quad \rho_0^2 = \frac{c'_2 c_1^2}{2\epsilon_i}.$$

There exists an absorbing set  $\mathcal{B}_0$  in  $L^2(S^2)$ , namely, any ball of  $L^2(S^2)$  centered at 0 of radius  $R > \rho_0$ , as if  $\mathcal{B}$  is a bounded set of  $L^2(S^2)$ , included in a ball  $B(0, R)$  of  $L^2(S^2)$ , then  $S(t)\mathcal{B} \in B(0, \rho'_0)$  for  $t \geq t_0(\mathcal{B}, \rho'_0)$ , with

$$t_0 = \frac{c_1^2}{2\epsilon_i} \ln\left(\frac{R^2}{(\rho'_0)^2 - \rho_0^2}\right).$$

In order to prove the uniform compactness of operators, we proceed using by an argument proposed by B. Nicolaenko (see Temam [7]) and making use of the absorbent set in  $L^2(S^2)$  whose existence was established in the previous paragraph.

By Holder inequality:

$$\int_{S^2} u^4 \geq \frac{1}{4\pi} \left( \int_{S^2} u^2 \right)^2.$$

Analogously to (15), we conclude that:

$$y' + \gamma y^2 \leq \delta,$$

where  $y = \|u\|_{L^2}^2, \gamma = \frac{1}{\pi}, \delta = 8\pi c'_1$ . Lemma 2 shows that:

$$y(t) \leq \left(\frac{\gamma}{\delta}\right)^{1/2} + \frac{1}{\gamma t}, \quad \forall t > 0.$$

Let  $\rho_2$  be a real number greater than  $(\gamma/\delta)^{1/2}$  and

$$T_0 = \frac{1}{\gamma} \left( \rho_2^2 - \left(\frac{\gamma}{\delta}\right)^{1/2} \right)^{-1}.$$

The above relations show that for any set  $\mathcal{B}$  of  $L^2(S^2)$ , bounded or not,  $S(t)\mathcal{B}$  is included in the ball  $\mathcal{B}_2$  centered at 0 of radius  $\rho_2$ , if  $t \geq T_0$ , thus demonstrating the existence of an absorbent set in  $H_1^2(S^2)$ . The uniform compactness of operators  $S(t)$  follows from the fact that a bounded set  $\mathcal{B}$  is included in a ball  $B(0, R)$  for all  $t \geq t_0$ , that which is bounded in  $H_1^2(S^2)$  and relatively compact in  $L^2(S^2)$  (corollary 1). The existence of the global attractor follows from theorem 1.

Having shown the existence of a global attractor, the question of characterizing its structure arises. This question can be answered provided there is a suitable Lyapunov functional.

**Definition 14.** A Liapunov functional for  $\{S(t)\}_{t \geq 0}$  on a set  $\mathcal{F} \subset H$  is a continuous function  $F: \mathcal{F} \rightarrow \mathbb{R}$  such that:

1. For each  $u_0 \in \mathcal{F}$ , the function  $t \rightarrow F(S(t)u_0)$  is non-increasing.
2. If  $F(S(\tau)u_1) = F(u_1)$  for some  $\tau > 0$ , then  $u_1$  is a fixed point of  $\{S(t)\}_{t \geq 0}$ , i.e.,  $S(t)u_1 = u_1, \forall t > 0$ .

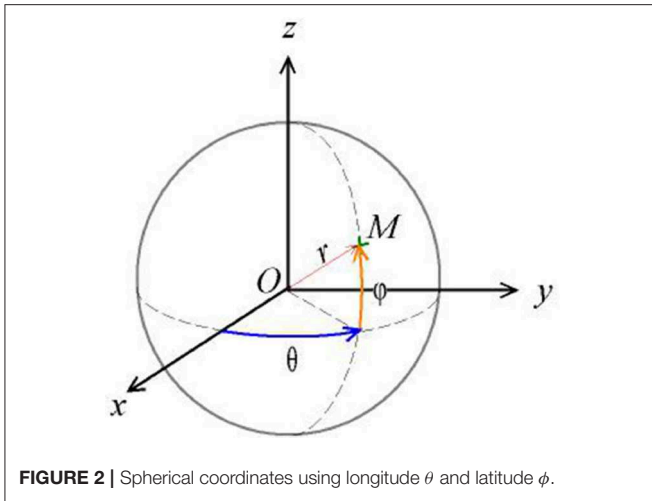


FIGURE 2 | Spherical coordinates using longitude  $\theta$  and latitude  $\phi$ .

The following standard theorem establishes the structure of the attractor.

**Theorem 4.** *Let there be a given semigroup  $\{S(t)\}_{t \geq 0}$  which enjoys the properties (6), (7). We assume that there exists a Lyapunov functional as in the definition 14, and a global attractor  $\mathcal{A} \subset \mathcal{F}$ . Let  $\mathcal{E}$  denote the set of fixed points of the semigroup. Then*

$$\mathcal{A} = \mathcal{M}_+(\mathcal{E}).$$

Furthermore, if  $\mathcal{E}$  is discrete,  $\mathcal{A}$  is the union of  $\mathcal{E}$  and of the heteroclinic curves joining points of  $\mathcal{E}$  and

$$\mathcal{A} = \bigcup_{z \in \mathcal{E}} \mathcal{M}_+(z).$$

Remember that,  $\mathcal{M}_+(X)$  is the set (maybe empty) of points  $u_*$ , which belongs to an orbit  $\{u(t), t \in \mathbb{R}\}$  such that  $d(u(t), X) \rightarrow 0$  as  $t \rightarrow \infty$ .

The details of this proof can be found in Temam [7] theorem 4.1 in chapter 7, Robinson [9] theorem 10.13, Ladyzhenskaya [17] theorem 3.2, or Sell [8] theorem 72.1.

### 4. THE EQUATION IN $S^2$

Once the existence of an attractor is proved, in this section we provide a numerical method for its characterization. In this implementation the Galerkin method is used.

$S^2$  is parametrized with spherical coordinates by  $(r \cos \theta \cos \phi, r \sin \theta \cos \phi, r \sin \phi)$ , where  $0 \leq \theta \leq 2\pi$   $-\frac{\pi}{2} \leq \phi \leq \frac{\pi}{2}$  (see Figure 2).

Then, the Laplacian in these coordinates is given by:

$$\begin{aligned} \Delta u &= \frac{1}{r^2 \cos \phi} \left( \frac{\partial}{\partial r} \left( (r^2 \cos \phi) \frac{\partial u}{\partial r} \right) \right. \\ &+ \frac{\partial}{\partial \theta} \left( (r^2 \cos \phi) \left( \frac{1}{r^2 \cos^2 \phi} \right) \frac{\partial u}{\partial \theta} \right) \\ &+ \left. \frac{\partial}{\partial \phi} \left( (r^2 \cos \phi) \left( \frac{1}{r^2} \right) \frac{\partial u}{\partial \phi} \right) \right) \\ &= \frac{\partial^2 u}{\partial r^2} + \frac{2}{r} \frac{\partial u}{\partial r} + \frac{1}{r^2 \cos^2 \phi} \frac{\partial^2 u}{\partial \theta^2} + \frac{1}{r^2} \frac{\partial^2 u}{\partial \phi^2} - \frac{\tan \phi}{r^2} \frac{\partial u}{\partial \phi}. \end{aligned}$$

Using  $r = 1$  in the above expression, the Laplace–Beltrami operator in  $S^2$  is obtained:

$$\Delta u = \frac{1}{\cos^2 \phi} \frac{\partial^2 u}{\partial \theta^2} + \frac{\partial^2 u}{\partial \phi^2} - \tan \phi \frac{\partial u}{\partial \phi}.$$

Then (4) becomes:

$$\frac{\partial u}{\partial t} - \epsilon \left( \frac{1}{\cos^2 \phi} \frac{\partial^2 u}{\partial \theta^2} + \frac{\partial^2 u}{\partial \phi^2} - \tan \phi \frac{\partial u}{\partial \phi} \right) - \frac{4}{\epsilon} u(1 - u^2) = 0. \tag{18}$$

By implementing Galerkin’s method, we can approximate the attractor. This is done by projecting Equation (18), with a suitable initial condition on a finite dimensional subspace, thus reducing it to a system of ordinary differential equations. The details are provided in the next section.

### 5. GALERKIN METHOD

The idea is to obtain a finite dimensional reduction of (18). One way to do this is using Galerkin method, which will be described below (for more details see Kythe et al. [15] and Evans [10]).

We consider the problem:

$$\frac{\partial u}{\partial t} - \epsilon \left( \frac{1}{\cos^2 \phi} \frac{\partial^2 u}{\partial \theta^2} + \frac{\partial u}{\partial \phi^2} - \tan \phi \frac{\partial u}{\partial \phi} \right) - \frac{4}{\epsilon} u(1 - u^2) = 0 \tag{19}$$

on  $S^2 \times (0, T]$

$$u(\theta, \phi) = g(\theta, \phi) \text{ en } S^2 \times \{t = 0\}. \tag{20}$$

Assume that the functions  $w_k = w_k(\theta, \phi)$ ,  $(k = 1, \dots)$  are smooth,  $\{w_k\}_{k=1}^\infty$  is an orthogonal basis of  $H_1^2(S^2)$  and an orthonormal basis of  $L^2(S^2)$ . For instance, we could take  $\{w_k\}_{k=1}^\infty$  to be the complete set of eigenfunctions of  $\Delta$  in  $S^2$ .

Fix now a positive integer  $m$ . We will look for an approximation  $u_m$  of the form

$$u_m(t) = u(x, t) = \sum_{k=1}^m d_m^k(t) w_k, \tag{21}$$

where we will select the coefficients  $d_m^k(t)$ ,  $(0 \leq t \leq T, k = 1, \dots, m)$  so that:

$$d_m^k(0) = (g, w_k) \tag{22}$$

and

$$(\mathbf{u}'_m(t), w_k) + B[\mathbf{u}_m(t), w_k; t] = (\mathbf{f}(t), w_k). \tag{23}$$

Here  $(\cdot, \cdot)$  denotes the inner product in  $L^2(S^2)$ ,  $' = \frac{d}{dt}$ ,  $B[\mathbf{u}_m, w_k; t]$  is the bilinear form:

$$- \int_{S^2} \left( \epsilon \left( \frac{1}{\cos^2 \phi} \frac{\partial^2 \mathbf{u}_m(t)}{\partial \theta^2} + \frac{\partial^2 \mathbf{u}_m(t)}{\partial \phi^2} - \tan \phi \frac{\partial \mathbf{u}_m(t)}{\partial \phi} \right) - \frac{4}{\epsilon} \mathbf{u}_m(t) \right) w_k, \tag{24}$$

and

$$\mathbf{f}(t) = -\frac{4}{\epsilon} (\mathbf{u}_m(t))^3. \tag{25}$$

Thus, we look for a function  $\mathbf{u}_m$  of the form (21) that satisfies the projection (23) of problem (19)–(20) onto the finite dimensional subspace spanned by  $\{w_k\}_{k=1}^m$ .

By the standard theorem on existence and uniqueness of systems of ordinary differential equations, we have the following result:

**Theorem 5.** For each integer  $m = 1, 2, \dots$ , there exists a unique function  $\mathbf{u}_m$  of the form (21) satisfying (22), (23).

Functions  $w_k$ , will be selected via the method of separation of variables, applied to the equation  $\Delta u = 0$  on  $S^2$ , i.e., we assume that  $u = \Theta(\theta)\Phi(\phi)$ , where we have:

$$\begin{aligned} \frac{1}{\cos^2 \phi} \frac{\partial^2 u}{\partial \theta^2} - \tan \phi \frac{\partial u}{\partial \phi} + \frac{\partial^2 u}{\partial \phi^2} &= 0, \\ \frac{1}{\cos^2 \phi} \Theta'' \Phi - (\tan \phi) \Theta \Phi' + \Theta \Phi'' &= 0, \\ \frac{1}{\cos^2 \phi} \Theta'' \Phi &= (\tan \phi) \Theta \Phi' - \Theta \Phi', \\ \frac{1}{\cos^2 \phi} \Theta'' \Phi &= \Theta [(\tan \phi) \Phi' - \Phi''], \\ \frac{\Theta''}{\Theta} &= -\frac{\cos^2 \phi [\Phi'' - (\tan \phi) \Phi']}{\Phi}. \end{aligned}$$

The corresponding solutions for  $\Theta$  are of the form sine and cosine, while those corresponding to  $\Phi$  are solutions to the Legendre equation, in which the substitution  $x = \sin \phi$  has been made. Thus, we use the associated Legendre polynomial denoted by  $P(k, l, x)$ , which is defined by:

$$P(k, l, x) = \frac{(-1)^k}{l! \cdot 2^l} \cdot (1 - x^2)^{\frac{m}{2}} \cdot \frac{d^{k+l}}{dx^{k+l}} (x^2 - 1)^l, \tag{26}$$

where  $k \geq 0$  and  $l \leq k$ . (For more details see Arfken [16]).

According to the above condition (5) we choose the functions  $\mathbf{u}_m$  as:

$$\mathbf{u}_m = \sum_{k=1}^m a_m^{k,l}(t) \sin(k\theta)P(k, l, \sin(\phi)) + b_m^{k,l}(t) \cos(k\theta)P(k, l, \sin(\phi)), \tag{27}$$

with  $m = 1$  and  $\epsilon = 0.001$ , (23) becomes:

$$\begin{aligned} 1110.33a_1^{1,0}(t)^3 + a_1^{1,0}(t)(-1973.92 + 1110.33a_1^{1,1}(t)^2) \\ + 1110.33b_1^{1,0}(t)^2 \\ + 370.11b_1^{1,1}(t)^2 + 740.22a_1^{1,1}(t)b_1^{1,0}(t)b_1^{1,1}(t) \\ + 4.9348 \frac{d}{dt} a_1^{1,0}(t) = 0, \\ 1110.33a_1^{1,1}(t)^3 + a_1^{1,1}(t)(-1973.82 + \\ 1110.33a_1^{1,1}(t)^2 + 370.11b_1^{1,0}(t)^2 + 1110.33b_1^{1,1}(t)^2) + \\ 740.22a_1^{1,0}(t)b_1^{1,0}(t)b_1^{1,1}(t) + 4.9348 \frac{d}{dt} a_1^{1,1}(t) = 0, \\ 1110.33b_1^{1,0}(t)^3 + 1110.33a_1^{1,0}(t)^2 b_1^{1,0}(t) + 370.11a_1^{1,1}(t)^2 b_1^{1,0}(t) + \\ 740.22a_1^{1,0}(t)a_1^{1,1}(t)b_1^{1,1}(t) + b_1^{1,0}(t)(-1973.92 + 1110.33b_1^{1,1}(t)^2) + \\ 4.9348 \frac{d}{dt} b_1^{1,0}(t) = 0, \\ 1110.33b_1^{1,1}(t)^3 + b_1^{1,1}(t)(-1973.82 + 1110.33a_1^{1,0}(t)^2 + \\ 1110.33b_1^{1,1}(t)^2) + 740.22a_1^{1,0}(t)a_1^{1,1}(t)b_1^{1,0}(t) + 370.11a_1^{1,0}(t)^2 b_1^{1,1}(t) \\ + 4.9348 \frac{d}{dt} b_1^{1,1}(t) = 0. \end{aligned} \tag{28}$$

## 6. NUMERICAL RESULTS

If the initial condition (22) is

$$a_1^{1,0}(0) = 0, a_1^{1,1}(0) = 1, b_1^{1,0}(0) = 0, b_1^{1,1}(0) = 0, \tag{29}$$

we obtain

$$\begin{aligned} a_1^{1,0}(t) = 0, b_1^{1,0}(t) = 0, b_1^{1,1}(t) = 0, \\ a_1^{1,1}(t) = \frac{65794}{\sqrt{2435101734 + 1893748702 \exp\left(-\frac{9869100}{12337}t\right)}}, \end{aligned}$$

and

$$\mathbf{u}_1 = \frac{65794}{\sqrt{2435101734 + 1893748702 \exp\left(-\frac{9869100}{12337}t\right)}} \sin(\theta) P(1, 1, \sin \phi).$$

Figure 3 show the behavior of  $\mathbf{u}_1$  at different times ( $t = 0, t = 0.0001, t = 1$ ).

If the initial condition is now,

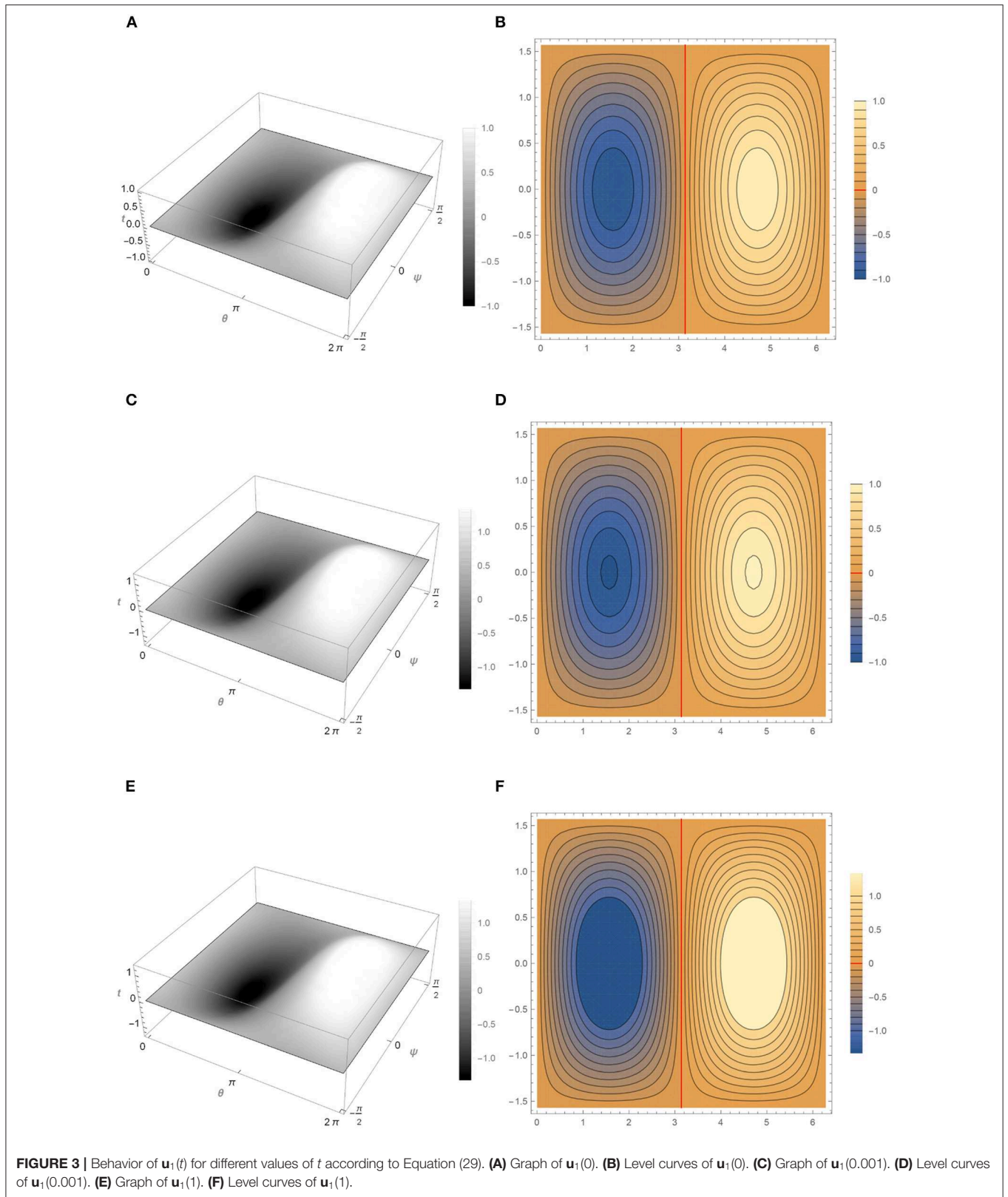
$$a_1^{1,0}(0) = 0, a_1^{1,1}(0) = 0, b_1^{1,0}(0) = 0, b_1^{1,1}(0) = 2, \tag{30}$$

then

$$a_1^{1,0}(t) = 0, a_1^{1,1}(t) = 0, b_1^{1,0}(t) = 0, b_1^{1,1}(t) = \frac{4}{\sqrt{9 - 5 \exp(-8000t)}},$$

and

$$\mathbf{u}_1 = \frac{4}{\sqrt{9 - 5 \exp(-8000t)}} \cos(\theta)P(1, 1, \sin \phi).$$



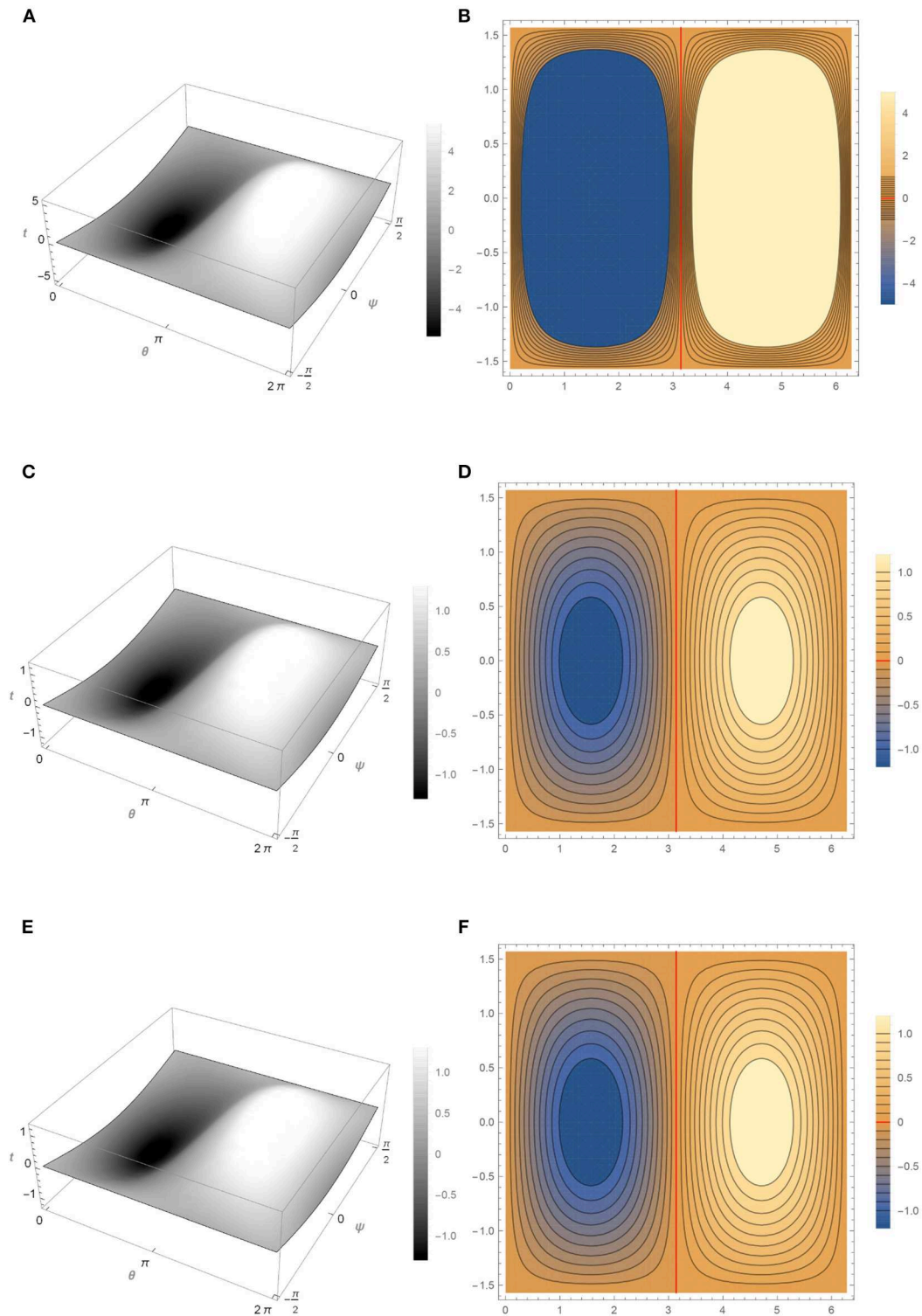


**FIGURE 4 |** Behavior of  $u_1(t)$  for different values of  $t$  according to Equation (29). **(A)** Graph of  $u_1(0)$ . **(B)** Level curves of  $u_1(0)$ . **(C)** Graph of  $u_1(0.01)$ . **(D)** Level curves of  $u_1(0.01)$ . **(E)** Graph of  $u_1(0.02)$ . **(F)** Level curves of  $u_1(0.02)$ .

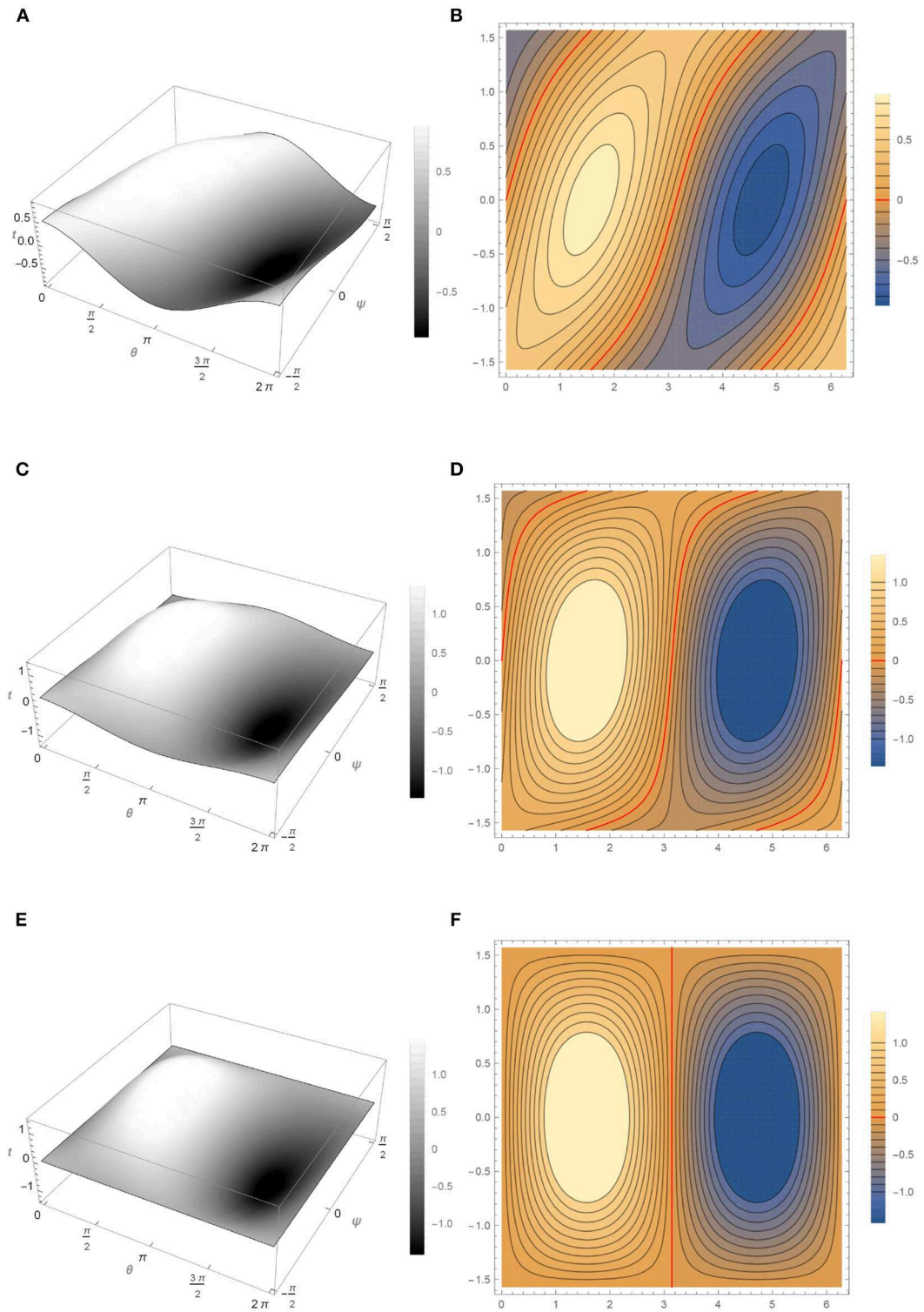


**FIGURE 5 |** Behavior of  $u_2(t)$  for different values of  $t$  according to Equations (34)–(36). **(A)** Graph of  $u_2(0)$ . **(B)** Level curves of  $u_2(0)$ . **(C)** Graph of  $u_2(0.0055)$ . **(D)** Level curves of  $u_1(0.0055)$ . **(E)** Graph of  $u_2(0.02)$ . **(F)** Level curves of  $u_2(0.02)$ .

**Figure 4** show the behavior of  $\mathbf{u}_1$  at different times ( $t = 0, t = 0.01, t = 0.02$ ).

As mentioned in the previous section the legendre equation is involved, we can also choose the Legendre polinomial as follows. If the following functions are now chosen,

$$\mathbf{u}_m = \sum_{k=1}^m (a_k(t) \sin(k\theta)P(k, \sin(\phi)) + b_k(t) \cos(k\theta)P(k \sin(\phi))), \tag{31}$$

where  $P(k, \sin(\phi))$  is the Legendre polynomial of  $k$  degree, with  $m = 2$  and  $\epsilon = 0.01$  the corresponding projection is,

$$\begin{aligned} &1110.33a_1(t)^3 + (-1973.92 + 1572.97a_2(t)^2 + 1110.33b_1(t)^2 \\ &+ 1592.97b_2(t)^2) a_1(t) + 4.9348 \frac{d}{dt} a_1(t) = 0, \\ &675.162a_2(t)^3 + (-1357.61 + 1572.97a_1(t)^2 + 1572.97b_1(t)^2 \\ &+ 675.162b_2(t)^2) a_2(t) + 3.392628 \frac{d}{dt} a_2(t) = 0, \\ &1110.33b_1(t)^3 + (-1973.92 + 1110.33a_1(t)^2 + 1572.97a_2(t)^2 \\ &+ 1572.97b_2(t)^2) b_1(t) + 4.9348 \frac{d}{dt} b_1(t) = 0, \\ &675.162b_2(t)^3 + (-1357.61 + 1572.97a_1(t)^2 + 675.162a_2(t)^2 \\ &+ 1572.97b_1(t)^2) b_2(t) + 3.392628 \frac{d}{dt} b_2(t) = 0. \end{aligned} \tag{32}$$

With the initial condition,

$$a_1(0) = -0.877583, a_2(0) = 0, b_1(0) = 0, b_2(0) = -0.479426, \tag{33}$$

we obtain the following expressions for  $\mathbf{u}_2$  for the values  $t = 0, t = 0.0055$ , and  $t = 0.02$ . **Figure 5**

shows the graph and level curves of  $\mathbf{u}_2$  for the values mentioned above.

$$\begin{aligned} \mathbf{u}_2(0) &= -0.877583 \sin(\theta)P(1, \sin(\phi)) \\ &- 0.479426 \cos(2\theta)P(2, \sin(\phi)), \end{aligned} \tag{34}$$

$$\begin{aligned} \mathbf{u}_2(0.0055) &= -1.2858 \sin(\theta)P(1, \sin(\phi)) \\ &- 0.1449 \cos(2\theta)P(2, \sin(\phi)), \end{aligned} \tag{35}$$

$$\mathbf{u}_2(0.02) = -1.3333 \sin(\theta)P(1, \sin(\phi)). \tag{36}$$

## 7. CONCLUSIONS

All the numerical simulations show that the graph of the solution on  $S^2$  approaches values close to 1 and  $-1$  when  $t$  increases, as can be seen in **Figures 3A,C,E-5A,C,E** found in grayscale color, while in the **Figures 3B,D, 4B,D**, the transition layer (show in red color) takes place along the level set  $\theta = \pi$  which is a closed geodesic (great circle). It can also be noted that in **Figure 5B** the transition layer at the value  $t = 0$  is not a straight line, but as  $t$  increases, this curve becomes a straight line,  $\theta = \pi$ , as mentioned above. This suggests that, for  $\epsilon$  sufficiently small, the attractor will consist of functions concentrating in  $-1$  or  $+1$  with transitions along great circles.

## DATA AVAILABILITY STATEMENT

All datasets generated for this study are included in the article/supplementary material.

## AUTHOR CONTRIBUTIONS

All authors listed have made a substantial, direct and intellectual contribution to the work, and approved it for publication.

## REFERENCES

1. Hutchinson JE, Tonewaga Y. Convergence of phase interfaces in the van der Waals - Cahn - Hilliard theory. *Calc Var.* (2000) **10**:49–84. doi: 10.1007/PL00013453
2. Padilla P, Tonewaga Y. On the convergence of stable phase transitions. *Commun Pure Appl Math.* (1998) **51**: 551–79.
3. Bronsard L, Kohn RV. Motion by mean curvature as the singular limit of Ginzburg-Landau dynamics. *J Diff Equat.* (1991) **90**:211–37.
4. Garza-Hume CE, Padilla P. Closed geodesics on oval surfaces and pattern formation. *Commun Anal Geometry.* (2003) **11**, 223–33. doi: 10.4310/CAG.2003.v11.n2.a3
5. Poincaré H. Sur les lignes géodésiques des surfaces convexes. *Trans Am Math Soc.* (1905) **6**:237–74.
6. Berger MS, Bombieri E. On Poincaré’s isoperimetric problem for simple closed goedesic. *J Funct Anal.* (1981) **42**:274–98.
7. Temam R. *Infinite Dimensional Dynamical Systems in Mechanics and Physics.* New York, NY: Springer - Verlag (1999).
8. Sell GR, You Y. *Dynamics of Evolutionary Equations.* New York, NY: Springer-Verlag (2002).
9. Robinson JC. *Infinite-Dimensional Dynamical Systems An Introduction to Dissipative Parabolic PDEs and the Theory of Global Attractors.* New York, NY: Cambridge University Press (2001).
10. Evans LC. *Partial Differential Equations, Graduate Studies in Mathematics, Vol. 19.* Providence, RI: American Mathematical Society (2000).

11. Hebey E. *Nonlinear Analysis on Manifolds: Sobolev Spaces and Inequalities.* Providence, RI: American Mathematical Society (2000).
12. Aubin T. *Nonlinear Analysis on Manifolds. Monge - Ampère Equations.* New York, NY: Springer - Verlag (1982).
13. Struwe M. *Variational Methods.* Berlin: Springer - Verlag (1990).
14. Del Río H, Garza C, Padilla P. Geodesics, soap bubbles and pattern formation in Riemannian surfaces. *J Geometr Anal.* (2003) **13**:595–604. doi: 10.1007/BF02921880
15. Kythe PK, Puri P, Schferkottter MR. *Partial Differential Equations and Boundary Value Problems with Mathematica.* 2nd ed. Boca Raton, FL: Chapman and Hall (2003).
16. Arfken G. *Mathematical Methods for Physicists.* Burlington, FL: Academic Press Inc. (1985).
17. Ladyzhenskaya O. *Attractors for Semigroups and Evolution Equations.* Cambridge, UK: Cambrbridge University Press (1991).

**Conflict of Interest:** The authors declare that the research was conducted in the absence of any commercial or financial relationships that could be construed as a potential conflict of interest.

Copyright © 2020 Medina and Padilla. This is an open-access article distributed under the terms of the Creative Commons Attribution License (CC BY). The use, distribution or reproduction in other forums is permitted, provided the original author(s) and the copyright owner(s) are credited and that the original publication in this journal is cited, in accordance with accepted academic practice. No use, distribution or reproduction is permitted which does not comply with these terms.



# Invariant Solutions and Conservation Laws of the Variable-Coefficient Heisenberg Ferromagnetic Spin Chain Equation

Na Liu<sup>1,2\*</sup>

<sup>1</sup> Business School, Shandong University of Political Science and Law, Jinan, China, <sup>2</sup> School of Mathematics and Statistics, Shandong Normal University, Jinan, China

The variable-coefficient Heisenberg ferromagnetic spin chain (vcHFSC) equation is investigated using the Lie group method. The infinitesimal generators and Lie point symmetries are reported. Four types of similarity reductions are acquired by virtue of the optimal system of one-dimensional subalgebras. Several invariant solutions are derived, including trigonometric and hyperbolic function solutions. Furthermore, conservation laws for the vcHFSC equation are obtained with the help of Lagrangian and non-linear self-adjointness.

## OPEN ACCESS

### Edited by:

Jesus Martin-Vaquero,  
University of Salamanca, Spain

### Reviewed by:

Abdullahi Yusuf,  
Federal University, Dutse, Nigeria  
Chaudry Masood Khalique,  
North-West University, South Africa  
Mahmoud Abdelrahman,  
Mansoura University, Egypt

### \*Correspondence:

Na Liu  
sna0531@126.com

### Specialty section:

This article was submitted to  
Mathematical and Statistical Physics,  
a section of the journal  
Frontiers in Physics

Received: 30 December 2019

Accepted: 10 June 2020

Published: 11 August 2020

### Citation:

Liu N (2020) Invariant Solutions and Conservation Laws of the Variable-Coefficient Heisenberg Ferromagnetic Spin Chain Equation. *Front. Phys.* 8:260. doi: 10.3389/fphy.2020.00260

**Keywords:** variable-coefficient Heisenberg ferromagnetic spin chain equation, Lie symmetry, invariant solutions, non-linear self-adjointness, conservation laws

## INTRODUCTION

The investigation of physical phenomenon modeled by non-linear partial differential equations (NLPDEs) and searching for their underlying dynamics remain the hot issue of research for applied and theoretical sciences. A lot of attention has been concentrated on looking for the explicit solutions of NLPDEs, for they can provide accurate information with which to understand some interesting physical phenomena. A great many powerful methods have been proposed to construct the explicit solutions of NLPDEs, such as the inverse scattering method [1], the Lie group method [2–5], the Hirota bilinear method [6, 7], the extended tanh method [8–10], the homoclinic test method [11–13], the F-expansion technique [14], and so on [15–18]. Among these methods, the Lie group method is a powerful and prolific method for the study of NLPDEs. On the one hand, based on the Lie group method, we can obtain new exact solutions directly or from the known ones or via similarity reductions; on the other hand, the conservation laws can be constructed via the corresponding Lie point symmetries. Recently, invariant solutions of a class of constant and variable coefficient NLPDEs have been obtained by virtue of this method, such as Keller-Segel models [19], generalized fifth-order non-linear integrable equation [20], KdV equation [21], and Davey-Stewartson equation [22].

So far, many effective methods have been extended to construct exact solutions of different types of differential equations. For example, the generalized Bernoulli sub-ODE and the generalized tanh methods have been applied to establish optical soliton solutions of the Chen-Lee-Liu equation [23]. The Lie group method has been used to find the exact solutions of the time fractional Abrahams–Tsuneto reaction diffusion system [24] and the non-linear transmission line equation [25].

In this work, we will focus on the (2+1)-dimensional variable-coefficient Heisenberg ferromagnetic spin chain (vcHFSC) equation

$$iq_t + \delta_1(t)q_{xx} + \delta_2(t)q_{yy} + \delta_3(t)q_{xy} + \delta_4(t)|q|^2q = 0, \quad (1)$$

where  $\delta_1(t)$ ,  $\delta_2(t)$ ,  $\delta_3(t)$ , and  $\delta_4(t)$  are arbitrary functions with respect to  $t$ . The interaction properties and stability of the bright and dark solitons are presented in [26]. Non-autonomous complex wave and analytic solutions are obtained in [27]. When  $\delta_i(t)$  ( $i = 1, \dots, 4$ ) are arbitrary constants, Equation (1) can be reduced to the following (2+1)-dimensional Heisenberg ferromagnetic spin chain (HFSC) equation:

$$iq_t + \delta_1q_{xx} + \delta_2q_{yy} + \delta_3q_{xy} + \delta_4|q|^2q = 0. \quad (2)$$

Latha and Vasanthi [28] obtained multisoliton solutions by employing Darboux transformation and analyzed the interaction properties of Equation (2). Anitha et al. [29] derived the dynamical equations of motion by employing long wavelength approximation and discussed the complete non-linear excitation with the aid of sine-cosine function method. Periodic solutions were obtained by Triki and Wazwaz [30], and they also discussed conditions for the existence and uniqueness of wave solutions. Tang et al. [31] reported the explicit power series solutions and bright and dark soliton solutions of Equation (2), and they also obtained some other exact solutions via the sub-ODE method.

However, the Lie symmetries, invariant solutions, and conservation laws of the (2+1)-dimensional vcHFSC equation (1) have not been studied. In the current work, we study the vcHFSC equation (1) via the Lie group method and obtain new invariant solutions, including the trigonometric and hyperbolic function solutions. Moreover, based on non-linear self-adjointness, conservation laws for vcHFSC equation (1) are constructed.

The main structure of this paper is as follows. In section Lie Symmetry Analysis and Optimal System, based on the Lie symmetry analysis, we construct the Lie point symmetries and the optimal system of one-dimensional subalgebras for Equation (1). In section Symmetry Reductions and Invariant Solutions, four types of similarity reductions and some invariant solutions are studied by virtue of the optimal system. In section Non-linear Self-Adjointness and Conservation Laws, conservation laws for Equation (1) are obtained with the help of Lagrangian and non-linear self-adjointness. Section Results and Discussion provides the results and discussion. Finally, the conclusion is given in section Conclusion.

## LIE SYMMETRY ANALYSIS AND OPTIMAL SYSTEM

In this section, our aim is to obtain the Lie point symmetries and the optimal system of the vcHFSC equation (1) by employing the Lie group method.

The vcHFSC equation (1) can be changed to the following system

$$\begin{cases} F_1 = u_t + \delta_1(t)v_{xx} + \delta_2(t)v_{yy} + \delta_3(t)v_{xy} \\ \quad + \delta_4(t)(u^2v + v^3) = 0, \\ F_2 = -v_t + \delta_1(t)u_{xx} + \delta_2(t)u_{yy} + \delta_3(t)u_{xy} \\ \quad + \delta_4(t)(u^3 + uv^2) = 0, \end{cases} \quad (3)$$

by using the transformation

$$q(x, y, t) = u(x, y, t) + iv(x, y, t), \quad (4)$$

where  $u(x, y, t)$  and  $v(x, y, t)$  are real and smooth functions.

Suppose that the associated vector field of system (3) is as follows:

$$V = \xi^1(x, y, t, u, v) \frac{\partial}{\partial x} + \xi^2(x, y, t, u, v) \frac{\partial}{\partial y} + \xi^3(x, y, t, u, v) \frac{\partial}{\partial t} \\ + \eta^1(x, y, t, u, v) \frac{\partial}{\partial u} + \eta^2(x, y, t, u, v) \frac{\partial}{\partial v}, \quad (5)$$

where  $\xi^1(x, y, t, u, v)$ ,  $\xi^2(x, y, t, u, v)$ ,  $\xi^3(x, y, t, u, v)$ ,  $\eta^1(x, y, t, u, v)$  and  $\eta^2(x, y, t, u, v)$  are unknown functions that need to be determined.

If vector field (5) generates a symmetry of system (3), then  $V$  must satisfy symmetry condition

$$pr^{(2)}V(\Delta_1) \Big|_{\Delta_1} = 0, pr^{(2)}V(\Delta_2) \Big|_{\Delta_2} = 0, \quad (6)$$

where

$$\begin{cases} \Delta_1 = u_t + \delta_1(t)v_{xx} + \delta_2(t)v_{yy} + \delta_3(t)v_{xy} + \delta_4(t)(u^2v + v^3), \\ \Delta_2 = -v_t + \delta_1(t)u_{xx} + \delta_2(t)u_{yy} + \delta_3(t)u_{xy} + \delta_4(t)(u^3 + uv^2). \end{cases}$$

The infinitesimals  $\xi^1$ ,  $\xi^2$ ,  $\xi^3$ ,  $\eta^1$ , and  $\eta^2$  must satisfy the following invariant conditions

$$\begin{cases} \eta_t^1 + \xi^3\delta_1'(t)v_{xx} + \delta_1(t)\eta_{xx}^2 + \xi^3\delta_2'(t)v_{yy} + \delta_2(t)\eta_{yy}^2 \\ \quad + \xi^3\delta_3'(t)v_{xy} \\ \quad + \delta_3(t)\eta_{xy}^2 + \xi^3\delta_4'(t)(u^2v + v^3) + \delta_4(t)(2u\eta^1v \\ \quad + u^2\eta^2 + 3v^2\eta^2) = 0, \\ -\eta_t^2 + \xi^3\delta_1'(t)u_{xx} + \delta_1(t)\eta_{xx}^1 + \xi^3\delta_2'(t)u_{yy} \\ \quad + \delta_2(t)\eta_{yy}^1 + \xi^3\delta_3'(t)u_{xy} \\ \quad + \delta_3(t)\eta_{xy}^1 + \xi^3\delta_4'(t)(u^3 + uv^2) + \delta_4(t)(3u^2\eta^1 \\ \quad + \eta^1v^2 + 2uv\eta^2) = 0, \end{cases} \quad (7)$$

where

$$\begin{aligned} \eta_t^1 &= D_t(\eta^1 - \xi^1u_x - \xi^2u_y - \xi^3u_t) + \xi^1u_{xt} + \xi^2u_{yt} \\ &\quad + \xi^3u_{tt}, \\ \eta_{xx}^1 &= D_{xx}(\eta^1 - \xi^1u_x - \xi^2u_y - \xi^3u_t) + \xi^1u_{xxx} \\ &\quad + \xi^2u_{xxy} + \xi^3u_{xxt}, \\ \eta_{xy}^1 &= D_{xy}(\eta^1 - \xi^1u_x - \xi^2u_y - \xi^3u_t) + \xi^1u_{xxy} \\ &\quad + \xi^2u_{xyy} + \xi^3u_{xyt}, \\ \eta_{yy}^1 &= D_{yy}(\eta^1 - \xi^1u_x - \xi^2u_y - \xi^3u_t) + \xi^1u_{xyy} \end{aligned}$$

$$\begin{aligned}
 & +\xi^2 u_{yyy} + \xi^3 u_{yyt}, \\
 \eta_t^2 & = D_t(\eta^2 - \xi^1 v_x - \xi^2 v_y - \xi^3 v_t) + \xi^1 v_{xt} \\
 & + \xi^2 v_{yt} + \xi^3 v_{tt}, \\
 \eta_{xx}^2 & = D_{xx}(\eta^2 - \xi^1 v_x - \xi^2 v_y - \xi^3 v_t) + \xi^1 v_{xxx} \\
 & + \xi^2 v_{xxy} + \xi^3 v_{xxt}, \\
 \eta_{xy}^2 & = D_{xy}(\eta^2 - \xi^1 v_x - \xi^2 v_y - \xi^3 v_t) \\
 & + \xi^1 v_{xxy} + \xi^2 v_{xyy} + \xi^3 v_{xyt}, \\
 \eta_{yy}^2 & = D_{yy}(\eta^2 - \xi^1 v_x - \xi^2 v_y \\
 & - \xi^3 v_t) + \xi^1 v_{xyy} + \xi^2 v_{yyy} + \xi^3 v_{yyt}.
 \end{aligned}$$

Solving Equation (7), one can obtain

$$\begin{aligned}
 \xi^1 & = c_1 x + c_2, \xi^2 = c_1 y + c_3, \xi^3 = \frac{2c_1 \int \delta_1(t) dt}{\delta_1(t)} \\
 & + \frac{c_4}{\delta_1(t)}, \eta^1 = c_1 u, \eta^2 = c_1 v, \quad (8)
 \end{aligned}$$

where  $c_1, c_2, c_3,$  and  $c_4$  are arbitrary constants, and the coefficient functions  $\delta_1(t), \delta_2(t), \delta_3(t),$  and  $\delta_4(t)$  are determined by

$$\begin{aligned}
 \xi^3 \delta_{2t} + \xi_t^3 \delta_2 - 2\delta_2 c_1 & = 0, \\
 \xi^3 \delta_{3t} + \xi_t^3 \delta_3 - 2\delta_3 c_1 & = 0, \\
 \xi^3 \delta_{4t} + \xi_t^3 \delta_4 + 2c_1 \delta_4 & = 0. \quad (9)
 \end{aligned}$$

The Lie algebra of infinitesimal symmetries of system (3) is generated by the four vector fields:

$$\begin{aligned}
 \tilde{\mathfrak{J}}_1 & = x \frac{\partial}{\partial x} + y \frac{\partial}{\partial y} + \frac{2 \int \delta_1(t) dt}{\delta_1(t)} \frac{\partial}{\partial t} + u \frac{\partial}{\partial u} + v \frac{\partial}{\partial v}, \\
 \tilde{\mathfrak{J}}_2 & = \frac{\partial}{\partial x}, \tilde{\mathfrak{J}}_3 = \frac{\partial}{\partial y}, \tilde{\mathfrak{J}}_4 = \frac{1}{\delta_1(t)} \frac{\partial}{\partial t}. \quad (10)
 \end{aligned}$$

The one-parameter groups  $g_i$  generated by the  $\tilde{\mathfrak{J}}_i$  are given as follows:

$$\begin{aligned}
 g_1 & : (x, y, t, u, v) \rightarrow \left( x e^\varepsilon, y e^\varepsilon, t + \varepsilon \frac{2 \int \delta_1(t) dt}{\delta_1(t)}, u e^\varepsilon, v e^\varepsilon \right), \\
 g_2 & : (x, y, t, u, v) \rightarrow (x + \varepsilon, y, t, u, v), \\
 g_3 & : (x, y, t, u, v) \rightarrow (x, y + \varepsilon, t, u, v), \\
 g_4 & : (x, y, t, u, v) \rightarrow \left( x, y, t + \frac{\varepsilon}{\delta_1(t)}, u, v \right). \quad (11)
 \end{aligned}$$

If  $\{u = U(x, y, t), v = V(x, y, t)\}$  is a solution of system (3), by employing symmetry groups  $g_i$  ( $i = 1, 2, 3, 4$ ), we can obtain the following new solutions

$$\begin{aligned}
 (u^{(1)}, v^{(1)}) & \rightarrow \left( e^\varepsilon U \left( x e^{-\varepsilon}, y e^{-\varepsilon}, t - \varepsilon \frac{2 \int \delta_1(t) dt}{\delta_1(t)} \right), \right. \\
 & \left. e^\varepsilon V \left( x e^{-\varepsilon}, y e^{-\varepsilon}, t - \varepsilon \frac{2 \int \delta_1(t) dt}{\delta_1(t)} \right) \right), \\
 (u^{(2)}, v^{(2)}) & \rightarrow (U(x - \varepsilon, y, t), V(x - \varepsilon, y, t)),
 \end{aligned}$$

TABLE 1 | Commutator table of the vector fields of system (3).

$[\tilde{\mathfrak{J}}_i, \tilde{\mathfrak{J}}_j]$	$\tilde{\mathfrak{J}}_1$	$\tilde{\mathfrak{J}}_2$	$\tilde{\mathfrak{J}}_3$	$\tilde{\mathfrak{J}}_4$
$\tilde{\mathfrak{J}}_1$	0	$-\tilde{\mathfrak{J}}_2$	$-\tilde{\mathfrak{J}}_3$	$-2\tilde{\mathfrak{J}}_4$
$\tilde{\mathfrak{J}}_2$	$\tilde{\mathfrak{J}}_2$	0	0	0
$\tilde{\mathfrak{J}}_3$	$\tilde{\mathfrak{J}}_3$	0	0	0
$\tilde{\mathfrak{J}}_4$	$2\tilde{\mathfrak{J}}_4$	0	0	0

TABLE 2 | Adjoint table of the vector fields of system (3).

Ad	$\tilde{\mathfrak{J}}_1$	$\tilde{\mathfrak{J}}_2$	$\tilde{\mathfrak{J}}_3$	$\tilde{\mathfrak{J}}_4$
$\tilde{\mathfrak{J}}_1$	$\tilde{\mathfrak{J}}_1$	$\tilde{\mathfrak{J}}_2 e^\varepsilon$	$\tilde{\mathfrak{J}}_3 e^\varepsilon$	$\tilde{\mathfrak{J}}_4 e^{2\varepsilon}$
$\tilde{\mathfrak{J}}_2$	$\tilde{\mathfrak{J}}_1 - \varepsilon \tilde{\mathfrak{J}}_2$	$\tilde{\mathfrak{J}}_2$	$\tilde{\mathfrak{J}}_3$	$\tilde{\mathfrak{J}}_4$
$\tilde{\mathfrak{J}}_3$	$\tilde{\mathfrak{J}}_1 - \varepsilon \tilde{\mathfrak{J}}_3$	$\tilde{\mathfrak{J}}_2$	$\tilde{\mathfrak{J}}_3$	$\tilde{\mathfrak{J}}_4$
$\tilde{\mathfrak{J}}_4$	$\tilde{\mathfrak{J}}_1 - 2\varepsilon \tilde{\mathfrak{J}}_4$	$\tilde{\mathfrak{J}}_2$	$\tilde{\mathfrak{J}}_3$	$\tilde{\mathfrak{J}}_4$

$$\begin{aligned}
 (u^{(3)}, v^{(3)}) & \rightarrow (U(x, y - \varepsilon, t), V(x, y - \varepsilon, t)), \\
 (u^{(4)}, v^{(4)}) & \rightarrow \left( U \left( x, y, t - \frac{\varepsilon}{\delta_1(t)} \right), V \left( x, y, t - \frac{\varepsilon}{\delta_1(t)} \right) \right). \quad (12)
 \end{aligned}$$

In order to construct the optimal system for system (3), we apply the formula

$$Ad(\exp(\varepsilon \tilde{\mathfrak{J}}_i)) \tilde{\mathfrak{J}}_j = \tilde{\mathfrak{J}}_j - \varepsilon [\tilde{\mathfrak{J}}_i, \tilde{\mathfrak{J}}_j] + \frac{\varepsilon^2}{2} [\tilde{\mathfrak{J}}_i, [\tilde{\mathfrak{J}}_i, \tilde{\mathfrak{J}}_j]] - \dots, \quad (13)$$

where  $[\tilde{\mathfrak{J}}_i, \tilde{\mathfrak{J}}_j] = \tilde{\mathfrak{J}}_i \tilde{\mathfrak{J}}_j - \tilde{\mathfrak{J}}_j \tilde{\mathfrak{J}}_i$  and  $\varepsilon$  is a parameter. The commutator table and the adjoint table of system (3) have been constructed and are presented in Tables 1, 2, respectively.

Based on Tables 1, 2, system (3) has the following optimal system [3, 32]

$$\text{(i) } \tilde{\mathfrak{J}}_1; \text{ (ii) } \tilde{\mathfrak{J}}_2 + \alpha \tilde{\mathfrak{J}}_3 + \beta \tilde{\mathfrak{J}}_4; \text{ (iii) } \tilde{\mathfrak{J}}_3 + \chi \tilde{\mathfrak{J}}_4; \text{ (iv) } \tilde{\mathfrak{J}}_4, \quad (14)$$

where  $\alpha, \beta,$  and  $\chi$  are arbitrary constants.

## SYMMETRY REDUCTIONS AND INVARIANT SOLUTIONS

Based on the optimal system (14), our major goal is to deal with the similarity reductions and invariant solutions for system (3).

### Subalgebra $\tilde{\mathfrak{J}}_1$

The characteristic equations of subalgebra  $\tilde{\mathfrak{J}}_1$  can be written as

$$\frac{dx}{x} = \frac{dy}{y} = \frac{dt}{\frac{2}{\delta_1(t)} \int \delta_1(t) dt} = \frac{du}{u} = \frac{dv}{v}. \quad (15)$$

Solving these equations yields the four similarity variables

$$\begin{aligned}
 r & = x \left( \int \delta_1(t) dt \right)^{-\frac{1}{2}}, s = y \left( \int \delta_1(t) dt \right)^{-\frac{1}{2}}, \\
 u & = F(r, s) \cdot \left( \int \delta_1(t) dt \right)^{\frac{1}{2}}, v = H(r, s) \cdot \left( \int \delta_1(t) dt \right)^{\frac{1}{2}}, \quad (16)
 \end{aligned}$$

and solving the constrained conditions (9), we get

$$\begin{aligned} \delta_2(t) &= k_1\delta_1(t), \delta_3(t) = k_2\delta_1(t), \\ \delta_4(t) &= k_3\delta_1(t) \left( \int \delta_1(t) dt \right)^{-2}, \end{aligned} \tag{17}$$

where  $k_1, k_2,$  and  $k_3$  are arbitrary constants. These variables reduce system (3) to the following (1+1)-dimensional PDEs

$$\begin{cases} F - rF_r - sF_s + 2H_{rr} + 2k_1H_{ss} + 2k_2H_{rs} \\ + 2k_3(F^2H + H^3) = 0, \\ -H + rH_r + sH_s + 2F_{rr} + 2k_1F_{ss} + 2k_2F_{rs} + 2k_3(F^3 \\ + FH^2) = 0. \end{cases} \tag{18}$$

Subalgebra  $\tilde{\mathcal{J}}_1$  does not give any group-invariant solutions.

### Subalgebra $\tilde{\mathcal{J}}_2 + \alpha\tilde{\mathcal{J}}_3 + \beta\tilde{\mathcal{J}}_4$

The similarity variables of this generator are

$$\begin{aligned} r &= \alpha x - y, s = \beta x - \int \delta_1(t) dt, \\ u &= F(r, s), v = H(r, s), \end{aligned} \tag{19}$$

and solving the constrained conditions (9), we get

$$\delta_2(t) = k_1\delta_1(t), \delta_3(t) = k_2\delta_1(t), \delta_4(t) = k_3\delta_1(t), \tag{20}$$

where  $k_i (i = 1, 2, 3, 4)$  are arbitrary constants. Substituting Equations (19) and (20) into (3), we have

$$\begin{cases} F_s - (\alpha^2 + k_1 - \alpha k_2)H_{rr} - \beta^2H_{ss} - (2\alpha\beta - \beta k_2)H_{rs} \\ - k_3(F^2H + H^3) = 0, \\ H_s + (\alpha^2 + k_1 - \alpha k_2)F_{rr} + \beta^2F_{ss} + (2\alpha\beta - \beta k_2)F_{rs} \\ + k_3(F^3 + FH^2) = 0. \end{cases} \tag{21}$$

For solving Equation (21), we use the transformation  $\zeta = r - \kappa s, F = f(\zeta), H = h(\zeta)$ , where  $\kappa$  is an arbitrary constant, and then (21) can be reduced to the following ODEs

$$\begin{cases} -\kappa f' + (2\alpha\beta\kappa - \beta k_2\kappa - \beta^2\kappa^2 - \alpha^2 - k_1 + \alpha k_2)h'' \\ - k_3(f^2h + h^3) = 0, \\ -\kappa h' - (2\alpha\beta\lambda - \beta k_2\lambda - \beta^2\lambda^2 - \alpha^2 - k_1 + \alpha k_2)f'' \\ + k_3(f^3 + fh^2) = 0. \end{cases} \tag{22}$$

Solving Equation (22) yields

$$\begin{cases} f = -B_1 \\ + A_1 \tan \left( r - \frac{4\alpha\beta - 2\beta k_2 + 1 - \sqrt{4\beta^2(k_2^2 - 4k_1) + 4\beta(2\alpha - k_2) + 1}}{4\beta^2} s \right), \\ h = A_1 \\ + B_1 \tan \left( r - \frac{4\alpha\beta - 2\beta k_2 + 1 - \sqrt{4\beta^2(k_2^2 - 4k_1) + 4\beta(2\alpha - k_2) + 1}}{4\beta^2} s \right), \end{cases} \tag{23}$$

and

$$\begin{cases} f = -B_1 \\ + A_1 \cot \left( r - \frac{4\alpha\beta - 2\beta k_2 + 1 - \sqrt{4\beta^2(k_2^2 - 4k_1) + 4\beta(2\alpha - k_2) + 1}}{4\beta^2} s \right), \\ h = A_1 \\ + B_1 \cot \left( r - \frac{4\alpha\beta - 2\beta k_2 + 1 - \sqrt{4\beta^2(k_2^2 - 4k_1) + 4\beta(2\alpha - k_2) + 1}}{4\beta^2} s \right), \end{cases} \tag{24}$$

where  $k_3 = -\frac{4\alpha\beta - 2\beta k_2 + 1 - \sqrt{4\beta^2(k_2^2 - 4k_1) + 4\beta(2\alpha - k_2) + 1}}{4\beta^2(A_1^2 + B_1^2)}$  and  $A_1, B_1$  are free parameters.

Based on Equations (19), (23), and (24), we obtain the following trigonometric function solutions for system (3)

$$\begin{cases} u = -B_1 \\ + A_1 \tan \left( \alpha x - y - \frac{4\alpha\beta - 2\beta k_2 + 1 - \sqrt{4\beta^2(k_2^2 - 4k_1) + 4\beta(2\alpha - k_2) + 1}}{4\beta^2} (\beta x - \int \delta_1(t) dt) \right), \\ v = A_1 \\ + B_1 \tan \left( \alpha x - y - \frac{4\alpha\beta - 2\beta k_2 + 1 - \sqrt{4\beta^2(k_2^2 - 4k_1) + 4\beta(2\alpha - k_2) + 1}}{4\beta^2} (\beta x - \int \delta_1(t) dt) \right), \end{cases} \tag{25}$$

and

$$\begin{cases} u = -B_1 \\ + A_1 \cot \left( \alpha x - y - \frac{4\alpha\beta - 2\beta k_2 + 1 - \sqrt{4\beta^2(k_2^2 - 4k_1) + 4\beta(2\alpha - k_2) + 1}}{4\beta^2} (\beta x - \int \delta_1(t) dt) \right), \\ v = A_1 \\ + B_1 \cot \left( \alpha x - y - \frac{4\alpha\beta - 2\beta k_2 + 1 - \sqrt{4\beta^2(k_2^2 - 4k_1) + 4\beta(2\alpha - k_2) + 1}}{4\beta^2} (\beta x - \int \delta_1(t) dt) \right), \end{cases} \tag{26}$$

where  $k_3 = -\frac{4\alpha\beta - 2\beta k_2 + 1 - \sqrt{4\beta^2(k_2^2 - 4k_1) + 4\beta(2\alpha - k_2) + 1}}{4\beta^2(A_1^2 + B_1^2)}$  and  $A_1, B_1$  are free parameters.

### Subalgebra $\tilde{\mathcal{J}}_3 + \chi\tilde{\mathcal{J}}_4$

The similarity variables of this generator are

$$\begin{aligned} r &= x, s = \chi y - \int \delta_1(t) dt, \\ u &= F(r, s), v = H(r, s), \end{aligned} \tag{27}$$

and solving the constrained conditions (9), we get

$$\delta_2(t) = k_1\delta_1(t), \delta_3(t) = k_2\delta_1(t), \delta_4(t) = k_3\delta_1(t), \tag{28}$$

where  $k_i (i = 1, 2, 3, 4)$  are arbitrary constants. System (3) can then be transformed to

$$\begin{cases} F_s - H_{rr} - \chi^2 k_1 H_{ss} - \chi k_2 H_{rs} - k_3(F^2H + H^3) = 0, \\ H_s + F_{rr} + \chi^2 k_1 F_{ss} + \chi k_2 F_{rs} + k_3(F^3 + FH^2) = 0. \end{cases} \tag{29}$$

For solving Equation (29), we use the transformation  $\zeta = r - \kappa s, F = f(\zeta), H = h(\zeta)$ , where  $\kappa$  is an arbitrary constant; Equation (29) can then be written as

$$\begin{cases} -\kappa f' + (\chi k_2\kappa - \chi^2\kappa^2 k_1 - 1)h'' - k_3(f^2h + h^3) = 0, \\ -\kappa h' - (\chi k_2\kappa - \chi^2\kappa^2 k_1 - 1)f'' + k_3(f^3 + fh^2) = 0. \end{cases} \tag{30}$$

To obtain the solutions of Equation (30), we shall apply the  $\left(\frac{G'}{G}\right)$  method, as described in [33].

Let us consider the solutions of (30), as

$$f = \sum_{i=0}^n A_i \left(\frac{G'}{G}\right)^i, h = \sum_{i=0}^m B_i \left(\frac{G'}{G}\right)^i. \tag{31}$$

By balancing the highest order derivative term and non-linear term in (30), we obtain  $m = n = 1$ , and  $G = G(\zeta)$  satisfies second-order ODE

$$G'' + \lambda G' + \mu G = 0.$$

Solving Equation (30), we obtain

$$\begin{aligned} \mu &= \frac{\lambda^2(A_1^2 + B_1^2) + 4B_0(B_0 - \lambda B_1)}{4A_1^2}, \\ A_0 &= \frac{\lambda(A_1^2 + B_1^2) - 2B_0B_1}{2A_1}, \kappa = \frac{k_3(A_1^2 + B_1^2)(2B_0 - \lambda B_1)}{2A_1}, \\ k_1 &= \frac{-2A_1((A_1^2 + B_1^2)(\lambda\chi B_1 k_2 k_3 - 2\chi A_1 B_0 k_2 k_3 + 2A_1 k_3) + 2A_1)}{\chi^2 k_3^2 (\lambda A_1^2 B_1 + \lambda B_1^3 - 2A_1^2 B_0 - 2B_0 B_1^2)}, \end{aligned} \tag{32}$$

where  $\lambda, \chi, d_1, B_0, B_1, k_2$ , and  $k_3$  are arbitrary constants.

Substituting (32) into (30), we obtain two types of solutions of (30), as follows:

When  $\lambda^2 - 4\mu > 0$ ,

$$\begin{cases} f = \frac{\lambda B_1 - 2B_0}{2i} \times \left( \frac{C_1 \cosh\left(\frac{1}{2}\sqrt{\lambda^2 - 4\mu}\zeta\right) + C_2 \sinh\left(\frac{1}{2}\sqrt{\lambda^2 - 4\mu}\zeta\right)}{C_1 \sinh\left(\frac{1}{2}\sqrt{\lambda^2 - 4\mu}\zeta\right) + C_2 \cosh\left(\frac{1}{2}\sqrt{\lambda^2 - 4\mu}\zeta\right)} \right) \\ \quad - \frac{\lambda(\lambda B_1 - 2B_0)}{2i\sqrt{\lambda^2 - 4\mu}} - \frac{\lambda B_0 - 2\mu B_1}{i\sqrt{\lambda^2 - 4\mu}}, \\ h = \frac{B_1}{2}\sqrt{\lambda^2 - 4\mu} \times \left( \frac{C_1 \cosh\left(\frac{1}{2}\sqrt{\lambda^2 - 4\mu}\zeta\right) + C_2 \sinh\left(\frac{1}{2}\sqrt{\lambda^2 - 4\mu}\zeta\right)}{C_1 \sinh\left(\frac{1}{2}\sqrt{\lambda^2 - 4\mu}\zeta\right) + C_2 \cosh\left(\frac{1}{2}\sqrt{\lambda^2 - 4\mu}\zeta\right)} \right) \\ \quad - \frac{\lambda B_1}{2} + B_0, \end{cases} \tag{33}$$

where

$$\begin{aligned} k_1 &= \frac{2k_3(\lambda B_0 B_1 - \mu B_1^2 - B_0^2) + \lambda^2 - 4\mu + 2i\chi k_2 k_3(\lambda B_0 B_1 - \mu B_1^2 - B_0^2)\sqrt{\lambda^2 - 4\mu}}{4\chi^2 k_3^2 (\lambda B_0 B_1 - \mu B_1^2 - B_0^2)^2}, \\ \zeta &= r - \frac{2k_3(\lambda B_0 B_1 - \mu B_1^2 - B_0^2)}{i\sqrt{\lambda^2 - 4\mu}} s, \lambda, \mu, \chi, B_0, B_1, \\ &\quad C_1, C_2, k_2, \text{ and } k_3 \text{ are arbitrary constants.} \end{aligned}$$

When  $\lambda^2 - 4\mu < 0$ ,

$$\begin{cases} f = \frac{\lambda B_1 - 2B_0}{2} \times \left( \frac{C_1 \cosh\left(\frac{1}{2}\sqrt{4\mu - \lambda^2}\zeta\right) - C_2 \sinh\left(\frac{1}{2}\sqrt{4\mu - \lambda^2}\zeta\right)}{C_1 \sinh\left(\frac{1}{2}\sqrt{4\mu - \lambda^2}\zeta\right) + C_2 \cosh\left(\frac{1}{2}\sqrt{4\mu - \lambda^2}\zeta\right)} \right) \\ \quad - \frac{\lambda(\lambda B_1 - 2B_0)}{2\sqrt{4\mu - \lambda^2}} - \frac{\lambda B_0 - 2\mu B_1}{\sqrt{4\mu - \lambda^2}}, \\ h = \frac{B_1}{2}\sqrt{4\mu - \lambda^2} \times \left( \frac{C_1 \cosh\left(\frac{1}{2}\sqrt{4\mu - \lambda^2}\zeta\right) - C_2 \sinh\left(\frac{1}{2}\sqrt{4\mu - \lambda^2}\zeta\right)}{C_1 \sinh\left(\frac{1}{2}\sqrt{4\mu - \lambda^2}\zeta\right) + C_2 \cosh\left(\frac{1}{2}\sqrt{4\mu - \lambda^2}\zeta\right)} \right) \\ \quad - \frac{\lambda B_1}{2} + B_0, \end{cases} \tag{34}$$

where

$$\begin{aligned} k_1 &= \frac{2k_3(\lambda B_0 B_1 - \mu B_1^2 - B_0^2) + \lambda^2 - 4\mu + 2\chi k_2 k_3(\lambda B_0 B_1 - \mu B_1^2 - B_0^2)\sqrt{4\mu - \lambda^2}}{4\chi^2 k_3^2 (\lambda B_0 B_1 - \mu B_1^2 - B_0^2)^2}, \\ \zeta &= r - \frac{2k_3(\mu B_1^2 + B_0^2 - \lambda B_0 B_1)}{\sqrt{\lambda^2 - 4\mu}} s, \lambda, \mu, \chi, B_0, B_1, C_1, C_2, k_2, \end{aligned}$$

and  $k_3$  are arbitrary constants.

Taking into account Equations (27), (33), and (34), we obtain the hyperbolic function solutions for system (3):

$$\begin{cases} u = \frac{\lambda B_1 - 2B_0}{2i} \times \left( \frac{C_1 \cosh\left(\frac{1}{2}\sqrt{\lambda^2 - 4\mu}\zeta\right) + C_2 \sinh\left(\frac{1}{2}\sqrt{\lambda^2 - 4\mu}\zeta\right)}{C_1 \sinh\left(\frac{1}{2}\sqrt{\lambda^2 - 4\mu}\zeta\right) + C_2 \cosh\left(\frac{1}{2}\sqrt{\lambda^2 - 4\mu}\zeta\right)} \right) \\ \quad - \frac{\lambda(\lambda B_1 - 2B_0)}{2i\sqrt{\lambda^2 - 4\mu}} - \frac{\lambda B_0 - 2\mu B_1}{i\sqrt{\lambda^2 - 4\mu}}, \\ v = \frac{B_1}{2}\sqrt{\lambda^2 - 4\mu} \times \left( \frac{C_1 \cosh\left(\frac{1}{2}\sqrt{\lambda^2 - 4\mu}\zeta\right) + C_2 \sinh\left(\frac{1}{2}\sqrt{\lambda^2 - 4\mu}\zeta\right)}{C_1 \sinh\left(\frac{1}{2}\sqrt{\lambda^2 - 4\mu}\zeta\right) + C_2 \cosh\left(\frac{1}{2}\sqrt{\lambda^2 - 4\mu}\zeta\right)} \right) \\ \quad - \frac{\lambda B_1}{2} + B_0, \end{cases} \tag{35}$$

where  $\lambda^2 - 4\mu > 0$ ,

$$\begin{aligned} k_1 &= \frac{2k_3(\lambda B_0 B_1 - \mu B_1^2 - B_0^2) + \lambda^2 - 4\mu + 2i\chi k_2 k_3(\lambda B_0 B_1 - \mu B_1^2 - B_0^2)\sqrt{\lambda^2 - 4\mu}}{4\chi^2 k_3^2 (\lambda B_0 B_1 - \mu B_1^2 - B_0^2)^2}, \\ \zeta &= x - \frac{2k_3(\lambda B_0 B_1 - \mu B_1^2 - B_0^2)}{i\sqrt{\lambda^2 - 4\mu}} \left( \chi y - \int \delta_1(t) dt \right), \\ &\quad \lambda, \mu, \chi, B_0, B_1, C_1, C_2, k_2, \\ &\quad \text{and } k_3 \text{ are arbitrary constants.} \end{aligned}$$

$$\begin{cases} u = \frac{\lambda B_1 - 2B_0}{2} \times \left( \frac{C_1 \cos\left(\frac{1}{2}\sqrt{4\mu - \lambda^2}\zeta\right) - C_2 \sin\left(\frac{1}{2}\sqrt{4\mu - \lambda^2}\zeta\right)}{C_1 \sin\left(\frac{1}{2}\sqrt{4\mu - \lambda^2}\zeta\right) + C_2 \cos\left(\frac{1}{2}\sqrt{4\mu - \lambda^2}\zeta\right)} \right) \\ \quad - \frac{\lambda(\lambda B_1 - 2B_0)}{2\sqrt{4\mu - \lambda^2}} - \frac{\lambda B_0 - 2\mu B_1}{\sqrt{4\mu - \lambda^2}}, \\ v = \frac{B_1}{2}\sqrt{4\mu - \lambda^2} \times \left( \frac{C_1 \cos\left(\frac{1}{2}\sqrt{4\mu - \lambda^2}\zeta\right) - C_2 \sin\left(\frac{1}{2}\sqrt{4\mu - \lambda^2}\zeta\right)}{C_1 \sin\left(\frac{1}{2}\sqrt{4\mu - \lambda^2}\zeta\right) + C_2 \cos\left(\frac{1}{2}\sqrt{4\mu - \lambda^2}\zeta\right)} \right) \\ \quad - \frac{\lambda B_1}{2} + B_0, \end{cases} \tag{36}$$

where  $\lambda^2 - 4\mu < 0$ ,

$$\begin{aligned} k_1 &= \frac{2k_3(\lambda B_0 B_1 - \mu B_1^2 - B_0^2) + \lambda^2 - 4\mu + 2\chi k_2 k_3(\lambda B_0 B_1 - \mu B_1^2 - B_0^2)\sqrt{4\mu - \lambda^2}}{4\chi^2 k_3^2 (\lambda B_0 B_1 - \mu B_1^2 - B_0^2)^2}, \\ \zeta &= x - \frac{2k_3(\mu B_1^2 + B_0^2 - \lambda B_0 B_1)}{\sqrt{\lambda^2 - 4\mu}} \left( \chi y - \int \delta_1(t) dt \right), \\ &\quad \lambda, \mu, \chi, B_0, B_1, C_1, C_2, k_2, \text{ and } k_3 \text{ are arbitrary constants.} \end{aligned}$$

### Subalgebra $\tilde{\mathcal{J}}_4 = \frac{1}{\delta_1(t)} \frac{\partial}{\partial t}$

The similarity variables of this generator are

$$\begin{aligned} r &= x, s = y, \\ u &= F(r, s), v = H(r, s), \end{aligned} \tag{37}$$

and solving the constrained conditions (9), we get

$$\delta_2(t) = k_1\delta_1(t), \delta_3(t) = k_2\delta_1(t), \delta_4(t) = k_3\delta_1(t), \quad (38)$$

where  $k_i$  ( $i = 1, 2, 3$ ) are arbitrary constants. Thus, system (3) can be transformed to

$$\begin{cases} H_{rr} + k_1H_{ss} + k_2H_{rs} + k_3(F^2H + H^3) = 0, \\ F_{rr} + k_1F_{ss} + k_2F_{rs} + k_3(F^3 + FH^2) = 0. \end{cases} \quad (39)$$

For solving Equation (39), we use the transformation  $\zeta = r - \kappa s$ ,  $F = f(\zeta)$ ,  $H = h(\zeta)$ , where  $\lambda$  is an arbitrary constant, and then (39) can be reduced to the following ODEs

$$\begin{cases} (1 + \kappa^2k_1 - \kappa k_2)h'' + k_3(f^2h + h^3) = 0, \\ (1 + \kappa^2k_1 - \kappa k_2)f'' + k_3(f^3 + fh^2) = 0. \end{cases} \quad (40)$$

Solving Equation (40) yields

$$\begin{cases} f = C_1 \sin\left(r - \frac{k_2 + \sqrt{4k_1k_3(C_1^2 + C_2^2) + k_2^2 - 4k_1}}{2k_1}s\right) \\ \quad - C_2 \cos\left(r - \frac{k_2 + \sqrt{4k_1k_3(C_1^2 + C_2^2) + k_2^2 - 4k_1}}{2k_1}s\right), \\ h = C_2 \sin\left(r - \frac{k_2 + \sqrt{4k_1k_3(C_1^2 + C_2^2) + k_2^2 - 4k_1}}{2k_1}s\right) \\ \quad + C_1 \cos\left(r - \frac{k_2 + \sqrt{4k_1k_3(C_1^2 + C_2^2) + k_2^2 - 4k_1}}{2k_1}s\right), \end{cases} \quad (41)$$

where  $C_1, C_2, k_1, k_2,$  and  $k_3$  are arbitrary constants.

On combining Equations (37) and (41), we obtain the periodic function solutions for system (3):

$$\begin{cases} u = C_1 \sin\left(x - \frac{k_2 + \sqrt{4k_1k_3(C_1^2 + C_2^2) + k_2^2 - 4k_1}}{2k_1}y\right) \\ \quad - C_2 \cos\left(x - \frac{k_2 + \sqrt{4k_1k_3(C_1^2 + C_2^2) + k_2^2 - 4k_1}}{2k_1}y\right), \\ v = C_2 \sin\left(x - \frac{k_2 + \sqrt{4k_1k_3(C_1^2 + C_2^2) + k_2^2 - 4k_1}}{2k_1}y\right) \\ \quad + C_1 \cos\left(x - \frac{k_2 + \sqrt{4k_1k_3(C_1^2 + C_2^2) + k_2^2 - 4k_1}}{2k_1}y\right), \end{cases} \quad (42)$$

where  $C_1, C_2, k_1, k_2,$  and  $k_3$  are arbitrary constants.

## NON-LINEAR SELF-ADJOINTNESS AND CONSERVATION LAWS

Conservation laws have been extensively researched due to their important physical significance. Many effective approaches have been proposed to construct conservation laws for NPDEs, such as Noether's theorem [34], the multiplier approach [35], and so on [36, 37]. Ibragimov [38, 39] proposed a new conservation theorem that does not require the existence of a Lagrangian and is based on the concept of an adjoint equation for NLPDEs. In this section, we will construct non-linear self-adjointness and conservation laws for vchFSC equation (1).

## Non-linear Self-Adjointness

Based on the method of constructing Lagrangians [38], we have the following formal Lagrangian  $\mathcal{L}$  in the symmetric form

$$\begin{aligned} \mathcal{L} = \bar{u} & \left[ u_t + \delta_1(t)v_{xx} + \delta_2(t)v_{yy} + \frac{1}{2}\delta_3(t)v_{xy} \right. \\ & \left. + \frac{1}{2}\delta_3(t)v_{yx} + \delta_4(t)(u^2v + v^3) \right] \\ & + \bar{v} \left[ -v_t + \delta_1(t)u_{xx} + \delta_2(t)u_{yy} + \frac{1}{2}\delta_3(t)u_{xy} \right. \\ & \left. + \frac{1}{2}\delta_3(t)u_{yx} + \delta_4(t)(u^3 + uv^2) \right], \end{aligned} \quad (43)$$

where  $\bar{u}$  and  $\bar{v}$  are two new dependent variables.

The adjoint system of system (3) is

$$\begin{cases} F_1^* = \frac{\delta \mathcal{L}}{\delta \bar{u}} = 0, \\ F_2^* = \frac{\delta \mathcal{L}}{\delta \bar{v}} = 0, \end{cases} \quad (44)$$

where

$$\frac{\delta \mathcal{L}}{\delta u} = \frac{\partial \mathcal{L}}{\partial u} - D_t \frac{\partial \mathcal{L}}{\partial u_t} + D_x D_x \frac{\partial \mathcal{L}}{\partial u_{xx}} + D_x D_y \frac{\partial \mathcal{L}}{\partial u_{xy}} + D_y D_y \frac{\partial \mathcal{L}}{\partial u_{yy}}, \quad (45)$$

$$\frac{\delta \mathcal{L}}{\delta v} = \frac{\partial \mathcal{L}}{\partial v} - D_t \frac{\partial \mathcal{L}}{\partial v_t} + D_x D_x \frac{\partial \mathcal{L}}{\partial v_{xx}} + D_x D_y \frac{\partial \mathcal{L}}{\partial v_{xy}} + D_y D_y \frac{\partial \mathcal{L}}{\partial v_{yy}}, \quad (46)$$

with  $D_x, D_y,$  and  $D_t$  the total differentiations with respect to  $x, y,$  and  $t$ .

For illustration,  $D_x$  can be expressed as

$$\begin{aligned} D_x = \frac{\partial}{\partial x} + u_x \frac{\partial}{\partial u} + v_x \frac{\partial}{\partial v} + u_{xx} \frac{\partial}{\partial u_x} + v_{xx} \frac{\partial}{\partial v_x} + u_{xt} \frac{\partial}{\partial u_t} \\ + v_{xt} \frac{\partial}{\partial v_t} + \dots \end{aligned}$$

Substituting (43), (45), and (46) into (44), the adjoint system for system (3) is

$$\begin{cases} F_1^* = -\bar{u}_t + \delta_1(t)\bar{v}_{xx} + \delta_2(t)\bar{v}_{yy} + \delta_3(t)\bar{v}_{xy} \\ \quad + 2\delta_4(t)\bar{u}uv + \delta_4(t)\bar{v}(3u^2 + v^2), \\ F_2^* = \bar{v}_t + \delta_1(t)\bar{u}_{xx} + \delta_2(t)\bar{u}_{yy} + \delta_3(t)\bar{u}_{xy} \\ \quad + 2\delta_4(t)\bar{v}uv + \delta_4(t)\bar{u}(u^2 + 3v^2). \end{cases} \quad (47)$$

The system (3) is non-linear self-adjoint when adjoint system (47) satisfy the following conditions

$$\begin{cases} F_1^* \Big|_{\bar{u} = \phi(x,y,t,u,v), \bar{v} = \psi(x,y,t,u,v)} = \lambda_{11}F_1 + \lambda_{12}F_2, \\ F_2^* \Big|_{\bar{u} = \phi(x,y,t,u,v), \bar{v} = \psi(x,y,t,u,v)} = \lambda_{21}F_1 + \lambda_{22}F_2, \end{cases} \quad (48)$$

where  $\phi(x, y, t, u, v) \neq 0$  or  $\psi(x, y, t, u, v) \neq 0$ , and  $\lambda_{ij}$  ( $i, j = 1, 2$ ) are undetermined coefficients.

Substituting the expressions of  $F_i$  ( $i=1,2$ ) and  $F_i^*$  ( $i=1,2$ ) into (48), we obtain the following equations

$$\begin{aligned}
 &(\lambda_{12} - \psi_u)(\delta_1(t)u_{xx} - \delta_2(t)u_{yy} - \delta_3(t)u_{xy}) \\
 & - (\lambda_{11} - \psi_v)(\delta_1(t)v_{xx} + \delta_2(t)v_{yy} + \delta_3(t)v_{xy}) \\
 & - (\lambda_{11} + \phi_u)u_t + (\lambda_{12} - \phi_v)v_t + \psi_{uv}(2\delta_1(t)u_x v_x \\
 & + 2\delta_2(t)u_y v_y + \delta_3(t)u_x v_y + \delta_3(t)u_y v_x) \\
 & + \psi_{uu}(\delta_1(t)u_x^2 + \delta_2(t)u_y^2 + \delta_3(t)u_x u_y) + \psi_{vv}(\delta_1(t)v_x^2 \\
 & + \delta_2(t)v_y^2 + \delta_3(t)v_x v_y) \\
 & + (2\delta_1(t)\psi_{xu} + \delta_3(t)\psi_{yu})u_x + (2\delta_2(t)\psi_{yu} + \delta_3(t)\psi_{xu})u_y \\
 & + (2\delta_1(t)\psi_{xv} + \delta_3(t)\psi_{yv})v_x \\
 & + (2\delta_2(t)\psi_{yv} + \delta_3(t)\psi_{xv})v_y + \delta_1(t)\psi_{xx} + \delta_2(t)\psi_{yy} \\
 & + \delta_3(t)\psi_{xy} - \lambda_{11}\delta_4(t)(u^2 v + v^3) \\
 & - \lambda_{12}\delta_4(t)(uv^2 + u^3) + 2\delta_4(t)\phi uv + 3\delta_4(t)\psi u^2 \\
 & + \delta_4(t)\psi v^2 - \phi_t = 0, \\
 & - (\lambda_{22} - \phi_u)(\delta_1(t)u_{xx} + \delta_2(t)u_{yy} + \delta_3(t)u_{xy}) \\
 & - (\lambda_{21} - \phi_v)(\delta_1(t)v_{xx} + \delta_2(t)v_{yy} + \delta_3(t)v_{xy}) \\
 & - (\lambda_{21} - \psi_u)u_t + (\lambda_{22} + \psi_v)v_t + \phi_{uv}(2\delta_1(t)u_x v_x \\
 & + 2\delta_2(t)u_y v_y + \delta_3(t)u_x v_y + \delta_3(t)u_y v_x) \\
 & + \phi_{uu}(\delta_1(t)u_x^2 + \delta_2(t)u_y^2 + \delta_3(t)u_x u_y) + \phi_{vv}(\delta_1(t)v_x^2 \\
 & + \delta_2(t)v_y^2 + \delta_3(t)v_x v_y) \\
 & + (2\delta_1(t)\phi_{xu} + \delta_3(t)\phi_{yu})u_x \\
 & + (2\delta_2(t)\phi_{yu} + \delta_3(t)\phi_{xu})u_y + (2\delta_1(t)\phi_{xv} + \delta_3(t)\phi_{yv})v_x \\
 & + (2\delta_2(t)\phi_{yv} + \delta_3(t)\phi_{xv})v_y + \delta_1(t)\phi_{xx} + \delta_2(t)\phi_{yy} \\
 & + \delta_3(t)\phi_{xy} - \lambda_{21}\delta_4(t)(u^2 v + v^3) \\
 & - \lambda_{22}\delta_4(t)(uv^2 + u^3) + 2\delta_4(t)\psi uv + 3\delta_4(t)\phi v^2 \\
 & + \delta_4(t)\phi u^2 + \psi_t = 0.
 \end{aligned} \tag{49}$$

Solving the above systems, we have

$$\phi = -Cu, \psi = Cv, \lambda_{12} = \lambda_{21} = 0, \lambda_{11} = C, \lambda_{22} = -C. \tag{51}$$

**Theorem 4.1.** System (3) is non-linearly self-adjoint.

The formal Lagrangian corresponding to (43) reads as,

$$\begin{aligned}
 L = & -Cu[u_t + \delta_1(t)v_{xx} + \delta_2(t)v_{yy} + \frac{1}{2}\delta_3(t)v_{xy} \\
 & + \frac{1}{2}\delta_3(t)v_{yx} + \delta_4(t)(u^2 v + v^3)] \\
 & + Cv[-v_t + \delta_1(t)u_{xx} + \delta_2(t)u_{yy} + \frac{1}{2}\delta_3(t)u_{xy} \\
 & + \frac{1}{2}\delta_3(t)u_{yx} + \delta_4(t)(u^3 + uv^2)].
 \end{aligned} \tag{52}$$

### Conservation Laws

In this section, we will construct the conservation laws for system (3) by Ibragimov's theorem. Next, we briefly review the notations used in the following sections. Let  $x = (x^1, x^2, \dots, x^n)$  be  $n$  independent variables,  $u = (u^1, u^2, \dots, u^m)$  be  $m$  dependent variables,

$$X = \xi_i(x, u, u_{(1)}, \dots) \frac{\partial}{\partial x^i} + \eta_s(x, u, u_{(1)}, \dots) \frac{\partial}{\partial u^s}, \tag{53}$$

be a symmetry of  $m$  equations

$$F_s(x, u, u_{(1)}, \dots, u_{(N)}) = 0, s = 1, 2, \dots, m. \tag{54}$$

and the corresponding adjoint equation

$$\begin{aligned}
 F_s^*(x, u, v, u_{(1)}, v_{(1)}, \dots, u_{(N)}, v_{(N)}) \\
 = \frac{\delta(v^i F_i)}{\delta u^s} = 0, s = 1, 2, \dots, m.
 \end{aligned} \tag{55}$$

**Theorem 4.2.** Any Lie point, Lie-Bäcklund and non-local symmetry  $X$ , as given in (53), of Equation (54) provides a conservation law for the system (54) and its adjoint system (55). The conserved vector is defined by

$$\begin{aligned}
 T^i = & \xi_i \mathcal{L} + W^s \left[ \frac{\partial \mathcal{L}}{\partial u_i^s} - D_{x^j} \left( \frac{\partial \mathcal{L}}{\partial u_{ij}^s} \right) + D_{x^j} D_{x^k} \left( \frac{\partial \mathcal{L}}{\partial u_{ijk}^s} \right) - \dots \right] \\
 & + D_{x^j} (W^s) \left[ \frac{\partial \mathcal{L}}{\partial u_{ij}^s} - D_{x^k} \left( \frac{\partial \mathcal{L}}{\partial u_{ijk}^s} \right) + D_{x^k} D_{x^r} \left( \frac{\partial \mathcal{L}}{\partial u_{ijk r}^s} \right) - \dots \right] \\
 & + D_{x^j} D_{x^k} (W^s) \left[ \frac{\partial \mathcal{L}}{\partial u_{ijk}^s} - D_{x^r} \left( \frac{\partial \mathcal{L}}{\partial u_{ijk r}^s} \right) + \dots \right] + \dots,
 \end{aligned} \tag{56}$$

where  $W^s = \eta_s - \xi_i u_i^s$  is the Lie characteristic function and  $\mathcal{L} = \sum_{i=1}^m v^i F_i$  is the formal Lagrangian.

Based on the formula in Theorem 4.2, we next construct conserved vectors for system (3) by employing the formal Lagrangian (43) and the symmetry operator (10). For system (3), Equation (56) becomes the following form

$$\begin{aligned}
 T^x = & \xi \mathcal{L} - W^1 \left[ D_x \left( \frac{\partial \mathcal{L}}{\partial u_{xx}} \right) + D_y \left( \frac{\partial \mathcal{L}}{\partial u_{xy}} \right) \right] \\
 & + D_x(W^1) \left( \frac{\partial \mathcal{L}}{\partial u_{xx}} \right) + D_y(W^1) \left( \frac{\partial \mathcal{L}}{\partial u_{xy}} \right) \\
 & - W^2 \left[ D_x \left( \frac{\partial \mathcal{L}}{\partial v_{xx}} \right) + D_y \left( \frac{\partial \mathcal{L}}{\partial v_{xy}} \right) \right] + D_x(W^2) \left( \frac{\partial \mathcal{L}}{\partial v_{xx}} \right) \\
 & + D_y(W^2) \left( \frac{\partial \mathcal{L}}{\partial v_{xy}} \right)
 \end{aligned} \tag{57}$$

$$\begin{aligned}
 = & \xi \mathcal{L} - W^1 C(\delta_1(t)v_x + \frac{1}{2}\delta_3(t)v_y) \\
 & + D_x(W^1) (C\delta_1(t)v) + D_y(W^1) (\frac{1}{2}C\delta_3(t)v) \\
 & + W^2 C(\delta_1(t)u_x + \frac{1}{2}\delta_3(t)u_y) - D_x(W^2) (C\delta_1(t)u) \\
 & - D_y(W^2) (\frac{1}{2}C\delta_3(t)u),
 \end{aligned}$$

$$\begin{aligned}
 T^y = & \eta \mathcal{L} - W^1 \left[ D_x \left( \frac{\partial \mathcal{L}}{\partial u_{yx}} \right) + D_y \left( \frac{\partial \mathcal{L}}{\partial u_{yy}} \right) \right] \\
 & + D_x(W^1) \left( \frac{\partial \mathcal{L}}{\partial u_{yx}} \right) + D_y(W^1) \left( \frac{\partial \mathcal{L}}{\partial u_{yy}} \right) \\
 & - W^2 \left[ D_x \left( \frac{\partial \mathcal{L}}{\partial v_{yx}} \right) + D_y \left( \frac{\partial \mathcal{L}}{\partial v_{yy}} \right) \right] \\
 & + D_x(W^2) \left( \frac{\partial \mathcal{L}}{\partial v_{yx}} \right) + D_y(W^2) \left( \frac{\partial \mathcal{L}}{\partial v_{yy}} \right) \\
 = & \eta \mathcal{L} - W^1 C \left[ \frac{1}{2}\delta_3(t)v_x + \delta_2(t)v_y \right] + D_x(W^1) (\frac{1}{2}C\delta_3(t)v) \\
 & + D_y(W^1) (C\delta_2(t)v) \\
 & + W^2 C \left[ \frac{1}{2}\delta_3(t)u_x + \delta_2(t)u_y \right] - D_x(W^2) (\frac{1}{2}C\delta_3(t)u) \\
 & - D_y(W^2) (C\delta_2(t)u),
 \end{aligned} \tag{58}$$

$$\begin{aligned}
 T^t = & \tau \mathcal{L} + W^1 \left( \frac{\partial \mathcal{L}}{\partial u_t} \right) + W^2 \left( \frac{\partial \mathcal{L}}{\partial v_t} \right) = \tau \\
 & \mathcal{L} - W^1 (Cu) - W^2 (Cv),
 \end{aligned} \tag{59}$$

with

$$\begin{aligned}
 W^1 = & \Phi - \xi u_x - \eta u_y - \tau u_t, \\
 W^2 = & \Omega - \xi v_x - \eta v_y - \tau v_t.
 \end{aligned}$$

Case 1  $\mathfrak{J}_1 = x \frac{\partial}{\partial x} + y \frac{\partial}{\partial y} + \frac{2 \int \delta_1(t) dt}{\delta_1(t)} \frac{\partial}{\partial t} + u \frac{\partial}{\partial u} + v \frac{\partial}{\partial v}$

The Lie characteristic functions for this operator are

$$W^1 = u - xu_x - yu_y - \frac{2 \int \delta_1(t) dt}{\delta_1(t)} u_t, \tag{60}$$

$$W^2 = v - xv_x - yv_y - \frac{2 \int \delta_1(t) dt}{\delta_1(t)} v_t. \tag{61}$$

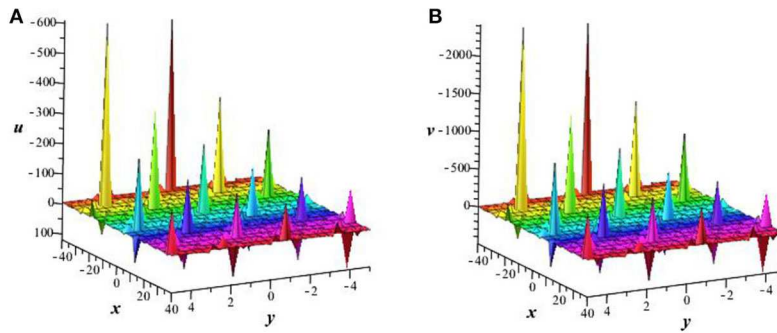


**FIGURE 1** | Plot of invariant solution (25) with  $\delta_1(t) = \sin t$ ,  $A_1 = 1$ ,  $B_1 = 4$ ,  $\alpha = \beta = k_1 = 1$ ,  $k_2 = 3$  at  $t = 0$ . **(A)** Perspective view of the solution  $u$ . **(B)** Perspective view of the solution  $v$ .

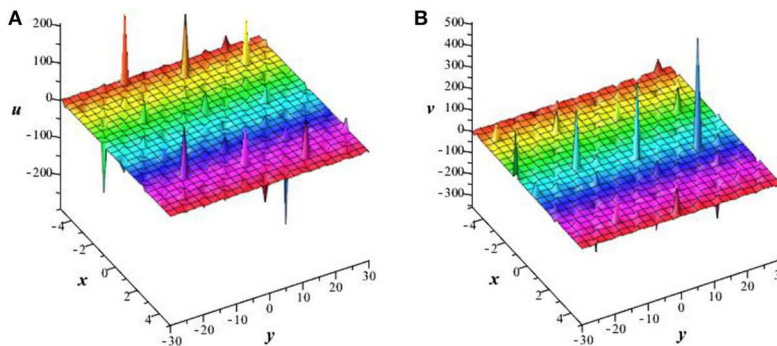


**FIGURE 2** | Plot of invariant solution (36) with  $\delta_1(t) = 1$ ,  $C_1 = 2$ ,  $C_2 = 1$ ,  $\lambda = \mu = \chi = 1$ ,  $B_0 = B_1 = k_2 = k_3 = 1$  at  $t = 5$ . **(A)** Perspective view of the solution  $u$ . **(B)** Perspective view of the solution  $v$ .

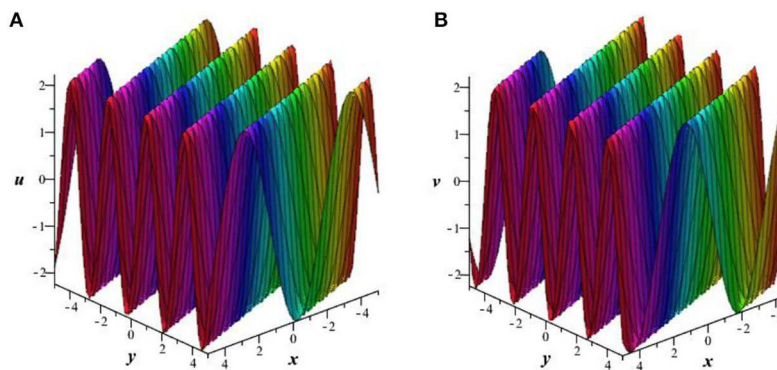


**FIGURE 3** | Plot of invariant solution (42) with  $C_1 = 1$ ,  $C_2 = 2$ ,  $k_1 = k_2 = k_3 = 1$  at  $t = 0$ . **(A)** Perspective view of the solution  $u$ . **(B)** Perspective view of the solution  $v$ .

The corresponding conservation laws are

$$\begin{aligned}
 T^x = & -\frac{1}{2}C [2k_1\delta_1(t)(uv_{yy} - u_{yy}v) + k_2\delta_1(t) \\
 & (uv_{xy} - u_xv_y + u_yv_x - u_{xy}v) + 2(uu_t + vv_t)]x \\
 & -\frac{1}{2}C [k_2\delta_1(t)(u_{yy}v - uv_{yy}) + 2\delta_1(t) \\
 & (u_{xy}v - u_yv_x - uv_{xy} + u_xv_y)]y \\
 & -\frac{1}{2}C \int \delta_1(t)dt [2k_2(u_{ty}v - uv_{ty} - u_tv_y + u_yv_t) \\
 & + 4(u_{tx}v - uv_{tx} - u_tv_x + u_xv_t)] \\
 & -\frac{1}{2}C [k_2\delta_1(t)(uv_y - u_yv) + 2\delta_1(t)(uv_x - u_xv)],
 \end{aligned} \tag{62}$$

$$\begin{aligned}
 T^y = & \frac{1}{2}C [2k_1\delta_1(t)(uv_{xy} + u_xv_y - u_yv_x - u_{xy}v) + k_2\delta_1(t) \\
 & (uv_{xx} - u_{xx}v)]x \\
 & +\frac{1}{2}C [2\delta_1(t)(u_{xx}v - uv_{xx}) + k_2\delta_1(t) \\
 & (u_yv_x + u_{xy}v - uv_{xy} - u_xv_y) - 2(uu_t + vv_t)]y
 \end{aligned} \tag{63}$$

$$\begin{aligned}
 T^t = & C [(uu_x + vv_x)x + (uu_y + vv_y)y - (u^2 + v^2)] \\
 & -C \int \delta_1(t)dt [2k_1(uv_{yy} - u_{yy}v) \\
 & + 2k_2(uv_{xy} - u_{xy}v) + 2(uv_{xx} - u_{xx}v)].
 \end{aligned} \tag{64}$$

Case 2  $\mathfrak{J}_2 = \frac{\partial}{\partial x}$

The Lie characteristic functions for this operator are

$$W^1 = -u_x, W^2 = -v_x. \quad (65)$$

The corresponding conservation laws are

$$T^x = -\frac{1}{2}C [2\delta_2(t)(uv_{yy} - u_{yy}v) + \delta_3(t)(uv_{xy} - u_{xy}v - u_xv_y + u_yv_x) + 2(uu_t + vv_t)], \quad (66)$$

$$T^y = \frac{1}{2}C [2\delta_2(t)(uv_{xy} - u_{xy}v + u_xv_y - u_yv_x) + \delta_3(t)(uv_{xx} - u_{xx}v)], \quad (67)$$

$$T^t = C(uu_x + vv_x). \quad (68)$$

Case 3  $\mathfrak{J}_3 = \frac{\partial}{\partial y}$

The Lie characteristic functions for this operator are

$$W^1 = -u_y, W^2 = -v_y. \quad (69)$$

The corresponding conservation laws are

$$T^x = \frac{1}{2}C [2\delta_1(t)(uv_{xy} - u_{xy}v - u_xv_y + u_yv_x) + \delta_3(t)(uv_{yy} - u_{yy}v)], \quad (70)$$

$$T^y = \frac{1}{2}C [2\delta_1(t)(u_{xx}v - uv_{xx}) - \delta_3(t)(uv_{xy} - u_{xy}v + u_xv_y - u_yv_x) - 2(uu_t + vv_t)], \quad (71)$$

$$T^t = C(uu_y + vv_y). \quad (72)$$

Case 4  $\mathfrak{J}_4 = \frac{1}{\delta_1(t)} \frac{\partial}{\partial t}$

The Lie characteristic functions for this operator are

$$W^1 = -\frac{1}{\delta_1(t)}u_t, W^2 = -\frac{1}{\delta_1(t)}v_t. \quad (73)$$

The corresponding conservation laws are,

$$T^x = \frac{1}{2}C [k_2(uv_{ty} - u_{ty}v + u_tv_y - u_yv_t) + 2(uv_{tx} - u_{tx}v + u_tv_x - u_xv_t)], \quad (74)$$

$$T^y = \frac{1}{2}C [k_2(uv_{tx} - u_{tx}v + u_tv_x - u_xv_t) + 2k_1(uv_{ty} - u_{ty}v + u_tv_y - u_yv_t)], \quad (75)$$

$$T^t = C [k_1(u_{yy}v - uv_{yy}) + k_2(u_{xy}v - uv_{xy}) + (u_{xx}v - uv_{xx})]. \quad (76)$$

## RESULTS AND DISCUSSION

The Lie group method has been successfully used to establish the invariant solutions for the vCHFSC equation. Some results for the vCHFSC equation have been published in the literature.

Huang et al. [26] used the Hirota bilinear method and found the bright and dark solitons to Equation (1). Peng [27] reported some new non-autonomous complex wave and analytic solutions to Equation (1) with the aid of the  $(G'/G)$  method. In this article, we constructed the trigonometric and hyperbolic function solutions to the studied equation. Compared with the solutions obtained in references [26, 27], our results are new. To better understand the characteristics of the obtained solutions, the 3D graphical illustrations are plotted in **Figures 1–3**.

With the Lagrangian, we find that the vCHFSC equation is non-linearly self-adjoint. Furthermore, a new conservation theorem has been used to construct conservation laws for the vCHFSC equation. Based on the four infinitesimal generators, we obtained four conserved vectors. It worth noting that the conservation laws obtained in this article have been verified by Maple software.

## CONCLUSION

In this research, the infinitesimal generators and Lie point symmetries of the vCHFSC equation have been investigated using the Lie group method. Based on the optimal system of one-dimensional subalgebras, four types of similarity reductions are presented. Taking similarity reductions into account, the invariant solutions are provided, including trigonometric and hyperbolic function solutions. Furthermore, conservation laws for the vCHFSC equation are derived by non-linear self-adjointness and a new conservation theorem.

## DATA AVAILABILITY STATEMENT

The original contributions presented in the study are included in the article; further inquiries can be directed to the corresponding author.

## AUTHOR CONTRIBUTIONS

The author confirms being the sole contributor of this work and has approved it for publication.

## FUNDING

This work was supported by Shandong Provincial Government Grants, the National Natural Science Foundation of China-Shandong Joint Fund (No. U1806203), Program for Young Innovative Research Team in Shandong University of Political Science and Law, and the Project of Shandong Province Higher Educational Science and Technology Program (No. J18KA234).

## ACKNOWLEDGMENTS

We would like to express our sincerest thanks to the editor and the reviewers for their valuable suggestions and comments, which lead to further improvement of our original manuscript.

## REFERENCES

- Mikhailov AV. The reduction problem and the inverse scattering method. *Phys D*. (1981) 3:73–117. doi: 10.1016/0167-2789(81)90120-2
- Olver PJ. *Applications of Lie Groups to Differential Equations*. Berlin: Springer (1993). doi: 10.1007/978-1-4612-4350-2
- Ovsiannikov LV. *Group Analysis of Differential Equations*. Cambridge: Academic (1982). doi: 10.1016/B978-0-12-531680-4.50012-5
- Bluman GW, Cheviakov AF, Anco SC. *Applications of Symmetry Methods to Partial Differential Equations*. Berlin: Springer (2010). doi: 10.1007/978-0-387-68028-6
- Hirota R, Satsuma J. Soliton solutions of a coupled Korteweg-de Vries equation. *Phys Lett A*. (1981) 85:407–8. doi: 10.1016/0375-9601(81)90423-0
- Ma WX. Lump solutions to the Kadomtsev-Petviashvili equation. *Phys Lett A*. (2015) 379:1975–8. doi: 10.1016/j.physleta.2015.06.061
- Fan EG. Extended Tanh-function method and its applications to nonlinear equations. *Phys Lett A*. (2000) 277:212–8. doi: 10.1016/S0375-9601(00)00725-8
- Abdou MA. The extended tanh method and its applications for solving nonlinear physical models. *Appl Math Comput*. (2010) 190:988–96. doi: 10.1016/j.amc.2007.01.070
- Wazwaz AM. The extended tanh method for the Zakharov-Kuznetsov (ZK) equation, the modified ZK equation, and its generalized forms. *Comm Nonlinear Sci Numer Simul*. (2008) 13:1039–47. doi: 10.1016/j.cnsns.2006.10.007
- Liu N, Liu YS. New multi-soliton solutions of a (3+1)-dimensional nonlinear evolution equation. *Comput. Math. Appl*. (2016) 71:1645–54. doi: 10.1016/j.camwa.2016.03.012
- Darvishi MT, Mohammad NA. Modification of extended homoclinic test approach to solve the (3+1)-dimensional potential-YTSE equation. *Chin Phys Lett*. (2011) 28:040201. doi: 10.1088/0256-307X/28/4/040202
- Wang CJ, Dai ZD, Lin L. Exact three-wave solution for higher dimensional KdV-type equation. *Appl Math Comput*. (2010) 216:501–5. doi: 10.1016/j.amc.2010.01.057
- Abdou MA. The extended F-expansion method and its application for a class of nonlinear evolution equations. *Chaos Solitons Fractals*. (2007) 31:95–104. doi: 10.1016/j.chaos.2005.09.030
- Emmanuel Y. The extended F-expansion method and its application for solving the nonlinear wave, CKGZ, GDS, DS and GZ equations. *Phys Lett A*. (2005) 340:149–60. doi: 10.1016/j.physleta.2005.03.066
- Liu N, Liu YS. Homoclinic breather wave, rouge wave and interaction solutions for a (3+1)-dimensional KdV-type equation. *Phys Scr*. (2019) 94:035201. doi: 10.1088/1402-4896/aaf654
- Liu N, Liu YS. Lump solitons and interaction phenomenon to a (3+1)-dimensional Kadomtsev-Petviashvili-Boussinesq-like equation. *Mod Phys Lett*. (2019) 33:1950395. doi: 10.1142/S0217984919503950
- Aliyu AI, Inc M, Yusuf A, Baleanu D, Bayram M. Dark-bright optical soliton and conserved vectors to the Biswas-Arshed equation with third-order dispersions in the absence of self-phase modulation. *Front Phys*. (2019) 7:28. doi: 10.3389/fphy.2019.00028
- Inc M, Aliyu AI, Yusuf A, Baleanu D. Optical solitons, conservation laws and modulation instability analysis for the modified nonlinear Schrödinger's equation for Davydov solitons. *J Electromagn Waves Appl*. (2018) 32:858–73. doi: 10.1080/09205071.2017.1408499
- Zhang LH, Xu FS. Conservation laws, symmetry reductions, and exact solutions of some Keller-Segel models. *Adv Differ Equat*. (2018) 2018:327. doi: 10.1186/s13662-018-1723-7
- Kaur L, Wazwaz AM. Painlevé analysis and invariant solutions of generalized fifth-order nonlinear integrable equation. *Nonlinear Dyn*. (2018) 94:2469–77. doi: 10.1007/s11071-018-4503-8
- Wang GW, Kara AH. A (2+1)-dimensional KdV equation and mKdV equation: symmetries, group invariant solutions and conservation laws. *Phys Lett A*. (2019) 383:728–31. doi: 10.1016/j.physleta.2018.11.040
- Wei GM, Lu YL, Xie YQ, Zheng WX. Lie symmetry analysis and conservation law of variable-coefficient Davey-Stewartson equation. *Comput Math Appl*. (2018) 75:3420–30. doi: 10.1016/j.camwa.2018.02.008
- Yusuf A, Inc M, Aliyu AI. Optical solitons possessing beta derivative of the Chen-Lee-Liu equation in optical fibers. *Front Phys*. (2019) 7:34. doi: 10.3389/fphy.2019.00034
- Yusuf A, Inc M, Bayram M. Invariant and simulation analysis to the time fractional Abrahams-Tsuneto reaction diffusion system. *Phys Scr*. (2019) 94:125005. doi: 10.1088/1402-4896/ab373b
- Tchier F, Yusuf A, Aliyu AI. Soliton solutions and conservation laws for lossy nonlinear transmission line equation. *Superlattices Microst*. (2017) 107:320–36. doi: 10.1016/j.spmi.2017.04.003
- Huang QM, Gao YT, Jia SL. Bright and dark solitons for a variable-coefficient (2+1) dimensional Heisenberg ferromagnetic spin chain equation. *Opt Quant Electron*. (2018) 50:183. doi: 10.1007/s11082-018-1428-x
- Peng LJ. Nonautonomous complex wave solutions for the (2+1)-dimensional Heisenberg ferromagnetic spin chain equation with variable coefficients. *Opt Quant Electron*. (2019) 51:168. doi: 10.1007/s11082-019-1883-z
- Latha MM, Vasanthi CC. An integrable model of (2+1)-dimensional Heisenberg ferromagnetic spin chain and soliton excitations. *Phys Scr*. (2014) 89:065204. doi: 10.1088/0031-8949/89/6/065204
- Anitha T, Latha MM, Vasanthi CC. Dromions in (2+1) dimensional ferromagnetic spin chain with bilinear and biquadratic interactions. *Phys A Stat Mech Appl*. (2014) 415:105–15. doi: 10.1016/j.physa.2014.07.078
- Triki H, Wazwaz AM. New solitons and periodic wave solutions for the (2+1)-dimensional Heisenberg ferromagnetic spin chain equation. *J Electromagn Wave*. (2016) 30:788–94. doi: 10.1080/09205071.2016.1153986
- Tang GS, Wang SH, Wang GW. Solitons and complexitons solutions of an integrable model of (2+1)-dimensional Heisenberg ferromagnetic spin chain. *Nonlinear Dyn*. (2017) 88:2319–27. doi: 10.1007/s11071-017-3379-3
- Olver, P.J. *Applications of Lie Groups to Differential Equations*. New York, NY: Springer (1986). doi: 10.1007/978-1-4684-0274-2
- Wang ML, Li X, Zhang J. The  $\left(\frac{G}{G}\right)$ -expansion method and travelling wave solutions of nonlinear evolution equations in mathematical physics. *Phys Lett A*. (2008) 372:417–23. doi: 10.1016/j.physleta.2007.07.051
- Marwat DNK, Kara AH, Hayat T. Conservation laws and associated Noether type vector fields via partial Lagrangians and Noether's theorem for the liang equation. *Int J Theor Phys*. (2008) 47:3075–81. doi: 10.1007/s10773-008-9739-5
- Naz R. Conservation laws for some compacton equations using the multiplier approach. *Appl Math Lett*. (2012) 25:257–61. doi: 10.1016/j.aml.2011.08.019
- Bokhari AH, Al-Dweik AY, Kara AH, Mahomed FM, Zaman FD. Double reduction of a nonlinear (2+1) wave equation via conservation laws. *Commun Nonlinear Sci Numer Simul*. (2011) 16:1244–53. doi: 10.1016/j.cnsns.2010.07.007
- Sjöberg A. On double reductions from symmetries and conservation laws. *Nonlinear Anal RWA*. (2009) 10:3472–7. doi: 10.1016/j.nonrwa.2008.09.029
- Ibragimov NH. A new conservation theorem. *J Math Anal Appl*. (2007) 333:311–28. doi: 10.1016/j.jmaa.2006.10.078
- Ibragimov NH, Khamitovaa RS, Valenti A. Self-adjointness of a generalized Camassa-Holm equation. *Appl Math Comput*. (2011) 218:2579–83. doi: 10.1016/j.amc.2011.07.074

**Conflict of Interest:** The author declares that the research was conducted in the absence of any commercial or financial relationships that could be construed as a potential conflict of interest.

Copyright © 2020 Liu. This is an open-access article distributed under the terms of the Creative Commons Attribution License (CC BY). The use, distribution or reproduction in other forums is permitted, provided the original author(s) and the copyright owner(s) are credited and that the original publication in this journal is cited, in accordance with accepted academic practice. No use, distribution or reproduction is permitted which does not comply with these terms.



# ESERK Methods to Numerically Solve Nonlinear Parabolic PDEs in Complex Geometries: Using Right Triangles

Jesús Martín-Vaquero\*

Department on Applied Mathematics, Instituto Universitario de Física Fundamental y Matemáticas, Universidad de Salamanca, Salamanca, Spain

In this paper Extrapolated Stabilized Explicit Runge-Kutta methods (ESERK) are proposed to solve nonlinear partial differential equations (PDEs) in right triangles. These algorithms evaluate more times the function than a standard explicit Runge-Kutta scheme ( $n_t$  times per step), and these extra evaluations do not increase the order of convergence but the stability region grows with  $\mathcal{O}(n_t^2)$ . Hence, the total computational cost is  $\mathcal{O}(n_t)$  times lower than with a traditional explicit algorithm. Thus, these algorithms have been traditionally considered to solve stiff PDEs in squares/rectangles or cubes. In this paper, for the first time, ESERK methods are considered in a right triangle. It is demonstrated that such type of codes keep the convergence and the stability properties under certain conditions. This new approach would allow to solve nonlinear parabolic PDEs with stabilized explicit Runge-Kutta schemes in complex domains, that would be decomposed in rectangles and right triangles.

## OPEN ACCESS

### Edited by:

Poom Kumam,  
King Mongkut's University of  
Technology Thonburi, Thailand

### Reviewed by:

Abdullahi Yusuf,  
Federal University Dutse, Nigeria  
Kazuharu Bamba,  
Fukushima University, Japan

### \*Correspondence:

Jesús Martín-Vaquero  
jesmarva@usal.es

### Specialty section:

This article was submitted to  
Mathematical and Statistical Physics,  
a section of the journal  
Frontiers in Physics

**Received:** 15 February 2020

**Accepted:** 29 July 2020

**Published:** 09 September 2020

### Citation:

Martín-Vaquero J (2020) ESERK  
Methods to Numerically Solve  
Nonlinear Parabolic PDEs in Complex  
Geometries: Using Right Triangles.  
Front. Phys. 8:367.  
doi: 10.3389/fphy.2020.00367

**Keywords:** complex geometries, higher-order codes, multi-dimensional partial differential equations, nonlinear PDEs, Stabilized Explicit Runge-Kutta methods

## 1. INTRODUCTION

Let us suppose that we have to solve a nonlinear PDE with dominating diffusion:

$$u_t = d(u_{\bar{x}\bar{x}} + u_{\bar{y}\bar{y}}) + f(t, \bar{x}, \bar{y}, u) \quad (\bar{x}, \bar{y}) \in \Omega \subset \mathbb{R}^2, \quad (1)$$

subject to traditional initial and Dirichlet boundary conditions:

$$u(0, \bar{x}, \bar{y}) = g_1(\bar{x}, \bar{y}) \quad (\bar{x}, \bar{y}) \in \Omega, \quad (2)$$

and

$$u(t, \bar{x}, \bar{y}) = g_2(\bar{x}, \bar{y}) \quad (\bar{x}, \bar{y}) \in \partial(\Omega). \quad (3)$$

These types of problems are very common in a large amount of areas such as atmospheric phenomena, biology, chemical reactions, combustion, financial mathematics, industrial engineering, laser modeling, malware propagation, medicine, mechanics, molecular dynamics, nuclear kinetics, etc., see [1–9], to mention a few.

A widely-used approach for solving these time-dependent and multi-dimensional PDEs is to first discretize the space variables (with finite difference or spectral methods) to obtain a very large system of ODEs of the form

$$y' = f(t, y); \quad y(t_0) = y_0; \quad (4)$$

where  $y, y_0 \in \mathbb{R}^n$ ,  $t \geq t_0$ , and  $f(t, y)$  takes value in  $\mathbb{R}^n$ , this procedure is well-known as the method of lines (MOL). But these systems of ODEs not only have a huge dimension, additionally they might become very stiff problems.

Hence, traditional explicit methods are usually very slow, due to absolute stability, it is necessary to use very small length steps, see [6, 7] and references therein. Therefore, these schemes are not usually considered.

Implicit schemes based on BDF and Runge–Kutta methods have much better stability properties. However, since the dimension of the ODE system is very high, then it is necessary to solve very large nonlinear systems at each iteration.

Other numerous techniques have also been proposed based on ETD schemes (but it is necessary to approximate operators including matrix exponentials), alternating direction implicit methods (they have limitations on the order of convergence) and explicit-implicit algorithms. However, in any case the number of operations is huge when the system dimension is high.

For those cases where it is known that the Jacobian eigenvalues of the function are all real negative or are very close to this semi-axis, there is another option: stabilized explicit Runge–Kutta methods (they are also called Runge–Kutta–Chebyshev methods). This happens, for example, when diffusion dominates in the PDE, when the Laplacian is discretized using finite differences or some spectral techniques, then the associated matrix has this type of eigenvalues.

These types of algorithms are totally explicit, but they have regions of stability extended along the real negative axis. These schemes typically have order 2 or 4 [8, 10–16]. Recently, we propose a new procedure combined with Richardson extrapolation to obtain methods with other orders of convergence [17, 18], but in all these methods, these integrators have many more stages than the order of convergence. Most of these extra stages seek to extend as much as possible the region of stability along the negative real axis. Regions of stability increase quadratically with the number of stages. Thus, the cost per step is greater than in a classic Runge–Kutta, because it is necessary to evaluate the function in Equation (4)  $n_i$  times. However, the number of steps reduce proportionally with  $n_i^2$ , thus the total computational cost is reduced proportionally with  $n_i$ .

These schemes have been traditionally considered in squares/rectangles or cubes. But this makes difficult to apply them in PDEs with complex geometries, which happens in most of the cases. Some different strategies have been proposed to apply them when the original domain is not a square nor a cube (see [3–5]). They implemented stabilized Runge–Kutta methods after using adaptive multiresolution techniques or fixed mesh codes in space. But simulations in complex geometries constitute a very challenging problem, see (section 4, [5]), where they stated for their results based on adaptive multiresolution techniques that they “will only present here 2D and 3D simulations in simplified geometries for the sake of assessing our results and perspectives in the field.”

As far as we know, stabilized explicit Runge–Kutta methods have not been tested in triangles yet. For this reason, in this paper, we are analysing how ESERK methods can be employed to solve nonlinear PDEs in these types of regions and their convergence.

In this paper, a summary on ESERK4 methods is provided in section 2. The major advance of our contribution is given in section 3: it is explained how ESERK4 can be utilized for (1) when  $\Omega$  is a right triangle. After some linear transformations and spatial discretizations ESERK4 is numerically stable and fourth-order convergence in time, and second-order in space is obtained. This allows a new way to numerically approach parabolic nonlinear PDEs in complex domains in the plane, which can be easier decomposed in a sum of triangles and rectangles. Finally, some conclusions and future goals are outlined.

## 2. ESERK4 METHODS

### 2.1. Construction of First-Order Stabilized Explicit Methods

In [17], ESERK4 schemes were developed for nonlinear PDEs in several dimensions with good stability properties and numerical results in squares and cubes. The idea is quite simple: first-order stabilized explicit Runge–Kutta (SERK) methods are derived using Chebyshev polynomials of the first kind:

$$T_0(x) = 1, \quad T_1(x) = x, \quad T_s(x) = 2xT_{s-1}(x) - T_{s-2}(x), \quad (5)$$

$s$  being the number of stages of the first-order method.

If we consider

$$R_s(z) = \frac{T_s(w_{0,s} + w_{1,s}z)}{T_s(w_{0,s})}, \quad w_{0,s} = 1 + \frac{\mu_4}{s^2}, \quad w_{1,s} = \frac{T_s(w_{0,s})}{T'_s(w_{0,s})}, \quad (6)$$

then  $|R_s(z)|$  oscillates between  $-\lambda_4$  and  $\lambda_4$  (for a value  $0 < \lambda_4 = 0.311688 < 1$  that we will calculate later) in a region which is  $O(s^2)$ , and  $R_s(z) = 1 + z + O(z^2)$ .

We can construct Runge–Kutta schemes with  $|R_s(z)|$  as stability functions by just changing  $x = 1 + \alpha_p \bar{x}$  (and considering that  $1, T_s(x)$  and  $\bar{x}$  are the stability functions of Identity operator,  $g_s$ , and  $hf(\cdot)$ , and writing  $R_s(z)$  as a linear combination of the Chebyshev polynomials, see Theorem 1 [12] for more details).

### 2.2. Construction of Higher-Order ESERK Schemes

Once first-order SERK methods have been derived, they approximate the solution of the initial value problem (4), by performing  $n_i$  steps with constant step size  $h_i$  at  $x_0 + h$ , i.e.,  $y_{h_i}(x_0 + h) := S_{i,1}$ , with step sizes  $h_1 > h_2 > h_3 > \dots$  (taking  $h_i = h/n_i$ ,  $n_i = 1, \dots, 4$ ).

Finally

$$S_{4,4} = \frac{-S_{1,1} + 24S_{2,1} - 81S_{3,1} + 64S_{4,1}}{6} = \frac{64y_{h/4}(x_0 + h) - 81y_{h/3}(x_0 + h) + 24y_{h/2}(x_0 + h) - y_h(x_0 + h)}{6} \quad (7)$$

is a fourth-order approximation with

$$P_{4s}(z) = \frac{-R_s(z) + 24(R_s(z/2))^2 - 81(R_s(z/3))^3 + 64(R_s(z/4))^4}{6} \quad (8)$$

as its stability function. Additionally, we have that

$$|P_{4s}(z)| \leq \frac{|R_s(z)| + 24|R_s(z/2)|^2 + 81|R_s(z/3)|^3 + 64|R_s(z/4)|^4}{6}$$

The positive real solution of

$$\frac{x + 24x^2 + 81x^3 + 64x^4}{6} = 0.95$$

is  $\lambda_4 = 0.311688$ . Hence, whenever  $|R_s(z)| < 0.311688$ , then  $|P_{4s}(z)| < 0.95$ . Taking  $\mu_4 = \frac{27}{16}$ , it can be checked numerically that  $|R_{s,4}(z)| \leq 0.311688$  for  $z \in [-s^2, -1]$  and  $9 \leq s \leq 4000$ , and therefore the ESERK4 methods derived in this way are fourth-order approximations and numerically stable in a region including  $[-s^2, 0]$ .

### 2.3. Parallel, Variable-Step, and Number of Stages Algorithm

In [17], we constructed a variable-step and number of stages algorithm combining all the schemes derived there, with  $s$  up to 4,000. The idea is quite simple: (i) First, we select the step size in order to control the local error; the best results were obtained using techniques considered for standard extrapolation methods (see Equations (8–11) in [17]). (ii) Later the minimum  $s$  is chosen so that the absolute stability is satisfied.

Recently, we are working developing the parallel version of this code (see [19]). Using 4 threads, CPU times are up to 2.5 times smaller than in the previous sequential algorithm. The new parallel code also has a decreasing memory demand, and therefore it is possible to solve problems with higher dimension in regular PCs.

## 3. DECOMPOSITION OF COMPLEX GEOMETRIES INTO RIGHT TRIANGLES

Complex geometric shapes are ubiquitous in our natural environment. In this paper, we are interested in numerically solving partial differential equations (PDEs) in such types of geometries, which are very common in problems related with human bodies, materials, or simply a complicated engine in classical engineering applications.

One very well-known strategy, within a finite element context, is to build the necessary modifications in the vicinity of the boundary. Such an approach is studied in the composite finite element method (FEM). Those methods based on finite element are usually proposed only for linear PDEs. FEM is a numerical method for solving problems of engineering and mathematical physics (typical problems include structural analysis, heat transfer, fluid flow, mass transport, or electromagnetic potential, because these problems generally require numerically approximating the solution of linear partial differential equations). The finite element method allows the transformation of the problem in a system of algebraic equations. Unfortunately, it is more difficult to employ these techniques with nonlinear parabolic PDEs in several dimensions, although some results have been obtained to know when the resulting

discrete Galerkin equations have a unique solution in [20]. However, for some problems, some of these techniques are not easy to be employed numerically, they are computationally very expensive because they require solving nonlinear systems with huge dimension at every step, or it is difficult to demonstrate that the numerical schemes have unique solution in a general case.

On the other hand, Implicit–Explicit (IMEX) methods have been employed to solve a very stiff nonlinear system of ODEs coming from the spatial discretization of nonlinear parabolic PDEs that appeared in the modelization of an ischemic stroke in [5]. The authors employed an adaptive multiresolution approach and a finite volume strategy for the spatial discretizations. And a Strang splitting method in time, combining ROCK4, an explicit Stalized Explicit Runge–Kutta scheme for the diffusion part, and Radau5, an implicit A-stable method for the reaction. These methods were previously analyzed in [3] for streamer discharge simulations, and the authors demonstrated second-order convergence in time. Later, they employed similar strategies for different physical problems in [4, 21]. As the authors state, some of these procedures are complicated except in simple domains like squares and cubes, and only second-order convergence in time is possible. However, there are complex problems where nonlinear terms have potentially large stiffness, and at the same time, it is necessary to efficiently solve the model with small errors. This motivates to derive high-order schemes with good internal stability properties.

In what follows we will explain a new strategy to numerically solve the nonlinear parabolic PDE given by Equation (1) where  $\Omega$  is any right triangle, and therefore any researcher can combine the theory (utilized with FEM) to spatially decomposed any complex geometry into triangles (since any acute triangle and obtuse triangle can be decomposed into two right triangles), and later employing the method described in this paper. Additionally, schemes proposed in this work are fourth-order ODE solvers (in time), and numerical spatial approximations will be second-order (although fourth-order formulae can be explored except for the closest points to vertices).

### 3.1. Higher-Order Spatial Approximations in the Triangle

Without loss of generality we can consider that our right triangle is  $T_R$ , the one with vertices  $(0, 1), (0, 0), (1, 0)$ . Otherwise we first use a linear transformation of the right triangle with vertices  $P_1 = (\bar{x}_1, \bar{y}_1), P_0 = (\bar{x}_0, \bar{y}_0), P_2 = (\bar{x}_2, \bar{y}_2)$  [where  $(\bar{x}_0, \bar{y}_0)$  is the vertex of the right angle]:

$$(x, y) = L(\bar{x}, \bar{y}) = (a_1(\bar{x} - \bar{x}_0) + a_2(\bar{y} - \bar{y}_0), b_1(\bar{x} - \bar{x}_0) + b_2(\bar{y} - \bar{y}_0)), \tag{9}$$

where the parameters  $a_1, a_2, b_1, b_2$  can be computed easily as

$$\begin{aligned} a_1 &= \frac{\bar{y}_2 - \bar{y}_0}{\text{Det}}, & a_2 &= \frac{\bar{x}_0 - \bar{x}_2}{\text{Det}}, \\ b_1 &= \frac{\bar{y}_0 - \bar{y}_1}{\text{Det}}, & a_2 &= \frac{\bar{x}_0 - \bar{x}_1}{\text{Det}}, \end{aligned} \tag{10}$$

where

$$\text{Det} = \begin{vmatrix} 1 & 1 & 1 \\ \bar{x}_0 & \bar{x}_1 & \bar{x}_2 \\ \bar{y}_0 & \bar{y}_1 & \bar{y}_2 \end{vmatrix} \tag{11}$$

and it is easy to check that  $\text{Det} \neq 0$  if and only the three points are not in a line (but we always have a triangle).

The main reason of decomposing our general region  $\Omega \in \mathbb{R}^2$  into right triangles (and not other triangles) is, that after this linear transformation given by Equations (9) and (10), our PDE given by Equation (1) transforms into the Equation

$$u_t = c_1 u_{xx} + c_2 u_{yy} + f(t, x, y, u) \quad (x, y) \in T_R, \quad (12)$$

subject to (traditional) initial and Dirichlet boundary conditions. Therefore, let us first study Equation (12), together with

$$u(0, x, y) = g_1(x, y) \quad (x, y) \in T_R, \quad (13)$$

and

$$u(t, x, y) = g_2(x, y) \quad (x, y) \in \partial(T_R), \quad (14)$$

where  $\partial(T_R)$  is the border of the triangle with vertices  $(0, 1), (0, 0), (1, 0)$ . One positive issue is that, after the traditional spatial discretization described below, the matrix obtained from the diffusion term has all the eigenvalues real, and therefore we can utilize the ESERK methods proposed in the previous section 2.

Now, let us define the spatial discretization of our continuous problem provided by Equation (12), the problem domain  $T_R$  is discretized by the grid points  $(x_i, y_j)$ , where

$$\begin{aligned} x_i &= i \cdot h, \quad i = 0, 1, \dots, N, \quad N = \frac{1}{h}, \quad y_j = j \cdot h, \\ j &= 0, 1, \dots, N - i, \quad h = \Delta x = \Delta y, \end{aligned} \quad (15)$$

since  $x_i + y_j \leq 1$ .

With this semidiscretizations we will approximate  $u_{xx}$  and  $u_{yy}$  at point  $(x_i, y_j)$  with the following second-order formulae:

$$\frac{\partial^2 u_{ij}}{\partial x^2} = \frac{u_{i+1,j} - 2u_{ij} + u_{i-1,j}}{h^2}, \quad \frac{\partial^2 u_{ij}}{\partial y^2} = \frac{u_{i,j+1} - 2u_{ij} + u_{i,j-1}}{h^2}. \quad (16)$$

After the linear transformation given by Equations (9) and (10), our PDE given by Equation (1) may transform into one Equation where one term in  $u_{xy}$  would appear. Normally, this term can be approximated in the square or the rectangle through the formula

$$\begin{aligned} &\frac{\partial^2 u_{ij}}{\partial x \partial y} \\ &= \frac{u_{i+1,j+1} - u_{i,j+1} - u_{i+1,j} + 2u_{ij} - u_{i-1,j} - u_{i,j-1} + u_{i-1,j-1}}{2h^2}, \end{aligned} \quad (17)$$

however, in  $T_R$ , we can obtain that the point  $(x_i, y_j)$  is in  $T_R$ , i.e.,  $x_i + y_j < 1$ , but the point  $(x_{i+1}, y_{j+1})$  might not satisfy that  $x_{i+1} + y_{j+1} \leq 1$ , and therefore we cannot employ these finite difference formulae if a term in  $u_{xy}$  appears. Fortunately, we will check that this term cancels after this transformation [given by Equations (9 and 10)] whenever the original triangle with vertices  $(\bar{x}_1, \bar{y}_1), (\bar{x}_0, \bar{y}_0)$ , and  $(\bar{x}_2, \bar{y}_2)$  is a right triangle and  $(\bar{x}_0, \bar{y}_0)$  is the vertex of the right angle. This fact is explained in **Figure 1**. If we

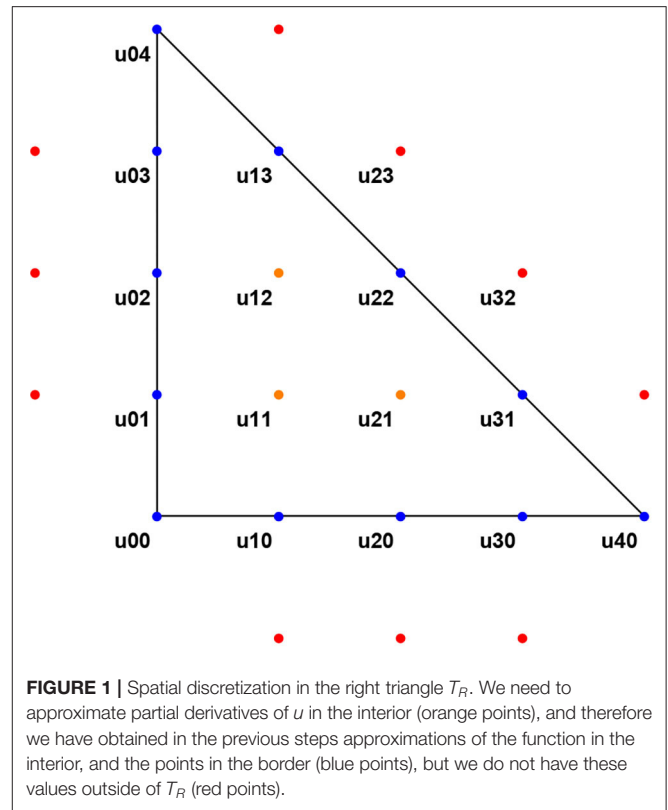


**FIGURE 1** | Spatial discretization in the right triangle  $T_R$ . We need to approximate partial derivatives of  $u$  in the interior (orange points), and therefore we have obtained in the previous steps approximations of the function in the interior, and the points in the border (blue points), but we do not have these values outside of  $T_R$  (red points).

would need to approximate  $\frac{\partial^2 u_{2,1}}{\partial x \partial y}$ , then it would be necessary to obtain an approximation of  $u_{3,2}$ , but this point is outside of the  $T_R$ , the region of study.

In this work, we are employing only second-order approximations in space. In other works, for example [13], we have also employed SERK codes after higher-order discretizations in space, but in rectangles. Normally, in rectangles, we can use formulae similar to

$$\frac{\partial^2 u_{ij}}{\partial x^2} = \frac{-u_{i+2,j} + 16u_{i+1,j} - 30u_{ij} + 16u_{i-1,j} - u_{i-2,j}}{12h^2}, \quad i = 2, \dots, N - 2, \quad (18)$$

and in the lower edge

$$\frac{\partial^2 u_{1,j}}{\partial x^2} = \frac{10u_{0,j} - 15u_{1,j} - 4u_{2,j} + 14u_{3,j} - 6u_{4,j} + u_{5,j}}{12h^2}. \quad (19)$$

However, in the triangle, again we can observe in **Figure 1**, that we would need to approximate the solution in points outside  $T_R$  before we can calculate (19) near the vertex  $(0, 1)$ . Obviously, one possible idea for the future is considering the decomposition of complex regions into bigger rectangles in the interior, and small right triangles near the border of the complex region where it is necessary to solve the PDE.

Now, we are ready to understand why we chose right triangles in the decomposition of complex regions. The main reason is,

that simple calculations give us [after linear transformations given by Equations (9–11)]:

$$u_{\bar{x}\bar{x}} + u_{\bar{y}\bar{y}} = a_1 (a_1 u_{xx} + b_1 u_{xy}) + b_1 (a_1 u_{xy} + b_1 u_{yy}) + a_2 (a_2 u_{xx} + b_2 u_{xy}) + b_2 (a_2 u_{xy} + b_2 u_{yy}), \tag{20}$$

and therefore, after this linear transformation,  $u_{\bar{x}\bar{x}} + u_{\bar{y}\bar{y}}$  has the following term in  $u_{xy}$

$$(2a_1 b_1 + 2a_2 b_2) u_{xy}. \tag{21}$$

If we change  $a_1, a_2, b_1,$  and  $b_2$  for their values given by Equation (10)

$$a_1 b_1 + a_2 b_2 = \frac{\bar{y}_2 - \bar{y}_0 \bar{x}_0 - \bar{x}_2}{Det} + \frac{\bar{y}_0 - \bar{y}_1 \bar{x}_0 - \bar{x}_1}{Det} \tag{22}$$

which is 0 if and only if the vectors  $\overrightarrow{P_2 P_0}$  and  $\overrightarrow{P_0 P_1}$  are orthogonal, i.e., if they form a right angle at  $P_0$ .

Thus, if the original triangle has a right angle at  $P_0$ , there is not a term in  $u_{xy}$ , and we can use the second-order approximations in space, with the spatial discretization described above. Additionally, the following theorem guarantee that ESERK methods can be employed (with numerical stability and good results) in this right triangle to solve the PDE given by Equations (1)–(3) after the linear transformation given by Equations (9)–(11) and the spatial discretization given by Equation (15):

**Theorem:** Let Equations (1)–(3) be the PDE to be solved, and  $\Omega$  a right triangle with a right angle at  $P_0$ . After linear transformation given by Equations (9) and (10), this PDE transforms into Equations (12)–(14), which can be discretized by Equations (15) and (16), transforming into the system of ODEs

$$\begin{pmatrix} u_{11} \\ u_{21} \\ \vdots \\ u_{N-2,1} \\ u_{12} \\ \vdots \\ u_{N-3,2} \\ \vdots \\ u_{1,N-2} \end{pmatrix}' = A \begin{pmatrix} u_{11} \\ u_{21} \\ \vdots \\ u_{N-2,1} \\ u_{12} \\ \vdots \\ u_{N-3,2} \\ \vdots \\ u_{1,N-2} \end{pmatrix} + \begin{pmatrix} F(t, x_1, y_1, u_{11}) \\ F(t, x_2, y_1, u_{21}) \\ \vdots \\ F(t, x_{N-2}, y_1, u_{N-2,1}) \\ F(t, x_1, y_2, u_{12}) \\ \vdots \\ F(t, x_{N-3}, y_2, u_{N-3,2}) \\ \vdots \\ F(t, x_1, y_{N-2}, u_{1,N-2}) \end{pmatrix}, \tag{23}$$

$F(t, x_i, y_j, u_{ij})$  being the sum of  $f(t, x, y, u)$  at the grid points plus the function given by the spatial discretization of the derivatives at the boundary.

The associate matrix,  $A$ , to the terms  $c_1 u_{xx} + c_2 u_{yy}$  (with  $c_1, c_2 \geq 0$ ) is real and symmetric, and therefore all the eigenvalues of this matrix are negative and real. Hence, Extrapolated Stabilized Explicit Runge–Kutta are numerically stable whenever  $\partial_u [F(t, x, y, u)]$  does not modify this type of eigenvalues (real and negative) in the Jacobian function and  $s > \sqrt{4\Delta t(\mu + \sigma)}$  ( $\mu$  being  $\frac{c_1}{h^2}$  and  $\sigma = \frac{c_2}{h^2}$ ). Therefore, ESERK4 methods can solve Equations (1)–(3) with a fourth-order convergence in time, and second in space.

**Proof:** It only remains to study the associate matrix  $A$ . But simple calculations allow us to obtain that

$$A = \begin{pmatrix} B_{N-2} & C_{N-2,N-3} & 0_{N-2,N-4} & \dots & 0_{N-2,2} & 0_{N-2,1} \\ C_{N-2,N-3}^t & B_{N-3} & C_{N-3,N-4} & \dots & 0_{N-3,2} & 0_{N-3,1} \\ 0_{N-4,N-2} & C_{N-3,N-4}^t & B_{N-4} & \ddots & \vdots & \vdots \\ \vdots & \vdots & \ddots & \ddots & \ddots & \ddots \\ 0_{2,N-2} & 0_{2,N-3} & \dots & \dots & B_2 & C_{2,1} \\ 0_{1,N-2} & 0_{1,N-3} & \dots & \dots & C_{2,1}^t & B_1 \end{pmatrix}, \tag{24}$$

where  $B_i$  is the square matrix with dimension  $i$

$$B_i = \begin{pmatrix} -2\mu - 2\sigma & \mu & 0 & \dots & 0 \\ \mu & -2\mu - 2\sigma & \mu & \ddots & 0 \\ 0 & \mu & -2\mu - 2\sigma & \ddots & \vdots \\ \vdots & \ddots & \ddots & \ddots & \mu \\ 0 & 0 & \dots & \mu & -2\mu - 2\sigma \end{pmatrix}, \tag{25}$$

$$C_{i+1,i} = \begin{pmatrix} \sigma \text{Id}_i \\ 0_{i,1} \end{pmatrix},$$

$0_{i,j}$  is the  $i \times j$  matrix with all the values equal 0,  $\text{Id}_i$  is the identity matrix of dimension  $i$ ,  $\mu = \frac{c_1}{h^2}$  and  $\sigma = \frac{c_2}{h^2}$ , and therefore  $A$  is a symmetric real matrix.

Finally, it is well-known that all the eigenvalues of any symmetric real matrix  $A$  are real. Let us suppose that  $(\lambda, v)$  is a complex pair of  $A$ , i.e., an eigenvector  $v = x + yi \in \mathbb{C}^n$ , where  $x, y \in \mathbb{R}^n$  and  $\lambda = a + bi \in \mathbb{C}$  is the corresponding eigenvalue with  $a, b \in \mathbb{R}$ . Therefore,

$$Ax + iAy = Av = \lambda v = (ax - by) + i(bx + ay). \tag{26}$$

Hence, equalizing real and imaginary parts, we have

$$Ax = (ax - by), \quad Ay = (bx + ay), \tag{27}$$

and therefore

$$Ax \cdot y = a(x \cdot y) - b\|y\|^2, \quad x \cdot Ay = b\|x\|^2 + a(x \cdot y). \tag{28}$$

In this way we can conclude that

$$0 = x \cdot Ay - Ax \cdot y = b(\|x\|^2 + \|y\|^2), \tag{29}$$

and, since  $\|x\|^2 + \|y\|^2 \neq 0$ , then  $b = 0$  and  $\lambda = a \in \mathbb{R}$

Additionally, since  $\sigma, \mu \geq 0$ , the Gershgoring theorem guarantees for all the eigenvalues of  $A$  that  $4(\mu + \sigma) \leq \lambda_i \leq 0$ .

Therefore, whenever the nonlinear part does not modify this type of eigenvalues (real and negative) in the Jacobian function, a bound of the spectral radius of the Jacobian is  $4(\mu + \sigma)$ , and we merely need to use an ESERK method with  $s > \sqrt{4\Delta t(\mu + \sigma)}$  to guarantee numerical stability.

**TABLE 1** | Analysis of the numerical convergence at points  $p_1 = (t, x, y) = (1, 0.15, 0.15)$  (top) and  $p_2 = (t, x, y) = (1, 0.5, 0.25)$  (bottom) for the ESERK4 algorithm with  $s = 100$  with  $k = \Delta t = 0.2, 0.1$  and  $0.05$ , and  $h = \Delta x = \Delta y = 0.025, 0.0125$ , and  $0.00625$ .

$s = 100, p_1$	$k = 0.2$	$k = 0.1$	$k = 0.05$	Temporal conv.
$h = 0.025$	$2.264e_{-4}$	$1.215e_{-5}$	$1.595e_{-5}$	
$h = 0.0125$	$3.355e_{-4}$	$6.364e_{-6}$	$2.479e_{-6}$	
$h = 0.00625$	$4.430e_{-4}$	$5.842e_{-5}$	$3.109e_{-6}$	<b>3.577</b>
Spatial conv.			1.180	

$s = 100, p_2$	$k = 0.2$	$k = 0.1$	$k = 0.05$	Temporal conv.
$h = 0.025$	$3.449e_{-4}$	$2.709e_{-6}$	$4.073e_{-5}$	
$h = 0.0125$	$1.412e_{-3}$	$8.117e_{-5}$	$1.479e_{-5}$	
$h = 0.00625$	$1.649e_{-3}$	$1.975e_{-5}$	$4.536e_{-6}$	<b>4.253</b>
Spatial conv.			1.583	

**TABLE 2** | Analysis of the numerical convergence at points  $p_1 = (t, x, y) = (1, 0.15, 0.15)$  (top) and  $p_2 = (t, x, y) = (1, 0.5, 0.25)$  (bottom) for the ESERK4 algorithm with  $s = 150$  with  $k = \Delta t = 0.2, 0.1$  and  $0.05$ , and  $h = \Delta x = \Delta y = 0.025, 0.0125$ , and  $0.00625$ .

$s = 150, p_1$	$k = 0.2$	$k = 0.1$	$k = 0.05$	Temporal conv.
$h = 0.025$	$2.150e_{-4}$	$1.228e_{-5}$	$1.599e_{-5}$	
$h = 0.0125$	$3.235e_{-4}$	$5.693e_{-6}$	$2.132e_{-6}$	
$h = 0.00625$	$4.401e_{-4}$	$5.842e_{-5}$	$2.625e_{-6}$	<b>3.695</b>
Spatial conv.			1.303	

$s = 150, p_2$	$k = 0.2$	$k = 0.1$	$k = 0.05$	Temporal conv.
$h = 0.025$	$3.275e_{-4}$	$3.657e_{-6}$	$4.042e_{-5}$	
$h = 0.0125$	$1.327e_{-3}$	$7.585e_{-5}$	$1.788e_{-5}$	
$h = 0.00625$	$1.568e_{-3}$	$1.975e_{-5}$	$3.824e_{-6}$	<b>4.340</b>
Spatial conv.			1.701	

### 4. NUMERICAL EXAMPLE

Let us now study the numerical behavior of ESERK methods in a right triangle with one example. We will consider

$$u_t = \frac{5}{\pi^2}(u_{\bar{x}\bar{x}} + u_{\bar{y}\bar{y}}) + (1 - u)^3 + f(t, \bar{x}, \bar{y}) \quad (\bar{x}, \bar{y}) \in \Omega \subset \mathbb{R}^2, \tag{30}$$

where

$$f(t, \bar{x}, \bar{y}) = e^{-3t} \left( \sin \left( \frac{\pi(\bar{y} - 2\bar{x} - 3)}{5} \right) - e^t \right)^3,$$

$\Omega$  is the triangle with vertices  $(-1, 1)$ ,  $(-3, 2)$ , and  $(0, 3)$  and initial and boundary conditions are taken such that  $u(t, \bar{x}, \bar{y}) = e^{-t} \sin \left( \frac{\pi(\bar{y} - 2\bar{x} - 3)}{5} \right)$  is its solution.

Hence, we first consider the linear transformation given by Equations (9) and (10), i.e.,  $a_1 = -2/5, a_2 = 1/5, b_1 = 1/5, b_2 = 2/5$ . In this way Equation (30) transforms into the Equation

$$u_t = \frac{1}{\pi^2}(u_{xx} + u_{yy}) + (1 - u)^3 + f(t, x, y) \quad (x, y) \in T_R, \tag{31}$$

where

$$f(t, x, y) = e^{-3t} \left( \sin(\pi x) - e^t \right)^3,$$

and initial and boundary conditions are taken such that  $u(t, x, y) = e^{-t} \sin(\pi x)$  is its solution.

Now, it is possible to utilize second-order approximations in space, as it was explained in the previous section. ESERK4 with  $s = 100$  and  $150$  where considered for this numerical experiment with different values of  $h = \Delta x = \Delta y$  and  $k = \Delta t$ . Numerical convergence at several points was analyzed with both methods, and numerical errors at two points [ $p_1 = (t, x, y) = (1, 0.15, 0.15)$  and  $p_2 = (t, x, y) = (1, 0.5, 0.25)$ ] are shown in **Tables 1, 2**.

First of all, we calculated all the eigenvalues of the matrix  $A$  after spatial discretization. As it was demonstrated in Theorem

**TABLE 3** | Analysis of the numerical convergence at points  $p_1 = (t, x, y) = (1, 0.15, 0.15)$ , and  $p_2 = (t, x, y) = (1, 0.5, 0.25)$  for the ESERK4 algorithm with  $s = 100$  and  $s = 150$  with  $k = \Delta t = 0.025$ , and  $h = \Delta x = \Delta y = 0.025, 0.0125$ , and  $0.00625$ .

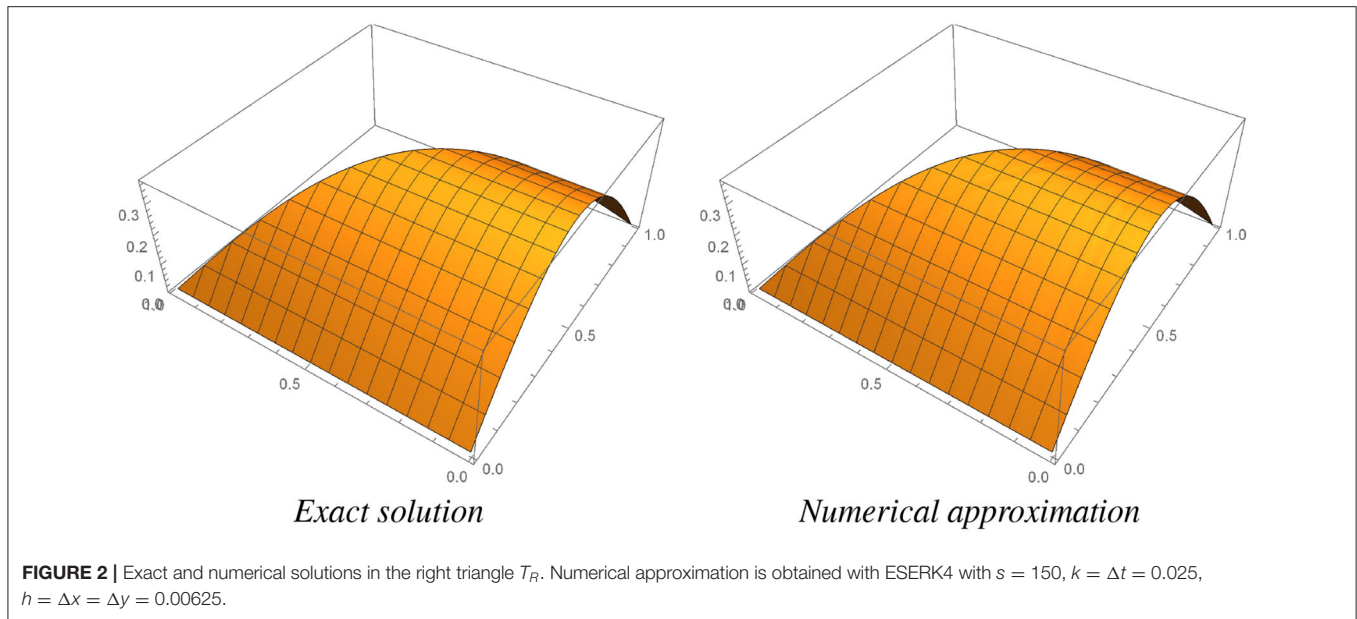
	$s = 100, p_1$	$s = 100, p_2$	$s = 150, p_1$	$s = 150, p_2$
$h = 0.025$	$1.749e_{-5}$	$3.489e_{-5}$	$1.750e_{-5}$	$3.490e_{-5}$
$h = 0.0125$	$4.544e_{-6}$	$9.593e_{-6}$	$4.542e_{-6}$	$9.575e_{-6}$
$h = 0.00625$	$2.086e_{-6}$	$9.398e_{-7}$	$2.026e_{-6}$	$7.835e_{-7}$
Spatial conv.	<b>1.534</b>	<b>2.607</b>	<b>1.555</b>	<b>2.738</b>

23, they are real and negative, and they are inside the intervals  $[-1, 292, 0]$  for  $h = 0.025$ ;  $[-5, 183, 0]$  for  $h = 0.0125$ ; and  $[-20, 746, 0]$  for  $h = 0.00625$ . In the three cases, the bound  $4(\mu + \sigma)$  given by Gershgorin theorem is a good approximation for the spectral radius  $[4(\mu + \sigma)]$  is  $1296.91$  for  $h = 0.025$ ,  $5187.64$  for  $h = 0.0125$ , and  $20750.6$  for  $h = 0.00625$ , less than a 1% over the real values].

ESERK4 schemes are stable in  $[-s^2, 0]$  therefore any ESERK method with  $s > \sqrt{20750.6k} \geq \sqrt{4150.2} = 64.4214$  (since our bigger  $k = 0.2$ ) is stable in this numerical example.

In both **Tables 1, 2**, if we take  $k = 0.2$  (also with  $k = 0.1$ ), we can observe that errors are similar with the three different values  $h = 0.025, 0.0125$ , and  $0.00625$  at many of the points. In this case, most of the error is due to the temporal discretization. Actually, in  $L_2$  norm, errors with constant  $k = 0.2$  grow when  $h$  decrease for the three step lengths in space, this is because there are more points and they are close to the border.

If we take  $h = 0.025$  constant, and we vary  $k = 0.2, 0.1$ , and  $k = 0.05$ , in general we observe that errors in most of the points decrease between  $k = 0.2$  and  $0.1$ , however, if we only compare the errors with  $h = 0.025, k = 0.1$  and  $k = 0.05$ , errors are similar at most points (and also in  $L_2$  norm). Obviously, this is because, with  $h = 0.025, k = 0.1$ , or  $k = 0.05$ , part of the error is due to the spatial discretization.



Therefore, it is not so easy to observe 4–th order convergence in time and 2–nd in space. If we choose  $h = 0.00625$ , then most of the error with  $k_1 = 0.2$ ,  $k_2 = 0.1$ , and  $k_3 = 0.05$  is due to temporal discretization. Hence, calculating  $\log_{k_1/k_3} \left( \frac{err_1}{err_3} \right)$  (these values are called Temporal convergence in **Tables 1, 2**,  $err_1$  being the error with  $k_1$ , and  $err_3$  being the error with  $k_3$ ) we can observe numerical rates in the range 3.6–4.3 in general, which gives us a good idea of the fourth-order convergence in time of ESERK4 schemes.

Now, if we fix  $k = 0.05$ , and we repeat the process with  $h_1 = 0.025$ ,  $h_2 = 0.0125$ , and  $h_3 = 0.00625$ , we observe that between  $h_1$  and  $h_2$  errors divide (more or less) by 4 which gives us a good idea of the second order in space of the discretization proposed for the right triangle. However, with  $k = 0.05$ , and  $h_3$  a part of the error is due to the temporal discretization. Thus, if we calculate  $\log_{h_1/h_3} \left( \frac{err_1}{err_3} \right)$  (these values are called Spatial convergence in **Tables 1, 2**,  $err_1$  being the error with  $h_1$ , and  $err_3$  being the error with  $h_3$ ), we observe numerical rates in the range 1.2–1.7.

Since, part of the error with  $k = 0.05$  is due to the temporal discretization, and the temporal convergence is fourth-order, let us choose a smaller  $k_4 = 0.025$ , and repeat the process with this length step in time. In **Table 3**, errors with both methods ( $s = 100$  and  $s = 150$ ), and  $h = \Delta x = \Delta y = 0.025, 0.0125$ , and  $0.00625$  are shown at both points,  $p_1$  and  $p_2$ .

Now, most of the errors are because of the spatial discretization, and we can observe that the numerical spatial convergence rates are in the range 1.5–2.7. They suggest that the numerical convergence rate is 2 as it was expected from the previous theoretical analysis.

In **Figure 2**, the exact solution and the numerical approximation obtained with ESERK4 with  $s = 150$ ,  $k = \Delta t = 0.025$ ,  $h = \Delta x = \Delta y = 0.00625$  are shown. We can check that both plots look identical.

## 5. CONCLUSIONS AND FUTURE GOALS

In this paper, for the first time, ESERK schemes are proposed to solve nonlinear partial differential equations (PDEs) in right triangles. These codes are explicit, they do not require to solve very large systems of linear nor nonlinear equations at each step. It is demonstrated that such type of codes are able to solve nonlinear PDEs in right triangles. They keep the order of convergence and the absolute stability property under certain conditions. Hence, this paper opens a new line of research, because this new approach will allow, in the future, to solve nonlinear parabolic PDEs with stabilized explicit Runge–Kutta schemes in complex domains, that would be decomposed in rectangles and right triangles.

Additionally, we consider that this procedure can be extended to tetrahedron and other simplexes for the solution of multi-dimensional nonlinear PDEs in complex regions in  $\mathbb{R}^n$ .

## DATA AVAILABILITY STATEMENT

The datasets generated for this study are available on request to the corresponding author.

## AUTHOR CONTRIBUTIONS

The author confirms being the sole contributor of this work and has approved it for publication.

## FUNDING

The authors acknowledges support from the University of Salamanca through its own Programa Propio I, Modalidad C2 grant 18.KB2B.

## REFERENCES

1. Aiken RC. *Stiff Computation*. New York, NY: Oxford University Press, Inc. (1985).
2. Cubillos-Moraga MA. *General-Domain Compressible Navier-Stokes Solvers Exhibiting Quasi-Unconditional Stability and High-Order Accuracy in Space and Time*. PhD thesis. Pasadena, CA: California Institute of Technology (2015). Available online at: <https://thesis.library.caltech.edu/8851/>
3. Duarte M, Bonaventura Z, Massot M, Bourdon A, Descombes S, Dumont T. A new numerical strategy with space-time adaptivity and error control for multi-scale streamer discharge simulations. *J Comput Phys*. (2012) **231**:1002–19. doi: 10.1016/j.jcp.2011.07.002
4. Duarte M, Descombes S, Tenaud C, Candel S, Massot M. Time-space adaptive numerical methods for the simulation of combustion fronts. *Combust Flame*. (2013) **160**:1083–101. doi: 10.1016/j.combustflame.2013.01.013
5. Dumont T, Duarte M, Descombes S, Dronne MA, Massot M, Louvet V. Simulation of human ischemic stroke in realistic 3D geometry. *Commun Nonlin Sci Numer Simul*. (2013) **18**:1539–57. doi: 10.1016/j.cnsns.2012.10.002
6. Hairer E, Wanner G. *Solving Ordinary Differential Equations. II: Stiff and Differential-Algebraic Problems*. Berlin: Springer (1996). doi: 10.1007/978-3-642-05221-7
7. Hundsdorfer WH, Verwer JG. *Numerical Solution of Time-Dependent Advection-Diffusion-Reaction Equations*. Berlin; Heidelberg: Springer (2007).
8. Martín-Vaquero J, Khaliq AQM, Kleefeld B. Stabilized explicit Runge-Kutta methods for multi-asset American options. *Comput Math Appl*. (2014) **67**:1293–308. doi: 10.1016/j.camwa.2014.01.018
9. Zlatev Z. *Computer Treatment of Large Air Pollution Models*. Dordrecht: Environmental Science and Technology Library; Springer Netherlands (2012). Available online at: <https://www.springer.com/gp/book/9780792333289>
10. Abdulle A, Medovikov AA. Second order Chebyshev methods based on orthogonal polynomials. *Numer Math*. (2001) **90**:1–18. doi: 10.1007/s002110100292
11. Abdulle A. Fourth order Chebyshev methods with recurrence relation. *SIAM J Sci Comput*. (2001) **23**:2041–54. doi: 10.1137/S1064827500379549
12. Kleefeld B, Martín-Vaquero J. SERK2v2: A new second-order stabilized explicit Runge-Kutta method for stiff problems. *Numer Methods Part Differ Equat*. (2013) **29**:170–85. doi: 10.1002/num.21704
13. Kleefeld B, Martín-Vaquero J. SERK2v3: solving mildly stiff nonlinear Partial Differential Equations. *J Comput Appl Math*. (2016) **299**:194–206. doi: 10.1016/j.cam.2015.11.045
14. Martín-Vaquero J, Janssen B. Second-order stabilized explicit Runge-Kutta methods for stiff problems. *Comput Phys Commun*. (2009) **180**:1802–10. doi: 10.1016/j.cpc.2009.05.006
15. Medovikov AA. High order explicit methods for parabolic equations. *BIT Numer Math*. (1998) **38**:372–90. doi: 10.1007/BF02512373
16. Sommeijer BP, Shampine LF, Verwer JG. RKC: An explicit solver for parabolic PDEs. *J Comput Appl Math*. (1997) **88**:315–26. doi: 10.1016/S0377-0427(97)00219-7
17. Martín-Vaquero J, Kleefeld B. Extrapolated stabilized explicit Runge-Kutta methods. *J Comput Phys*. (2016) **326**:141–155. doi: 10.1016/j.jcp.2016.08.042
18. Martín-Vaquero J, Kleefeld A. ESERK5: A fifth-order extrapolated stabilized explicit Runge-Kutta method. *J Comput Appl Math*. (2019) **356**:22–36. doi: 10.1016/j.cam.2019.01.040
19. Martín-Vaquero J, Kleefeld A. Solving nonlinear parabolic PDEs in several dimensions: parallelized ESERK codes. *J. Comput. Phys*. (2020) 109771. doi: 10.1016/j.jcp.2020.109771 Available online at: <https://www.sciencedirect.com/science/article/pii/S0021999120305453>
20. Farago I. Finite element method for solving nonlinear parabolic equations. *Comput Math Appl*. (1991) **21**:59–69. doi: 10.1016/0898-1221(91)90231-R
21. Duarte M, Bonaventura Z, Massot M, Bourdon A. A numerical strategy to discretize and solve the Poisson equation on dynamically adapted multiresolution grids for time-dependent streamer discharge simulations. *J Comput Phys*. (2015) **289**:129–48. doi: 10.1016/j.jcp.2015.02.038

**Conflict of Interest:** The author declares that the research was conducted in the absence of any commercial or financial relationships that could be construed as a potential conflict of interest.

Copyright © 2020 Martín-Vaquero. This is an open-access article distributed under the terms of the Creative Commons Attribution License (CC BY). The use, distribution or reproduction in other forums is permitted, provided the original author(s) and the copyright owner(s) are credited and that the original publication in this journal is cited, in accordance with accepted academic practice. No use, distribution or reproduction is permitted which does not comply with these terms.



# Numerical Solutions of Quantum Mechanical Eigenvalue Problems

Asif Mushtaq<sup>1\*</sup>, Amna Noreen<sup>2</sup> and Kåre Olaussen<sup>3</sup>

<sup>1</sup> Seksjon for Matematikk, Nord Universitet, Bodø, Norway, <sup>2</sup> Bodin videregående skole, Nordland fylkeskommune, Bodø, Norway, <sup>3</sup> MJAU, Trondheim, Norway

A large class of problems in quantum physics involve solution of the time independent Schrödinger equation in one or more space dimensions. These are boundary value problems, which in many cases only have solutions for specific (quantized) values of the total energy. In this article we describe a Python package that “automagically” transforms an analytically formulated Quantum Mechanical eigenvalue problem to a numerical form which can be handled by existing (or novel) numerical solvers. We illustrate some uses of this package. The problem is specified in terms of a small set of parameters and selectors (all provided with default values) that are easy to modify, and should be straightforward to interpret. From this the numerical details required by the solver is generated by the package, and the selected numerical solver is executed. In all cases the spatial continuum is replaced by a finite rectangular lattice. We compare common stencil discretizations of the Laplace operator with formulations involving Fast Fourier (and related trigonometric) Transforms. The numerical solutions are based on the NumPy and SciPy packages for Python 3, in particular routines from the `scipy.linalg`, `scipy.sparse.linalg`, and `scipy.fftpack` libraries. These, like most Python resources, are freely available for Linux, MacOS, and MSWindows. We demonstrate that some interesting problems, like the lowest eigenvalues of anharmonic oscillators, can be solved quite accurately in up to three space dimensions on a modern laptop—with some patience in the 3-dimensional case. We demonstrate that a reduction in the lattice distance, for a fixed the spatial volume, does not necessarily lead to more accurate results: A smaller lattice length increases the spectral width of the lattice Laplace operator, which in turn leads to an enhanced amplification of the numerical noise generated by round-off errors.

## OPEN ACCESS

### Edited by:

Jesus Martin-Vaquero,  
University of Salamanca, Spain

### Reviewed by:

Kazuharu Bamba,  
Fukushima University, Japan  
Jan Sladkowski,  
University of Silesia of Katowice,  
Poland

### \*Correspondence:

Asif Mushtaq  
asif.mushtaq@nord.no

### Specialty section:

This article was submitted to  
Mathematical and Statistical Physics,  
a section of the journal  
Frontiers in Physics

**Received:** 30 November 2019

**Accepted:** 11 August 2020

**Published:** 28 September 2020

### Citation:

Mushtaq A, Noreen A and Olaussen K  
(2020) Numerical Solutions of  
Quantum Mechanical Eigenvalue  
Problems. *Front. Phys.* 8:390.  
doi: 10.3389/fphy.2020.00390

**Keywords:** numpy array, FFT (fast fourier transform), quantum mechanics, python classes, eigenvalue problems, sparse SciPy routines, Schrödinger equations

## 1. INTRODUCTION

The Schrödinger equation has been a central part of “modern” physics for almost a century. When interpreted broadly, it can be formulated in a multitude of ways [1]. Here we mainly restrict our discussion to the non-relativistic, time independent form,

$$[-\Delta_{\mathbf{q}} + V(\mathbf{q})] \psi(\mathbf{q}) = E\psi(\mathbf{q}). \quad (1)$$

This constitutes an eigenvalue problem for  $E$  (there are many cases where the operator defined by Equation (1) allows for a continuous spectrum of  $E$ -values, but this will not directly influence the treatment of finite discretizations of such systems). In Equation (1),  $\mathbf{q}$

denotes the configuration space coordinate for a system of one or more particles in one or more spatial dimensions, and  $\Delta_{\mathbf{q}}$  is a Laplace operator on this configuration space.  $V(\mathbf{q})$  is the interaction potential, and  $E$  the eigenvalue parameter, interpreted as an allowed energy for the quantum system.

Despite its appearance as a single-particle equation, Equation (1) can also be used to model  $N$ -particle systems, with  $\mathbf{q} = (\mathbf{r}_1, \dots, \mathbf{r}_N)$  and  $\Delta_{\mathbf{q}} = (c_1 \Delta_1, \dots, c_N \Delta_N)$ . Here each  $\Delta_k$  is an ordinary flat space Laplace operator, and  $c_k$  is a numerical coefficient inversely proportional to the mass  $m_k$  of particle  $k$ ; this mass may differ from particle to particle. By a suitable scaling of each coordinate  $\mathbf{r}_k$ , one can mathematically transform all  $c_k$  to (for instance) unity. But such transformations may obscure physical interpretations of the coordinates, and make mathematical formulations more error-prone.

How to solve eigenvalue problems like (1)? Fortunately for the rapid initial development of quantum mechanics, for many important physical cases [like the hydrogen atom [2, 3] and harmonic oscillators [4]] it could be reduced to a set of one-dimensional eigenvalue problems, through the separation of variables method. Moreover, the resulting one-dimensional problems could all be solved exactly by analytic methods. The origins for such fortunate states of affairs can invariably be traced to an enhanced set of symmetries. However, not every system of physical interest enjoy a high degree of symmetry. Even most one-dimensional problems of the form (1) have no known analytic solution. A popular and much investigated system is the anharmonic oscillator,

$$\left[ -\frac{d^2}{dx^2} + \mu x^2 + \varepsilon x^4 \right] \psi(x) = E\psi(x). \quad (2)$$

This model has often functioned as a theoretical laboratory [5, 6], for instance to investigate the behavior and properties of perturbative [7, 8] and other [9–12] expansions, and alternative solution methods [13–15].

In this article we describe some attempts to simplify numerical solutions of eigenvalue problems like (1). Our approach relies on standard numerical algorithms, already coded and freely available through Python packages like `numpy` [16] and `scipy` [17, 18]. The main aim is to automatize the transformation of (1) to function calls accepted by the numerical eigenvalue solvers. Within the above class of models, the problem is completely defined by the coefficient vector  $(c_1, c_2, \dots, c_N)$  and the real function  $V(\mathbf{q})$ . In principle, this should be the only user input required for a numerical solution.

In practice some additional decisions must be made, like how a possibly infinite configuration space should be reduced to a region of finite extent, how the boundaries of this region should be treated, and how this region should be further approximated by a finite lattice. Other options involve selection of numerical approaches, like whether dense or iterative sparse matrix solvers should be used. Such decisions have consequences for many “trivial” details of the numerical programs, but they can be provided in the form of parameters and selectors, automatically implemented without further tedious and error-prone human intervention. Even many of the decisions indicated above may

ultimately be delegated to artificial intelligence systems, but this is beyond our current scope.

## 2. AVAILABLE PYTHON PROCEDURES FOR NUMERICAL SOLUTION

Numerical approaches to problems like those above are in principle straightforward: The operator

$$H = T + V$$

defined by Equation (1) is approximated by a finite real symmetric matrix

$$M_H = M_T + M_V$$

where we have introduced the symbol  $T = -\Delta_{\mathbf{q}}$ . For densely defined matrices  $M_H$  there are several standard numerical eigenvalue solvers available, like `eig` and `eigvals` in the `scipy.linalg` package. A  $10^4 \times 10^4$  matrix of double precision numbers requires 800 Mb of storage space; this is indicative of the problem magnitudes that can be handled by dense matrix methods on (for instance) modern laptops. That is, such computers have more than enough memory for numerical treatment of one-dimensional problems, and usually also sufficient memory for two-dimensional ones.

For higher-dimensional problems one may utilize the sparse nature of  $M_H$  to find solutions through iterative procedures, like the `eigsh` eigenvalue solver in the `scipy.sparse.linalg` package. This solver does not require any explicit matrix construction of  $M_H$ , only a `LinearOperator` function that returns the vector  $M_H\psi$  for any input vector  $\psi$ . In the representations we consider,  $M_V$  is always diagonal, and  $M_T$  can be made diagonal by a Fast Fourier Transform (FFT), or some of its discrete trigonometric variants. This opens the possibility it to handle non-sparse matrix problems, where  $T$  is replaced by more general expressions of  $F(T)$ , by the same procedures. For instance functions  $F$  that involves fractional and/or inverse powers of its arguments.

## 3. REQUIRED PARAMETERS AND SELECTORS

In this section we describe the additional quantities that a user must input for a full specification of the numerical problem. They assume that configuration space has been modeled by a rectangular point lattice, with a selection of possible boundary conditions.

### 3.1. Lattice Shape

The most basic quantity of the numerical model is the discrete lattice approximating the relevant region of configuration space. For rectangular approximations this is defined by the `shape` parameter, a Python *tuple*,

$$\text{shape} = (s_0, s_1, \dots, s_{d-1}), \quad (3)$$

where each  $s_k$  is a positive integer specifying the number of lattice points in the  $k$ 'th direction, and  $d$  is the (effective) dimension of configuration space. For models with continuous symmetries (for instance rotational ones) the effective dimension may be chosen smaller than the physical one, by separation of variables. Likewise, discrete symmetries may be used to reduce the size of configuration space that this lattice must approximate.

In Python programs, quantities like the wave function  $\psi$  and the potential  $V$  are defined as floating point NumPy arrays of shape **shape**.

### 3.2. Edge Lengths and Offsets

The geometric extent of the selected region is specified by its edge lengths **xe**. This is a NumPy array of positive floating point numbers,

$$\mathbf{xe} = [e_0, e_1, \dots, e_{d-1}]. \tag{4}$$

A secondary quantity, derived from **xe** and **shape** is the elementary lattice cell,

$$\mathbf{dx} = \mathbf{xe}/\mathbf{shape} = [e_0/s_0, e_1/s_1, \dots, e_{d-1}/s_{d-1}]. \tag{5}$$

The absolute positioning of the region, with respect to some fixed coordinate system, is specified by a NumPy array of floating point numbers,

$$\mathbf{xo} = [x_0, x_1, \dots, x_{d-1}]. \tag{6}$$

This is defined as the position of the “lower left” corner of the selected region. The placement of the lattice points within the region still needs to be specified, as will be discussed below.

### 3.3. Boundary Conditions

The restriction to finite regions of space requires imposition of boundary conditions. For regions of rectangular shape (generalized to arbitrary dimensions), as considered here, the perhaps simplest choice is *periodic* boundary conditions in each direction. This may be viewed as a topological property of configuration space itself. Other boundary conditions are really properties of functions defined on this space, as specifications of how the functions should be extended beyond the boundary. Two natural choices are *symmetric* and *anti-symmetric* extensions. With a lattice approximation a further distinction can be made, related to how the lattice points are positioned relative to the boundary.

In this connection, it is natural to consider the cases handled by the trigonometric cousins of the fast Fourier transform (FFT). In the one-dimensional case the extension may be symmetric or anti-symmetric with respect to a boundary, which is situated either (i) at a lattice point, or (ii) midway between two lattice points. Thus, at each boundary there is  $2 \times 2$  matrix of possibilities, as indicated by **Table 1**.

With two boundaries there are altogether  $4 \times 4 = 16$  possibilities. However, the routines in **scipy.fftpack** (**dct** and **dst** of types I–IV) only implement cases where both options come from the same row of **Table 1**. With the periodic extension

**TABLE 1** | Individual boundary conditions covered by standard discrete trigonometric transforms (**DCT** and **DST**).

Function extension	Symmetric	Anti-symmetric
Boundary at lattice point	“S”	“A”
Boundary midway between points	“s”	“a”

**P** in addition, one ends up with a set of nine possibilities in each direction:

$$\mathcal{B} = \{ 'PP', 'SS', 'SA', 'AS', 'AA', 'ss', 'sa', 'as', 'aa' \}. \tag{7}$$

Hence, the numerical model must be further specified by a Python tuple of two-character strings, defining the selected boundary condition in all directions,

$$\mathbf{bc} = (b_0, b_1, \dots, b_{d-1}) \tag{8}$$

with each  $b_k \in \mathcal{B}$  (or in an enlarged set of possibilities).

### 3.4. Lattice Positions. Dual Lattice Squared Positions

When **bc** is given, one may automatically calculate the positions of all lattice points

$$\mathbf{xlat} = (\mathbf{X}_0, \mathbf{X}_1, \dots, \mathbf{X}_{d-1}), \tag{9}$$

provided **shape**, **xe**, and **xo** are also known. In Equation (9), the property **xlat** is a tuple of one-dimensional arrays. For illustration, consider the case of a 3-dimensional lattice of shape  $(s_x, s_y, s_z)$ . Then **xlat** is a Python tuple  $(\mathbf{X}, \mathbf{Y}, \mathbf{Z})$ , where **X** is a **numpy** array of shape  $(s_x, 1, 1)$ , **Y** is a **numpy** array of shape  $(1, s_y, 1)$ , and **Z** is a **numpy** array of shape  $(1, 1, s_z)$ . These are all one-dimensional arrays, but their shape information implies that (for instance) the Python expression  $\mathbf{X} * \mathbf{Y}$  automatically evaluates to a **numpy** array of shape  $(s_x, s_y, 1)$ .

A Python function  $V(x, y, z)$ , defined by an expression that can involve “standard” functions, may then be evaluated on the complete lattice by the short and simple expression  $V(*\mathbf{xlat})$ . When  $V$  depends on all its arguments, the result will be a **numpy** array of shape  $(s_x, s_y, s_z)$ .

In general, when Fourier transforming a periodic function  $f(\mathbf{x})$ , where  $\mathbf{x}$  takes values on some discrete lattice, the result becomes another periodic function  $\tilde{f}(\mathbf{k})$ , where  $\mathbf{k}$  takes values on another discrete lattice (the dual lattice/reciprocal space). Modulo an overall scaling, a set of  $\mathbf{k}$ -values (labeling the points of some complete, minimal subdomain to be extended by periodicity) can be defined such that  $f(\mathbf{x} + \mathbf{a})$  transforms to  $e^{-i\mathbf{k} \cdot \mathbf{a}} \tilde{f}(\mathbf{k})$ . A natural choice for that minimal domain is, in physicists language, the *first Brillouin zone* (this choice may still leave a somewhat arbitrary selection of boundary points to be included). On this subdomain of the dual lattice, derivatives can be defined as the multiplication operators  $-i\mathbf{k}$ . But these operators must still be extended to the full dual

lattice by periodicity. The common stencil expressions for lattice derivatives correspond to the lowest Fourier components of the (periodically extended) multiplication operator  $-i\mathbf{k}$ .

For the other (discrete trigonometric) transformations a complication arises, because a derivation also induces a transposition of the boundary conditions in  $\mathcal{B}$ . However, two derivations in the same direction leave the boundary conditions unchanged, and hence can be represented as a multiplication operator  $\mathbf{q}$  on the transformed functions. Let  $\partial_k$  be shorthand notation for  $\partial/\partial x_k$ . The previous conclusion implies that all operators of the form  $F(\partial_0^2, \partial_1^2, \dots, \partial_{d-1}^2)$  can be evaluated through multiplications and fast discrete transforms,

$$F(\partial_0^2, \partial_1^2, \dots, \partial_{d-1}^2) = \mathcal{T}^{-1} F(q_0, q_1, \dots, q_{d-1}) \mathcal{T}. \tag{10}$$

We have implemented code that performs  $\mathcal{T}$  and  $\mathcal{T}^{-1}$  through a sequence of discrete trigonometric or fast Fourier transforms, dependent on  $\mathbf{bc}$  and the other parameters. Analogous to the arrays  $\mathbf{xlat}$  of lattice positions (Equation 9), one may automatically calculate similar arrays of squared positions for reciprocal lattice,

$$\mathbf{qlat} = (\mathbf{Q}_0, \mathbf{Q}_1, \dots, \mathbf{Q}_{d-1}). \tag{11}$$

### 3.5. Lattice Laplacian. Stencil Representations

Instead of relying on FFT type transforms, one may directly construct discrete approximations (stencils) of the Laplace operator, and similar differential operators. The simplest implementation of a lattice Laplacian in one dimension is obtained by use of the formula

$$\frac{d^2\psi}{dx^2}(x_n) \approx \frac{\psi(x_n + \delta x) - 2\psi(x_n) + \psi(x_n - \delta x)}{\delta x^2}, \tag{12}$$

where  $\delta x$  is the distance between nearest-neighbor lattice points. The formal discretizations error of this approximation is of order  $\delta x^2$ . By summing such expression in  $d$  orthogonal directions one finds the  $(2d + 1)$ -stencil expression for the lattice Laplacian.

A more accurate approximation is the  $(4d + 1)$ -stencil,

$$\Delta\varphi(\mathbf{x}_n) \approx \sum_{k=0}^{d-1} \frac{-\varphi(\mathbf{x}_n + 2\delta_k) + 16\varphi(\mathbf{x}_n + \delta_k) - 30\varphi(\mathbf{x}_n) + 16\varphi(\mathbf{x}_n - \delta_k) - \varphi(\mathbf{x}_n - 2\delta_k)}{12|\delta_k|^2}. \tag{13}$$

Here  $\delta_k$  denotes a vector of length  $|\delta_k|$  pointing in positive  $k$ -direction.

An arbitrary (short-range) position independent operator  $O$  can in general be represented by a stencil  $s_O(\mathbf{b})$  such that

$$(O\psi)(\mathbf{x}_n) = \sum_{\mathbf{b}} s_O(\mathbf{b}) \psi(\mathbf{x}_{n-\mathbf{b}}). \tag{14}$$

When  $\mathbf{n} - \mathbf{b}$  falls outside the lattice, the value of  $\psi(\mathbf{x}_{n-\mathbf{b}})$  must be interpreted according to the boundary conditions  $\mathbf{bc}$ . This can again be automatized. We have implemented an algorithm for this, currently only for 5 of the 9 cases in  $\mathcal{B}$  in each direction, but for an arbitrary number of directions.

The various ways to approximate the Laplace operator, or more generally the kinetic energy operator, is made available through the selector  $\mathbf{ke}$ , whose value is currently limited to the set of options  $\{ '2dplus1', '4dplus1', 'fft2k2' \}$ . The last of these options is discussed in section 5.

## 4. SIMPLE APPLICATIONS

In this section we will demonstrate some applications of our automatic code. The main requirement is that in each case only a set of parameters and selectors should be provided, with no coding required by the application itself. This should be sufficient to generate eigenvalues  $E_n$  as requested, and optionally also the associated eigenfunctions (an issue which we have not yet tested).

### 4.1. Example: One-Dimensional Harmonic Oscillator

Consider the eigenvalue problem of the one-dimensional harmonic oscillator,

$$-\psi_n''(x) + x^2 \psi_n(x) = E_n \psi_n(x). \tag{15}$$

The eigenvalues are  $E_n = 2n + 1$  for  $n = 0, 1, \dots$ , and the extent of the wavefunction  $\psi_n(x)$  can be estimated from the requirement that a classical particle of energy  $E_n$  is restricted to  $x^2 \leq E_n$ . A quantum particle requires a little more space than the classically restricted one.

For a numerical analysis we provide the parameters

`shape = (128,)`, `bc = ('a', 'a')`, `xe = (25,)`, `xo = (-12.5)`,  
`v = lambda x : x * * 2`,

selects the 3-stencil approximation for  $\mathbf{T}$  (default choice), and the dense matrix solver `eigvalsh` (default choice). This instantly returns 128 eigenvalues as plotted in **Figure 1**. We may easily change `shape` to (1024), for a much better result. The potential for additional explorations, without any coding whatsoever, should be obvious.

For a better quantitative assessment of the accuracy obtained we plot some energy differences,  $E_n^{(\text{exact})} - E_n$ , in **Figure 2**.

This *brute force* method leads to a dramatic increase in memory requirement with increasing lattice size. For a lattice with  $N = 2^m$  sites, the matrix requires storage of  $4^m$  double precision (8 byte) numbers. For  $m = 13$  this corresponds to about  $\frac{1}{2}$  Gb of memory, for  $m = 14$  about 2 Gb. The situation becomes even worse in higher dimensions.

Assuming that we are only interested some of the lowest eigenvalues, an alternative approach is to calculate these by the iterative routine `eigsh` from `scipy.sparse.linalg`. This allows extension to larger lattices, as shown in **Figure 3**.

With a sparse eigenvalue solver the calculation becomes limited by available computation time, which in many cases is a

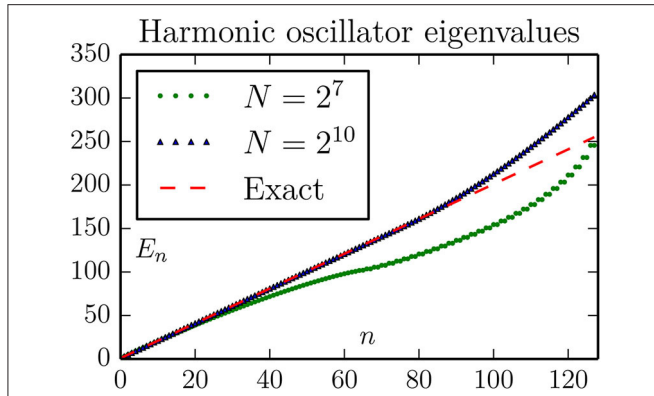


**FIGURE 1** | The 128 lowest eigenvalues of Equation (15), computed with the standard 3-stencil approximation for the Laplace operator (here the kinetic energy  $T$ ). The parameters are chosen to illustrate two typical effects: With the  $\mathbf{bc}=(\mathbf{a}, \mathbf{a})$  boundary conditions the harmonic oscillator potential is effectively changed to  $V = \infty$  for  $x \geq 12.5$ , thereby modifying the behavior of extended (highly excited) states. The effect of this is to increase the eigenenergies of such states, to a behavior more similar to a particle-in-box. This is visible for  $n \gtrsim 80$ . The effect of using the 3-stencil approximation for  $T$  is to change the spectrum of this operator from  $k^2$  to (the slower rising)  $(2/\delta x)^2 \sin^2(k\delta x/2)$ . This is visible in the sub-linear rise of the spectrum for  $N = 2^7$ .

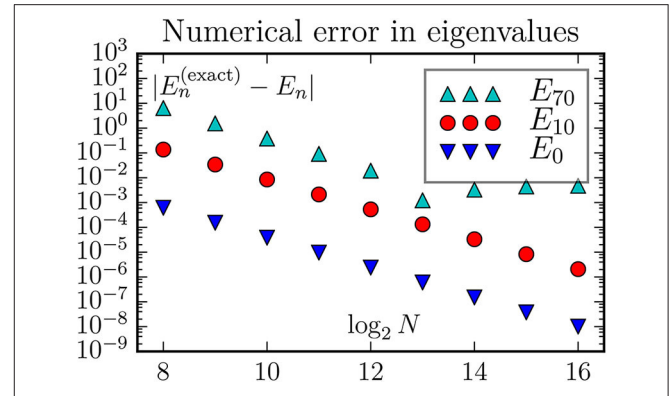


**FIGURE 3** | The discretizations error computed by the routine `eigsh` from `scipy.sparse.linalg`. For a fixed lattice size the discretizations error is essentially the same as with dense matrix routines. However, with a memory requirement proportional to the lattice size (instead of its square) it becomes possible to go to much larger lattices. This figure also demonstrates ( $E_{70}$ ) that the error can be limited by boundary effects instead of the finite discretization length  $\delta x$ .

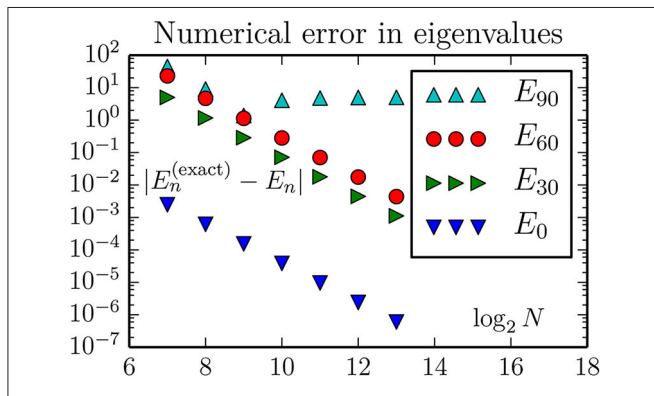


**FIGURE 2** | The discretizations error of energy eigenvalues when using the standard 3-stencil approximation for the one-dimensional Laplace operator (here the kinetic energy  $T$ ). There is no improvement in  $E_{90}$  beyond a certain lattice size  $N$ , because the corresponding oscillator state is too large for the geometric region. Hence, for improved accuracy of higher eigenvalues one should instead increase the  $\mathbf{x}_e$ , while maintaining  $\mathbf{x}_o = -\mathbf{x}_e/2$ . For the other states the improvement is consistent with the expectation of an error proportional to  $\delta x^2$ . This predicts an accuracy improvement of magnitude  $2^{12} = 4,096$  when the number of lattice sites increases from  $N = 2^7$  to  $N = 2^{13}$  for a fixed geometry. The eigenvalues are computed by the dense matrix routine `eigvalsh` from `scipy.linalg`.

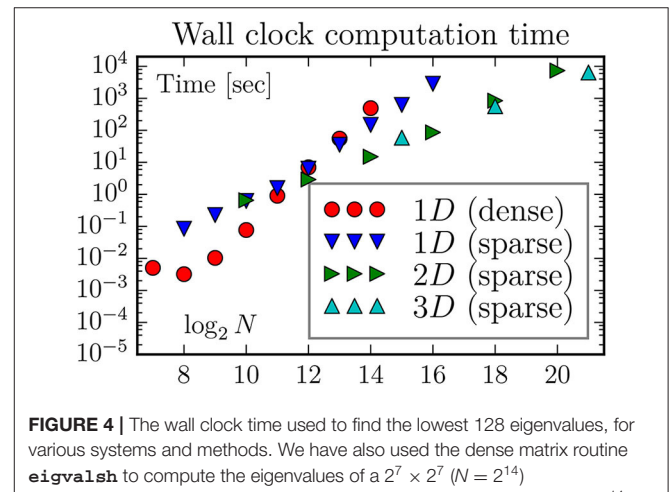


**FIGURE 4** | The wall clock time used to find the lowest 128 eigenvalues, for various systems and methods. We have also used the dense matrix routine `eigvalsh` to compute the eigenvalues of a  $2^7 \times 2^7$  ( $N = 2^{14}$ ) two-dimensional lattice; not unexpected it takes the same time as for a  $2^{14}$  one-dimensional lattice. Somewhat surprisingly, with `eigsh` it is much faster to find the eigenvalues for two-dimensional lattice than for a one-dimensional with the same number of sites, and somewhat faster to find the eigenvalues for a three-dimensional lattice than for the two-dimensional with the same number of sites.

much weaker constraint: With proper planning and organization of calculations, the relevant timescale is the time to analyze and publish results (i.e., weeks or months). The computation time is nevertheless of interest (it shouldn't be years). We have measured the wall clock time used to perform the computations for **Figures 2, 3**, performed on a 2012 Mac Mini with 16 Gb of memory, and equipped with a parallelized `scipy` library.

Hence, the `eigvalsh` and `eigsh` routines are running with four threads. The results are plotted in **Figure 4**.

Here we have used the `eigsh` routine in the most straightforward manner, using default settings for most parameters. This means, in particular, that the initial vector for the iteration (and the subsequent set of trial vectors) may not be chosen in an optimal manner for our category of problems. It is interesting to observe that `eigsh` works better for higher-dimensional problems. The (brief) `scipy` documentation [17] says that the underlying routines works best when computing eigenvalues of largest magnitude, which are of no physical interest for our type of problems. It is our experience that the

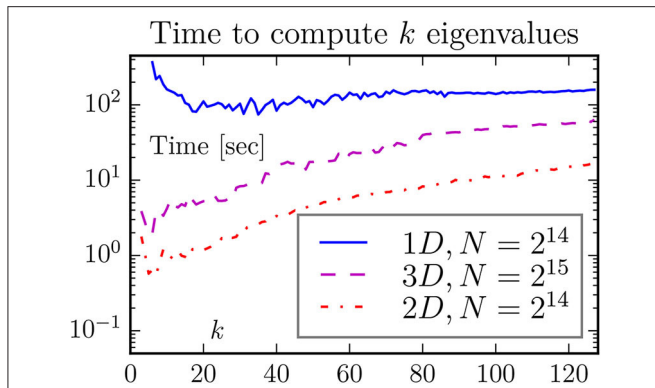


**FIGURE 5** | One may think that it takes longer to compute more eigenvalues. This is not always the case when the number of eigenvalues is small, as demonstrated by this figure. The default choice of `eigsh` is to compute  $k = 6$  eigenvalues. For our two- and three-dimensional problems this looks close to the optimal value, but it is too low for the one-dimensional problem.

suggested strategy, of using the *shift-invert* mode instead, does not work right out-of-the-box for problems of interesting size (i.e., where dense solvers cannot be used). We were somewhat surprised to observe that the computation time may *decrease* if the number of computed eigenvalues increases (cf. **Figure 5**).

### 4.2. Example: 2- and 3-Dimensional Harmonic Oscillators

The  $d$ -dimensional harmonic oscillator

$$[-\Delta + r^2] \psi_n(\mathbf{r}) = E_n \psi_n(\mathbf{r}), \tag{16}$$

has eigenvalues  $E_n = (d + 2n)$ , for  $n = 0, 1, \dots$ . The degeneracy of the energy level  $E_n$  is  $g_n = (n + 1)$  in two dimensions, and  $g_n = \frac{1}{2}(n + 1)(n + 2)$  in three dimensions<sup>1</sup>. This degeneracy may be significantly broken by the numerical approximation. For a numerical solution we only have to change the previous parameters slightly:

$$\text{shape} = (128,) * \text{dim}, \text{bc} = (('a', 'a'),) * \text{dim},$$

$$\text{xe} = (25,) * \text{dim}, \text{xo} = (-12.5,) * \text{dim}, \tag{17a}$$

$$\mathbf{V} = \text{lambd} \ x, y : x * * 2 + y * * 2 \quad (\text{dim} = 2), \tag{17b}$$

$$\mathbf{V} = \text{lambd} \ x, y, z : x * * 2 + y * * 2 + z * * 2 \quad (\text{dim} = 3), \tag{17c}$$

for  $\text{dim} = 2, 3$ .

As already discussed, the routine `eigsh` works somewhat faster in higher dimensions than in one dimension (for the same *total* number  $N$  of lattice points). The corresponding discretizations errors are shown in **Figures 6, 7**.

The discretizations error continues to scale like  $\delta x^2$ . This means that a reduction of this error by a factor  $2^2 = 4$  requires an increase in the number of lattice points by a factor  $2^d$  in  $d$  dimensions. This means that it becomes more urgent

<sup>1</sup>The general formula is  $g_n = \binom{d-1+n}{d-1}$ .

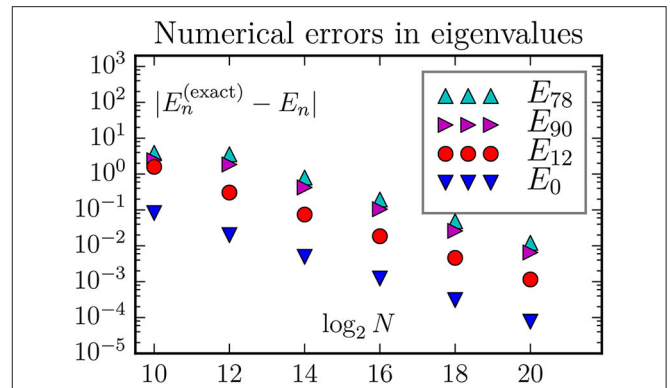


**FIGURE 6** | The discretization error of energy eigenvalues when using the standard 5-stencil approximation for the two-dimensional Laplace operator. Exactly, the states  $E_{78}$  and  $E_{90}$  are the two edges of a 13-member multiplet with energy 26, and the state  $E_{12}$  is the middle member of a 5-member multiplet with energy 10. With the chosen parameters all states considered are well confined inside the geometric region; hence we do not observe any boundary correction effects.

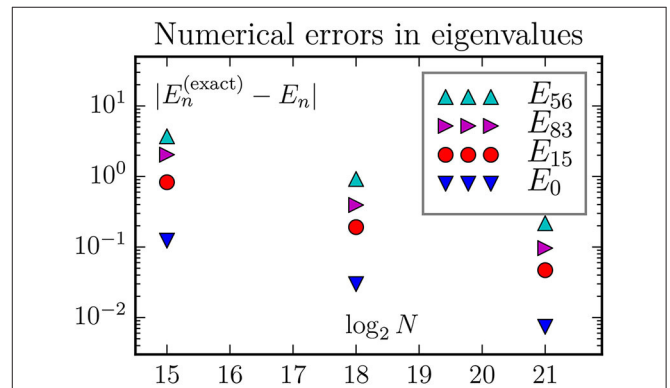


**FIGURE 7** | The discretization error of energy eigenvalues when using the standard 7-stencil approximation for the three-dimensional Laplace operator. Exactly, the states  $E_{56}$  and  $E_{83}$  are the two edges of a 28-member multiplet with energy 15, and the state  $E_{15}$  is the middle member of a 10-member multiplet with energy 9.

to use a better representation of the Laplace operator in higher dimensions. Fortunately, as we shall see in the next sections, better representations are available for our type of problems.

## 5. FFT CALCULATION OF THE LAPLACE OPERATOR

One improvement is to use the reflection symmetry of each axis ( $x \rightarrow -x, y \rightarrow -y$ , etc.) to reduce the size of the spatial domain. This reduces  $\delta x$  by a half, without changing the number of lattice points.

A much more dramatic improvement is to use some variant of a Fast Fourier Transform (FFT): After a Fourier transformation,  $\psi(\mathbf{r}) \rightarrow \tilde{\psi}(\mathbf{k})$ , the Laplace operator turns into

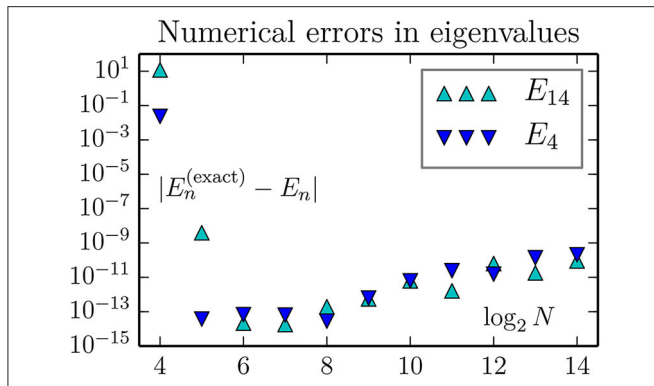


**FIGURE 8** | With a FFT representation of the Laplace operator the discretization error drops exceptionally fast with  $\delta x \propto N^{-1}$ . When it becomes “small enough” the effect of numerical roundoff becomes visible; the latter leads to an *increase* in error with  $\delta x$ . The results in this figure is for a one-dimensional lattice, but the behavior is the same in all dimensions. The lesson is that we should make  $\delta x$  “small enough” (which in general may be difficult to determine *a priori*), but not smaller. It may also be possible to rewrite the eigenvalue problem to a form with less amplification of roundoff errors.

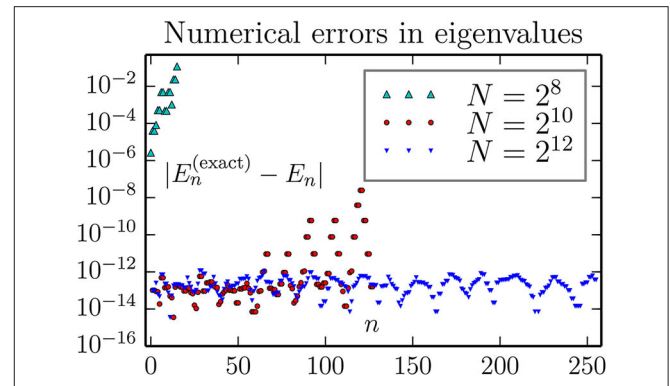


**FIGURE 10** | Accuracy of computed eigenvalues for a 2D oscillator, using the FFT approximation for kinetic energy  $T$ . As can be seen, a large number of the lowest eigenvalues can be computed to an absolute accuracy in the range  $10^{-14}$ – $10^{-12}$  with a lattice of size  $2^6 \times 2^6$ . We observe not improvement by going to  $2^7 \times 2^7$  lattice, but no harm either (except for an increase in the wall clock execution time from about 3 to 30 s for each combination of boundary conditions).

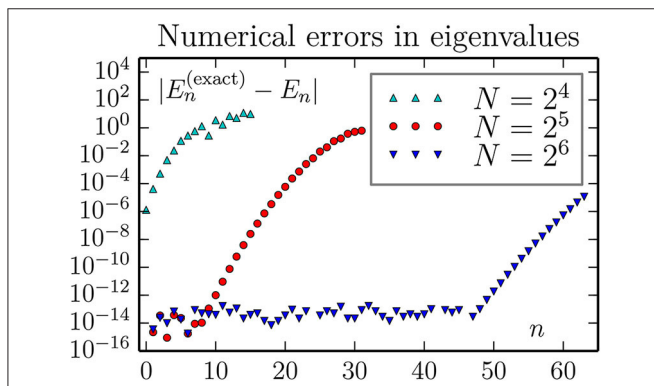


**FIGURE 9** | Accuracy of computed eigenvalues for a 1D oscillator, using the FFT approximation for kinetic energy  $T$ . This figure may suggest that an increase in the number of lattice size  $N$  will lead to an accurate treatment of states with higher  $n$ . Our findings are that this is *not* the case: The results for  $N = 2^7$  and  $N = 2^8$  have essentially the same behavior as for  $N = 2^6$ .

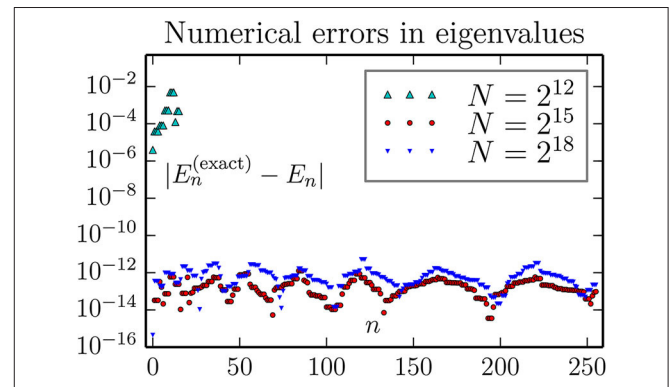


**FIGURE 11** | Accuracy of computed eigenvalues for a 3D oscillator, using the FFT approximation for kinetic energy  $T$ . As can be seen, a large number of the lowest eigenvalues can be computed to an absolute accuracy in the range  $10^{-14}$  to  $10^{-12}$  with lattice of size  $2^6 \times 2^6 \times 2^6$ . We observe no improvement by going to  $2^7 \times 2^7 \times 2^7$  lattice, but no harm either (except for an increase in the wall clock execution time from about 6 to 95 min for each combination of boundary conditions).

multiplication operator,

$$(-\Delta\psi)(\mathbf{r}) \rightarrow \mathbf{k}^2 \tilde{\psi}(\mathbf{k}).$$

This means that application of the Laplace operator can be represented by (i) a Fourier transform, followed by (ii) multiplication by  $\mathbf{k}^2$ , and finally (iii) an inverse Fourier transform. Essentially the same procedure works for the related trigonometric transforms.

For rectangular lattices, these options can also be implemented as practical procedures, due to the existence of efficient and accurate<sup>2</sup> algorithms for discrete Fourier

and trigonometric transforms. The time to perform the above procedure is not very much longer than the corresponding stencil operations. The benefit is that the Laplace operator becomes exact on the space of functions which can be represented by the modes included in the discrete transform.

We have coded this FFT-type representation of the Laplace operator for the various types of boundary conditions listed in **Table 1**. This possibility can be chosen as an option for the kinetic energy selector,  $\mathbf{ke}$ . The obtainable accuracy through this option increases dramatically, as illustrated in **Figures 8–11**. As shown in **Figure 8**, a decrease of the lattice length  $\delta x$  does not necessarily

<sup>2</sup>The error of a back-and-forth FFT is a few times the numerical accuracy, i.e., in the range  $10^{-14}$  to  $10^{-15}$ , with double precision numbers. However, when an error of this order is multiplied by  $\mathbf{k}^2$  it can be amplified by several orders of

magnitude. Hence, the range of  $\mathbf{k}^2$ -values should not be chosen significantly larger than required to represent  $\psi(\mathbf{r})$  to sufficient accuracy.

**TABLE 2** | The 10 lowest eigenvalues of the quantum anharmonic oscillator, calculated to high precision by the method described in [14], from the Schrödinger equation  $\left(-\frac{d^2}{d\xi^2} + \xi^4\right) \psi_n(\xi) = \varepsilon_n \psi_n(\xi)$ .

$n$	$\varepsilon_n$
1	1.060 362 090 484 182 899 647 046 016 693
2	3.799 673 029 801 394 168 783 094 188 513
3	7.455 697 937 986 738 392 156 591 347 186
4	11.644 745 511 378 162 020 850 373 281 371
5	16.261 826 018 850 225 937 894 954 430 385
6	21.238 372 918 235 940 024 149 711 113 589
7	26.528 471 183 682 518 191 813 828 183 681
8	32.098 597 710 968 326 634 272 106 438 332
9	37.923 001 027 033 985 146 516 378 551 910
10	43.981 158 097 289 730 785 318 113 752 827

The eigenfunctions obey the (anti-)symmetry property,  $\psi_n(\xi) = (-1)^{n-1} \psi_n(-\xi)$ .

lead to a more accurate result. We attribute this to an enhanced amplification of roundoff errors.

It might be that the harmonic oscillator systems are particularly favorable for application of the FFT representation. One important feature is that the Fourier components of the harmonic oscillator wave functions vanishes exponentially fast, like  $e^{-k^2/2}$ , with increasing wave-numbers  $k^2$ . This feature is shared with all eigenfunctions of polynomial potential Schrödinger equations, but usually with different powers of  $k$  in the exponent, which quantitatively leads to a somewhat different behavior. Furthermore, the onset of exponential decay will occur for larger values of  $k^2$  for the more excited states (i.e., with larger eigenvalue numbers).

For systems with singular wavefunctions the corresponding Fourier components may vanish only algebraically with  $k^2$ . An equally dramatic increase in accuracy cannot be expected for such cases.

### 6. ANHARMONIC OSCILLATORS

Our general setup allows for any computable potential, by simply changing the definition of the function assigned to  $\mathbf{V}$  (This does not mean that every potential will lead to a successful calculation of eigenvalues). For demonstration and comparison purposes, like here, one encounters the problem that the exact answers are no longer known. This makes it more difficult to assess the accuracy and other qualities of the code. As an example where some instructive comparisons are possible, we consider the two-dimensional anharmonic oscillator obeying the Schrödinger equation,

$$\frac{1}{2} \left( -\frac{d^2}{dx^2} - \frac{d^2}{dy^2} + x^4 + 6x^2y^2 + y^4 \right) \Psi_E(x, y) = E \Psi(x, y). \tag{18}$$

By construction, this problem has separable solutions of the form

$$\Psi_E(x, y) = \psi_m(\xi) \psi_n(\eta), \text{ with } \xi = (x+y)/\sqrt{2}, \eta = (x-y)/\sqrt{2}, \tag{19}$$

**TABLE 3** | The 22 lowest eigenvalues  $E$  of the two-dimensional quantum anharmonic oscillator, as defined by the Schrödinger equation  $\frac{1}{2} \left( -\frac{d^2}{dx^2} - \frac{d^2}{dy^2} + x^4 + 6x^2y^2 + y^4 \right) \Psi_E(x, y) = E \Psi_E(x, y)$ , displayed to 30 decimals accuracy.

$(P_x, P_y)$	Comp	$E$
(S, S)	$\varepsilon_1 + \varepsilon_1$	2.120 724 180 968 365 799 294 092 033 385
(S, A)	$\varepsilon_1 + \varepsilon_2$	4.860 035 120 285 577 068 430 140 205 205
(A, S)	$\varepsilon_1 + \varepsilon_2$	4.860 035 120 285 577 068 430 140 205 205
(S, S)	$\varepsilon_2 + \varepsilon_2$	7.599 346 059 602 788 337 566 188 377 025
(S, S)	$\varepsilon_1 + \varepsilon_3$	8.516 060 028 470 921 291 803 637 363 878
(A, A)	$\varepsilon_1 + \varepsilon_3$	8.516 060 028 470 921 291 803 637 363 878
(S, A)	$\varepsilon_2 + \varepsilon_3$	11.255 370 967 788 132 560 939 685 535 698
(A, S)	$\varepsilon_2 + \varepsilon_3$	11.255 370 967 788 132 560 939 685 535 698
(S, A)	$\varepsilon_1 + \varepsilon_4$	12.705 107 601 862 344 920 497 419 298 064
(A, S)	$\varepsilon_1 + \varepsilon_4$	12.705 107 601 862 344 920 497 419 298 064
(S, S)	$\varepsilon_3 + \varepsilon_3$	14.911 395 875 973 476 784 313 182 694 372
(S, S)	$\varepsilon_2 + \varepsilon_4$	15.444 418 541 179 556 189 633 467 469 884
(A, A)	$\varepsilon_2 + \varepsilon_4$	15.444 418 541 179 556 189 633 467 469 884
(S, S)	$\varepsilon_1 + \varepsilon_5$	17.322 188 109 334 408 837 542 000 447 077
(A, A)	$\varepsilon_1 + \varepsilon_5$	17.322 188 109 334 408 837 542 000 447 077
(S, A)	$\varepsilon_3 + \varepsilon_4$	19.100 443 449 364 900 413 006 964 628 557
(A, S)	$\varepsilon_3 + \varepsilon_4$	19.100 443 449 364 900 413 006 964 628 557
(S, A)	$\varepsilon_2 + \varepsilon_5$	20.061 499 048 651 620 106 678 048 618 897
(A, S)	$\varepsilon_2 + \varepsilon_5$	20.061 499 048 651 620 106 678 048 618 897
(S, A)	$\varepsilon_1 + \varepsilon_6$	22.298 735 008 720 122 923 796 757 130 281
(A, S)	$\varepsilon_1 + \varepsilon_6$	22.298 735 008 720 122 923 796 757 130 281
(S, S)	$\varepsilon_4 + \varepsilon_4$	23.289 491 022 756 324 041 700 746 562 742

This equation is separable in terms of two identical one-dimensional problems, with eigenvalues  $\varepsilon_m$  as listed in **Table 2**. Hence each eigenvalues  $E$  is composed of two eigenvalues  $\varepsilon_m, \varepsilon_n$  as indicated in the second column. The reflection parities  $(P_x, P_y)$  listed in the first column indicate how the wavefunctions  $\Psi_E(x, y)$  can be chosen symmetric (S) or anti-symmetric (A) under the reflections  $x \rightarrow -x$  or  $y \rightarrow -y$ .

where the factors  $\psi$  obey a one-dimensional equation,

$$\left( -\frac{d^2}{d\xi^2} + \xi^4 \right) \psi_m(\xi) = \varepsilon_m \psi_m(\xi), \tag{20}$$

and  $E = \varepsilon_m + \varepsilon_n$ . As mentioned in the introduction, equations like the latter have been quite intensely studied in the literature. Accurate values for the even parity eigenvalues of Equation (20) can for instance be found in Table 1 of [9]. In **Table 2**, we list the 10 lowest eigenvalues to 30 decimals precision, calculated by the very-high-precision method described in [14]. Hence, for practical purposes all  $\varepsilon_m$  of interest can be considered exactly known. This means that the eigenvalues  $E$  of Equation (18) can also be considered exactly known. We list the 22 lowest ones of them in **Table 3**. These are the values we want to compare against the standard solution methods. The latter make no use of the separability property of the problem, which anyway is destroyed by the lattice approximation.

The first column of **Table 3** associates a symmetry classification  $(P_x, P_y)$  to each eigenvalue  $E$ , or rather to its corresponding eigenfunction  $\Psi_E(x, y)$ . Since Equation (18) are

**TABLE 4** | Numerical calculations of the lowest eigenvalues of the two-dimensional quantum anharmonic oscillator, by various approximations and lattice sizes.

$(P_x, P_y)$	Stencil ( $2^{10} \times 2^{10}$ )	“FFT” ( $2^4 \times 2^4$ )	“FFT” ( $2^5 \times 2^5$ )	“FFT” ( $2^7 \times 2^7$ )
(S, S)	2.120574864327	2.121724631908	2.120724180968	2.120724180969
(S, A)	4.859463304350	4.863978042739	4.860035120276	4.860035120286
(A, S)	4.859463304350	4.863978042731	4.860035120269	4.860035120289
(S, S)	7.597839625245	7.580886360302	7.599346064273	7.599346059599
(S, S)	8.514505169411	8.443877132728	8.516060033426	8.516060028467
(A, A)	8.514700940122	8.466735662572	8.516060024420	8.516060028467
(S, A)	11.252295795135	11.091953034554	11.255371027420	11.255370967792
(A, S)	11.252295795137	11.091953034552	11.255371027446	11.255370967784
(S, A)	12.702160201238	12.713861518776	12.705107605729	12.705107601868
(A, S)	12.702160201248	12.713861518777	12.705107605757	12.705107601861
(S, S)	14.905839565650	16.827495880048	14.911396413962	14.911395875970
(S, S)	15.438616444914	17.044711067731	15.444418909471	15.444418541178
(A, A)	15.439522886891	14.126665759659	15.444418063518	15.444418541175
(S, S)	17.316965583271	18.162997853055	17.322188195788	17.322188109337
(A, A)	17.317047769535	16.740653634905	17.322187929414	17.322188109328
(S, A)	19.091567414142	18.071825773508	19.100442397522	19.100443449360
(A, S)	19.091567414151	18.071825773501	19.100442397503	19.100443449361
(S, A)	20.053053266697	20.244253292135	20.061496254183	20.061499048648
(A, S)	20.053053266716	20.244253292132	20.061496254153	20.061499048648
(S, A)	22.290449617012	22.809096276441	22.298734848064	22.298735008720
(A, S)	22.290449617033	22.809096276438	22.298734848071	22.298735008718
(S, S)	23.276097201666	35.427997419504	23.289486014610	23.289491022749

The accuracy obtained is indicated by an underscore of the first inaccurate position (when taking roundoffs into account). The first column list the symmetry types (reflection parities) of the associated wavefunction.

invariant under reflections,

$$\mathcal{P}_x : x \rightarrow -x \quad \text{or} \quad \mathcal{P}_y : y \rightarrow -y,$$

all eigenfunctions can be constructed to transform symmetrically (S) or anti-symmetrically (A) under such reflections. For  $m < n$ , such a construction is

$$\Psi_{mn}^{(\pm)}(x, y) = \frac{1}{\sqrt{2}} [\psi_m(\xi) \psi_n(\eta) \pm \psi_n(\xi) \psi_m(\eta)]. \quad (21a)$$

For  $m = n$  there is only one possibility,

$$\Psi_{mm}(x, y) = \psi_m(\xi) \psi_m(\eta). \quad (21b)$$

By use of the properties that

$$\psi_m(-\xi) = (-1)^{m-1} \psi_m(\xi), \quad \mathcal{P}_x : (\xi, \eta) \rightarrow -(\eta, \xi), \quad \text{and} \\ \mathcal{P}_y : (\xi, \eta) \rightarrow (\eta, \xi),$$

we find that

$$\Psi_{mn}^{(\pm)}(-x, y) = \pm (-1)^{m+n} \Psi_{mn}^{(\pm)}(x, y), \quad \text{and} \\ \Psi_{mn}^{(\pm)}(x, -y) = \pm \Psi_{mn}^{(\pm)}(x, y). \quad (22)$$

and further that  $\Psi_{mm}(-x, y) = \Psi_{mm}(x, -y) = \Psi_{mm}(x, y)$ . The conclusion is that in an exact calculation the states  $\Psi_{mn}$  will be double degenerate when  $m \neq n$ , with parities  $(P_x, P_y)$  equal to (S, S) and (A, A) when  $m, n$  are both even or both odd, otherwise with parities (S, A) and (A, S). The states  $\Psi_{mm}$

are singlets with parities (S, S). The first column of **Table 3** is constructed according to these rules.

**Table 4** displays the results of some standard numerical solutions to Equation (18), “automagically” generated in the same way as the previous treatments of the harmonic (linear) oscillators. In the second column we show the results of using the minimal 5-point stencil approximation of the Laplace operator on a  $1,024 \times 1,024$  lattice (approximating the whole space). The resulting numerical problem is solved with the **eigsh** sparse solver. The numerical accuracy is indicated by an underscore of the first inaccurate position, when taking proper roundoffs into account: The exact and numerical results are rounded off to the same number of digits, and compared; the underscore indicates the first position where the results differ.

As can be seen, the results are less than impressive, taking into account the amount computational work invested. One straightforward improvement is to utilize the reflection symmetries of the problem to reduce the magnitude of the problem (with the same lattice cell size  $\delta x^2$ ) by a factor 4, or to reduce the lattice cell size  $\delta x^2$  (with the same problem magnitude) by a factor 4. Another option is to use a higher order stencil approximation like (13). However, as already discussed in section 5, an even better option (for this class of problems) is to use a FFT type of approximation of the Laplace operator. The resulting eigenvalues are listed in columns 3–5, for various lattice sizes approximating the upper right quadrant ( $x \geq 0, y \geq 0$ ) of space. For each lattice size the problem must be solved 4 times, with symmetric (S) and anti-symmetric (A) boundary conditions at the axes  $x = 0$  and  $y = 0$ .

By symmetry under interchange,  $x \leftrightarrow y$ , we expect the  $(S, A)$  and  $(A, S)$  to give identical results (as long as the lattice approximation respects this symmetry). As can be seen, the numerical results satisfy the symmetry within a numerical accuracy of  $\text{few} \times 10^{-12}$ , regardless how close the results are to the exact values. The degeneracy of states with  $(S, S)$ , respectively,  $(A, A)$  symmetry cannot be deduced in the same way from the lattice approximated problem. In the infinite space formulation the problem is separable, which in turn implies this degeneracy. However, the lattice approximation introduces boundaries that are non-factorizable in the  $(\xi, \eta)$ -coordinates. This means that the problem is no longer separable in the lattice approximation. As a result the degeneracy of the  $(S, S)$  and  $(A, A)$  energies are split by a much larger amount, of the same order as the difference between exact and numerical results. (In this case, the lattice problem could be made separable by a rotation of the lattice orientation by 45 degrees.)

We observe that even a  $2^4 \times 2^4$  lattice with in the “FFT approximated” Laplace operator provide almost equally accurate results as a  $2^{10} \times 2^{10}$  lattice with the 5-stencil approximation. The results from a  $2^5 \times 2^5$  lattice seems more than sufficient for practical purposes (say compared to experimental obtainable accuracy), with little to be gained by further decrease of the lattice length  $\delta x$ .

The computation times for the “FFT approximation” are about 0.06, 0.8, and 75 s for respectively  $16 \times 16$ ,  $32 \times 32$ , and  $128 \times 128$  lattice sizes. For the same number of lattice points, the

5-stencil formulation may lead to somewhat shorter computation times. But this is completely offset by the need to work with a much larger number of lattice points: The computation time for the  $1,024 \times 1,024$  stencil approximation was about 30 min.

The Python package described in this paper is available at [19].

## DATA AVAILABILITY STATEMENT

The raw data [19] supporting the conclusions of this article will be made available by the authors, without undue reservation.

## AUTHOR CONTRIBUTIONS

All authors listed have made a substantial, direct and intellectual contribution to the work, and approved it for publication.

## ACKNOWLEDGMENTS

An early version of this work was presented at the IAENG International MultiConference of Engineers and Computer Scientists, Hong Kong March 18–20, 2015, as documented in [20].

AM would like to thank *Mathematics Teaching and Learning Research Group* within *The department of mathematics, Bodø, Nord University* for partial support.

## REFERENCES

- Dirac PAM. The fundamental equations of quantum mechanics. *Proc R Soc A*. (1925) **109**:642–53. doi: 10.1098/rspa.1925.0150
- Schrödinger E. An undulatory theory of the mechanics of atoms and molecules. *Phys Rev*. (1926) **28**:1049–70. doi: 10.1103/PhysRev.28.1049
- Pauli W. Über die Wasserstoffspektrum vom Standpunkt der neuen Quantenmechanik. *Zeitsch Phys*. (1926) **36**:336–63.
- Heisenberg W. Über quantentheoretische Umdeutung kinematischer und mechanischer Beziehungen [Quantum-theoretical reinterpretation of kinematic and mechanical relations]. *Zeitsch Phys*. (1925) **33**:879–93.
- Bender CM, Wu TT. Analytic structure of energy levels in a field-theory model. *Phys Rev Lett*. (1968) **21**:406–9. doi: 10.1103/PhysRevLett.21.406
- Bender CM, Wu TT. Anharmonic oscillator. *Phys Rev*. (1969) **184**:1231–60. doi: 10.1103/PhysRev.184.1231
- Bender CM, Wu TT. Large-order behavior of perturbation theory. *Phys Rev Lett*. (1971) **27**:461–5. doi: 10.1103/PhysRevLett.27.461
- Bender CM, Wu TT. Anharmonic oscillator. II. A study of perturbation theory in large order. *Phys Rev D*. (1973) **7**:1620–36. doi: 10.1103/PhysRevD.7.1620
- Bender CM, Olaussen K, Wang PS. Numerological analysis of the WKB approximation in large order. *Phys Rev D*. (1977) **16**:1740–8. doi: 10.1103/PhysRevD.16.1740
- Zinn-Justin J, Jentschura UD. Multi-instantons and exact results I: conjectures, WKB expansions, and instanton interactions. *Ann Phys*. (2004) **313**:197–267. doi: 10.1016/j.aop.2004.04.004
- Zinn-Justin J, Jentschura UD. Multi-instantons and exact results II: specific cases, higher-order effects, and numerical calculations. *Ann Phys*. (2004) **313**:269–325. doi: 10.1016/j.aop.2004.04.003
- Noreen A, Olaussen K. Quantum loop expansion to high orders, extended borel summation, and comparison with exact results. *Phys Rev Lett*. (2013) **111**:040402. doi: 10.1103/PhysRevLett.111.040402
- Janke W, Kleinert H. Convergent strong-coupling expansions from divergent weak-coupling perturbation theory. *Phys Rev Lett*. (1995) **75**:2787–91. doi: 10.1103/PhysRevLett.75.2787
- Mushtaq A, Noreen A, Olaussen K, Øverbø I. Very-high-precision solutions of a class of Schrödinger type equations. *Comput Phys Commun*. (2011) **182**:1810–3. doi: 10.1016/j.cpc.2010.12.046
- Noreen A, Olaussen K. High precision series solutions of differential equations: ordinary and regular singular points of second order ODEs. *Comput Phys Commun*. (2012) **183**:2291–7. doi: 10.1016/j.cpc.2012.05.015
- Van Der Walt S, Colbert SC, Varoquaux G. The NumPy array: a structure for efficient numerical computation. *Comput Sci Eng*. (2011) **13**:22–30. doi: 10.1109/MCSE.2011.37
- Jones E, Oliphant T, Peterson P. *SciPy: Open Source Scientific Tools for Python*. (2014). Available online at: <http://www.scipy.org/>
- Oliphant TE. Python for scientific computing. *Comput Sci Eng*. (2007) **9**:10–20. doi: 10.1109/MCSE.2007.58
- Mushtaq A, Noreen A, Olaussen A. *Python Package for Numerical Solutions of Quantum Mechanical Eigenvalue Problems* (2020). doi: 10.6084/m9.figshare.127655
- Noreen A, Olaussen A. A python class for higher-dimensional schrödinger equations. In: *Proceedings of the International MultiConference of Engineers and Computer Scientists IMECS 2015*. Hong Kong (2015). p. 206–11.

**Conflict of Interest:** The authors declare that the research was conducted in the absence of any commercial or financial relationships that could be construed as a potential conflict of interest.

Copyright © 2020 Mushtaq, Noreen and Olaussen. This is an open-access article distributed under the terms of the Creative Commons Attribution License (CC BY). The use, distribution or reproduction in other forums is permitted, provided the original author(s) and the copyright owner(s) are credited and that the original publication in this journal is cited, in accordance with accepted academic practice. No use, distribution or reproduction is permitted which does not comply with these terms.



# A Vector Series Solution for a Class of Hyperbolic System of Caputo Time-Fractional Partial Differential Equations With Variable Coefficients

Ahmad El-Ajou<sup>1\*</sup> and Zeyad Al-Zhour<sup>2\*</sup>

<sup>1</sup>Department of Mathematics, Faculty of Science, Al-Balqa' Applied University, Al-Salt, Jordan, <sup>2</sup>Department of Basic Engineering Sciences, College of Engineering, Imam Abdulrahman Bin Faisal University, Dammam, Saudi Arabia

## OPEN ACCESS

### Edited by:

Feliz Minhós,  
University of Evora, Portugal

### Reviewed by:

Yang Liu,  
Inner Mongolia University, China  
Ndolane Sene,  
Cheikh Anta Diop University, Senegal  
Sania Qureshi,  
Mehran University of Engineering and  
Technology, Pakistan

### \*Correspondence:

Ahmad El-Ajou  
ajou44@bau.edu.jo  
Zeyad Al-Zhour  
zalzhour@iau.edu.sa

### Specialty section:

This article was submitted to  
Mathematical and Statistical Physics,  
a section of the journal  
Frontiers in Physics

Received: 08 January 2020

Accepted: 30 April 2021

Published: 28 May 2021

### Citation:

El-Ajou A and Al-Zhour Z (2021) A  
Vector Series Solution for a Class of  
Hyperbolic System of Caputo Time-  
Fractional Partial Differential Equations  
With Variable Coefficients.  
Front. Phys. 9:525250.  
doi: 10.3389/fphy.2021.525250

In this paper, we introduce a series solution to a class of hyperbolic system of time-fractional partial differential equations with variable coefficients. The fractional derivative has been considered by the concept of Caputo. Two expansions of matrix functions are proposed and used to create series solutions for the target problem. The first one is a fractional Laurent series, and the second is a fractional power series. A new approach, via the residual power series method and the Laplace transform, is also used to find the coefficients of the series solution. In order to test our proposed method, we discuss four interesting and important applications. Numerical results are given to authenticate the efficiency and accuracy of our method and to test the validity of our obtained results. Moreover, solution surface graphs are plotted to illustrate the effect of fractional derivative arrangement on the behavior of the solution.

**Keywords:** hyperbolic systems, power series, analytical-numerical methods, fractional derivatives, Laplace transform

## 1 INTRODUCTION

Many natural phenomena have been modeled through partial differential equations (PDEs), especially in physics, engineering, chemistry, and biology, as well as in humanities [1, 2]. A wide range of PDEs can be classified under the name of hyperbolic PDEs that have the following general form [2–6]:

$$u_t(x, t) = a(x, t)u_x(x, t) + b(x, t)u(x, t) + f(x, t), x \in \mathfrak{I}, t > 0, \quad (1)$$

subject to the following initial condition:

$$u(x, 0) = u_0(x). \quad (2)$$

The equations of compressible fluid flow and the Euler equations are examples of PDEs that can be reduced to hyperbolic PDEs when the effects of viscosity and heat conduction are neglected [6]. In addition, many mathematical models are appearing as hyperbolic systems of PDEs that have the following general form:

$$U_t(x, t) = A(x, t)U_x(x, t) + B(x, t)U(x, t) + F(x, t), x \in \mathfrak{I}, t \geq 0, \quad (3)$$

subject to

$$U(x, 0) = U_0(x), \quad (4)$$

where  $U(x, t), F(x, t) \in M_{n \times 1}, n \in \mathbb{N}$  are vector functions of two variables  $x$  and  $t, U_0(x) \in M_{n \times 1}$  is a vector function of  $x, A(x, t), B(x, t) \in M_{n \times n}$  are matrix functions of two variables  $x$  and  $t,$  and  $A(x_0, t_0)$  is diagonalizable with real eigenvalues for every  $(x_0, t_0) \in \mathfrak{X} \times [0, \infty)$ . The system in **Eqs 3, 4** is said to be strictly hyperbolic if the eigenvalues of  $A(x_0, t_0)$  are all distinct, whereas it is said to be elliptic at a point  $(x_0, t_0)$  if none of the eigenvalues of  $A(x_0, t_0)$  are real for every  $(x_0, t_0) \in \mathfrak{X} \times [0, \infty)$ .

In recent decades, many mathematical models have been reformulated using the concept of fractional calculus because they are found to reflect the phenomenon that has been modeled in a more precise and realistic way by replacing the ordinary derivative with a fractional derivative (FD) of the model. The concept of fractional calculus dates back to the 17th century [7, 8] and has recently gained considerable interest because of its extensive use in widespread fields, for instance, engineering, biological, chemical, and applied physics such as in nonlinear oscillation, waves, and diffusion as we mentioned [7–13]. In fact, from that date until now, there are many definitions of the FD. The most popular definition is the Caputo FD that is denoted and defined as [7, 8]

$$\mathfrak{D}_t^\alpha u(x, t) = \begin{cases} J_t^{m-\alpha} \partial_t^m u(x, t), & m - 1 < \alpha < m, \\ \partial_t^m u(x, t), & \alpha = m, \end{cases}, t > t_0 \geq 0, \quad (5)$$

where  $m \in \mathbb{N}$  and  $J_t^\alpha$  is the Riemann–Liouville fractional integral operator (R-LFIO) of order  $\alpha > 0$  with respect to  $t \geq t_0 \geq 0,$  which is defined by

$$J_t^\alpha u(x, t) = \frac{1}{\Gamma(\alpha)} \int_{t_0}^t (t - \tau)^{\alpha-1} u(x, \tau) d\tau, t > \tau > t_0 \geq 0. \quad (6)$$

For more details about the properties of the two previous definitions, readers can refer to the references [7–12]. The most useful properties that we need in this research are

$$J_t^\alpha (t - t_0)^\mu = \frac{\Gamma(\mu + 1)}{\Gamma(\mu + \alpha + 1)} (t - t_0)^{\mu + \alpha}, \mu > -1, t \geq t_0 \geq 0, \quad (7)$$

$$J_t^\alpha \lambda = \frac{\lambda}{\Gamma(\alpha + 1)} (t - t_0)^\alpha, \lambda \text{ is a constant}, \quad (8)$$

$$\mathfrak{D}_t^\alpha (t - t_0)^\mu = \begin{cases} \frac{\Gamma(\mu + 1)}{\Gamma(\mu - \alpha + 1)} (t - t_0)^{\mu - \alpha}, & \mu \notin \{0, 1, 2, \dots, m - 1\} \\ 0 & \mu \in \{0, 1, 2, \dots, m - 1\} \end{cases}, \quad (9)$$

$$\mathfrak{D}_t^\alpha \lambda = 0, \lambda \text{ is a constant}. \quad (10)$$

As mentioned, the definition of Caputo is one of the most important definitions of the FD, since it was and still is an appropriate and effective tool in the modeling of many natural phenomena in all sciences and fields. For example, but not limited to, the definition of Caputo has recently been used to construct a mathematical model to illustrate the impacts of deforestation on wildlife species [13], in a fractional investigation of bank data [14], to model the spread of hookworm infection [15], and newly to model and analyze the dynamics of novel coronavirus (COVID-19) [16].

It is difficult to find exact solutions (ESs) for the fractional differential and integral equations; for this reason, analytical and numerical methods are usually used to find approximate solutions (ASs) for those equations. In recent decades, many methods have been used to find analytical and numerical solutions for fractional differential and integral equations such as the variational iteration method [17], the Adomian decomposition method [18], the homotopy perturbation method [17], the homotopy analysis method, the fractional transform method [19], Green’s function method [20], and other methods [21, 22].

In the last five years, the residual power series method (RPSM) has achieved an advanced rank among the methods used to find ASs for many fractional differential and integral equations. It has been used in determining ESs and ASs for many equations such as homogeneous and non-homogeneous time- and space-fractional telegraph equation [23], time-fractional Boussinesq-type and space-fractional Klein–Gordon-type equations [24], fractional multi-pantograph system [25], space- and time-fractional linear and nonlinear KdV–Burgers equation [26], multi-energy groups of neutron diffusion equations [27], and other equations. The RPSM is characterized by its ease and speed in finding solutions for equations in the form of a power series. In fact, the RPSM is a mechanism for finding the coefficients of the fractional power series (FPS) without having to find a recurrence relation that we normally obtain from equating the corresponding coefficients in the series. The RPSM is a good alternate proceeding for gaining analytic solutions for fractional PDEs.

Despite all the features we mentioned about the RPSM, we will present in this paper a major modification to the method. We use the concept of limit at infinity instead of the concept of FD in determining the coefficients of the power series solution (SS). As is well known, finding an FD manually is not easy and sometimes takes tens of minutes when it is calculated by software packages, while calculating the limit is much easier than calculating the FD manually and faster by compute. Indeed, the RPSM determines the coefficients of the power SS of the differential or integral equations, whereas the proposed technique determines the coefficients of the expansion that represents the Laplace transform (LT) of the solution. Therefore, we do not need FDs during the transaction-finding process. To be able to implement the new method, we need to provide two expansions of the matrix functions, one to represent the solution of the equation and the other to represent the LT of the solution. Moreover, the convergence of the introduced expansions is studied. In fact, the proposed method called the Laplace-RPSM (L-RPSM) was first introduced by the authors in [28] and used for introducing exact and approximate SSs to the linear and nonlinear neutral FDEs. El-Ajou [29] then adapted the new method in creating solitary solutions for the nonlinear time-fractional partial differential equations (T-FPDEs).

Several articles are interested in providing ASs to T-FPDEs of hyperbolic type, such as the Caputo time-fractional-order hyperbolic telegraph equation [30], hyperbolic T-FPDEs [31–35], the time-fractional diffusion equation [36], fractional

advection–dispersion flow equations [37], and other hyperbolic equations. However, a limited number of research studies provided analytical and numerical solutions for hyperbolic systems of T-FPDEs. Kochubei [38] presented a numerical–analytical solution for homogeneous hyperbolic fractional systems, and Hendy et al. [39] introduced a solution for two-dimensional fractional systems that was provided by a separate contrast scheme. Therefore, more research is needed in providing analytical and numerical solutions for such systems due to their importance in many applications as mentioned above.

The present work aims to apply the L-RPSM to construct ASs of a hyperbolic system of T-FPDEs with variable coefficients in the sense of Caputo’s FD, which are given in the form of the following model:

$$U_t^{(\alpha)}(x, t) = A(x, t)U_x^{(\beta)}(x, t) + B(x, t)U(x, t) + F(x, t), 0 < \alpha, \beta \leq 1, x \in \mathfrak{F}, t \geq 0, \tag{11}$$

subject to

$$U(x, 0) = U_0(x), \tag{12}$$

where  $U_t^{(\alpha)}(x, t) = \mathfrak{D}_t^\alpha U(x, t)$  refers to Caputo’s time-FD of order  $\alpha$  of the multivariable vector function  $U(x, t)$ ,  $U_x^{(\beta)}(x, t) = \mathfrak{D}_x^\beta U(x, t)$  refers to Caputo’s space-FD of order  $\beta$  of the multivariable vector function  $U(x, t)$ , and the definitions of all terms and variables in Eqs 11, 12 are the same as those in Eqs 3, 4.

This paper is organized as follows: In Section 2, the analysis of matrix FPS is prepared. In Section 3, the construction of FPS solution to a hyperbolic system of T-FPDEs with variable coefficients in the sense of Caputo’s FD is presented using the L-RPSM. In Section 4, application models and graphical and numerical simulations are performed in order to illustrate the capability and the simplicity of the proposed method. Finally, the conclusion is presented in Section 5.

## 2 PRELIMINARIES OF MATRIX FPS

Here, we present some definitions and theories regarding matrix analysis and the matrix FPS, which are playing a central role in constructing the L-RPSM solution to a hyperbolic system of T-FPDEs with variable coefficients.

**Definition 2.1.** The R-LFIO of order  $\alpha > 0$  of a matrix function  $U(x, t) = [u_{ij}(x, t)] \in M_{r \times k}$ ,  $1 \leq i \leq r$ ,  $1 \leq j \leq k$ , is defined as

$$J_t^\alpha U(x, t) = [J_t^\alpha u_{ij}(x, t)]_{r \times k}, x \in \mathfrak{F}, t \geq t_0. \tag{13}$$

**Definition 2.2.** Caputo’s time-FD operator of order  $\alpha > 0$  of a matrix function  $U(x, t) = [u_{ij}(x, t)] \in M_{r \times k}$ ,  $1 \leq i \leq r$ ,  $1 \leq j \leq k$ , is

$$\mathfrak{D}_t^\alpha U(x, t) = [\mathfrak{D}_t^\alpha u_{ij}(x, t)]_{r \times k}, x \in \mathfrak{F}, t \geq t_0. \tag{14}$$

**Lemma 2.1.** If  $m - 1 < \alpha \leq m$  and  $m \in \mathbb{N}$ , then

1.  $\mathfrak{D}_t^\alpha J_t^\alpha U(x, t) = U(x, t)$ ,
2.  $J_t^\alpha \mathfrak{D}_t^\alpha U(x, t) = U(x, t) - \sum_{j=0}^{m-1} \frac{\partial^j U(x, 0^+)}{\partial t^j} \frac{(t-t_0)^j}{j!}, t > t_0$ .

**Definition 2.3** Let  $A_k \in M_{m \times n}$ . We say that a sequence  $\{A_k\}$  converges to a matrix  $A \in M_{m \times n}$  with respect to a matrix norm  $\|\bullet\|$  on  $M_{m \times n}$  if and only if  $\lim_{k \rightarrow \infty} \|A_k - A\| = 0$ . If  $\{A_k\}$  converges to  $A$ , we write  $\lim_{k \rightarrow \infty} A_k = A$ .

**Definition 2.4** For  $0 < \alpha \leq 1$ ,  $x \in \mathfrak{F}$ , and  $t \geq t_0$ , a matrix power series of the following form:

$$\sum_{m=0}^{\infty} H_m(x)(t-t_0)^{m\alpha} = H_0(x) + H_1(x)(t-t_0)^\alpha + H_2(x)(t-t_0)^{2\alpha} + \dots, x \in \mathfrak{F} t \geq t_0, \tag{15}$$

is called a bivariate matrix FPS around  $t_0$ , where  $t$  is an independent variable and  $H_m(x) \in M_{r \times k}$  are matrix functions of the independent variable  $x$  called series coefficients.

**Theorem 2.1.** Assume that  $U(x, t) = [u_{ij}(x, t)] \in M_{r \times k}$ ,  $1 \leq i \leq r$ ,  $1 \leq j \leq k$ , such that  $u_{ij}(x, t) \in C(\mathfrak{F} \times [t_0, t_0 + T])$  and  $\mathfrak{D}_t^{m\alpha} u_{ij}(x, t) \in C(\mathfrak{F} \times (t_0, t_0 + T))$  for  $1 \leq i \leq r$ ,  $1 \leq j \leq k$ ,  $w = 0, 1, 2, \dots, n + 1$ , where  $\mathfrak{D}_t^{m\alpha} = \mathfrak{D}_t^\alpha \cdot \mathfrak{D}_t^\alpha \dots \mathfrak{D}_t^\alpha$  ( $m$ -times) and  $\alpha > 0$ . Then,

$$J_t^{(n+1)\alpha} \mathfrak{D}_t^{(n+1)\alpha} U(x, t) = \frac{\mathfrak{D}_t^{(n+1)\alpha} U(x, \xi)}{\Gamma((n+1)\alpha + 1)} (t-t_0)^{(n+1)\alpha}, t_0 \leq \xi \leq t < t_0 + T. \tag{16}$$

**Proof.** Of the operator definition in Eqs 6, 13 we have

$$J_t^{(n+1)\alpha} \mathfrak{D}_t^{(n+1)\alpha} U(x, t) = \frac{1}{\Gamma((n+1)\alpha)} \int_{t_0}^t (t-y)^{(n+1)\alpha-1} \mathfrak{D}_y^{(n+1)\alpha} U(x, y) dy = \frac{\mathfrak{D}_t^{(n+1)\alpha} U(x, \xi)}{\Gamma((n+1)\alpha)} \int_{t_0}^t (t-y)^{(n+1)\alpha-1} dy$$

(based on the second mean value theorem for integral [4])

$$= \frac{\mathfrak{D}_t^{(n+1)\alpha} U(x, \xi)}{\Gamma((n+1)\alpha + 1)} (t-t_0)^{(n+1)\alpha}, t_0 \leq \xi \leq t < t_0 + T.$$

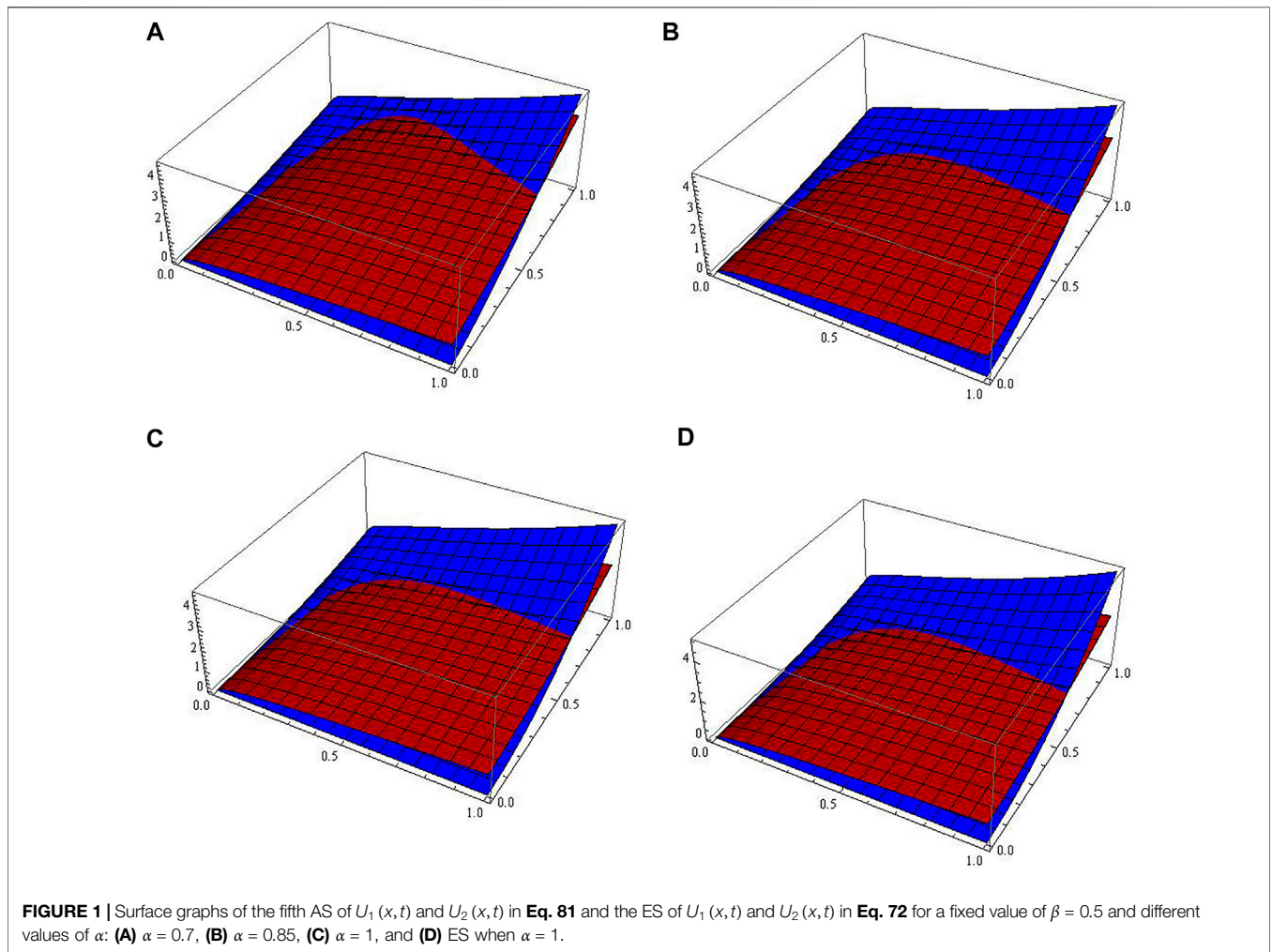
**Theorem 2.2.** Assume that  $U(x, t) = [u_{ij}(x, t)] \in M_{r \times k}$ ,  $1 \leq i \leq r$ ,  $1 \leq j \leq k$ , such that  $u_{ij}(x, t) \in C(\mathfrak{F} \times [t_0, t_0 + T])$  and  $\mathfrak{D}_t^{m\alpha} u_{ij}(x, t) \in C(\mathfrak{F} \times (t_0, t_0 + T))$  for  $1 \leq i \leq r$ ,  $1 \leq j \leq k$ ,  $m = 0, 1, 2, \dots, n + 1$ , where  $\alpha \in (0, 1]$ . Then,

$$U(x, t) = \sum_{m=0}^n \frac{\mathfrak{D}_t^{m\alpha} U(x, t_0)}{\Gamma(m\alpha + 1)} (t-t_0)^{m\alpha} + \frac{\mathfrak{D}_t^{(n+1)\alpha} U(x, \xi)}{\Gamma((n+1)\alpha + 1)} (t-t_0)^{(n+1)\alpha}, t_0 \leq \xi \leq t \leq t_0 + T. \tag{17}$$

**Proof.** From Theorem 2.1, it suffices to demonstrate that

$$J_t^{(n+1)\alpha} \mathfrak{D}_t^{(n+1)\alpha} U(x, t) = U(x, t) - \sum_{m=0}^n \frac{\mathfrak{D}_t^{m\alpha} U(x, t_0)}{\Gamma(m\alpha + 1)} (t-t_0)^{m\alpha}.$$

According to Lemma 2.1, it is easy to show that the formula is correct for  $n = 0$  and  $n = 1$ . Thus, inductively, we prove the theorem as follows:



$$\begin{aligned}
 & J_t^{(n+2)\alpha} \mathfrak{D}_t^{(n+2)\alpha} U(x, t) = J_t^\alpha \left( (J_t^{(n+1)\alpha} \mathfrak{D}_t^{(n+1)\alpha}) \mathfrak{D}_t^\alpha U(x, t) \right) \\
 & = J_t^\alpha \left( \mathfrak{D}_t^\alpha U(x, t) - \sum_{m=0}^n \frac{\mathfrak{D}_t^{(m+1)\alpha} U(x, t_0)}{\Gamma(m\alpha + 1)} (t - t_0)^{m\alpha} \right) \text{ (by Lemma 2.1)} \\
 & = J_t^\alpha \mathfrak{D}_t^\alpha U(x, t) - \sum_{m=0}^n \frac{\mathfrak{D}_t^{(m+1)\alpha} U(x, t_0)}{\Gamma((m+1)\alpha + 1)} (t - t_0)^{(m+1)\alpha} \text{ (by Eq. (7))} \\
 & = U(x, t) - U(x, t_0) - \sum_{m=1}^{n+1} \frac{\mathfrak{D}_t^{m\alpha} U(x, t_0)}{\Gamma(m\alpha + 1)} (t - t_0)^{m\alpha} \text{ (by Lemma 2.1)} \\
 & = U(x, t) - \sum_{m=0}^{n+1} \frac{\mathfrak{D}_t^{m\alpha} U(x, t_0)}{\Gamma(m\alpha + 1)} (t - t_0)^{m\alpha}.
 \end{aligned}$$

Thus, the proof of Theorem 2.2 has been completed.  
 Let us call the series (Eq. 17) the bivariate fractional matrix Taylor’s formula (BFMTF) of the matrix function  $U(x, t)$ . As any series, the tail of the series (Eq. 17),  $\mathcal{R}_n(x, t) = \frac{\mathfrak{D}_t^{(n+1)\alpha} U(x, t)}{\Gamma((n+1)\alpha + 1)} (t - t_0)^{(n+1)\alpha}$ , is called the  $n$ th remainder for the Taylor series of  $U(x, t)$ . The function  $P(x, t) = U(x, t) - \mathcal{R}_n(x, t)$  is an approximate function

for  $U(x, t)$ , and the accuracy of the approximation increases as  $\mathcal{R}_n(x, t)$  decreases. Finding a bound for  $\mathcal{R}_n(x, t)$  gives an indication of the accuracy of the approximation  $P(x, t) \approx U(x, t)$ . The following theorem provides such a bound.

**Theorem 23. (The Remainder Estimation Theorem)** Assume that  $\mathfrak{D}_t^{(n+1)\alpha} U(x, t)$ ,  $\alpha \in (0, 1]$  is defined on  $(\mathfrak{S} \times (t_0, t_0 + d))$ . If  $\|\mathfrak{D}_t^{(n+1)\alpha} U(x, t)\| \leq \mathcal{M}(x)$  on  $t_0 \leq t \leq d$  and fixed  $x$  for some matrix norm  $\|\bullet\|$ , then the remainder  $\mathcal{R}_n(x, t)$  of the BFMTF of  $U(x, t)$  satisfies

$$\mathcal{R}_n(x, t) \leq \frac{\mathcal{M}(x)}{\Gamma((n+1)\alpha + 1)} (t - t_0)^{(n+1)\alpha}, t_0 \leq t \leq d. \tag{18}$$

**Proof.** The definition of the remainder of the BFMTF of  $U(x, t)$  as in Eq. 17 is given by

$$\begin{aligned}
 \mathcal{R}_n(x, t) & = \frac{\mathfrak{D}_t^{(n+1)\alpha} U(x, t)}{\Gamma((n+1)\alpha + 1)} (t - t_0)^{(n+1)\alpha} \\
 & = U(x, t) - \sum_{m=0}^n \frac{\mathfrak{D}_t^{m\alpha} U(x, t_0)}{\Gamma(m\alpha + 1)} (t - t_0)^{m\alpha}.
 \end{aligned} \tag{19}$$

According to Theorem 2.2, the remainder can be expressed as

$$J_t^{(n+1)\alpha} \mathfrak{D}_t^{(n+1)\alpha} U(x, t) = U(x, t) - \sum_{m=0}^n \frac{\mathfrak{D}_t^{m\alpha} U(x, t_0)}{\Gamma(m\alpha + 1)} (t - t_0)^{m\alpha}.$$

So, for  $t_0 \leq \tau \leq t \leq d$ , we have

$$\begin{aligned} \|\mathcal{R}_n(x, t)\| &= \left\| J_t^{(n+1)\alpha} \mathfrak{D}_t^{(n+1)\alpha} U(x, t) \right\| \\ &= \left\| \frac{1}{\Gamma((n+1)\alpha)} \int_{t_0}^t (t - \tau)^{(n+1)\alpha-1} \mathfrak{D}_t^{(n+1)\alpha} U(x, \tau) d\tau \right\| \\ &\leq \frac{1}{\Gamma((n+1)\alpha)} \int_{t_0}^t |(t - \tau)^{(n+1)\alpha-1}| \left\| \mathfrak{D}_t^{(n+1)\alpha} U(x, \tau) \right\| d\tau \\ &\leq \frac{1}{\Gamma((n+1)\alpha)} \int_{t_0}^t |(t - \tau)^{(n+1)\alpha-1}| \mathcal{M}(x) d\tau \\ &= \frac{\mathcal{M}(x)}{\Gamma((n+1)\alpha)} \int_{t_0}^t (t - \tau)^{(n+1)\alpha-1} d\tau \\ &= \frac{\mathcal{M}(x)}{\Gamma((n+1)\alpha + 1)} (t - t_0)^{(n+1)\alpha}. \end{aligned}$$

Thus, the proof is completed.

Note that when  $n \rightarrow \infty$ , Taylor’s formula (17) is of the form

$$U(x, t) = \sum_{m=0}^{\infty} \frac{U_t^{(m\alpha)}(x, t_0)}{\Gamma(m\alpha + 1)} (t - t_0)^{m\alpha}, \quad x \in I, t_0 \leq t < t_0 + T, \quad (21)$$

which can be applied throughout this work.

Finally, it is worth to mention that if  $\alpha = 1$ , then the BFMTF (Eq. 21) becomes

$$U(x, t) = \sum_{m=0}^{\infty} \frac{\partial^m U(x, t_0)}{m! \partial t^m} (t - t_0)^m, \quad t_0 \leq t < t_0 + T, \quad (22)$$

which is the bivariate classical matrix Taylor’s formula of a matrix function.

Lemma 2.2. Let  $U(x, t) = [u_{ij}(x, t)] \in M_{r \times k}$ ,  $1 \leq i \leq r$ ,  $1 \leq j \leq k$ , such that  $u_{ij}(x, t)$  are of exponential orders (EOs)  $\lambda_{ij}$  and piecewise continuous functions (PCFs) on  $\mathfrak{F} \times [t_0, \infty)$ , respectively. Then,

- $\mathcal{L}[J_t^\alpha U(x, t)] = s^{\alpha-1} \mathcal{L}[U(x, t - t_0)]$ ,  $\alpha > 0$ .
- $\mathcal{L}[\mathfrak{D}_t^\alpha U(x, t)] = s^\alpha \mathcal{L}[U(x, t - t_0)] - \sum_{k=0}^{m-1} s^{\alpha-k-1} \partial_t^k U(x, t_0)$ ,  $m - 1 < \alpha < m$ .
- $\mathcal{L}[\mathfrak{D}_t^{n\alpha} U(x, t)] = s^{n\alpha} \mathcal{L}[U(x, t - t_0)] - \sum_{k=0}^{n-1} s^{(n-k)\alpha-1} \mathfrak{D}_t^{k\alpha} U(x, t_0)$ ,  $0 < \alpha < 1$ .

Corollary 2.1. Let  $U(x, t) = [u_{ij}(x, t)] \in M_{r \times k}$ ,  $1 \leq i \leq r$ ,  $1 \leq j \leq k$ , such that  $u_{ij}(x, t)$  are PCFs on  $\mathfrak{F} \times [t_0, \infty)$  and of EOs  $\lambda_{ij}$ , respectively. Assume that  $U(x, t)$  can be represented as a BFMTF as in Eq. 21. Then, the inverse LT of  $U(x, t)$  has the following fractional matrix expansion (FME):

$$\mathbb{U}(x, s) = e^{-t_0 s} \sum_{n=0}^{\infty} \frac{U_t^{(n\alpha)}(x, t_0)}{s^{1+n\alpha}}, \quad 0 < \alpha \leq 1, x \in \mathfrak{F}, s > \lambda, \quad (23)$$

where  $\lambda = \min \lambda_{ij}$ ,  $1 \leq i \leq r$ ,  $1 \leq j \leq k$ , which can be applied directly throughout this work when  $t_0 = 0$ .

TABLE 1 | Values of  $\|\text{RES}_6(x, t)\|$  for different values of  $\alpha$ .

(x, t)	$\alpha = 0.6$	$\alpha = 0.8$	$\alpha = 1.0$
(0.0, 0.0)	0.000000	0.000000	0.000000
(0.2, 0.2)	$3.5563 \times 10^{-3}$	$1.6882 \times 10^{-4}$	$7.6648 \times 10^{-6}$
(0.4, 0.4)	$4.8228 \times 10^{-2}$	$5.1980 \times 10^{-3}$	$5.3168 \times 10^{-4}$
(0.6, 0.6)	$2.2559 \times 10^{-1}$	$3.9524 \times 10^{-2}$	$6.5249 \times 10^{-3}$
(0.8, 0.8)	$6.8021 \times 10^{-1}$	$1.6888 \times 10^{-1}$	$3.9295 \times 10^{-2}$
(1.0, 1.0)	$1.6103 \times 10^0$	$5.2523 \times 10^{-1}$	$1.5995 \times 10^{-1}$

TABLE 2 | Values of  $\text{RES}_7(x, t)$  for different values of  $\alpha$ .

(x, t)	$\alpha = 0.6$	$\alpha = 0.8$	$\alpha = 1.0$
(0.0, 0.0)	0.000000	0.000000	0.000000
(0.2, 0.2)	$9.6895 \times 10^{-4}$	$2.6675 \times 10^{-5}$	$6.82732 \times 10^{-7}$
(0.4, 0.4)	$1.9432 \times 10^{-2}$	$1.3932 \times 10^{-3}$	$9.2535 \times 10^{-5}$
(0.6, 0.6)	$1.1395 \times 10^{-1}$	$1.4361 \times 10^{-2}$	$1.6690 \times 10^{-3}$
(0.8, 0.8)	$4.0283 \times 10^{-1}$	$7.5982 \times 10^{-2}$	$1.3162 \times 10^{-2}$
(1.0, 1.0)	$1.0780 \times 10^0$	$2.7858 \times 10^{-1}$	$6.5901 \times 10^{-2}$

Theorem 2.4. Let  $U(x, t) = [u_{ij}(x, t)] \in M_{r \times k}$ ,  $1 \leq i \leq r$ ,  $1 \leq j \leq k$ , such that  $u_{ij}(x, t)$  are PCFs on  $\mathfrak{F} \times [t_0, \infty)$  and of EOs  $\lambda_{ij}$ , respectively, and  $\mathbb{U}(x, s) = \mathcal{L}[U(x, t)]$  can be represented as the FME in Eq. 23. For some matrix norm  $\|\bullet\|$ , if  $\|se^{-t_0 s} \mathcal{L}[\mathfrak{D}_t^{(n+1)\alpha} U(x, t)]\| \leq \mathcal{M}(x)$ ,  $0 < \alpha \leq 1$ , on  $\mathfrak{F} \times (\lambda, \gamma]$  and at a fixed point  $x$ , then the norm of the remainder of the FME in Eq. 23 satisfies

$$\|\mathcal{R}_n(x, s)\| \leq \frac{\mathcal{M}(x)}{s^{1+(n+1)\alpha}}, \quad x \in \mathfrak{F}, \lambda < s \leq \gamma. \quad (24)$$

Proof. As it is assumed in the text of the theorem, suppose that

$$\|se^{-t_0 s} \mathcal{L}[\mathfrak{D}_t^{(n+1)\alpha} \psi(x, t)]\| \leq \mathcal{M}(x), \quad x \in \mathfrak{F}, \lambda < s \leq \gamma. \quad (25)$$

As in Eq. 19, the remainder of the FME in Eq. 23 is

$$\mathcal{R}_n(x, s) = \mathbb{U}(x, s) - e^{-t_0 s} \sum_{k=0}^n \frac{\mathfrak{D}_t^{k\alpha} U(x, t_0)}{s^{1+k\alpha}}. \quad (26)$$

Multiplying Eq. 26 by  $s^{1+(n+1)\alpha}$ , we get

$$\begin{aligned} s^{1+(n+1)\alpha} \mathcal{R}_n(x, s) &= s^{1+(n+1)\alpha} \mathbb{U}(x, s) - e^{-t_0 s} \sum_{k=0}^n s^{(n+1-k)\alpha} \mathfrak{D}_t^{k\alpha} U(x, t_0) \\ &= se^{-t_0 s} \left( s^{(n+1)\alpha} \mathcal{L}[U(x, t - t_0)] - \sum_{k=0}^n s^{(n+1-k)\alpha-1} \mathfrak{D}_t^{k\alpha} U(x, t_0) \right) \\ &= se^{-t_0 s} \mathcal{L}[\mathfrak{D}_t^{(n+1)\alpha} U(x, t)]. \end{aligned}$$

Thus, it follows that

$$\mathcal{R}_n(x, s) = \frac{se^{-t_0 s}}{s^{1+(n+1)\alpha}} \mathcal{L}[\mathfrak{D}_t^{(n+1)\alpha} U(x, t)]. \quad (28)$$

Finally, for  $0 \leq \lambda < s \leq \gamma$  and fixed  $x$ , we have

$$\begin{aligned} \|\mathcal{R}_n(x, s)\| &= \frac{1}{s^{1+(n+1)\alpha}} \|s e^{-t_0 s} \mathcal{L}[\mathfrak{D}_t^{(n+1)\alpha} U(x, t)]\| \\ &\leq \frac{\mathcal{M}(x)}{s^{1+(n+1)\alpha}} \end{aligned} \tag{29}$$

Thus, we reach the end of the proof.

### 3 APPLYING THE L-RPSM TO THE HYPERBOLIC SYSTEM OF T-FPDES

In this section, we construct an AS to the hyperbolic system of T-FPDEs with variable coefficients given in Eqs 11, 12 by using the L-RPSM. To achieve it, firstly, we apply the LT on both sides of Eq. 11, and use Lemma 2.2, and Eq. 12; then, we have

$$\begin{aligned} \mathbb{U}(x, s) &= \frac{U_0(x)}{s} + \frac{\mathcal{L}[\mathcal{L}^{-1}[\mathbb{A}(x, s)] \partial_x^\beta (\mathcal{L}^{-1}[\mathbb{U}(x, s)])]}{s^\alpha} \\ &+ \frac{\mathcal{L}[\mathcal{L}^{-1}[\mathbb{B}(x, s)] \mathcal{L}^{-1}[\mathbb{U}(x, s)]]}{s^\alpha} + \frac{\mathbb{F}(x, t)}{s^\alpha}, \quad x \in \mathfrak{I}, s > \lambda \geq 0, \end{aligned} \tag{30}$$

where  $\mathbb{U}(x, s) = \mathcal{L}[U(x, t)](s)$ ,  $\mathbb{A}(x, s) = \mathcal{L}[A(x, t)](s)$ ,  $\mathbb{B}(x, s) = \mathcal{L}[B(x, t)](s)$ , and  $\mathbb{F}(x, s) = \mathcal{L}[F(x, t)](s)$ . Let the solution of Eq. 30 have the following FME:

$$\mathbb{U}(x, s) = \sum_{m=0}^{\infty} \frac{H_m(x)}{s^{1+m\alpha}}, \quad x \in \mathfrak{I}, s > \lambda \geq 0, \tag{31}$$

where  $H_m(x) = U_t^{(m\alpha)}(x, 0) \in M_{r \times 1}$ ,  $m = 0, 1, 2, \dots$ ,  $0 < \alpha \leq 1$ , and  $A(x, t), B(x, t)$ , and  $F(x, t)$  have a BFMTEF.

Of course, treating with a finite series is acceptable more than an infinite series. For this reason, the L-RPSM deals with a finite series while calculating coefficients of the SS. So, we express the  $k$ th truncated series ( $k$ th TS) of  $\mathbb{U}(x, s)$  as follows:

$$\mathbb{U}_k(x, s) = \frac{U_0(x)}{s} + \sum_{m=1}^k \frac{H_m(x)}{s^{1+m\alpha}}. \tag{32}$$

To apply the L-RPSM for determining the coefficients  $H_m(x)$ ,  $m = 1, 2, 3, \dots, k$ , in the  $k$ th TS in Eq. 32, we define the so-called residual matrix function (RMF) for Eq. 30 as

$$\begin{aligned} \text{RMF}(x, s) &= \mathbb{U}(x, s) - \frac{U_0(x)}{s} - \frac{\mathcal{L}[\mathcal{L}^{-1}[\mathbb{A}(x, s)] \partial_x^\beta (\mathcal{L}^{-1}[\mathbb{U}(x, s)])]}{s^\alpha} \\ &- \frac{\mathcal{L}[\mathcal{L}^{-1}[\mathbb{B}(x, s)] \mathcal{L}^{-1}[\mathbb{U}(x, s)]]}{s^\alpha} - \frac{\mathbb{F}(x, t)}{s^\alpha}, \quad x \in \mathfrak{I}, s > \lambda \geq 0, \end{aligned} \tag{33}$$

and the  $k$ th residual matrix function (RMF<sub>*k*</sub>) of the style form

$$\begin{aligned} \text{RMF}_k(x, s) &= \mathbb{U}_k(x, s) - \frac{U_0(x)}{s} - \frac{\mathcal{L}[\mathcal{L}^{-1}[\mathbb{A}(x, s)] \partial_x^\beta (\mathcal{L}^{-1}[\mathbb{U}_k(x, s)])]}{s^\alpha} \\ &- \frac{\mathcal{L}[\mathcal{L}^{-1}[\mathbb{B}(x, s)] \mathcal{L}^{-1}[\mathbb{U}_k(x, s)]]}{s^\alpha} - \frac{\mathbb{F}(x, t)}{s^\alpha}, \quad x \in \mathfrak{I}, s > \lambda \geq 0. \end{aligned} \tag{34}$$

The main idea of the L-RPSM can be shown in the following clear facts related to the RMF and RMF<sub>*k*</sub>:

1.  $\lim_{k \rightarrow \infty} \text{RMF}_k(x, s) = \text{RMF}(x, s)$ ,  $x \in \mathfrak{I}$ ,  $s > \lambda \geq 0$
2.  $\text{RMF}(x, s) = 0 \in M_{r \times 1}$ ,  $x \in I$ ,  $s > \lambda \geq 0$
3. RMF( $x, s$ ) has an FME. So, we can express it as follows:

$$\text{RMF}(x, s) = \sum_{m=1}^{\infty} \frac{H_m(x) - N_m[H_i(x)]}{s^{1+m\alpha}}, \quad i \in \{0, 1, 2, \dots, m-1\}, \tag{35}$$

where  $N_m$ ,  $m = 1, 2, 3, \dots$ , are operators depending on the operators  $\mathcal{L}$  and  $\partial_x^\beta$ .

4. Thus,  $H_m(x) - N_m[H_i(x)] = 0 \in M_{r \times 1}$ , for  $m = 1, 2, 3, \dots$  and  $i \in \{0, 1, 2, \dots, m-1\}$ .
5. RMF<sub>*k*</sub>( $x, s$ ) is not a TS of the expansion of RMF( $x, s$ ), but it is obtained by substituting  $\mathbb{U}_k(x, s)$  into Eq. 35. So, it takes the following form:

$$\text{RMF}_k(x, s) = \sum_{m=1}^k \frac{H_m(x) - N_m[H_i(x)]}{s^{1+m\alpha}} + \sum_{m=k+1}^{n_k} \frac{\mathcal{N}_m[H_j(x)]}{s^{1+m\alpha}}, \tag{36}$$

where  $j \in \{0, 1, 2, \dots, k\}$ ,  $i \in \{0, 1, 2, \dots, m-1\}$ ,  $\mathcal{N}_m$ ,  $m = k+1, k+2, \dots, n_k$ , are operators, and  $\mathcal{N}_m[H_j(x)] \neq 0$ .

6. Using the following fact determines the unknown coefficients  $H_k(x)$ ,  $k = 1, 2, 3, \dots$ , in the FME (Eq. 31):

$$\begin{aligned} \lim_{s \rightarrow \infty} (s^{1+k\alpha} \text{RMF}(x, s)) &= \lim_{s \rightarrow \infty} (s^{1+k\alpha} \text{RMF}_k(x, s)) \\ &= H_k(x) - N_k[H_i(x)] = 0, \quad k = 1, 2, 3, \dots, \quad i \in \{0, 1, 2, \dots, k-1\}. \end{aligned} \tag{37}$$

Now, to find  $H_1(x)$ , in Eq. 32, substitute the 1st TS,  $\mathbb{U}_1(x, s) = \frac{U_0(x)}{s} + \frac{H_1(x)}{s^{1+\alpha}}$ , into the 1st RMF, RMF<sub>1</sub>( $x, s$ ), to get

$$\begin{aligned} \text{RMF}_1(x, s) &= \frac{H_1(x) - N_1 U_0(x)}{s^{1+\alpha}} + \frac{\mathcal{N}_2[U_0(x), H_1(x)]}{s^{1+2\alpha}} + \dots \\ &+ \frac{\mathcal{N}_{n_1}[U_0(x), H_1(x)]}{s^{1+n_1\alpha}}. \end{aligned} \tag{38}$$

Multiply Eq. 38 by  $s^{1+\alpha}$  to obtain

$$\begin{aligned} s^{1+\alpha} \text{RMF}_1(x, s) &= H_1(x) - N_1[U_0(x)] + \frac{\mathcal{N}_2[U_0(x), H_1(x)]}{s^\alpha} + \dots \\ &+ \frac{\mathcal{N}_{n_1}[U_0(x), H_1(x)]}{s^{(n_1-1)\alpha}}. \end{aligned} \tag{39}$$

Compute the limit to Eq. 39 as  $s \rightarrow \infty$ , use the fact in Eq. 37, and solve the new obtained equation for  $H_1(x)$  to have

$$H_1(x) = N_1[U_0(x)]. \tag{40}$$

Similarly, to determine the second unknown coefficient in Eq. 32,  $H_2(x)$ , we substitute  $\mathbb{U}_2(x, s) = \frac{U_0(x)}{s} + \frac{H_1(x)}{s^{1+\alpha}} + \frac{H_2(x)}{s^{1+2\alpha}}$  into RMF<sub>2</sub>( $x, s$ ) to get

$$\begin{aligned}
 \text{RMF}_2(x, s) &= \frac{H_2(x) - N_2[U_0(x), H_1(x)]}{s^{1+2\alpha}} + \frac{N_3[U_0(x), H_1(x), H_2(x)]}{s^{1+3\alpha}} + \dots \\
 &+ \frac{N_{n_2}[U_0(x), H_1(x), H_2(x)]}{s^{1+n_2\alpha}}.
 \end{aligned} \tag{41}$$

$$U(x, 0) = \begin{pmatrix} x \\ 1 \end{pmatrix}, \tag{47}$$

where

$$\begin{aligned}
 A(x, t) &= \begin{pmatrix} t^\alpha x & \frac{1}{2x} \\ x^2 & -\frac{t^{3\alpha}}{2x} \end{pmatrix}, \\
 B(x, t) &= \begin{pmatrix} t^{4\alpha} x - t^\alpha & -t^{2\alpha} \\ \frac{t^{5\alpha} + t^{2\alpha} x^4}{x} + \frac{t^\alpha x \Gamma(1+2\alpha)}{\Gamma(1+\alpha)} & -x^2 \end{pmatrix},
 \end{aligned}$$

and the ES is  $U(x, t) = \begin{pmatrix} x \\ 1 + t^{2\alpha} x^2 \end{pmatrix}$ .

To obtain an FME solution for this application using the L-RPSM, transform Eq. 46 to the Laplace space as follows:

$$\begin{aligned}
 \mathbb{U}(x, s) - \frac{U(x, 0)}{s} - \frac{\mathcal{L}[\mathcal{L}^{-1}[A(x, s)]\partial_x^1(\mathcal{L}^{-1}[\mathbb{U}(x, s)])]}{s^\alpha} \\
 - \frac{\mathcal{L}[\mathcal{L}^{-1}[B(x, s)]\mathcal{L}^{-1}[\mathbb{U}(x, s)]]}{s^\alpha} = 0, \quad x \in \mathfrak{R}, s > \lambda \geq 0.
 \end{aligned} \tag{48}$$

Let the solution of Eq. 48 have a form of the FME as in Eq. 31. According to the condition in Eq. 47, the first coefficient of the FME in Eq. 31,  $H_0(x) = U(x, 0) = \begin{pmatrix} x \\ 1 \end{pmatrix}$ . Therefore, the  $k$ th TS of Eq. 31 takes the following expression:

$$\mathbb{U}_k(x, s) = \begin{pmatrix} x \\ 1 \end{pmatrix} \frac{1}{s} + \sum_{m=1}^k \frac{H_m(x)}{s^{1+m\alpha}}, \quad 0 < \alpha \leq 1, x \in \mathfrak{R}, s > \lambda \geq 0, \tag{49}$$

and the  $k$ th RMF of Eq. 48 is

$$\begin{aligned}
 \text{RMF}_k(x, s) &= \mathbb{U}_k(x, s) - \begin{pmatrix} x \\ 1 \end{pmatrix} \frac{1}{s} - \frac{\mathcal{L}[\mathcal{L}^{-1}[A(x, s)]\partial_x^1(\mathcal{L}^{-1}[\mathbb{U}_k(x, s)])]}{s^\alpha} \\
 &- \frac{\mathcal{L}[\mathcal{L}^{-1}[B(x, s)]\mathcal{L}^{-1}[\mathbb{U}_k(x, s)]]}{s^\alpha}, \quad x \in \mathfrak{R}, s > \lambda \geq 0.
 \end{aligned} \tag{50}$$

To find the first unknown coefficient  $H_1(x) = \begin{pmatrix} h_{11}(x) \\ h_{12}(x) \end{pmatrix}$  in Eq. 49, we put the 1st TS,  $\mathbb{U}_1(x, s) = \begin{pmatrix} x \\ 1 \end{pmatrix} \frac{1}{s} + \frac{H_1(x)}{s^{1+\alpha}}$ , into the 1st RMF to get the following abbreviated expression:

$$\begin{aligned}
 \text{RMF}_1(x, s) &= \begin{pmatrix} h_{11}(x) \\ h_{12}(x) \end{pmatrix} \frac{1}{s^{1+\alpha}} + \begin{pmatrix} 0 \\ h_{12}(x) - \Gamma(1+2\alpha) \end{pmatrix} \frac{x^2}{s^{1+2\alpha}} \\
 &+ \begin{pmatrix} 1 + \frac{h_{11}(x)}{\Gamma(1+\alpha)} \\ -x^4 - \frac{x h_{11}(x) \Gamma(1+2\alpha)}{\Gamma(1+\alpha)^2} \end{pmatrix} \frac{\Gamma(1+2\alpha)}{s^{1+3\alpha}} + \begin{pmatrix} h_{12}(x) \\ -h_{11}(x)x^3 \end{pmatrix} \frac{\Gamma(1+3\alpha)}{\Gamma(1+\alpha)s^{1+4\alpha}} \\
 &- \begin{pmatrix} x^2 \\ 0 \end{pmatrix} \frac{\Gamma(1+4\alpha)}{s^{1+5\alpha}} - \begin{pmatrix} x h_{11}(x) \\ 1 \end{pmatrix} \frac{\Gamma(1+5\alpha)}{s^{1+6\alpha}} - \begin{pmatrix} 0 \\ h_{11}(x) \\ x \end{pmatrix} \frac{\Gamma(1+6\alpha)}{\Gamma(1+\alpha)s^{1+7\alpha}}.
 \end{aligned} \tag{51}$$

Multiply Eq. 51 by  $s^{1+\alpha}$  to obtain

Multiply Eq. 41 by  $s^{1+2\alpha}$  and compute the limit at infinity for both sides of a new obtained equation, according to Eq. 37, to have

$$H_2(x) = N_2[U_0(x), H_1(x)]. \tag{42}$$

In general, to determine the  $n$ th unknown coefficient in Eq. 32,  $H_n(x)$ , we substitute  $\mathbb{U}_n(x, s) = \frac{U_0(x)}{s} + \frac{H_1(x)}{s^{1+\alpha}} + \dots + \frac{H_n(x)}{s^{1+n\alpha}}$  into  $\text{RMF}_k(x, s)$  for  $k = n$ , re-multiplying both sides of the new obtained formula by  $s^{1+n\alpha}$ , and use the fact in Eq. 37 to obtain

$$H_n(x) = N_n[U_0(x), H_1(x), \dots, H_{n-1}(x)]. \tag{43}$$

This procedure can be repeated for the required number of FME coefficients representing the solution of Eq. 30. Therefore, the  $k$ th approximation of the solution of Eq. 30 can be represented as the following finite series:

$$\begin{aligned}
 \mathbb{U}_k(x, s) &= \frac{U_0(x)}{s} + \frac{N_1[U_0(x)]}{s^{\alpha+1}} + \frac{N_2[U_0(x), H_1(x)]}{s^{2\alpha+1}} + \dots \\
 &+ \frac{N_k[U_0(x), H_1(x), \dots, H_{k-1}(x)]}{s^{k\alpha+1}}.
 \end{aligned} \tag{44}$$

If we act the inverse LT on both sides of Eq. 44, then we obtain the  $k$ th approximation of the solution of the initial value problem (IVP) (Eqs 11, 12), which takes the following expression:

$$\begin{aligned}
 U_k(x, s) &= \frac{U_0(x)}{s} + \frac{N_1[U_0(x)]}{\Gamma(1+\alpha)} t^\alpha + \frac{N_2[U_0(x), H_1(x)]}{\Gamma(1+2\alpha)} t^{2\alpha} + \dots \\
 &+ \frac{N_k[U_0(x), H_1(x), \dots, H_{k-1}(x)]}{\Gamma(1+k\alpha)} t^{k\alpha}.
 \end{aligned} \tag{45}$$

### 4 APPLICATIONS AND NUMERICAL SIMULATIONS

To test our proposed method, we present in this section four interesting and important applications. The first three applications are prepared so that the ES is already known, while the last application is prepared without knowing the solution in advance to test the predictability of the solution or obtain a suitable AS.

Application 4.1. Consider the following homogeneous hyperbolic system of T-FPDEs with variable coefficients:

$$\begin{aligned}
 U_t^{(\alpha)}(x, t) - A(x, t)U_x^{(1)}(x, t) - B(x, t)U(x, t) &= 0, \\
 0 < \alpha \leq 1, x \in \mathfrak{R}, t \geq 0,
 \end{aligned} \tag{46}$$

subject to

$$\begin{aligned}
 s^{1+\alpha}RMF_1(x,s) &= \begin{pmatrix} h_{11}(x) \\ h_{12}(x) \end{pmatrix} + \begin{pmatrix} 0 \\ h_{12}(x) - \Gamma(1+2\alpha) \end{pmatrix} \frac{x^2}{s^\alpha} \\
 &+ \begin{pmatrix} 1 + \frac{h_{11}(x)}{\Gamma(1+\alpha)} \\ -x^4 - \frac{xh_{11}(x)\Gamma(1+2\alpha)}{\Gamma(1+\alpha)^2} \end{pmatrix} \frac{\Gamma(1+2\alpha)}{s^{2\alpha}} + \begin{pmatrix} h_{12}(x) \\ -h_{11}(x)x^3 \end{pmatrix} \frac{\Gamma(1+3\alpha)}{\Gamma(1+\alpha)s^{3\alpha}} \\
 &- \begin{pmatrix} x^2 \\ 0 \end{pmatrix} \frac{\Gamma(1+4\alpha)}{s^{4\alpha}} - \begin{pmatrix} xh_{11}(x) \\ 1 \end{pmatrix} \frac{\Gamma(1+5\alpha)}{s^{5\alpha}} - \begin{pmatrix} 0 \\ \frac{h_{11}(x)}{x} \end{pmatrix} \frac{\Gamma(1+6\alpha)}{\Gamma(1+\alpha)s^{6\alpha}}.
 \end{aligned} \tag{52}$$

Take the limit at infinity for Eq. 52 and use Eq. 37 to get

$$H_1(x) = \begin{pmatrix} h_{11}(x) \\ h_{12}(x) \end{pmatrix} = \begin{pmatrix} 0 \\ 0 \end{pmatrix}. \tag{53}$$

Similarly, we can obtain the second unknown coefficient in Eq. 49,  $H_2(x) = \begin{pmatrix} h_{21}(x) \\ h_{22}(x) \end{pmatrix}$ . Substitute  $\mathbb{U}_2(x,s) = \begin{pmatrix} x \\ 1 \end{pmatrix} \frac{1}{s} + \frac{H_2(x)}{s^{1+2\alpha}}$  into  $RMF_2(x,s)$  to get the next summarized expression of the second RMF of Eq. 48:

$$\begin{aligned}
 RMF_2(x,s) &= \begin{pmatrix} h_{21}(x) \\ h_{22}(x) - x^2\Gamma(1+2\alpha) \end{pmatrix} \frac{1}{s^{1+2\alpha}} + \begin{pmatrix} \Gamma(1+2\alpha) \\ x^2h_{22}(x) - x^4\Gamma(1+2\alpha) \end{pmatrix} \frac{1}{s^{1+3\alpha}} \\
 &+ \begin{pmatrix} \frac{h_{21}(x)}{\Gamma(1+2\alpha)} \\ \frac{xh_{21}(x)}{\Gamma(1+\alpha)} \end{pmatrix} \frac{\Gamma(1+3\alpha)}{s^{1+4\alpha}} - \begin{pmatrix} x^2 - h_{22}(x) \\ x^3h_{21}(x) \end{pmatrix} \frac{\Gamma(1+4\alpha)}{\Gamma(1+2\alpha)s^{1+5\alpha}} \\
 &- \begin{pmatrix} 0 \\ 1 \end{pmatrix} \frac{\Gamma(1+5\alpha)}{s^{1+6\alpha}} - \begin{pmatrix} xh_{21}(x) \\ 0 \end{pmatrix} \frac{\Gamma(1+6\alpha)}{\Gamma(1+2\alpha)s^{1+7\alpha}} - \begin{pmatrix} 0 \\ \frac{h_{21}(x)}{x} \end{pmatrix} \frac{\Gamma(1+7\alpha)}{\Gamma(1+2\alpha)s^{1+8\alpha}}.
 \end{aligned} \tag{54}$$

Multiply Eq. 54 by  $s^{1+2\alpha}$ , apply the limit at infinity of the obtained equation, and use Eq. 37 to get

$$H_2(x) = \begin{pmatrix} h_{11}(x) \\ h_{12}(x) \end{pmatrix} = \begin{pmatrix} 0 \\ x^2\Gamma(1+2\alpha) \end{pmatrix}. \tag{55}$$

If we repeat the previous procedure for  $k = 3, 4, \dots$ , we can see that

$$H_k(x) = \begin{pmatrix} 0 \\ 0 \end{pmatrix}, \text{ for } k = 3, 4, \dots \tag{56}$$

So, the ES for Eq. 48 will be as follows:

$$\mathbb{U}(x,s) = \frac{1}{s} \begin{pmatrix} x \\ 1 \end{pmatrix} + \begin{pmatrix} 0 \\ x^2 \end{pmatrix} \frac{\Gamma(1+2\alpha)}{s^{1+2\alpha}}. \tag{57}$$

If we apply the inverse LT on Eq. 57, then the SS of the IVP (Eqs 46, 47) will take the following form:

$$U(x,t) = \begin{pmatrix} x \\ 1 \end{pmatrix} + \begin{pmatrix} 0 \\ x^2 \end{pmatrix} t^{2\alpha}, \tag{58}$$

which coincides with the ES.

Application 4.2. Consider the following non-homogeneous hyperbolic system of T-FPDEs with variable coefficients:

$$\begin{aligned}
 U_t^{(\alpha)}(x,t) + A(x,t)U_x^{(1)}(x,t) + B(x,t)U(x,t) \\
 = F(x,t), 0 < \alpha \leq 1, x \in \mathfrak{R}, t \geq 0,
 \end{aligned} \tag{59}$$

subject to

$$U(x,0) = \begin{pmatrix} 0 \\ x^2 \end{pmatrix}, \tag{60}$$

where

$$A(x,t) = \begin{pmatrix} x & t^\alpha \\ 2x + t^{2\alpha} & 0 \end{pmatrix}, B(x,t) = \begin{pmatrix} t^\alpha & x \\ 0 & 2x + t^{2\alpha} \end{pmatrix},$$

$$F(x,t) = \begin{pmatrix} x^3 + e^x\Gamma(1+\alpha) + (2+e^x)xt^\alpha + (x+e^x)t^{2\alpha} \\ 2x^3 + \left(2xe^x + \frac{\Gamma(1+2\alpha)}{\Gamma(1+\alpha)}\right)t^\alpha + (2+x)xt^{2\alpha} + e^xt^{3\alpha} + t^{4\alpha} \end{pmatrix}.$$

According to the construction in Section 3, the LT of Eq. 59 can be represented by

$$\mathbb{U}(x,s) - \begin{pmatrix} 0 \\ x^2 \end{pmatrix} \frac{1}{s} + \frac{\mathcal{L}[\mathcal{L}^{-1}[A(x,s)]\partial_x^1(\mathcal{L}^{-1}[\mathbb{U}(x,s)])]}{s^\alpha} \tag{61}$$

$$+ \frac{\mathcal{L}[\mathcal{L}^{-1}[B(x,s)]\mathcal{L}^{-1}[\mathbb{U}(x,s)]]}{s^\alpha} - \frac{\mathbb{F}(x,t)}{s^\alpha} = 0.$$

The  $k$ th TS of the FME of the solution of Eq. 61 has the following form:

$$\mathbb{U}_k(x,s) = \begin{pmatrix} 0 \\ x^2 \end{pmatrix} \frac{1}{s} + \sum_{m=1}^k \frac{H_m(x)}{s^{1+m\alpha}}, 0 < \alpha \leq 1, x \in \mathfrak{R}, s > \lambda \geq 0, \tag{62}$$

and the  $k$ th RMF of Eq. 61 is

$$\begin{aligned}
 RMF_k(x,s) &= \mathbb{U}_k(x,s) - \begin{pmatrix} 0 \\ x^2 \end{pmatrix} \frac{1}{s} \\
 &+ \frac{\mathcal{L}[\mathcal{L}^{-1}[A(x,s)]\partial_x^1(\mathcal{L}^{-1}[\mathbb{U}_k(x,s)])]}{s^\alpha} \\
 &+ \frac{\mathcal{L}[\mathcal{L}^{-1}[B(x,s)]\mathcal{L}^{-1}[\mathbb{U}_k(x,s)]]}{s^\alpha} - \frac{\mathbb{F}(x,t)}{s^\alpha}, x \in \mathfrak{R}, s > \lambda \geq 0.
 \end{aligned} \tag{63}$$

So, to set the first unknown coefficient of Eq. 62, substitute  $\mathbb{U}_1(x,s)$  into  $s^{1+\alpha}RMF_1(x,s)$  to get

$$\begin{aligned}
 s^{1+\alpha}RMF_1(x,s) &= \begin{pmatrix} h_{11}(x) - e^x\Gamma(1+\alpha) \\ h_{12}(x) \end{pmatrix} \\
 &+ \begin{pmatrix} xh_{12}(x) - 4x\Gamma(1+\alpha) - xe^x\Gamma(1+\alpha) \\ 2xh_{12}(x) - 2xe^x\Gamma(1+\alpha) - \Gamma(1+2\alpha) \end{pmatrix} \frac{1}{s^\alpha} \\
 &- \begin{pmatrix} e^x + x - \frac{h_{11}(x)}{\Gamma(1+\alpha)} \\ 2x \end{pmatrix} \frac{\Gamma(1+2\alpha)}{s^{2\alpha}} \\
 &- \begin{pmatrix} 0 \\ e^x - \frac{h_{12}(x)}{\Gamma(1+\alpha)} \end{pmatrix} \frac{\Gamma(1+3\alpha)}{s^{3\alpha}} - \begin{pmatrix} 0 \\ 1 \end{pmatrix} \frac{\Gamma(1+4\alpha)}{s^{4\alpha}}
 \end{aligned} \tag{64}$$

and use the result in Eq. 37 to obtain

$$H_1(x) = \begin{pmatrix} h_{11}(x) \\ h_{12}(x) \end{pmatrix} = \begin{pmatrix} e^{x\Gamma(1+\alpha)} \\ 0 \end{pmatrix}. \tag{65}$$

Again, substitute  $\mathbb{U}_2(x, s)$  into  $s^{1+2\alpha}RMF_2(x, s)$  to get

$$\begin{aligned} s^{1+2\alpha}RMF_2(x, s) &= \begin{pmatrix} h_{21}(x) \\ h_{22}(x) - \Gamma(1+2\alpha) \end{pmatrix} \\ &+ \begin{pmatrix} xh_{22}(x) - x\Gamma(1+2\alpha) \\ 2xh_{22}(x) - 2x\Gamma(1+2\alpha) \end{pmatrix} \frac{1}{s^\alpha} \\ &- \begin{pmatrix} \frac{h_{21}(x)\Gamma(1+3\alpha)}{\Gamma(1+2\alpha)} \\ 0 \end{pmatrix} \frac{\Gamma(1+2\alpha)}{s^{2\alpha}} \\ &- \begin{pmatrix} 0 \\ 1 - \frac{h_{22}(x)}{\Gamma(1+2\alpha)} \end{pmatrix} \frac{\Gamma(1+4\alpha)}{s^{3\alpha}}. \end{aligned} \tag{66}$$

According to the fact in Eq. 37, we have

$$H_2(x) = \begin{pmatrix} h_{21}(x) \\ h_{22}(x) \end{pmatrix} = \begin{pmatrix} 0 \\ \Gamma(1+2\alpha) \end{pmatrix}. \tag{67}$$

Similarly, anyone can check that  $H_k(x) = 0$ , for  $k = 3, 4, \dots$ . So, the ES for Eq. 61 can be expressed as

$$\mathbb{U}(x, s) = \begin{pmatrix} 0 \\ x^2 \end{pmatrix} \frac{1}{s} + \begin{pmatrix} 1 \\ 0 \end{pmatrix} \frac{e^{x\Gamma(1+\alpha)}}{s^{1+\alpha}} + \begin{pmatrix} 0 \\ 1 \end{pmatrix} \frac{\Gamma(1+2\alpha)}{s^{1+2\alpha}}. \tag{68}$$

Thus, the FME solution of the IVP (Eqs 59, 60) would be as follows:

$$U(x, t) = \begin{pmatrix} 0 \\ x^2 \end{pmatrix} + \begin{pmatrix} e^x \\ 0 \end{pmatrix} t^\alpha + \begin{pmatrix} 0 \\ 1 \end{pmatrix} t^{2\alpha}, \tag{69}$$

which is identical to the ES  $U(x, t) = \begin{pmatrix} e^x t^\alpha \\ x^2 + t^{2\alpha} \end{pmatrix}$ .

Application 4.3. Consider the following non-homogeneous hyperbolic system of T-FPDEs with variable coefficients:

$$\begin{aligned} U_t^{(\alpha)}(x, t) + A(x, t)U_x^{(\beta)}(x, t) + B(x, t)U(x, t) \\ = F(x, t), 0 < \alpha, \beta \leq 1, x \in \mathfrak{R}, t \geq 0, \end{aligned} \tag{70}$$

subject to

$$U(x, 0) = \begin{pmatrix} 0 \\ x^\beta \end{pmatrix}, \tag{71}$$

where

$$A(x, t) = \begin{pmatrix} x^\beta & 0 \\ 0 & x^\beta \end{pmatrix}, B(x, t) = \begin{pmatrix} 1 & t^\alpha \\ t^\alpha & 1 \end{pmatrix},$$

$$F(x, t) = \begin{pmatrix} t^\alpha x^\beta E_\alpha(t^\alpha) + \left( t^\alpha + t^\alpha x^\beta + \frac{\Gamma(1+2\alpha)}{\Gamma(1+\alpha)} \right) t^\alpha E_\beta(x^\beta) \\ (2 + \Gamma(1+\beta))x^\beta E_\alpha(t^\alpha) + t^{3\alpha} E_\beta(x^\beta) \end{pmatrix},$$

and the ES is

$$U(x, t) = \begin{pmatrix} t^{2\alpha} E_\beta(x^\beta) \\ x^\beta E_\alpha(t^\alpha) \end{pmatrix}, \tag{72}$$

where  $E_\alpha(t)$  is the Mittag-Leffler function defined by the following expansion [40]:

$$E_\alpha(t) = \sum_{m=0}^{\infty} \frac{t^m}{\Gamma(1+m\alpha)}. \tag{73}$$

Mathematica 7 software has been used through a low-RAM PC for obtaining all numerical calculations and symbolism. Since the Mittag-Leffler function is an infinite expansion, it was difficult to perform the calculations using the Mittag-Leffler function as it is. For this, the fifth truncated series of the expansion in Eq. 73 was used throughout the calculations.

Like the previous applications, transform Eq. 70 to the Laplace space using the initial condition in Eq. 71 to read as follows:

$$\begin{aligned} \mathbb{U}(x, s) - \frac{U_0(x)}{s} + \frac{\mathcal{L}[\mathcal{L}^{-1}[A(x, s)]\partial_x^\beta(\mathcal{L}^{-1}[\mathbb{U}(x, s)])]}{s^\alpha} \\ + \frac{\mathcal{L}[\mathcal{L}^{-1}[B(x, s)]\mathcal{L}^{-1}[\mathbb{U}(x, s)]]}{s^\alpha} \\ - \frac{\mathbb{F}(x, t)}{s^\alpha} = 0, 0 < \alpha, \beta \leq 1, x \in \mathfrak{R}, s > \lambda \geq 0. \end{aligned} \tag{74}$$

Let the solution of the algebraic equation (74) has an FME as in Eq. 31. Then, the  $k$ th TS of the FME of  $\mathbb{U}(x, s)$  can be given by

$$\mathbb{U}_k(x, s) = \begin{pmatrix} 0 \\ x^\beta \end{pmatrix} \frac{1}{s} + \sum_{m=1}^k \frac{H_m(x)}{s^{1+m\alpha}}, 0 < \alpha, \beta \leq 1, x \in \mathfrak{R}, s > \lambda \geq 0, \tag{75}$$

and the  $k$ th RMF of Eq. 74 is given by

$$\begin{aligned} RMF_k(x, s) = \mathbb{U}_k(x, s) - \begin{pmatrix} 0 \\ x^\beta \end{pmatrix} \frac{1}{s} \\ + \frac{\mathcal{L}[\mathcal{L}^{-1}[A(x, s)]\partial_x^\beta(\mathcal{L}^{-1}[\mathbb{U}_k(x, s)])]}{s^\alpha} \\ + \frac{\mathcal{L}[\mathcal{L}^{-1}[B(x, s)]\mathcal{L}^{-1}[\mathbb{U}_k(x, s)]]}{s^\alpha} \\ - \frac{\mathbb{F}(x, t)}{s^\alpha}, x \in \mathfrak{R}, s > \lambda \geq 0. \end{aligned} \tag{76}$$

Now, to determine  $H_1(x)$  in Eq. 73, we substitute  $\mathbb{U}_1(x, s) = \begin{pmatrix} 0 \\ x^\beta \end{pmatrix} \frac{1}{s} + \frac{H_1(x)}{s^{1+\alpha}}$  into Eq. 76 for  $k = 1$ , and multiplying the obtained equation by  $s^{1+\alpha}$  gives the following formula:

$$\begin{aligned} s^{1+\alpha}RMF_1(x, s) &= \begin{pmatrix} h_{11}(x) \\ h_{12}(x) - x^\beta \end{pmatrix} + \frac{\mathcal{H}_{12}(x; \alpha, \beta)}{s^\alpha} \\ &+ \frac{\mathcal{H}_{13}(x; \alpha, \beta)}{s^{2\alpha}} + \frac{\mathcal{H}_{14}(x; \alpha, \beta)}{s^{3\alpha}} + \frac{\mathcal{H}_{15}(x; \alpha, \beta)}{s^{4\alpha}} \\ &+ \frac{\mathcal{H}_{16}(x; \alpha, \beta)}{s^{5\alpha}} + \frac{\mathcal{H}_{17}(x; \alpha, \beta)}{s^{6\alpha}}, \end{aligned} \tag{77}$$

where  $\mathcal{H}_{1j}(x; \alpha, \beta) \in M_{2 \times 1}$ ,  $j = 1, 2, \dots, 7$ , are vector functions free from  $s$ . So, according to Eq. 37, we have

$$H_1(x) = \begin{pmatrix} h_{11}(x) \\ h_{12}(x) \end{pmatrix} = \begin{pmatrix} 0 \\ x^\beta \end{pmatrix}. \tag{78}$$

Using the same previous approach, we find the following vector coefficients of Eq. 75:

$$\begin{aligned} H_2(x) &= \begin{pmatrix} \Gamma(1 + 2\alpha)E_\beta(x^\beta) \\ x^\beta \end{pmatrix}, \\ H_3(x) &= \begin{pmatrix} 0 \\ x^\beta \end{pmatrix}, \\ H_4(x) &= \begin{pmatrix} 0 \\ x^\beta \end{pmatrix}, \\ H_5(x) &= \begin{pmatrix} 0 \\ x^\beta \end{pmatrix}. \end{aligned} \tag{79}$$

So, the fifth AS of Eq. 74 can be written as follows:

$$\begin{aligned} \mathbb{U}_5(x, s) &= \begin{pmatrix} 0 \\ x^\beta \end{pmatrix} \frac{1}{s} + \begin{pmatrix} 0 \\ x^\beta \end{pmatrix} \frac{1}{s^{1+\alpha}} + \begin{pmatrix} \Gamma(1 + 2\alpha)E_\beta(x^\beta) \\ x^\beta \end{pmatrix} \frac{1}{s^{1+2\alpha}} \\ &+ \begin{pmatrix} 0 \\ x^\beta \end{pmatrix} \frac{1}{s^{1+3\alpha}} + \begin{pmatrix} 0 \\ x^\beta \end{pmatrix} \frac{1}{s^{1+4\alpha}} + \begin{pmatrix} 0 \\ x^\beta \end{pmatrix} \frac{1}{s^{1+5\alpha}}. \end{aligned} \tag{80}$$

Transforming the AS in Eq. 80 to the  $t$ -space by the inverse LT, we get the fifth approximation of the solution of the IVP (Eqs 70, 71) as follows:

$$\begin{aligned} U_5(x, t) &= \begin{pmatrix} 0 \\ x^\beta \end{pmatrix} + \begin{pmatrix} 0 \\ x^\beta \end{pmatrix} \frac{t^\alpha}{\Gamma(1 + \alpha)} \\ &+ \begin{pmatrix} \Gamma(1 + 2\alpha)E_\beta(x^\beta) \\ x^\beta \end{pmatrix} \frac{t^{2\alpha}}{\Gamma(1 + 2\alpha)} \\ &+ \begin{pmatrix} 0 \\ x^\beta \end{pmatrix} \frac{t^{3\alpha}}{\Gamma(1 + 3\alpha)} + \begin{pmatrix} 0 \\ x^\beta \end{pmatrix} \frac{t^{4\alpha}}{\Gamma(1 + 4\alpha)} + \begin{pmatrix} 0 \\ x^\beta \end{pmatrix} \frac{t^{5\alpha}}{\Gamma(1 + 5\alpha)}. \end{aligned} \tag{81}$$

Obviously, there is a pattern between the terms of Eq. 81 that gives us the ES as in Eq. 72.

The mathematical behavior of the solution of the IVP (Eqs 70, 71) is illustrated next by plotting the three-dimensional space figures of the fifth approximation of the two components of the vector solution in Eq. 81 for different values of  $\alpha$  and a fixed value of  $\beta = 0.5$ . Figures 1A–C show the fifth AS,  $(U_1)_5(x, t)$  and  $(U_2)_5(x, t)$ , when  $\alpha = 0.7$ ,  $\alpha = 0.85$ , and  $\alpha = 1$ , respectively, on the square  $[0, 1] \times [0, 1]$ . Figure 1D shows the ES expressed by Eq. 72 for  $\alpha = 1$ .

Figures 1C,D show that the fifth AS of the IVP (Eq. 70, 71) is excellent compared to the ES, as well as in the previous cases, which have not been documented in order not to increase the numbers of graphs. It is known that, by increasing the number

of terms in the series, the accuracy of the solution increases and, thus, the error of solution reduces; therefore, we can reduce the error of the solution by calculating more coefficients of the FME solution as in Eq. 31.

In the next application, the ES is unknown. Therefore, we are trying to find the ES or an appropriate approximation of the solution.

Application 4.4. Consider the following non-homogeneous hyperbolic system of T-FPDEs with variable coefficients:

$$\begin{aligned} U_t^{(\alpha)}(x, t) - A(x, t)U_x^{(1)}(x, t) - B(x, t)U(x, t) \\ = F(x, t), 0 < \alpha \leq 1, x \in \mathfrak{R}, t \geq 0, \end{aligned} \tag{82}$$

subject to

$$U(x, 0) = \begin{pmatrix} x + 1 \\ e^x \end{pmatrix}, \tag{83}$$

where

$$\begin{aligned} A(x, t) &= \begin{pmatrix} 0 & -e^{-x}(e^x + (x-1)E_\alpha(t^\alpha) + (1+x)t^\alpha) \\ \Gamma(1 + \alpha) - e^x x - t^\alpha x & 0 \end{pmatrix}, \\ B(x, t) &= \begin{pmatrix} t^\alpha & 1 \\ 0 & x \end{pmatrix}, \quad F(x, t) = \begin{pmatrix} xE_\alpha(t^\alpha) \\ 0 \end{pmatrix}. \end{aligned}$$

Similar to the previous applications, the LT of Eq. 82 is given by

$$\begin{aligned} \mathbb{U}(x, s) - \begin{pmatrix} x + 1 \\ e^x \end{pmatrix} \frac{1}{s} - \frac{\mathcal{L}[\mathcal{L}^{-1}[A(x, s)]\partial_x^1(\mathcal{L}^{-1}[\mathbb{U}(x, s)])]}{s^\alpha} \\ - \frac{\mathcal{L}[\mathcal{L}^{-1}[B(x, s)]\mathcal{L}^{-1}[\mathbb{U}(x, s)]]}{s^\alpha} - \frac{\mathbb{F}(x, t)}{s^\alpha} \\ = 0, 0 < \alpha \leq 1, x \in \mathfrak{R}, s > \lambda \geq 0, \end{aligned} \tag{84}$$

the  $k$ th TS of the expansion of the solution of Eq. 84 is given as

$$\mathbb{U}_k(x, s) = \begin{pmatrix} x + 1 \\ e^x \end{pmatrix} \frac{1}{s} + \sum_{m=1}^k \frac{H_m(x)}{s^{1+m\alpha}}, 0 < \alpha \leq 1, x \in \mathfrak{R}, s > \lambda \geq 0, \tag{85}$$

and the  $k$ th RMF of Eq. 84 is given by

$$\begin{aligned} \text{RMF}_k(x, s) &= \mathbb{U}_k(x, s) - \begin{pmatrix} x + 1 \\ e^x \end{pmatrix} \frac{1}{s} \\ &- \frac{\mathcal{L}[\mathcal{L}^{-1}[F(x, s)]\partial_x^1(\mathcal{L}^{-1}[\mathbb{U}_k(x, s)])]}{s^\alpha} \\ &- \frac{\mathcal{L}[\mathcal{L}^{-1}[B(x, s)]\mathcal{L}^{-1}[\mathbb{U}_k(x, s)]]}{s^\alpha} - \frac{\mathbb{F}(x, t)}{s^\alpha}, x \in \mathfrak{R}, s > \lambda \geq 0. \end{aligned} \tag{86}$$

According to the fact in Eq. 37, we can create, successively, the following first eight coefficients of the expansion in Eq. 31 for this application:

$$\begin{aligned}
 H_0(x) &= \begin{pmatrix} x+1 \\ e^x \end{pmatrix}, \\
 H_1(x) &= \begin{pmatrix} 1 \\ \Gamma(1+\alpha) \end{pmatrix}, \\
 H_2(x) &= \begin{pmatrix} 1+\Gamma(1+\alpha) \\ 0 \end{pmatrix}, \\
 H_3(x) &= \begin{pmatrix} 1+\frac{\Gamma(1+2\alpha)}{\Gamma(1+\alpha)} \\ 0 \end{pmatrix}, \\
 H_4(x) &= \begin{pmatrix} 1+\frac{(1+\Gamma(1+\alpha))\Gamma(1+3\alpha)}{\Gamma(1+2\alpha)} \\ 0 \end{pmatrix}, \\
 H_5(x) &= \begin{pmatrix} 1+\frac{(\Gamma(1+\alpha)+\Gamma(1+2\alpha))\Gamma(1+4\alpha)}{\Gamma(1+\alpha)\Gamma(1+3\alpha)} \\ 0 \end{pmatrix}, \\
 H_6(x) &= \begin{pmatrix} 1+\frac{(\Gamma(1+2\alpha)+(1+\Gamma(1+\alpha))\Gamma(1+3\alpha))\Gamma(1+5\alpha)}{\Gamma(1+2\alpha)\Gamma(1+4\alpha)} \\ 0 \end{pmatrix}, \\
 H_7(x) &= \begin{pmatrix} 1+\frac{(\Gamma(1+\alpha)\Gamma(1+3\alpha)+(\Gamma(1+\alpha)+\Gamma(1+2\alpha))\Gamma(1+4\alpha))\Gamma(1+6\alpha)}{\Gamma(1+3\alpha)\Gamma(1+5\alpha)} \\ 0 \end{pmatrix}.
 \end{aligned}
 \tag{87}$$

Thus, the seventh AS of Eq. 84 has the following expression:

$$\begin{aligned}
 \cup_7(x, s) &= \frac{H_0(x)}{s} + \frac{H_1(x)}{s^{1+\alpha}} + \frac{H_2(x)}{s^{1+2\alpha}} + \frac{H_3(x)}{s^{1+3\alpha}} + \frac{H_4(x)}{s^{1+4\alpha}} + \frac{H_5(x)}{s^{1+5\alpha}} \\
 &\quad + \frac{H_6(x)}{s^{1+6\alpha}} + \frac{H_7(x)}{s^{1+7\alpha}},
 \end{aligned}
 \tag{88}$$

so the seventh AS of the IVP (Eqs 82, 83) can be expressed as follows:

$$\begin{aligned}
 U_7(x, t) &= H_0(x) + H_1(x) \frac{t^\alpha}{\Gamma(1+\alpha)} + H_2(x) \frac{t^{2\alpha}}{\Gamma(1+2\alpha)} \\
 &\quad + H_3(x) \frac{t^{3\alpha}}{\Gamma(1+3\alpha)} \\
 &\quad + H_4(x) \frac{t^{4\alpha}}{\Gamma(1+4\alpha)} + H_5(x) \frac{t^{5\alpha}}{\Gamma(1+5\alpha)} + H_6(x) \frac{t^{6\alpha}}{\Gamma(1+6\alpha)} \\
 &\quad + H_7(x) \frac{t^{7\alpha}}{\Gamma(1+7\alpha)}.
 \end{aligned}
 \tag{89}$$

To test the AS in Eq. 89, we need to find the norm of residual error vector (RES(x, t)) for different values of t and x in the region [0, 1] × [0, 1], where the residual error vector is defined by

$$\begin{aligned}
 \text{RES}_k(x, t) &= (U_k)_t^{(\alpha)}(x, t) - A(x, t)(U_k)_x^{(1)}(x, t) \\
 &\quad - B(x, t)U_k(x, t) - F(x, t),
 \end{aligned}
 \tag{90}$$

and the Frobenius norm is chosen for error analysis and defined by

$$\|U(x, t)\| = \sqrt{\left(\sum_{i=1}^m \sum_{j=1}^n |u_{ij}(x, t)|^2\right)}, \quad U(x, t) = [u_{ij}(x, t)] \in M_{m \times n}.
 \tag{91}$$

Tables 1, 2 show the values of ||RES<sub>6</sub>(x, t)|| and ||RES<sub>7</sub>(x, t)||, respectively, for different values of α. The data in the tables indicate that the norm of the residual error of the obtained AS decreases as (x, t) → (0, 0) as well as when α → 1. This indicates that the convergence of the BFMTF in Eq. 17 depends on t, x, and α as illustrated in Theorem 2.3. As we know, we can reduce the error in the FME solution as we increase the number of terms of the expansion. As we can see from the data in Tables 1, 2, the seventh approximation is more accurate than the sixth approximation. Anyway, it can be said that the L-RPSM is good at providing an accurate AS of a hyperbolic system of T-FPDEs with variable coefficients.

### 5 CONCLUSION

We have found that the ES for the hyperbolic system of T-FPDEs with variable coefficients is available if the solution is a linear combination of power functions or if it is a composite of an elementary function and a power function. In case the ES is not available, a good approximation of the solution can be obtained. The L-RPSM is an effective, accurate, easy, and speed technique in obtaining the values of coefficients for the SS. Through this work, we have presented a solution that may be missing for this kind of problem and we have opened the way for researchers to provide other ways to solve this class of equations. Moreover, the newly proposed technique can be used to construct many types of the ordinary or partial DEs of fractional order such as Lane–Emden, Boussinesq, KdV–Burgers, K(m, n), Klein–Gordon, and B(l, m, n) equations.

### DATA AVAILABILITY STATEMENT

All datasets generated for this study are included in the article/ supplementary files.

### AUTHOR CONTRIBUTIONS

The idea of this work, implementation, and output of this form was carried out by both authors.

### ACKNOWLEDGMENTS

The first author expresses his appreciation and thanks to Al-Balqa Applied University for granting him a sabbatical leave that made this research possible.

## REFERENCES

1. Burger M, Caffarelli L, and Markowich PA. Partial Differential Equation Models in the Socio-Economic Sciences. *Phil Trans R Soc A* (2014) 372: 20130406. doi:10.1098/rsta.2013.0406
2. Mattheij R, Rienstra S, and Boonkcamp J. *Partial Differential Equations: Modeling, Analysis, Computation, Technische Universiteit Eindhoven Eindhoven*. Netherlands: Siam (2005). doi:10.1137/1.9780898718270
3. Evans LC. *Partial Differential Equations*. American Mathematical Society (2002). doi:10.1090/gsm/019
4. Leray J. *Hyperbolic Differential Equations*. Princeton, NJ: Institute for Advanced Study (1953). doi:10.11948/2017095
5. Sanchez Y, and Vickers J. Generalised Hyperbolicity in Spacetimes with Lipschitz Regularity. *J Math Phys* (2017) 58:022502. doi:10.1063/1.4975216
6. Toro EF. Notions on Hyperbolic Partial Differential Equations. In: *Riemann Solvers and Numerical Methods for Fluid Dynamics*. Heidelberg, Berlin: Springer (2009). doi:10.1007/b79761
7. Caputo M. Linear Models of Dissipation Whose Q Is Almost Frequency Independent-II. *Geophys J Int* (1967) 13:529–39. doi:10.1111/j.1365-246x.1967.tb02303.x
8. Mainardi F. *Fractional Calculus and Waves in Linear Viscoelasticity*, Imperial College Press. London, UK: Imperial College (2010). doi:10.1142/p614
9. Kilbas AA, Srivastava HM, and Trujillo JJ. *Theory and Applications of Fractional Differential Equations*. Netherlands: Elsevier, Amsterdam (2006).
10. Magin RL, Ingo C, Colon-Perez L, Triplett W, and Mareci TH. Characterization of Anomalous Diffusion in Porous Biological Tissues Using Fractional Order Derivatives and Entropy. *Microporous Mesoporous Mater* (2013) 178:39–43. doi:10.1016/j.micromeso.2013.02.054
11. Tarasov VE. *Fractional Dynamics: Applications of Fractional Calculus to Dynamics of Particles, Fields and Media*. Berlin, Germany: Springer (2011).
12. West B, Bologna M, and Grigolini P. *Physics of Fractal Operators*. New York: Springer (2003).
13. Qureshi S, and Yusuf A. Mathematical Modeling for the Impacts of Deforestation on Wildlife Species Using Caputo Differential Operator. *Chaos, Solitons & Fractals* (2019) 126:32–40. doi:10.1016/j.chaos.2019.05.037
14. Li Z, Liu Z, and Khan MA. Fractional Investigation of Bank Data with Fractal-Fractional Caputo Derivative. *Chaos, Solitons & Fractals* (2020) 131:109528. doi:10.1016/j.chaos.2019.109528
15. Mustapha UT, Qureshi S, Yusuf A, and Hincal E. Fractional Modeling for the Spread of Hookworm Infection under Caputo Operator. *Chaos, Solitons & Fractals* (2020) 137:109878. doi:10.1016/j.chaos.2020.109878
16. Ali A, Alshammari FS, Islam S, Khan MA, and Ullah S. Modeling and Analysis of the Dynamics of Novel Coronavirus (COVID-19) with Caputo Fractional Derivative. *Results Phys* (2021) 20:103669. doi:10.1016/j.rinp.2020.103669
17. Momani S, and Odibat Z. Comparison between the Homotopy Perturbation Method and the Variational Iteration Method for Linear Fractional Partial Differential Equations. *Comput Maths Appl* (2007) 54:910–9. doi:10.1016/j.camwa.2006.12.037
18. Daftardar-Gejji V, and Bhalekar S. Solving Multi-Term Linear and Non-linear Diffusion-Wave Equations of Fractional Order by Adomian Decomposition Method. *Appl Maths Comput* (2008) 202:113–20. doi:10.1016/j.amc.2008.01.027
19. Das S, and Gupta PK. Homotopy Analysis Method for Solving Fractional Hyperbolic Partial Differential Equations. *Int J Comput Maths* (2011) 88: 578–88. doi:10.1080/00207161003631901
20. Momani S, and Odibat ZM. Fractional Green Function for Linear Time-Fractional Inhomogeneous Partial Differential Equations in Fluid Mechanics. *J Appl Math Comput* (2007) 24:167–78. doi:10.1007/bf02832308
21. El-Ajou A. Taylor's Expansion for Fractional Matrix Functions: Theory and Applications. *J Math Comput Sci* (2020) 21(2):1–17. doi:10.22436/jmcs.021.01.01
22. Oqielat Ma. N, El-Ajou A, Al-Zhour Z, Alkhasawneh R, and Alrabaiah H. Series Solutions for Nonlinear Time-Fractional Schrödinger Equations: Comparisons between Conformable and Caputo Derivatives. *Alexandria Eng J* (2020) 59(4):2101–14. doi:10.1016/j.aej.2020.01.023
23. El-Ajou A, Oqielat Ma. N, Al-Zhour Z, and Momani S. A Class of Linear Non-homogenous Higher Order Matrix Fractional Differential Equations: Analytical Solutions and New Technique. *Fract Calc Appl Anal* (2020) 23(2):356–77. doi:10.1515/fca-2020-0017
24. El-Ajou A, Al-Smadi M, Oqielat Ma. N, Momani S, and Hadid S. Smooth Expansion to Solve High-Order Linear Conformable Fractional PDEs via Residual Power Series Method: Applications to Physical and Engineering Equations. *Ain Shams Eng J* (2020) 11(4):1243–54. doi:10.1016/j.aesej.2020.03.016
25. El-Ajou A, Oqielat Ma. N, Al-Zhour Z, and Momani S. Analytical Numerical Solutions of the Fractional Multi-Pantograph System: Two Attractive Methods and Comparisons. *Results Phys* (2019) 14:102500. doi:10.1016/j.rinp.2019.102500
26. El-Ajou A, Al-Zhour Z, Oqielat Ma., Momani S, and Hayat T. Series Solutions of Nonlinear Conformable Fractional KdV-Burgers Equation with Some Applications. *Eur Phys J Plus* (2019) 134(8):402. doi:10.1140/epjp/i2019-12731-x
27. Shqair M, El-Ajou A, and Nairat M. Analytical Solution for Multi-Energy Groups of Neutron Diffusion Equations by a Residual Power Series Method. *Mathematics* (2019) 7(7):633. doi:10.3390/math7070633
28. Eriqat T, El-Ajou A, Oqielat Ma. N, Al-Zhour Z, and Momani S. A New Attractive Analytic Approach for Solutions of Linear and Nonlinear Neutral Fractional Pantograph Equations. *Chaos, Solitons & Fractals* (2020) 138: 109957. doi:10.1016/j.chaos.2020.109957
29. El-Ajou A. Adapting the Laplace Transform to Create Solitary Solutions for the Nonlinear Time-Fractional Dispersive PDEs via a New Approach. *Eur Phys J Plus* (2021) 136:229. doi:10.1140/epjp/s13360-020-01061-9
30. Srivastava VK, Awasthi MK, and Tamsir M. RDTM Solution of Caputo Time Fractional-Order Hyperbolic Telegraph Equation. *AIP Adv* (2013) 3(3): 032142. doi:10.1063/1.4799548
31. Abbas S, and Benchohra M. Fractional Order Partial Hyperbolic Differential Equations Involving Caputo Derivative. *Stud Univ Babeş-bolyai Math* (2012) 57:469–79.
32. Akilandeewari A, Balachandran K, and Annapoorani N. Solvability of Hyperbolic Fractional Partial Differential Equations. *J App Anal Comp* (2017) 7:1570–85. doi:10.11948/2017095
33. Ashyralyev A, Dal F, and Pinar Z. On the Numerical Solution of Fractional Hyperbolic Partial Differential Equations. *Math Probl Eng* (2009) 2009:1–11. doi:10.1155/2009/730465
34. Khan H, Shah R, Baleanu D, Kumam P, and Arif M. Analytical Solution of Fractional-Order Hyperbolic Telegraph Equation, Using Natural Transform Decomposition Method. *Electronics* (2019) 8(9):1015. doi:10.3390/electronics8091015
35. Modanl M. Two Numerical Methods for Fractional Partial Differential Equation with Nonlocal Boundary Value Problem. *Adv Differ Equ* (2018) 333:333. doi:10.1186/s13662-018-1789-2
36. Lin Y, and Xu C. Finite Difference/spectral Approximations for the Time-Fractional Diffusion Equation. *J Comput Phys* (2007) 225:1533–52. doi:10.1016/j.jcp.2007.02.001
37. Meerschaert MM, and Tadjeran C. Finite Difference Approximations for Fractional Advection-Dispersion Flow Equations. *J Comput Appl Maths* (2004) 172:65–77. doi:10.1016/j.cam.2004.01.033
38. Kochubei AN. Fractional-hyperbolic Systems. *Fract Calc Appl Anal* (2013) 16: 860–73. doi:10.2478/s13540-013-0053-4
39. Hendy AS, Macias-Díaz JE, and Serna-Reyes AJ. On the Solution of Hyperbolic Two-Dimensional Fractional Systems via Discrete Variational Schemes of High Order of Accuracy. *J Comput Appl Maths* (2019) 354:612–22. doi:10.1016/j.cam.2018.10.059
40. Simon T. Mittag-Leffler Functions and Complete Monotonicity. *Integral Transforms Special Fun* (2015) 26 (1):36–50. doi:10.1080/10652469.2014.965704

**Conflict of Interest:** The authors declare that the research was conducted in the absence of any commercial or financial relationships that could be construed as a potential conflict of interest.

Copyright © 2021 El-Ajou and Al-Zhour. This is an open-access article distributed under the terms of the Creative Commons Attribution License (CC BY). The use, distribution or reproduction in other forums is permitted, provided the original author(s) and the copyright owner(s) are credited and that the original publication in this journal is cited, in accordance with accepted academic practice. No use, distribution or reproduction is permitted which does not comply with these terms.

# Advantages of publishing in Frontiers



## OPEN ACCESS

Articles are free to read for greatest visibility and readership



## FAST PUBLICATION

Around 90 days from submission to decision



## HIGH QUALITY PEER-REVIEW

Rigorous, collaborative, and constructive peer-review



## TRANSPARENT PEER-REVIEW

Editors and reviewers acknowledged by name on published articles

## Frontiers

Avenue du Tribunal-Fédéral 34  
1005 Lausanne | Switzerland

Visit us: [www.frontiersin.org](http://www.frontiersin.org)

Contact us: [frontiersin.org/about/contact](http://frontiersin.org/about/contact)



## REPRODUCIBILITY OF RESEARCH

Support open data and methods to enhance research reproducibility



## DIGITAL PUBLISHING

Articles designed for optimal readership across devices



## FOLLOW US

@frontiersin



## IMPACT METRICS

Advanced article metrics track visibility across digital media



## EXTENSIVE PROMOTION

Marketing and promotion of impactful research



## LOOP RESEARCH NETWORK

Our network increases your article's readership